This electronic thesis or dissertation has been downloaded from the King's Research Portal at https://kclpure.kcl.ac.uk/portal/

Ab initio prediction of thermomagnetic and thermoelectric transport phenomena in 3d and 2d materials

MacHeda, Francesco

Awarding institution:
King's College London

The copyright of this thesis rests with the author and no quotation from it or information derived from it may be published without proper acknowledgement.

END USER LICENCE AGREEMENT

Unless another licence is stated on the immediately following page this work is licensed

under a Creative Commons Attribution-NonCommercial-NoDerivatives 4.0 International

licence. https://creativecommons.org/licenses/by-nc-nd/4.0/

You are free to copy, distribute and transmit the work

Under the following conditions:

- Attribution: You must attribute the work in the manner specified by the author (but not in any way that suggests that they endorse you or your use of the work).
- Non Commercial: You may not use this work for commercial purposes.
- No Derivative Works - You may not alter, transform, or build upon this work.

Any of these conditions can be waived if you receive permission from the author. Your fair dealings and other rights are in no way affected by the above.

Take down policy

If you believe that this document breaches copyright please contact librarypure@kcl.ac.uk providing details, and we will remove access to the work immediately and investigate your claim.

Download date: 25. Dec. 2024

KING'S COLLEGE LONDON

DOCTORAL THESIS

Ab initio prediction of thermomagnetic and thermoelectric transport phenomena in 3d and 2d materials

---

Author:
Francesco Macheda

Supervisor:
Dr. Nicola Bonini

Department of Physics

A thesis submitted in fulfilment of the requirements
for the degree of Doctor of Philosophy

July 1, 2021

KING'S COLLEGE LONDON

Abstract

Faculty of Natural and Mathematical Sciences
Department of Physics

Doctor of Philosophy

***Ab initio* prediction of thermomagnetic and thermoelectric transport phenomena in 3d and 2d materials**

by Francesco Macheda

In this work we study the thermomagnetic and thermoelectric transport phenomena in 3d and 2d crystals. We first present the general theory for transport in presence of electric and magnetic external fields. In this context, we introduce the linearised Boltzmann Transport Equation and the Kubo formalism, with a focus on their derivation from first-principles and on the *ab-initio* evaluation of their main ingredients. Here, a particular emphasis is given to the development of an efficient approach to determine magneto-transport coefficients, that firmly relies on our highly scalable and strongly optimized computational implementation. Then, we apply the theory to three different systems: bulk p-doped diamond, graphene and the tetrahedrite compound $Cu_{12}Sb_4S_{13}$. Each one of these systems, beside being of interest for technological applications, poses its own challenge to the calculation of transport properties. p-doped diamond presents a complex interplay between the electronic and vibrational properties, that has prevented detailed experimental investigation to extract the true value of transport observables; in graphene, the electrons near the Dirac cone have very large momenta that generate non-trivial trends and values of the transport properties, that are in sharp contrast with known behaviours of traditional semiconductors; finally, the tetrahedrite system displays a complex crystal structure stabilized by temperature so that the description of its transport properties requires a proper sampling of the electron-ion dynamics of the system. In this perspective, the theoretical study of these systems and the comparison with experimental data serve both purposes of increasing the knowledge of specific material properties and of testing the theory on challenging cases.

Acknowledgements

This work would have not been possible without the support of many people.

First and foremost, I want to heartfeltly thank my supervisor Dr. Nicola Bonini for his guidance, teachings and feedback during all my PhD.

I thank my second supervisor Dr. Cedric Weber, my collaborators Prof. Feliciano Giustino, Dr. Cono di Paola, Dr. Savio Laricchia and Dr. Samuel Poncé. I also thank my Master Degree supervisor Prof. Giuseppe Grosso, Dr. Guido Menichetti and all the people that have inspired me in all these years.

A special thank goes to Giulia, Marcello, Paolo and Giuseppe for our never-ending friendship and intellectual discussions (to put it mildly).

A thought goes to my friends of a lifetime Cristian and Mattia, you have always been there for me.

All of this would have never been possible without the constant support of my family. To you go my biggest thank, every achievement that I earn is also yours. To Athos, Giovanna, Monica, Saverio and my beloved Chiara.

Contents

List of Figures

List of Abbreviations

BTE	**B**oltzmann **T**ransport **E**quation
DFT	**D**ensity **F**unctional **T**heory
GS	**G**round **S**tate
DFPT	**D**ensity **F**unctional **P**erturbation **T**heory
BZ	**B**rillouin **Z**one
SMA	**S**ingle **M**ode **A**pproximation
FS	**F**ermi **S**urface
SERTA	**S**elf **E**nergy **R**elaxation **T**ime **A**pproximation
MRTA	**M**omentum **R**elaxation **T**ime **A**pproximation
CRT	**C**onstant **R**elaxation **T**ime
MLWF	**M**aximally **L**ocalized **W**annier **F**unctions
HSF	**H**all **S**cattering **F**actor
K-G	**K**ubo **G**reenwood
NEGF	**N**on **E**quilibrium **G**reen's **F**unction
QBTE	**Q**uantum **B**oltzmann **T**ransport **E**quation

List of Symbols

σ	Electrical conductivity
ρ	Electrical resistivity
μ^d	Drift mobility
μ^H	Hall mobility
k^{th}	Thermal conductivity
S	Seebeck coefficient
S^p	Phonon drag contribution to Seebeck coefficient
r	Hall scattering factor
E_F	Fermi level
v_F	Fermi velocity
g	Electron phonon vertex
a	Lattice parameter
L	Lorenz number

Introduction

Electronic and thermal transport properties are central quantities in order to characterize a material; it is well known that these properties are not independent one from another because small electrical fields and thermal gradients generate interdependent currents which are governed by the Onsager relations [1, 2]. The detailed understanding of these phenomena is at the hearth of the development and the optimization of new electronic and thermoelectric devices, that can outperform traditional silicon-based technology and pave the way for a more sustainable and eco-friendly technological progress. In recent years, electrical and thermal transport coefficients of some elemental materials have been computed by means of the linearised Boltzmann Transport Equation (BTE) [3, 4, 5, 6]. The Boltzmann formalism was developed by L. E. Boltzmann in 1872 to describe the microscopical behaviour of classical diluted gases formed by weakly interacting particles [7]; in particular, the Boltzmann equation describes the evolution of the statistical one-particle density f in the phase space of momentum and position, equating diffusion-force processes and collision mechanisms. It was only later in 1929 that R. Peierls pioneered the use of the Boltzmann equation to study the transport properties of crystals in presence of small external fields [8]. Here, the classical motion observables such as the momentum or the velocity are identified with the expectation values of the corresponding quantum-mechanical operators and the collisional integral is written using the Fermi golden rule. It might surprise that such a seemingly heuristic approach still represents one of the most successful framework in order to study transport in materials. Actually, it has be shown that more advanced methods such as the non-equilibrium Green's function formalism, in appropriate simplifying hypotheses, have the same structure of the Boltzmann scheme [9, 10, 11]. In particular, the Boltzmann equation is recovered in the limit of the quasiparticles approximation [12] (with some additional features that we will highlight in the body of this thesis). Also, a generalized Boltzmann equation can be derived starting from the Kubo formula for the conductivity [13]. It is thus at last not so surprising that for weakly interacting particles the Boltzmann framework is so successful in predicting the non equilibrium linear response of a system to external fields within a very good precision.

In this work we mainly specialize to the study of electron and phonons and their mutual interaction—defects, doping, finite size effects, isotopic scattering etc. are included only when necessary—in presence of small external perturbing fields (electric and magnetic fields and/or thermal gradients). In this case electrons and phonons possess two BTEs that are coupled through their mutual interaction; these equations have to be solved, in principle, at the same time. In practice, they can most often be treated separately. When this is possible, we will focus on the electronic BTE and calculate the electronic transport properties. When this is not possible, phenomena like the phonon-drag of electrons show up from the coupling between electron and phonons populations [14] that can be particularly strong, so that we will have to deal with both equations.

The theory of the solution of the BTE of simple models in simplifying assumption is well studied [15]. Nonetheless, such approximations are most often not suitable for an accurate reproduction of the experimental data. For that reason, in the last years there has been a huge effort to solve the BTE equation exactly, using *ab-initio* techniques to calculate the one-particle quantities and the particle interactions (see for example Refs. [4, 16, 3, 17, 18, 19, 20, 21, 22, 23] for the electronic BTE and Refs. [24, 25, 26, 27, 28] for the phonon BTE). The difficulty of solving the BTE equations from first principles is mainly related to the huge number of quantities that have to be computed starting from Density Functional Theory (DFT) and Density Functional Perturbation Theory (DFPT).

For the phonon BTE the main ingredients are the phonon dispersions, the phonon velocities and all the possible scattering processes that can influence heat transport in a crystal. The main computational bottleneck here is represented by the calculation of the matrix of the third order derivatives of the total energy with respect to phonon eigendisplacement [27]. This matrix is related to the three-phonons anharmonic scattering processes, which are the principal intrinsic mechanism that limit the heat transport in crystals. The three-phonon processes involve summation over the whole Brillouin Zone (BZ) on uniform $\mathbf{q}$-point grids and over the complete phonon frequency spectrum (phonon branches); in many materials, such as diamond or graphene, there is no valid simplifying assumption that can reduce the portion of the BZ considered because the thermal conductivity gets a non-negligible contribution for each of the allowed processes. Energetically, at low temperatures one could exclude high frequency optical phonons from the summations; this improvement would be significant for compounds with many atoms per unit cell, but here the calculation of the phonons alone is already a complicate task. Moreover, if one is interested in the asymptotic behaviour of

the out of equilibrium phonon populations near the center of the BZ, then the computational cost becomes prohibitive due to the grid sizes—unless one can find an accurate simplifying assumption to calculate the populations in this region. Such asymptotic behaviours are of interest because, as we will show later, they determine the strength of the phonon-drag contribution to the Seebeck coefficient. In this work we find that in diamond the Single Mode Approximation (SMA) is appropriate to describe the out of equilibrium populations near the BZ center, and therefore we can access the asymptotic behaviours without extreme efforts.

For the electron BTE the main ingredients are the electronic band structure, the electronic velocity and the possible scattering between electrons and other particles. In particular one can count many scattering sources: phonons, plasmons, polarons, impurities, boundaries and possibly other collective modes. In this work we will concentrate on the effects of the electron-phonon coupling scattering and we will consider scattering with impurities only when necessary. Scattering with collective modes are usually important at very high doping concentrations, which are never accessed in this work. The electronic transport, in contraposition to what happens in the case of the phonon transport, gets contributions from a well defined region of the BZ. This region corresponds to the neighbourhood of the Fermi Surface (FS) because, as we will see, only those states give a significant contribution to the electron and heat flows. When dealing with doped semiconductors, which may not possess a well-defined FS because of the electronic band gap, the particles that contribute to the transport properties are the ones that are energetically nearer to the Fermi Level (E_F), which is instead always well defined through the charge neutrality condition. To understand which states around E_F are active for transport we can look at the physical scales: the electronic energies usually vary on the scale of the eV, while the phonons energies are usually in the range $0-200$ meV; the electron-phonon coupling too is of the meV order, while the room-temperature thermal energy–which is the scale for the Fermi Dirac distribution– is around 25 meV. Since in this work we mainly consider electron-phonon coupling, we expect—and we find—that the out of equilibrium populations used to find the transport observables vary on the meV scale. This basically means on one side that the portions of the electronic band structure that really contribute to transport are distant some meV from E_F (or from the band extrema if E_F falls in the gap); on the other side it means that this small energy window has to be sampled very accurately in order to describe the variation of the momentum resolved transport quantities. This implies the use of very dense homogeneous electronic $\mathbf{k}$ and phonon $\mathbf{q}$-point grids, unless some simplifying assumption can be made. As we will see, some approximation such as the Self Energy Relaxation Time Approximation (SERTA) do not need the solution of the

Boltzmann equation on homogeneous grids, but the accuracy of this approximation is not always sufficient.

Since for the electronic BTE we need to sample a tiny energetic window but with high precision, the calculation of the *ab-initio* quantities needs to be performed with great accuracy. The effort it would take to calculate all the quantities directly from first principles is overwhelming. Luckily, it has been shown that the electronic quantities and the electron-phonon coupling matrix elements are prone to be interpolated via the use of Maximally Localized Wannier Functions (MLWFs) [29, 30, 31] with several computational infrastructures [32, 33, 34, 35]. MLWFs are obtained as a unitary transformation of the Bloch states; the transformation is built in a way that the elements of the arrival basis set are as much localized in real space as possible. In the MLWFs basis set the crystal Hamiltonian is no more diagonal; the idea is to trade the localization in the quasi-momentum/energy with localization in space, so that when we express an operator in the MLWF basis set we can justify the truncation of the basis set with real space arguments. We can understand the usefulness of MLWFs with a practical example: let's suppose that we are able to calculate the eigenvalues of a crystal Hamiltonian from first-principles on a certain given $\mathbf{k}$-point grid of dimensions $n_1 \times n_2 \times n_3$. We now consider the restriction of the Hamiltonian to a set of n_b eigenvalues (energy bands) that are relevant for our problem, so that we have $n_b \times n_1 \times n_1 \times n_3$ Bloch functions. From these Bloch functions we generate our set of MLWF and express the Hamiltonian in this basis set; if—and this usually happens for reasonable dimensions of the electronic grids—the Hamiltonian displays a localization in real space then we can use the inverse transformation and back-interpolate the Hamiltonian safely on a generic $\mathbf{k}$-point of the BZ. This process is called Wannier interpolation and is, as we will see, of primary importance in order to access the transport quantities on grids of (almost) arbitrary dimensions.

The techniques outlined above have given the possibility to perform accurate calculations for the transport properties that have developed unprecedented insights on the processes involved in electronic and thermal transport. These promise to provide useful guidelines for experimental investigation and for material engineering. Amongst the most promising bulk materials for a new generation of energy-efficient, high-performance and tough electronic devices, diamond surely assumes a leading role for applications ranging from power electronics to bio-sensors and high-energy-physics detectors [36, 37]. The reason is that diamond has some extreme physical properties which make it suitable for a broad range of applications [38]: it is very hard, chemically inert and heat tolerant, and it has extraordinary high values of breakdown voltage, thermal conductivity and carrier mobility, as well as one of the largest known energy

gaps of all semiconductors. In particular, the hole mobility of p-doped diamond is of great interest in modelling new electronic devices [37, 39]. Despite several experimental and theoretical investigations, the value for the hole mobility vary significantly in literature, ranging from 2000 to 3800 $cm^2V^{-1}s^{-1}$ at room temperature [40, 41, 42, 43, 44, 45]. In the same fashion, the link between hole drift and Hall mobility is still not completely clear [46] and the comparison between experimental data and theoretical calculations is often difficult. In addition, the relation between the charge carriers flow and phonon out of equilibrium populations (both exceptionally high in diamond), that leads to a strikingly large Seebeck coefficient at low temperatures [47] (as large as five times the value for Silicon [3]), has not yet been precisely characterized. In this work, we will determine the transport properties of p-doped diamond and determine how these can be affected or controlled by doping, temperature and magnetic fields.

When talking about potential materials for electronic device applications, it is impossible not to mention graphene. Since its discovery in 2004 [48], graphene has drawn attention from all the scientific community for its incredible and peculiar properties. The possibility of reducing the dimensionality of a working device in conjunction with the formidable transport phenomena that arise in graphene has generated unique expectations around this material. Of course, at the basis of all the possible applications lies the precise understanding of electronic transport in graphene. A lot of work has already been done in order to quantify the temperature dependence and predict the value of the electronic resistivity and mobility of graphene (see for example Refs. [49, 50, 51, 52, 16, 53]. The previous works—together with experimental evidence such as Ref. [54]—showed that the electrical resistivity ρ in graphene follows two temperature trends. At low temperatures $\rho \propto T^4$ while at high temperatures $\rho \propto T$; the change in behaviour is due to the fact that at high enough temperatures the thermal energy scale k_BT "hides" the presence of low frequency phonons while at low temperatures this does not happen. Nonetheless, even with the most advanced types of calculations the numerical agreement with experiments is still arguable [16], especially at high temperatures. An hypothesis that is put forward in Ref. [16] is that the value of the coupling between electrons near the Dirac cone and phonons with wave-vectors around the $\mathbf{K}$ special point is underestimated by a factor 3 in the theoretical calculations. On the other side, what is always implicitly assumed when doing comparison between theory and experiments is that the carrier concentrations are well estimated with Hall measurements. In fact, the estimate of the carrier density relies on the assumption that the Hall Scattering Factor (HSF) r [55], defined as the ratio between Hall and drift mobilities, can be taken as 1. In this work we show that this assumption for low dopings does not hold in graphene as a consequence of the linear band dispersion and the particular

form of coupling between electron and acoustic phonons. Therefore the comparison with experimental data has to be performed carefully. Moreover, we will show that at a given carrier density r is highly sensitive to the value of the Fermi velocity v_F, which can be highly dependent on the substrate on which graphene is grown [56]. The whole of these aspect are usually not taken in account in experiments.

Thus far we have considered transport properties in systems where we have well-defined quasi-particles that weakly interact and generate charge and heat fluxes when small external fields are turned on. Though, it is not always guaranteed that we have well defined excitation of the electronic or of the nuclear systems. In fact, for a system it may happen that the Fermi liquid picture does not hold—but we don't consider this case in this work—or that the DFT phonon dispersions at zero temperature shows negative phonons for a given geometrical structure which is known to be stable at another temperature. This is usually the mark of low temperature structural instabilities that are renormalized by the temperature dependence of the free energy. If one wants to study the transport phenomena in such a system with the Boltzmann formalism, one should consider the temperature effect on the phonon dispersions (as done for example in Refs. [57]). This approach is very difficult because every quantity in the Boltzmann equation should be calculated ab-initio for each temperature (whereas usually temperature enters just in the statistical factors). In alternative, another possible approach is to study transport phenomena with the Kubo-Greenwood (K-G) formalism [58, 59] applied to crystals [60]. There exist a wide number of systems that show phonon instabilities and that are actually of great technological interest because they show very good thermoelectric properties in connection with their very low thermal conductivity. This is linked to the previously mentioned renormalization of phonon frequencies that ultimately leads to very low phonon group velocities—and then low heat transport—in the temperatures of interest. In this work we will study the tetrahedrite compound $Cu_{12}Sb_4S_{13}$, that in its pristine form posseses a remarkably high figure of merit value, $zT \sim 0.6$ at 700K, due to a very low thermal conductivity (below 1 $Wm^{-1}K^{-1}$ from 300 to 700K) and a very high power factor. At room temperature this system crystallizes in a cubic structure ($I\bar{4}3m$) while at around 70K there are hints of a structural transition [61, 62]; coherently, DFT calculations show several soft phonons modes at zero temperature for the cubic structure. Since we want to study the high temperature thermoelectric properties of this compound, we adopt here the K-G formula for transport and estimate the intrinsic lowest bound for the electrical conductivity and the value for the Seebeck coefficient. In particular, we will perform an *ab-initio* Molecular Dynamics (MD) to simulate the electronic and atomic systems at a given temperature, where the phonons are well defined, and then extract snapshots on which we will

apply the K-G formulas (as done in Ref. [63]). Moreover, we will show that a simplified Boltzmann formalism with arbitrary scattering rates—even though not formally justified—can reproduce the temperature trends (but not the values) of the electrical conductivity and the values of the Seebeck coefficient. The result is not very surprising for the Seebeck coefficient because it is quite known that its value is almost entirely determined by the electronic band structure while it is almost insensitive to the scattering type. The parallelism with the Boltzmann formalism also allows us to extract an "effective" scattering rate by matching the two electrical resistivity results.

In summary, in this thesis we will study transport phenomena in systems with different dimensionality, electronic and atomic structure, and for each of those we will use the appropriate tools in order to grasp the physical mechanisms at the basis of transport. The outline of this thesis is as follows:

- In Chapter 1 we present the theoretical framework of this thesis, with a brief introduction to the electronic ground state calculations via DFT, the description of vibrational properties via DFPT, the Wannier interpolation with MLWFs, the BTE formalism, the transport coefficients and the Kubo formula.;

- In Chapter 2 we give a theoretical derivation of the electronic BTE from first-principles using the theory of NEGFs;

- In Chapter 3 we study the magneto-transport properties of bulk p-doped diamond—part of this work has been published in: Francesco Macheda and Nicola Bonini. "Magnetotransport phenomena in p-doped diamond from first principles". In: *Phys. Rev. B* 98 (20 2018), p. 201201. DOI: 10.1103/PhysRevB.98.201201. URL: https://link.aps.org/doi/10.1103/PhysRevB.98.201201 (Ref. [4] in the text);

- In Chapter 4 we calculate the Hall scattering factor for 2d graphene—part of this work has been published in: Francesco Macheda, Samuel Poncé, Feliciano Giustino, and Nicola Bonini. "Theory and Computation of Hall Scattering Factor in Graphene". In: *Nano Letters* 20.12 (2020), pp. 8861–8865. ISSN: 1530-6984. DOI: 10.1021/acs.nanolett.0c03874. URL: https://doi.org/10.1021/acs.nanolett.0c03874 (Ref. [64] in the text);

- In Chapter 5 we compute the thermoelectric coefficient for the high-temperature phase of the $Cu_{12}Sb_4S_{13}$ compound—part of this work has been published in: Cono Di Paola, Francesco Macheda, Savio Laricchia, Cedric Weber, and Nicola Bonini. "First-principles study of electronic transport and structural properties

of $Cu_{12}Sb_4S_{13}$ in its high-temperature phase". In: *Phys. Rev. Research* 2 (3 2020), p. 033055. DOI: 10.1103/PhysRevResearch.2.033055. URL: https://link.aps.org/doi/10.1103/PhysRevResearch.2.033055 (Ref. [65] in the text).

We also summarize the computational infrastructures used for the calculations, with a particular focus on the ones developed by the authors of the present work:

- QUANTUM ESPRESSO [66] for DFT and DFPT calculations;
- WANNIER90 [32, 33] for MLWFs determination;
- D3Q [27] and THERMAL2 [25], together with in-house built post-processing tools, in order to study thermal conductivity and phonon out of equilibrium populations;
- An in-house built code which contains solvers of the BTE in absence or presence of a magnetic field, used to determine the magneto-transport coefficients of diamond in Chapter 3;
- A private, highly scalable and strongly optimized version of EPW [30, 34] used to solve the BTE in absence or presence of magnetic field and calculate transport coefficients for graphene in Chapter 4;
- VASP [67, 68] which is used, in conjunction with in-house built post-processing tools, to simulate the *ab-initio* molecular dynamics and compute the Kubo-Greenwood formula for tetrahedrite in Chapter 5.

Most of the technical details and proofs are postponed in the Appendices in order to facilitate readability.

Chapter 1

Theoretical framework

In this chapter we introduce the theoretical framework of this thesis. In the first section we present the main tools to calculate from first principles the electronic and vibrational properties of a material, and their mutual interaction. In the second section, we present the general physical problem of the non equilibrium response of a system to external perturbations; from here, we start analysing the two different methods to study non equilibrium that are used in this thesis, namely the Boltzmann formalism and the KG formula. We start presenting the coupled linearised Boltzmann equations for phonons and electrons and discuss the conditions for their decoupling. Once we have decoupled equations, we show how to efficiently calculate the ingredients needed to approach their solution. In particular, we discuss the one-particle quantities and the collision terms that are considered in this work, and in which way they can be interpolated. In the last section we present the general theory for transport in linear response introducing the KG formula in crystals and describing its use in conjunction with MD simulations. A work-flow and a flowchart of the practical implementation of the techniques described in this chapter and used throughout all this work is given in App. A.

1.1 Electronic and vibrational properties and electron-phonon coupling

Solids are composed by mutually interacting electrons and nuclei. The total non-relativistic Hamiltonian of a system of electrons (of coordinates $\mathbf{r}_i$, momenta $\mathbf{p}_i$, and charge -e) and nuclei (of coordinates $\mathbf{R}_I$, momenta $\mathbf{P}_I$, and charge +$z_I e$) in mutual interaction via Coulomb forces and in absence of external perturbations, can be written

as:

$$\hat{H} = \sum_i \frac{\hat{\mathbf{p}}_i^2}{2m_e} + \sum_I \frac{\hat{\mathbf{P}}_I^2}{2m_I} - \sum_{iI} \frac{z_I e^2}{|\hat{\mathbf{r}}_i - \hat{\mathbf{R}}_I|} + \frac{1}{2}\sum_{i\neq j} \frac{e^2}{|\hat{\mathbf{r}}_i - \hat{\mathbf{r}}_j|} + \frac{1}{2}\sum_{I\neq J} \frac{z_I z_J e^2}{|\hat{\mathbf{R}}_I - \hat{\mathbf{R}}_J|} \quad (1.1)$$

where we will call:

$$V_{nucl}(\hat{\mathbf{r}}) \coloneqq -\sum_I \frac{z_I e^2}{|\hat{\mathbf{r}} - \hat{\mathbf{R}}_I|} \quad (1.2)$$

The solution of the Schrödinger equation for this Hamiltonian is impossible to be approached consistently from first principles because the typical number of particles in a solid is $N \sim 10^{23}$. Luckily, for most of the practical purposes one is mostly interested in physical quantities that can be computed in simplifying assumptions. The starting one is based on the large mass difference between electrons and nuclei; in common practice, this allows to decouple the fast dynamics of electrons from the slow dynamics of nuclei and think at the nuclei as moving on an adiabatic potential surface generated by electrons [69] (even though in some cases, when the energy of the nuclear motion is much larger than their coupling with electrons, this is not entirely possible [70]). It is therefore in general frequent to study first the electronic problem at fixed (clamped) nuclei and then determine the nuclear dynamics in a second step; this procedure is known as the Born-Oppenheimer approximation [71].

1.1.1 DFT for electronic properties

In crystals, DFT studies the ground state properties of a system of electrons in presence of an external potential generated by the nuclei considered as fixed in certain clamped positions R_{cl}, where with R we indicate the set of multidimensional nuclear positions. The nuclear coordinates of Eq. 1.1 become then classical parameters and we can disregard the nuclear kinetic term; such assumption is justified by the large difference between nuclear and electronic masses. Moreover, the total inter-nuclear Coulomb interaction becomes a constant and we can neglect it if we are interested in the difference of energies of the electronic states in the rigid lattice approximation. At last, we are left with an Hamiltonian depending only on the electronic set of coordinates $\{\mathbf{r}_1, \mathbf{r}_2, ..\}$ with an external potential due to the nuclei.

According to the theorems of Hohenberg-Kohn (HK) [72], for a system of interacting electrons in an external potential $V_{ext}(\mathbf{r})$, the potential $V_{ext}(\mathbf{r})$ is in a one-to-one correspondence, except for constants, with the Ground State (GS) density $n^{GS}(\mathbf{r})$. Moreover, there exists a functional for the energy, $E[n]$, that has a global minimum for $n = n^{GS}(\mathbf{r})$. The minimization is subjected to the constraint that $\int n(\mathbf{r})d\mathbf{r} = N$

where N is the total number of electrons in the system. At the end of the minimization procedure, we obtain the ground state energy $E^{GS} = E[n^{GS}(\mathbf{r})]$. The fundamental aspect of this approach is that, except for the part involving the external potential, the energy functional is universal. In fact, we can write:

$$E[n] = T_e[n] + V_{e-e}[n] + \int V_{nucl}(\mathbf{r})n(\mathbf{r})d\mathbf{r} = F[n] + \int V_{nucl}(\mathbf{r})n(\mathbf{r})d\mathbf{r} \tag{1.3}$$

where $F[n]$ is an universal functional including both the kinetic and the interaction contributions (respectively, $T_e[n]$ and $V_{e-e}[n]$). Therefore, the focus of the ground state property calculations is completely moved from the wave-function to the density, greatly reducing the number of degrees of freedom.

The implementation of the theory is not straightforward, especially because the form of the functional $F[n]$ is not known practically since the theorems only guarantee its existence. The fundamental practical calculation scheme has been introduced by Kohn and Sham [73]. The Kohn-Sham (KS) ansatz states that for each non-uniform ground-state density $n(\mathbf{r})$ of N interacting electrons there exists a non-interacting N-electron system with the same non-uniform ground-state density. Therefore, the density of the interacting system can be written as $n(\mathbf{r}) = \sum_i \phi_i^*(\mathbf{r})\phi_i(\mathbf{r})$ where $\phi_i(\mathbf{r})(i = 1, 2, ...N)$ are orthonormal orbitals to be determined consistently. The Hamiltonian of the Kohn-Sham system is:

$$\hat{H}_{KS} = T_{KS}(\hat{\mathbf{p}}) + V_{KS}(\hat{\mathbf{r}}) = \sum_i \frac{\hat{\mathbf{p}}_i^2}{2m} + V_{KS}(\hat{\mathbf{r}}) \tag{1.4}$$

where V_{KS} is an appropriate potential to be determined. The Kohn-Sham ansatz is used performing a variational minimization of the energy functional of Eq. 1.3. One of the fundamental points of this approach is that, before doing the variation, the functional of equation 1.3 is recast in the following form:

$$E[n] = T_{KS}[n] + V_H[n] + \int V_{nucl}(\mathbf{r})n(\mathbf{r})d\mathbf{r} + E_{xc}[n] \tag{1.5}$$

where $T_{KS}[n]$ is the kinetic term density functional for the non interacting system, and:

$$\begin{aligned} V_H[n] &= \frac{1}{2}\int n(\mathbf{r})\frac{e^2}{|\mathbf{r}-\mathbf{r}'|}n(\mathbf{r}')d\mathbf{r}d\mathbf{r}' \\ E_{xc}[n] &\equiv T_e[n] - T_{KS}[n] + V_{e-e}[n] - V_H[n] \end{aligned} \tag{1.6}$$

If now the variation is performed the Kohn-Sham equations are obtained:

$$H_{KS}(-\nabla_{\mathbf{r}}, \mathbf{r})\phi_i(\mathbf{r}) = \left(-\frac{\nabla^2_{\mathbf{r}}}{2m} + V_{KS}(\mathbf{r})\right)\phi_i(\mathbf{r}) =$$
$$= \left(-\frac{\nabla^2_{\mathbf{r}}}{2m} + V_{nucl}(\mathbf{r}) + V_{Coul}(\mathbf{r}) + V_{xc}(\mathbf{r})\right)\phi_i(\mathbf{r}) = \epsilon_i\phi_i(\mathbf{r}) \tag{1.7}$$

where we have the non-interacting kinetic energy term $-\frac{\nabla^2_{\mathbf{r}}}{2m}$, the external potential $V_{nucl}(\mathbf{r})$, the Hartree potential $V_{Coul}(\mathbf{r}) = \frac{\delta V_H[n(\mathbf{r})]}{\delta n(\mathbf{r})}$, and the exchange-correlation term $V_{xc}(\mathbf{r}) = \frac{\delta E_{xc}[n(\mathbf{r})]}{\delta n(\mathbf{r})}$ which contains statistical and dynamical correlations.

In principle, the KS equations describe a fictitious system that enables us to calculate the ground state charge density of our real system. The eigenvalues ϵ_i and the eigenfunctions $\phi_i(\mathbf{r})$ of Eq. 1.7 do not have in general a direct physical meaning. Nonetheless, it is common practice to use the KS equations to deduce the band energy structure of crystals and to consider the Slater determinant of the lowest N eigenfunctions of Eq. 1.7 $|\phi_1(\mathbf{r}_1)..\phi_N(\mathbf{r_N})\rangle$ as the total wave-function for the electrons. The rational behind this approach is that we can interpret the KS equations as an approximation to the quasi-particle equations coming from the many-body Green's function formalism [74]:

$$\left(-\frac{\nabla^2_{\mathbf{r}}}{2m} + V(\mathbf{r})\right)\psi_i(\mathbf{r}) + \int d\mathbf{r}'\Sigma(\mathbf{r}, \mathbf{r}'; E_i)\psi_i(\mathbf{r}') = E_i\psi_i(\mathbf{r}) \tag{1.8}$$

where V denotes a one body external potential and Σ is the non-local, energy-dependent, complex self energy that determines the Green's function via the Dyson equation. Eq. 1.8 describes the physical quasi-particle energies and wave-functions E_i and $\psi_i(\mathbf{r})$ that have a well defined meaning in many-body theory.

Therefore, the identification $\epsilon_i \rightarrow E_i$ and $\phi_i \rightarrow \psi_i$ is just an approximation and may lead to severe errors, such as the well known band-gap underestimation typical of DFT. Nonetheless, the simplicity of the KS equations makes them a fundamental tool to study the crystal band structures for weakly interacting systems within a reasonable precision.

1.1.2 DFPT for the theory of lattice vibrations

Once that we are able to describe the electronic properties of a crystal at a given set of nuclear positions R_{cl}, we can try to study the dynamics of the nuclei. As already mentioned at the beginning of this section, Eq. 1.1 governs the coupled dynamics of

electrons and nuclei. We can schematically rewrite the various terms as [69]:

$$\hat{H} = T_N(\hat{R}) + T_e(\hat{r}) + V(\hat{r}, \hat{R}) = T_N(\hat{R}) + H_e(\hat{r}, \hat{R}) \tag{1.9}$$

where we have indicated with $\hat{r}$ and $\hat{R}$ the multidimensional sets of electronic and nuclear momentum and spatial variables, and we have regrouped all the terms that depends on different sets of variables. In the previous subsection we have learnt how to solve $H_e\Psi^{GS}(r, R) = E^{GS}(R)\Psi^{GS}(r, R)$ for fixed R. As we vary R, $E^{GS}(R)$ describes the so called adiabatic ground-state potential-energy surface (PES). Our central assumption is that we can now consider the nuclei as moving on $E^{GS}(R)$ following the classical equation of motion:

$$M_I\ddot{\mathbf{R}}_I = -\frac{\partial E_0(R)}{\mathbf{R}_I} \tag{1.10}$$

This is of course an approximation because the nuclei are not strictly confined on $E^{GS}(R)$ but they couple also to the other adiabatic surfaces/sheets that are obtained from the spectrum of H_e [69]. Nonetheless, for most practical purposes this approximation is usually good. Often one is interested in the behaviour of the ground-state adiabatic surface near its absolute minimum at R_0, i.e. around the nuclear equilibrium positions. In this case we can expand the energy as a function of the nuclear displacements $\mathbf{u}_I = \mathbf{R}_I - \mathbf{R}_0$:

$$E^{GS}(R) = E^{GS}(R_0) + \frac{1}{2}\sum_{IJ}\left(\frac{\partial^2 E^{GS}(R)}{\partial\mathbf{R}_I\partial\mathbf{R}_J}\right)\mathbf{u}_I\mathbf{u}_J + o(R^3) \tag{1.11}$$

and define the inter-atomic force constant square matrix as:

$$D(\mathbf{R}_I, \mathbf{R}_J) = \frac{\partial^2 E^{GS}(R)}{\partial\mathbf{R}_I\partial\mathbf{R}_J} \tag{1.12}$$

For translational symmetry it holds that $D(\mathbf{R}_I, \mathbf{R}_J) = D(\mathbf{R}_I - \mathbf{R}_J) := D_{\alpha i,\beta j}(\mathbf{R})$ where now αi and βj are indexes that run over the Cartesian coordinates and the number of atoms in the unit cell respectively [75], and $\mathbf{R}$ is a lattice vector. We can also perform the Fourier transform of Eq. 1.12 and define the dynamical matrix:

$$\tilde{D}_{\alpha i,\beta j}(\mathbf{q}) = \sum_{\mathbf{R}} e^{i\mathbf{q}\cdot\mathbf{R}}\frac{D_{\alpha i,\beta j}(\mathbf{R})}{\sqrt{m_I m_J}} \tag{1.13}$$

where we are neglecting the time dependence of the atomic positions, following the adiabatic approximation, so that the dynamical matrix is frequency independent (this

is not always possible, see for example Ref. [76]). The phonon eigenvalues $\omega^2_{\lambda\mathbf{q}}$ and eigenvectors $\mathbf{e}^{\lambda}(\mathbf{q})$ are defined as the quantities that diagonalize the dynamical matrix:

$$\sum_{\beta j} \tilde{D}_{\alpha i,\beta j}(\mathbf{q}) e^{\lambda}_{\beta j}(\mathbf{q}) = \omega^2_{\lambda\mathbf{q}} e^{\lambda}_{\alpha i}(\mathbf{q}) \tag{1.14}$$

where λ—called the phonon branch index—can assume as many values as the number of rows/columns of the dynamical matrix. In order to practically solve Eq. 1.14 for a certain $\mathbf{q}$ we first have to know the dynamical matrix at that same wave-vector. Two main approaches are possible: the first one, known as frozen-phonon, consists in calculating the interatomic-force constant numerically on a supercell in real space and then use Eq. 1.13. The second approach is to use perturbation theory within the DFT framework in order to calculate the response of the electron system to an external perturbation directly in reciprocal space and then link it to the dynamical matrix. This approach is known as DFPT [77] and is the one used in this work.

The DFPT starting point is represented by the variation of the ground-state density (we drop the GS superscript from now on):

$$\Delta n(\mathbf{r}) = 4\mathrm{Re} \sum_{n=1}^{N/2} \phi^*_n(\mathbf{r}) \Delta\phi_n(\mathbf{r}) \tag{1.15}$$

where N is the total number of electrons in the system and spin degeneracy is assumed for sake of simplicity. The variation of the KS orbitals can be calculated from:

$$\left(H_{KS}(-\nabla_{\mathbf{r}}, \mathbf{r}) - \epsilon_n\right) |\Delta\phi_n(\mathbf{r})\rangle = -\left(\Delta V_{KS}(\mathbf{r}) - \Delta\epsilon_n\right) |\phi_n(\mathbf{r})\rangle \tag{1.16}$$

where:

$$\Delta V_{KS}(\mathbf{r}) = \Delta V_{ext} + e^2 \int \frac{\Delta n(\mathbf{r}')}{|\mathbf{r} - \mathbf{r}'|} d\mathbf{r}' + \frac{dv_{xc}(n)}{dn}|_{n=n(\mathbf{r})} \Delta n(\mathbf{r}) \tag{1.17}$$

$$\Delta\epsilon_n = \langle\psi_n(\mathbf{r})| \Delta V_{KS} |\psi_n(\mathbf{r})\rangle \tag{1.18}$$

One of the greatest advantages of Eq. 1.16 is that the variations can be done with respect to monochromatic external perturbations for any arbitrary $\mathbf{q}$ wave-vector. The dynamical matrix is then recovered using:

$$\tilde{D}_{\alpha i,\beta j}(\mathbf{q}) = \int \frac{\partial^2 V_{nucl}(\mathbf{r}, R)}{\partial u_{\alpha i}(\mathbf{q}) \partial u_{\beta j}(\mathbf{q})} n(\mathbf{r}) d\mathbf{r} + \int \frac{\partial V_{nucl}(\mathbf{r}, R)}{\partial u_{\alpha i}(\mathbf{q})} \frac{\partial n(\mathbf{r})}{\partial u_{\beta j}(\mathbf{q})} d\mathbf{r} + \frac{\partial^2 E^{ion-ion}(R)}{\partial u_{\alpha i}(\mathbf{q}) \partial u_{\beta j}(\mathbf{q})} \tag{1.19}$$

where $u_{\alpha i}(\mathbf{q})$ is a generic perturbation of the atomic positions of wave-vector $\mathbf{q}$ and $E^{ion-ion}(R)$ is the part of the ground state energy that depends only on the nuclear positions. A complete expression of this second piece can be found in Ref. [75].

1.1.3 Electron-phonon coupling using DFT and DFPT

Once that we have introduced the theoretical framework to compute the electronic properties at fixed nuclear positions and the nuclear dynamics, we now study the interaction between the electronic and vibrational systems. The approximation of neglecting the coupling between different adiabatic PESs is adequate in order to reproduce the experimental phonon frequencies, but has the major drawback of decoupling entirely the nuclear motion from the electronic excitations. This approximation is quite rough and, for example, would imply the absence of any intrinsic resistivity in the electron conduction in metals. In particular, it is the nuclear kinetic term $T_N(R)$ that induces a coupling between electrons and phonons.

We can deduce the electron-phonon coupling even with a more intuitive approach. We consider the electronic Hamiltonian of Eq. 1.7; if we move the nuclear coordinates, the potential felt by the electrons change and we can treat it perturbatively for small nuclear displacements. Indeed, at the first order in the nuclear displacements u, we can write:

$$V_{KS}(\hat{\mathbf{r}}, \hat{R}) = V_{KS}(\hat{\mathbf{r}}, \hat{R}_0) + \sum_{\kappa\alpha p} \frac{\partial V_{KS}(\hat{\mathbf{r}}, \hat{R})}{\partial \hat{u}_{\kappa\alpha p}} \Delta\hat{u}_{\kappa\alpha p} \tag{1.20}$$

where the index κ runs on the number of atoms of the unit cell, α is the Cartesian index and p is the index indicating the cell of the crystal that we are considering. Eq. 1.20 can also be rewritten in the basis of the phonon perturbation and of phonons creation and annihilation operators $\hat{a}, \hat{a}^\dagger$ using [78]:

$$\Delta\hat{u}_{\kappa\alpha p} = \left(\frac{\hbar}{N_p M_\kappa}\right)^{1/2} \sum_{\lambda\mathbf{q}} \frac{1}{\sqrt{2\omega_{\lambda\mathbf{q}}}} e^{i\mathbf{q}\cdot\mathbf{R}_p} e^{\lambda}_{\kappa\alpha}(\mathbf{q})(\hat{a}_{\lambda\mathbf{q}} + \hat{a}^\dagger_{\lambda-\mathbf{q}}) \tag{1.21}$$

where N_p is the number of real space cells included in the summation. We can now express the change of the potential in the Khon-Sham electron basis set and obtain the perturbing potential $\hat{H}_{e-ph}$ as a function of the electronic creation and annihilation

operators $\hat{c}, \hat{c}^\dagger$:

$$\hat{H}_{e-ph} = \frac{1}{\sqrt{N_p}} \sum_{\substack{\mathbf{kq} \\ mn\lambda}} g^{\lambda}_{m\mathbf{k+q},n\mathbf{k}} \hat{c}^\dagger_{m\mathbf{k+q}} \hat{c}_{n\mathbf{k}} (\hat{a}_{\lambda\mathbf{q}} + \hat{a}^\dagger_{\lambda-\mathbf{q}})$$

$$g^{\lambda}_{m\mathbf{k+q},n\mathbf{k}} = \sqrt{\frac{\hbar}{2M_0\omega_{\lambda\mathbf{q}}}} \langle u_{m\mathbf{k+q}} | \, \partial_{\lambda\mathbf{q}} v_{KS} \, | u_{n\mathbf{k}} \rangle_{uc} \tag{1.22}$$

where $v_{KS} = e^{-i\mathbf{q}\cdot\mathbf{r}} V_{KS}$, $\partial_{\nu\mathbf{q}} v_{KS}$ is the derivative of the Khon-Sham potential with respect to the $(\lambda\mathbf{q})$ phonon displacement , M_0 is a reference mass and $\langle u_{n'\mathbf{k+q}}|$ and $|u_{n\mathbf{k}}\rangle$ are the cell periodic part of the Bloch functions in Dirac's notation for a given band and quasi-momentum index and uc indicates that the scalar product has to be taken in the unit cell. The ingredients to evaluate Eq. 1.22 are obtained using Eqs. 1.7 and 1.16, which give access to the eigenfunctions and the variation of the potential.

To conclude the discussion on the EPC, we shall point out some remarks. First of all, the expansion of Eq. 1.20 at first order is enough for the purposes of calculating scattering between well defined quasi-particles without including energy renormalization effects. Renormalization effects indeed need a coherent expansion of the potential V_{KS} to the second order in u (Debye-Waller term)[79]. Secondly, Eq. 1.22 can be understood from a many-body point of view as an approximation to the Fan-Migdal self-energy where [78]:

1. the vertex corrections are neglected;
2. the fully interacting Green's function is replaced by the Khon-Sham Green's function at clamped nuclei;
3. the fully interacting phonon propagator is replaced by the adiabatic phonon propagator;
4. the screened electron-phonon vertex is evaluated using the RPA+*xc* electronic screening from a DFT calculation;
5. the phonon frequency of the EPC is neglected.

Once that we have access to the basic electronic and vibrational quantities of a crystal in equilibrium, we can wonder what happens when we apply external perturbations such as electromagnetic fields or thermal gradients. This is matter of the next sections.

1.2 Non equilibrium and Onsager relations

The macroscopic extension of thermodynamics to non equilibrium phenomena can be done in the linear regime for external fields following Ref. [80]. The assumption is that, given a set of N thermodynamic variables, their fluctuation around the equilibrium state $\{x_1, .., x_N\}$ completely determines the out of equilibrium state. In particular, we can express their time evolution as:

$$\dot{x}_i = \dot{x}_i(x_1..x_N) \tag{1.23}$$

and, if we are near enough to the equilibrium, we can expand the above relation as:

$$\dot{x}_i = -\sum_k \lambda_{ik} x_k \tag{1.24}$$

where λ_{ik} are constant coefficients. If we express Eq. 1.24 as a function of the conjugate variables $X_i = -\frac{\partial S(x_1..x_N)}{\partial x_i}$ and in the hypothesis of microscopic reversible processes, we have [1]:

$$\dot{x}_i = -\sum_k \gamma_{ik} X_k \tag{1.25}$$

$$\gamma_{ik} = \gamma_{ki} \tag{1.26}$$

where γ are known as kinetic coefficients, X as driving forces and x as flux variables. To correctly identify conjugate variables, we require that the entropy production $\dot{S} = \sum_i X_i x_i$ is unchanged for any possible set of legitimate variables.

Following the above general principles, we can study the case where non equilibrium is induced by an electrical field $\mathbf{E}$, a concentration gradient $\nabla_{\mathbf{r}}\mu$ and a temperature gradient $\nabla_{\mathbf{r}}T$; in this case the entropy production reads [81]:

$$\dot{S} = \frac{1}{T}\left\{\left(\mathbf{E} + \frac{\nabla_{\mathbf{r}}\mu}{e}\right)\cdot \mathbf{J}_e - \left(\frac{\nabla_{\mathbf{r}}T}{T}\right)\cdot \mathbf{J}_Q\right\} \tag{1.27}$$

where $\mathbf{J}_e$ and $\mathbf{J}_Q$ are the electric and heat current densities respectively. The identification of the driving forces and flux variables is immediate. Therefore, we can write

immediately:

$$\mathbf{J}_e = L_{11}\left(\mathbf{E} + \frac{\nabla_{\mathbf{r}}\mu}{\mathbf{e}}\right) + L_{12}\left(-\frac{\nabla_{\mathbf{r}}T}{T}\right) \tag{1.28}$$

$$\mathbf{J}_Q = L_{21}\left(\mathbf{E} + \frac{\nabla_{\mathbf{r}}\mu}{\mathbf{e}}\right) + L_{22}\left(-\frac{\nabla_{\mathbf{r}}T}{T}\right) \tag{1.29}$$

where L are in general tensors of dimension 3×3 (whose independent components may be reduced by symmetry arguments) and:

$$L_{11} = L_{11}^T \quad L_{22} = L_{22}^T \quad L_{12} = L_{21}^T \tag{1.30}$$

where ^{T} is the transposition symbol [82, 83]. The relations between the L tensors usually go under the name of Onager relations.

In case the microscopic reversibility is not respected, the relation between the coefficients does not hold. Anyway, in presence of a uniform magnetic field $\mathbf{B}$, the Onsager relations can be generalized to [84, 85]:

$$L_{11}(\mathbf{B}) = L_{11}^T(-\mathbf{B}) \quad L_{22}(\mathbf{B}) = L_{22}^T(-\mathbf{B}) \quad L_{12}(\mathbf{B}) = L_{21}^T(-\mathbf{B}) \tag{1.31}$$

The physical electronic transport coefficients that we will study in this work relate to the L tensors trough the following expressions, in absence of magnetic field [86, 87]:

$$\sigma = L_{11} \tag{1.32}$$

$$\kappa_e = \frac{1}{T}\left(L_{22} - L_{12}L_{11}^{-1}L_{12}\right) \tag{1.33}$$

$$S = \frac{1}{T}L_{11}^{-1}L_{12} \tag{1.34}$$

$$\Pi = L_{11}^{-1}L_{21} \tag{1.35}$$

where σ is the electrical conductivity tensor, κ_e is the electronic thermal conductivity, S is the Seebeck coefficient and Π is the Peltier coefficient. We refer to Ref. [86] for the discussion of the tensor symmetries in the Boltzmann formalism. In particular, it can be shown that the L_{12} (and therefore the Seebeck coefficient) is symmetric in absence of magnetic field, whereas it may present asymmetries in presence of a magnetic field in

a general direction [88]. When a magnetic field is present, the above relations become:

$$\sigma = L_{11}(\mathbf{B}) \tag{1.36}$$

$$\kappa_e = \frac{1}{T}\left(L_{22}(\mathbf{B}) - L_{21}(\mathbf{B})L_{11}^{-1}(\mathbf{B})L_{12}(\mathbf{B})\right) \tag{1.37}$$

$$S = \frac{1}{T}L_{11}^{-1}(\mathbf{B})L_{12}(\mathbf{B}) \tag{1.38}$$

$$\Pi = L_{11}^{-1}(\mathbf{B})L_{21}(\mathbf{B}) \tag{1.39}$$

The lattice thermal conductivity in presence of a thermal gradient is instead simply defined by

$$\mathbf{J}_Q^{latt.} = -k^{th}\nabla_{\mathbf{r}}T \tag{1.40}$$

where $\mathbf{J}_Q^{latt.}$ is the heat current density due only to lattice dynamics. In order to compute the kinetic coefficients described in this sections, we can resort to different theoretical frameworks. In this thesis, we make use of the Boltzmann formalism and of the Kubo approach, which are matter of the next sections.

1.3 Coupled Boltzmann equations

When external fields are applied to a crystal otherwise in equilibrium, the balance of its microscopic components (nuclei and electrons) changes; these components evolve dynamically according to the laws of quantum mechanics. The exact description of this dynamics is highly non-trivial; it is thus necessary to resort to a single-particle approximation where the dynamics of the system is representable by the interaction of well-defined particles (electrons and phonons in our case). This semi-classical approximation is valid under the assumptions that the particles' wave-packets width is narrow if compared to the external field variation and that such a field is of sufficiently small intensity [89] (see Chap. 2 for a much more detailed discussion). In this case, the dynamics can be described by wave-packets possessing a group velocity and subject to external forces that weakly interact amongst themselves via the Fermi golden rule. Moreover, the wave-packets' physical quantities (energy and velocity) are calculated in absence of external perturbations, enabling us to use the theory developed in section 1.1.

Within this picture, we can introduce single-particle statistical distribution functions in the space-momentum phase space (f for electrons and n for phonons— f^0 is the Fermi-Dirac distribution and n^0 is the Bose-Einstein distribution) to represent all the particles of the system. In crystals, Bloch's theorem allows us to label electronic

states with a couple of number $\{n\mathbf{k}\}$ that identify band and quasi-momentum indexes [69]. Analogously, we can label phonon states with the branch and momentum indexes $\{\lambda\mathbf{q}\}$. The particle statistical weights are thereby written as $f_{n\mathbf{k}} \coloneqq f(\epsilon_{m\mathbf{k}})$ and $n_{\lambda\mathbf{q}} \coloneqq n(\omega_{\lambda\mathbf{q}})$. Their time-space evolution is described by the coupled BTE equations, which read as:

$$\begin{cases} \frac{\partial f_{n\mathbf{k}}}{\partial t} + \mathbf{v}_{n\mathbf{k}} \cdot \nabla_{\mathbf{r}} f_{n\mathbf{k}} + \frac{\mathbf{F}}{\hbar} \cdot \nabla_{\mathbf{k}} f_{n\mathbf{k}} = \left(\frac{\partial f_{n\mathbf{k}}}{\partial t}\right)_{coll.} \\ \frac{\partial n_{\lambda\mathbf{q}}}{\partial t} + \mathbf{v}_{\lambda\mathbf{q}} \cdot \nabla_{\mathbf{r}} n_{\lambda\mathbf{q}} = \left(\frac{\partial n_{\lambda\mathbf{q}}}{\partial t}\right)_{coll.} \end{cases} \tag{1.41}$$

where $\mathbf{v}_{m\mathbf{k}}$ and $\mathbf{v}_{\lambda\mathbf{q}}$ are the semi-classical electronic and phonon group velocities, $\mathbf{F}$ is an external electrochemical-magnetic force [90], and the right hand side members represent the collisional terms that include all the possible interactions between the particle and the surrounding environment. In particular, it is the collisional term containing the mutual electron-phonon scattering interaction that couples the two equations in 1.41. The real-space dependence of the statistical functions stems from the assumption of a local thermodynamic equilibrium characterized by a temperature $T = T(\mathbf{r})$. As long as in this work we are interested in steady state conditions, equation 1.41 reduces to:

$$\begin{cases} \mathbf{v}_{n\mathbf{k}} \cdot \nabla_{\mathbf{r}} T \frac{\partial f_{n\mathbf{k}}}{\partial T} + \frac{\mathbf{F}}{\hbar} \cdot \nabla_{\mathbf{k}} f_{n\mathbf{k}} = \left(\frac{\partial f_{n\mathbf{k}}}{\partial t}\right)_{coll.} \\ \mathbf{v}_{\lambda\mathbf{q}} \cdot \nabla_{\mathbf{r}} T \frac{\partial n_{\lambda\mathbf{q}}}{\partial T} = \left(\frac{\partial n_{\lambda\mathbf{q}}}{\partial t}\right)_{coll.} \end{cases} . \tag{1.42}$$

Since the Eq. 1.42 is valid only in the assumption of small external fields, we can without losing generality expand the electronic and phonon populations around the thermal equilibrium values $f^0_{n\mathbf{k}}$ and $n^0_{\lambda\mathbf{q}}$:

$$f_{n\mathbf{k}} = f^0_{n\mathbf{k}} - \frac{\partial f^0_{n\mathbf{k}}}{\partial \epsilon_{n\mathbf{k}}} \chi_{n\mathbf{k}} \tag{1.43}$$

$$n_{\lambda\mathbf{q}} = n^0_{\lambda\mathbf{q}} - \frac{\partial n^0_{\lambda\mathbf{q}}}{\partial \omega_{\lambda\mathbf{q}}} \Psi_{\lambda\mathbf{q}} \tag{1.44}$$

where $\chi_{n\mathbf{k}}$ and $\Psi_{\lambda\mathbf{q}}$ depends linearly on all the external fields. Even with this expansion, finding an exact solution to the coupled equations1.42 is very demanding. We therefore need a systematic way to decouple the equations or retain only the leading terms stemming from the coupling. In order to do so, we first need to look at the expressions of $\left(\frac{\partial f_{n\mathbf{k}}}{\partial t}\right)_{coll.}$ and $\left(\frac{\partial n_{\lambda\mathbf{q}}}{\partial t}\right)_{coll.}$ in terms of the Electron-Phonon Coupling (EPC).

1.3.1 Decoupling of equations

For the moment we limit our attention to the part of the collisional terms that depend on the EPC. As seen in section 1.1.3, the electron phonon vertex is described by the function $g^{\lambda}_{n\mathbf{k},n'\mathbf{k}'} = \sqrt{\frac{\hbar}{2M\omega_{\lambda\mathbf{q}}}} \langle n\mathbf{k}| \partial_{\lambda\mathbf{k}-\mathbf{k}'} V |n\mathbf{k}'\rangle$. Using the Fermi golden rule the electronic collisional term reads as:

$$\left(\frac{\partial f_{n\mathbf{k}}}{\partial t}\right)^{e-ph.}_{coll.} = \frac{1}{N_{\mathbf{k}}} \sum_{n'\mathbf{k}'} \{f_{n'\mathbf{k}'} W_{n'\mathbf{k}'\to n\mathbf{k}}[1 - f_{n\mathbf{k}}] - f_{n\mathbf{k}} W_{n\mathbf{k}\to n'\mathbf{k}'}[1 - f_{n'\mathbf{k}'}]\} \quad (1.45)$$

where we define the scattering rate:

$$W_{n\mathbf{k}\to n'\mathbf{k}+\mathbf{q}} = \frac{2\pi}{\hbar} \sum_{\lambda} |g^{\lambda}_{n'\mathbf{k}+\mathbf{q},n\mathbf{k}}|^2 \{n_{\lambda\mathbf{q}} \delta(\epsilon_{n'\mathbf{k}+\mathbf{q}} - \epsilon_{n\mathbf{k}} - \hbar\omega_{\lambda\mathbf{q}}) + [n_{\lambda-\mathbf{q}} + 1]\delta(\epsilon_{n'\mathbf{k}+\mathbf{q}} - \epsilon_{n\mathbf{k}} + \hbar\omega_{\lambda\mathbf{q}})\} \quad (1.46)$$

In Eq. 1.46 we have supposed time reversal symmetry to write $\omega_{\lambda\mathbf{q}} = \omega_{\lambda-\mathbf{q}}$. The signs in Eq. 1.45 show that the processes where the final state is $\{n\mathbf{k}\}$ contributes positively to the collisional term (they tend to increase $f_{n\mathbf{k}}$ over time); vice versa, when $\{n\mathbf{k}\}$ is the initial state that scatters, the collisional term gets a negative contribution. With the same rational we can deduce the collisional term for the phonons:

$$\left(\frac{\partial n_{\lambda\mathbf{q}}}{\partial t}\right)^{e-ph.}_{coll.} = \frac{1}{N_{\mathbf{k}}} \sum_{nn'\mathbf{k}} |g^{\lambda}_{n'\mathbf{k}+\mathbf{q},n\mathbf{k}}|^2 \{[n_{\lambda\mathbf{q}} + 1] f_{n'\mathbf{k}+\mathbf{q}}[1 - f_{n\mathbf{k}}] - n_{\lambda\mathbf{q}} f_{n\mathbf{k}}[1 - f_{n'\mathbf{k}+\mathbf{q}}]\} \delta(\epsilon_{n'\mathbf{k}+\mathbf{q}} - \epsilon_{n\mathbf{k}} - \hbar\omega_{\lambda\mathbf{q}}) \quad (1.47)$$

As a check for the previous expressions, we notice that both the electron and phonon collisional terms are coherently zero if evaluated inserting the equilibrium populations $f^0_{n\mathbf{k}}$ and $n^0_{\lambda\mathbf{q}}$. This is a consequence of the detailed balance relations :

$$\begin{aligned} \{f^0_{n'\mathbf{k}+\mathbf{q}}[1 - f^0_{n\mathbf{k}}] n^0_{\lambda\mathbf{q}} - f^0_{n\mathbf{k}}[1 - f^0_{n'\mathbf{k}+\mathbf{q}}][n^0_{\lambda\mathbf{q}} + 1]\} \delta(\epsilon_{n'\mathbf{k}+\mathbf{q}} - \epsilon_{n\mathbf{k}} + \hbar\omega_{\lambda\mathbf{q}}) = 0 \\ \{f^0_{n'\mathbf{k}+\mathbf{q}}[1 - f^0_{n\mathbf{k}}][n^0_{\lambda\mathbf{q}} + 1] - f^0_{n\mathbf{k}}[1 - f^0_{n'\mathbf{k}+\mathbf{q}}] n^0_{\lambda\mathbf{q}}\} \delta(\epsilon_{n'\mathbf{k}+\mathbf{q}} - \epsilon_{n\mathbf{k}} - \hbar\omega_{\lambda\mathbf{q}}) = 0 \end{aligned} \quad (1.48)$$

and confirms that without any external field all the information on the thermodynamic is contained in $f^0_{n\mathbf{k}}$ and $n^0_{\lambda\mathbf{q}}$.

The terms of Eqs. 1.45 and 1.47 couple the electron and phonon BTE as they depend on both the out of equilibrium populations. While the effect of the EPC on the electron transport has been widely studied and has become almost a textbook topic, its

effects on phonon transport has remained largely unexplored. This is mostly because the impact of the EPC on phonon transport is important for bulk doped semiconductors only at very high doping [91] and for metals at very low temperatures [15]. In the typical treatment therefore the collisional term of Eq. 1.47 is neglected. Only recently there has been a self-consistent solution of the coupling induced by Eqs. 1.45 and 1.47 in the case of n-doped GaAs for different doping concentrations [92]. The simultaneous solutions of both equations at linear order in the perturbing fields shows that [92]: 1) the phonon thermal conductivity is unaffected by the EPC collisional term; 2) the mobility of a semiconductor, provided that scattering with impurities may be made weak, can gain a substantial contribution by mutual drag effects at high doping; 3) there is a strong enhancement of the Seebeck coefficient at low temperatures which is clearly visible also in experiments.

Given the previous considerations, in this thesis we will safely work in a regime where the collisional term of Eq. 1.47 can be safely neglected, so that the phonon transport is dominated by the anharmonic three-phonon processes. Our assumption implies that $\Psi_{\lambda\mathbf{q}}$ of Eq. 1.44 is non-zero only in presence of a thermal gradient. If we now insert the expressions of Eqs. 1.43 and 1.44 inside Eq. 1.45 and retain only the linear terms in the out of equilibrium populations, we can separate the contributions coming from the pieces containing only in equilibrium phonon or electron populations (denoted respectively with the superscript $n = n^0$ and $f = f^0$):

$$\left(\frac{\partial f_{n\mathbf{k}}}{\partial t}\right)^{e-ph.}_{coll.} = \left(\frac{\partial f_{n\mathbf{k}}}{\partial t}\right)^{n=n^0}_{coll.} + \left(\frac{\partial f_{n\mathbf{k}}}{\partial t}\right)^{f=f^0}_{coll.} \tag{1.49}$$

$$\left(\frac{\partial f_{n\mathbf{k}}}{\partial t}\right)^{n=n^0}_{coll.} = \frac{1}{k_B T}\sum_{n'\mathbf{k}'} f^0_{n'\mathbf{k}'}[1 - f^0_{n\mathbf{k}}]W^{n=n^0}_{n'\mathbf{k}'\to n\mathbf{k}}\left[\chi_{n'\mathbf{k}'} - \chi_{n\mathbf{k}}\right] \tag{1.50}$$

$$\left(\frac{\partial f_{n\mathbf{k}}}{\partial t}\right)^{f=f^0}_{coll.} = -\frac{2\pi}{\hbar}\sum_{\lambda} |g^{\lambda}_{n\mathbf{k},n'\mathbf{k}+\mathbf{q}}|^2\{\frac{\partial n^0_{\lambda\mathbf{q}}}{\partial \omega_{\lambda\mathbf{q}}}\Psi_{\lambda\mathbf{q}}\delta(\epsilon_{n'\mathbf{k}+\mathbf{q}} - \epsilon_{n\mathbf{k}} - \hbar\omega_{\lambda\mathbf{q}}) +$$
$$\frac{\partial n^0_{\lambda\mathbf{q}}}{\partial \omega_{\lambda\mathbf{q}}}\Psi_{\lambda-\mathbf{q}}\delta(\epsilon_{n'\mathbf{k}+\mathbf{q}} - \epsilon_{n\mathbf{k}} + \hbar\omega_{\lambda\mathbf{q}})\} \times [f^0_{n'\mathbf{k}'} - f^0_{n\mathbf{k}}] \tag{1.51}$$

In the term 1.50 the scattering rate is evaluated using the equilibrium phonon population; therefore its value is independent from the presence of a thermal gradient. On the contrary, the term 1.51—the so called phonon-drag—arises only when the phonon populations are brought out of equilibrium. In our approximation, this drag term is non zero only in presence of a thermal gradient. The term 1.51 is of particular importance at low temperatures to determine the Seebeck coefficient for materials that have a very high thermal lattice conductivity, such as diamond.

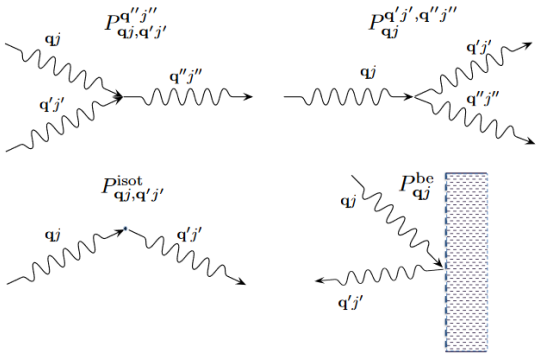

Figure 1.1: Scattering processes that enters the phonon BTE of Eq. 1.53. Reprinted from Ref. [25].

1.4 BTE for phonons

As discussed in the previous section, in this work we consider the BTE for phonons in steady state disregarding the EPC contribution to the collisional term. We start rewriting Eq. 1.44 supposing—without losing generality for the aims of this thesis—that the thermal gradient is along the $\hat{x}$ direction, in the following form:

$$n_{\lambda\mathbf{q}} = n^0_{\lambda\mathbf{q}} + \frac{n^0_{\lambda\mathbf{q}}(n^0_{\lambda\mathbf{q}}+1)}{k_B T^2}\frac{\partial T}{\partial x}\tilde{f}_{\lambda\mathbf{q}}. \tag{1.52}$$

where we have made the dependence on the external field explicit. In terms of $\tilde{f}$ the phonon BTE is written as:

$$\sum_{\lambda'\mathbf{q}',\lambda''\mathbf{q}''}\left[P^{\lambda''\mathbf{q}''}_{\lambda\mathbf{q},\lambda'\mathbf{q}'}(\tilde{f}_{\lambda\mathbf{q}}+\tilde{f}_{\lambda'\mathbf{q}'}-\tilde{f}_{\lambda''\mathbf{q}''})+\frac{1}{2}P^{\lambda'\mathbf{q}',\lambda''\mathbf{q}''}_{\lambda\mathbf{q}}(\tilde{f}_{\lambda\mathbf{q}}-\tilde{f}_{\lambda'\mathbf{q}'}-\tilde{f}_{\lambda''\mathbf{q}''})\right]+$$
$$\sum_{\lambda'\mathbf{q}'}P^{isot}_{\lambda\mathbf{q},\lambda'\mathbf{q}'}(\tilde{f}_{\lambda\mathbf{q}}-\tilde{f}_{\lambda'\mathbf{q}'})+P^{be}_{\lambda\mathbf{q}}\tilde{f}_{\lambda\mathbf{q}} = -\mathbf{v}_{\lambda\mathbf{q}}\frac{\partial n^0_{\lambda\mathbf{q}}}{\partial T} \tag{1.53}$$

where the P-matrices represent the scattering rate for phonon due to anharmonic phonon-phonon scattering, isotope scattering ($isot$) and boundary-elastic (be) scattering [25]. The graphical description of the scatterings is given in Fig. 1.1.

P^{isot} and P^{be} are usually described by models, while the anharmonic processes can be evaluated *ab initio*. In particular,

$$P^{\lambda''\mathbf{q}''}_{\lambda\mathbf{q},\lambda'\mathbf{q}'} = \frac{2\pi}{N\hbar^2}\sum_{\mathbf{G}}|V^{(3)}(\lambda\mathbf{q},\lambda'\mathbf{q}',\lambda''-\mathbf{q}'')|^2 n^0_{\lambda\mathbf{q}}n^0_{\lambda'\mathbf{q}'}(n^0_{\lambda''\mathbf{q}''}+1)\times \\ \delta_{\mathbf{q}+\mathbf{q}'-\mathbf{q}'',\mathbf{G}}\delta(\hbar\omega_{\lambda\mathbf{q}}+\hbar\omega_{\lambda'\mathbf{q}'}-\hbar\omega_{\lambda''\mathbf{q}''}) \tag{1.54}$$

$$P^{\lambda'\mathbf{q}',\lambda''\mathbf{q}''}_{\lambda\mathbf{q}} = \frac{2\pi}{N\hbar^2}\sum_{\mathbf{G}}|V^{(3)}(\lambda\mathbf{q},\lambda'-\mathbf{q}',\lambda''-\mathbf{q}'')|^2 n^0_{\lambda\mathbf{q}}(n^0_{\lambda'\mathbf{q}'}+1)(n^0_{\lambda''\mathbf{q}''}+1)\times \\ \delta_{\mathbf{q}-\mathbf{q}'-\mathbf{q}'',\mathbf{G}}\delta(\hbar\omega_{\lambda\mathbf{q}}-\hbar\omega_{\lambda'\mathbf{q}'}-\hbar\omega_{\lambda''\mathbf{q}''}) \tag{1.55}$$

where N is the number of vectors that enter the sum, $\mathbf{G}$ are reciprocal lattice vectors and $V^{(3)}$ is the Fourier transform of the third order derivative of the energy with respect to the atomic displacements. The $\mathbf{G}$ vectors different from 0 are the origin of the *U*-processes that contribute to a non-zero thermal conductivity (while *N*-processes do not contribute [15]). $V^{(3)}$ can be calculated directly in real space, as done in Refs. [93, 94] for $\mathbf{q}\neq 0$, or in reciprocal space, following the recipe of Ref. [27] within the DFT formalism. Such calculations can be done on relatively coarse grids with respect to the grids needed to solve the BTE. Therefore, usually $V^{(3)}$ is Fourier interpolated on fine grids.

Eq. 1.53 is in the form of a linear system where the unknown is the phonon out of equilibrium population. Incidentally, we notice that the populations change sign under the transformation $\mathbf{q}\rightarrow-\mathbf{q}$; this means that the mean number of phonons is conserved when the crystal is in slightly out of equilibrium conditions and therefore there is no increment in the internal energy $u(T)$ over time due to heat accumulation. A variational approach, derived from consideration over the entropy production [15], may be used to calculate the lattice thermal conductivity k^{th}. Otherwise, the expression of k^{th} as a function of $\tilde{f}$ is:

$$k^{th} = -\frac{\hbar}{N_k\Omega k_B T^2}\sum_{\lambda\mathbf{q}} v_{\lambda\mathbf{q}}\omega_{\lambda\mathbf{q}}n^0_{\lambda\mathbf{q}}(n^0_{\lambda\mathbf{q}}+1)\tilde{f}_{\lambda\mathbf{q}} \tag{1.56}$$

where Ω is the volume of the primitive crystal cell. An useful approximation to describe the out of equilibrium populations is the Single Mode Approximation (SMA), in which only the off-diagonal entries of the collisional matrix are put to 0. The validity of this approximation depends on the material and on the dimensionality of the system[95], and should always be investigated carefully.

1.5 BTE for electrons

As already seen in Sec. 1.3, the electron BTE intrinsic collisional term can be written by considering the scattering with equilibrium vibrations via Eq. 1.50 and the drag exercised by out of equilibrium phonons via Eq. 1.51. The ingredients to calculate these terms can be computed via *ab initio* techniques. The extrinsic collisional terms, such as scattering with impurities, are usually are treated via simplified models—see Sec. 1.5.1.

The electron BTE can be rewritten formally as a linear system where the unknown is the out of equilibrium population χ; we define:

$$\Pi^0_{n'\mathbf{k}',n\mathbf{k}} := f^0_{n'\mathbf{k}'}(1-f^0_{n\mathbf{k}})\left[W^{n=n^0}_{n'\mathbf{k}'\to n\mathbf{k}} + W^{imp.}_{n'\mathbf{k}'\to n\mathbf{k}}\right] \tag{1.57}$$

where $W^{imp.}$ includes the scattering of electrons from impurities. Then we can write the BTE in a form $\mathbf{b} = A\mathbf{x}$ where:

$$\begin{aligned}
&\mathbf{x} = \chi_{n\mathbf{k}} \\
&\mathbf{b} = -\frac{\partial f^0_{n\mathbf{k}}}{\partial \epsilon_{n\mathbf{k}}}\mathbf{v}_{n\mathbf{k}} \cdot \left[e\mathbf{E} + \frac{\nabla_{\mathbf{r}} T}{T}(\epsilon_{n\mathbf{k}} - \mu)\right] - \left(\frac{\partial f_{n\mathbf{k}}}{\partial t}\right)^{f=f^0}_{coll.} + \\
&+ \frac{e}{\hbar}\frac{\partial f^0_{n\mathbf{k}}}{\partial \epsilon_{n\mathbf{k}}}(\mathbf{v}_{n\mathbf{k}} \wedge \mathbf{B}) \cdot \nabla_{\mathbf{k}} \chi_{n\mathbf{k}} \\
&A_{n'\mathbf{k}',n\mathbf{k}} = \frac{1}{N_k k_B T}\left[\Pi^0_{n'\mathbf{k}',n\mathbf{k}} - \delta_{n'\mathbf{k}',n\mathbf{k}} \sum_{n''\mathbf{k}''} \Pi^0_{n''\mathbf{k}'',n\mathbf{k}}\right]
\end{aligned} \tag{1.58}$$

where $\mathbf{E}$ and $\mathbf{B}$ are the external electro-magnetic fields and μ is the electronic chemical potential. In absence of magnetic field the $\mathbf{b}$ term is completely determined by equilibrium electronic quantities and out of equilibrium phonon populations; on the contrary, in presence of a magnetic field, it depends on the derivative of the solution. Therefore, the electronic BTE becomes an integro-differential equation. When $\mathbf{B} = 0$ the BTE can be solved exactly and efficiently using a Conjugate Gradient (CG) algorithm since A is a semi-definite positive matrix [15]. Care has to be taken to avoid overlap between the solution and the kernel of A, which is represented by the vectorial space spanned by $\mathbf{x}_{Ker} = (1, 1, .., 1)$; physically, we have to restrict to all the vectors orthogonal to $\mathbf{x}_{Ker}$ because they have the properties that $\sum_{n\mathbf{k}} \chi_{n\mathbf{k}} = 0$, which means that the total number of electrons is conserved. When $\mathbf{B} \neq 0$, at first sight we could try to include the magnetic term inside the collisional term; in this case, we would end up with a *not* definite positive matrix [15] and therefore the conjugate gradient method would be unsuitable. Hence, the strategy used here will be to solve the BTE iteratively:

at the i-th iteration the magnetic term is calculated from the output population of the $i-1$-th iteration and then included in $\mathbf{b}$; then the equation is solved by means of the CG scheme and the output of the i-th iteration is produced. The procedure is iterated until convergence. We can thus reduce the complex problem of an integro-differential BTE to the collection of linear systems solvable by the CG method; the number of such linear systems is equal to the number of iterations N_{it} needed to converge the solution—i.e. to obtain a population that changes less than a predetermined threshold between two consecutive iterations. Different iterative schemes based on the mixing of the input and the output of the N-th iteration can be used when convergence is hard to achieve. Another possible approach is to replace the CG scheme with an iterative procedure, which is less efficient but easier to implement [21].

In particular cases, the electron BTE can be solved using simplifying expressions for the collisional term. Two of the most known are the Energy Relaxation Time Approximation (ERTA)—also known as Self Energy Relaxation Time Approximation (SERTA)—and the Momentum Relaxation Time Approximation (MRTA). For A these approximations read as:

$$A^{SERTA}_{m\mathbf{k},m'\mathbf{k}'} = -\frac{1}{k_B T N_{\mathbf{k}}} \sum_{m'',\mathbf{k}''} \delta_{m'\mathbf{k}',m\mathbf{k}} \Pi^0_{m\mathbf{k},m''\mathbf{k}''} \tag{1.59}$$

$$A^{MRTA}_{m\mathbf{k},m'\mathbf{k}'} = -\frac{1}{k_B T N_{\mathbf{k}}} \sum_{m'',\mathbf{k}''} \delta_{m'\mathbf{k}',m\mathbf{k}} \Pi^0_{m\mathbf{k},m''\mathbf{k}''} \frac{\mathbf{v}_{m\mathbf{k}} \cdot \mathbf{v}_{m''\mathbf{k}''}}{|\mathbf{v}_{m\mathbf{k}}||\mathbf{v}_{m''\mathbf{k}''}|}. \tag{1.60}$$

The SERTA approximations takes in account only the diagonal components of the A matrix, that represent the rate at which a certain electronic state $\{n\mathbf{k}\}$ is depopulating due to scattering; we thus neglect the scatterings that have $\{n\mathbf{k}\}$ as final asymptotic product. Physically, this rate is coincident with the quasi-particle inverse lifetime. This approximation can never be exact, but it is very efficient when any diagonal element of A is much larger than any single out diagonal element. The MRTA approximation instead is exact for a system where the band structure is isotropic and the scattering is purely elastic [15]. Therefore, we expect it to be especially good for materials with spherical or circular Fermi surfaces when the scattering with low energy acoustic phonon may be considered elastic (at intermediate-low temperatures) or when the elastic impurity scattering is dominant (high doping regime).

1.5.1 Scattering with doping impurities

Elastic interaction between electrons and ionized or neutral impurities (by means of the medium-shielded Coulomb potential) is a scattering channel which can dominate the

value of the electronic transport properties at high doping. In 3 dimensional materials, ionized scattering is dealt with the Brooks and Herring formula [96]:

$$W^{ion}_{m\mathbf{k},m'\mathbf{k}+\mathbf{q}} = \frac{2\pi Z^2 n_I e^4}{\hbar\Omega_{BZ}(\epsilon_r\epsilon_0)^2}\frac{1}{(\beta_s^2+\mathbf{q}^2)^2} \tag{1.61}$$

where Ze is the charge of the impurity, n_I the impurity density, Ω_{BZ} is the BZ volume, ϵ_r and ϵ_0 are the relative and vacuum permittivity. β_s is the reciprocal of the Debye screening length given as:

$$\beta_s = \sqrt{\frac{e^2 n_I}{\epsilon_r\epsilon_0 k_B T}}. \tag{1.62}$$

For 3 dimensional zincblend materials neutral scattering can be added, as in Ref. [97], as a lifetime, i.e. as a diagonal element to the total scattering amplitude:

$$W^{neu}_{m\mathbf{k},m\mathbf{k}} = A(w)\frac{\hbar^3 n_n \epsilon_r\epsilon_0}{m^2_{h,dos}e^2} \tag{1.63}$$

$$\begin{aligned} A(w) = &\frac{35.2}{w^{1/2}}\frac{(1+e^{-50w})(1+80.6w+23.7w^2)}{1+41.3w+133w^2} \\ &\times\left[\frac{1}{w}ln(1+w) - \frac{1+0.5w-0.17w^2}{(1+w)^3}\right] \end{aligned} \tag{1.64}$$

where $w = \frac{\epsilon_{m\mathbf{k}}-\epsilon_{vtb}}{E_a}$, ϵ_{vtb} is the highest valence band electronic energy, E_a is the dopant activation energy, n_n the neutral impurity concentration and $m_{h,dos}$ is the doss effective mass for the top valence band. The total impurity scattering is therefore $W^{imp.} = W^{ion} + W^{neu}$.

1.5.2 Transport coefficients

We conclude the section giving the expression of the transport coefficients for the BTE formalism. We first notice that Eq. 1.58 can be solved turning on $\mathbf{E}$ and $\nabla_{\mathbf{r}}T$ one at a time, obtaining $\chi^{\mathbf{E}}_{n\mathbf{k}}$ and $\chi^{\nabla_{\mathbf{r}}T}_{n\mathbf{k}}$. The total solution is then $\chi_{n\mathbf{k}} = \chi^{\mathbf{E}}_{n\mathbf{k}} + \chi^{\nabla_{\mathbf{r}}T}_{n\mathbf{k}}$. Moreover, we can solve Eq. 1.58 independently for all the three Cartesian orientations of the electric field/thermal gradient. We can thus introduce a vector $\chi^{\alpha}_{n\mathbf{k}}$, where α is a Cartesian index, such that $\chi^{\alpha}_{n\mathbf{k}} = \chi^{\mathbf{E}_\alpha}_{n\mathbf{k}} + \chi^{\nabla_\alpha T}_{n\mathbf{k}}$. The solution of the BTE for a generic $\{\mathbf{E}, \nabla_{\mathbf{r}}T\}$ is then obtained as $\chi^{\{\mathbf{E},\nabla_{\mathbf{r}}T\}}_{n\mathbf{k}} = \sum_\alpha E_\alpha \chi^{\mathbf{E}_\alpha}_{n\mathbf{k}} + \nabla_\alpha T \chi^{\nabla_\alpha T}_{n\mathbf{k}}$.

For a generic electric field and in presence of an additional magnetic field, we can write the electronic and heat current densities as:

$$\mathbf{J}_e = \frac{2e}{\Omega N_k} \sum_{n\mathbf{k}} \mathbf{v}_{n\mathbf{k}} \frac{\partial f^0_{n\mathbf{k}}}{\partial \epsilon_{n\mathbf{k}}} \chi^{\{\mathbf{E},\nabla_\mathbf{r} T\}}_{n\mathbf{k}}(\mathbf{B}) \tag{1.65}$$

$$\mathbf{J}_Q = -\frac{2}{\Omega N_k} \sum_{n\mathbf{k}} \mathbf{v}_{n\mathbf{k}} (\epsilon_{n\mathbf{k}} - \mu) \frac{\partial f^0_{n\mathbf{k}}}{\partial \epsilon_{n\mathbf{k}}} \chi^{\{\mathbf{E},\nabla_\mathbf{r} T\}}_{n\mathbf{k}}(\mathbf{B}) \tag{1.66}$$

$\mathbf{J}_Q$ can be interpreted as the heat exchanged by the particles with a reservoir at a chemical potential μ. In order to obtain the values of the kinetic coefficients, it is convenient to rewrite:

$$\chi^\alpha_{n\mathbf{k}} = -v^\alpha_{n\mathbf{k}} \left[eE_\alpha \tau^e_{n\mathbf{k}}(\mathbf{B}) + \frac{\nabla_\alpha T}{T} (\epsilon_{n\mathbf{k}} - \mu) \tau^t_{n\mathbf{k}}(\mathbf{B}) \right] \tag{1.67}$$

where $\tau^e_{n\mathbf{k}}$ and $\tau^t_{n\mathbf{k}}$ are determined from $\chi^{\mathbf{E}}_{n\mathbf{k}}$ and $\chi^{\nabla_\mathbf{r} T}_{n\mathbf{k}}$ and are independent of field orientation. Therefore the expressions for the currents become:

$$J^\alpha_e = -\frac{2e}{\Omega N_k} \sum_{n\mathbf{k}\beta} v^\alpha_{n\mathbf{k}} v^\beta_{n\mathbf{k}} \frac{\partial f^0_{n\mathbf{k}}}{\partial \epsilon_{n\mathbf{k}}} \left[eE_\beta \tau^e_{n\mathbf{k}}(\mathbf{B}) + \frac{\nabla_\beta T}{T} (\epsilon_{n\mathbf{k}} - \mu) \tau^t_{n\mathbf{k}}(\mathbf{B}) \right] \tag{1.68}$$

$$J^\alpha_Q = \frac{2}{\Omega N_k} \sum_{n\mathbf{k}\beta} v^\alpha_{n\mathbf{k}} v^\beta_{n\mathbf{k}} (\epsilon_{n\mathbf{k}} - \mu) \frac{\partial f^0_{n\mathbf{k}}}{\partial \epsilon_{n\mathbf{k}}} \left[eE_\beta \tau^e_{n\mathbf{k}}(\mathbf{B}) + \frac{\nabla_\beta T}{T} (\epsilon_{n\mathbf{k}} - \mu) \tau^t_{n\mathbf{k}}(\mathbf{B}) \right] \tag{1.69}$$

so that now we can identify the expression for the kinetic coefficients:

$$L_{11\alpha\beta} = -\frac{2e^2}{\Omega N_k} \sum_{n} v^\alpha_{n\mathbf{k}} v^\beta_{n\mathbf{k}} \frac{\partial f^0_{n\mathbf{k}}}{\partial \epsilon_{n\mathbf{k}}} \tau^e_{n\mathbf{k}}(\mathbf{B}) \tag{1.70}$$

$$L_{12\alpha\beta} = \frac{2e}{\Omega N_k} \sum_{n} v^\alpha_{n\mathbf{k}} v^\beta_{n\mathbf{k}} \frac{\partial f^0_{n\mathbf{k}}}{\partial \epsilon_{n\mathbf{k}}} (\epsilon_{n\mathbf{k}} - \mu) \tau^t_{n\mathbf{k}}(\mathbf{B}) \tag{1.71}$$

$$L_{21\alpha\beta} = \frac{2e}{\Omega N_k} \sum_{n} v^\alpha_{n\mathbf{k}} v^\beta_{n\mathbf{k}} \frac{\partial f^0_{n\mathbf{k}}}{\partial \epsilon_{n\mathbf{k}}} (\epsilon_{n\mathbf{k}} - \mu) \tau^e_{n\mathbf{k}}(\mathbf{B}) \tag{1.72}$$

$$L_{22\alpha\beta} = -\frac{2}{\Omega N_k} \sum_{n} v^\alpha_{n\mathbf{k}} v^\beta_{n\mathbf{k}} \frac{\partial f^0_{n\mathbf{k}}}{\partial \epsilon_{n\mathbf{k}}} (\epsilon_{n\mathbf{k}} - \mu)^2 \tau^t_{n\mathbf{k}}(\mathbf{B}) \tag{1.73}$$

where the Onsager relations discussed in Sec. 1.2 must be respected.

1.6 Wannier interpolation of electronic properties

The electronic transport properties depend relevantly on a well defined region of states in the BZ with energies near the Fermi level E_F. It is usually found that the electron-phonon coupling induces out of equilibrium populations that vary on the meV scale. This means that the set of the states that contribute significantly to transport includes only electronic energies distant some meV from E_F (or from the band extrema if E_F falls in the gap); at the same time this small energy window has to be sampled very accurately in order to describe the variation of the momentum resolved transport quantities. Therefore, the solution of the electronic BTE has to be performed on very dense homogeneous electronic $\mathbf{k}$ and phonon $\mathbf{q}$-point grids; the main bottleneck of the calculation is here represented by the *ab initio* calculation of the EPC elements. It turns out that it is practically impossible to calculate directly all the scattering rates on the needed grids. Therefore, an accurate and sufficiently fast interpolation method for the EPC needs to be introduced. This method relies on the use of Wannier functions, which are defined as the Fourier transform of the Bloch functions $|n\mathbf{k}\rangle$ of the crystal:

$$|n\mathbf{R}\rangle = \frac{\Omega}{(2\pi)^3} \sum_{\mathbf{k}} e^{-i\mathbf{k}\cdot\mathbf{R}} \sum_{m=i_i}^{i_f} U_{mn}(\mathbf{k}) \, |m\mathbf{k}\rangle \tag{1.74}$$

where $\mathbf{R}$ is a real-space lattice vector and $U_{mn}(\mathbf{k})$ is a unitary gauge matrix mixing $i_f - i_i + 1$ Bloch functions at the same wave-vector, with smoothness properties as a function of $\mathbf{k}$. The U matrices can be chosen in a way such that the Wannier function basis set is the most localized possible in real space [29]. The procedure consists in finding the U matrices that minimize the spread functional $\mathbf{\Omega}$ defined as:

$$\mathbf{\Omega} = \sum_{\nu} \langle \nu\mathbf{0}| \, r^2 \, |\nu\mathbf{0}\rangle - [\langle \nu\mathbf{0}| \, \mathbf{r} \, |\nu\mathbf{0}\rangle]^2 \tag{1.75}$$

The resulting Wannier functions are known as Maximally Localized Wannier Functions (MLWF). The relevance of the procedure lies on the fact that components of a generic localized operator between different MLWFs have the least possible overlap; therefore, we have control over the basis set truncation to represent short range operators. As an example, the electronic energies may be written as:

$$\epsilon_{n\mathbf{k}} = \sum_{\nu\nu' p} e^{-i\mathbf{k}\cdot\mathbf{R}_p} U_{n\nu'}(\mathbf{k}) \, \langle \nu'\mathbf{0}| \, H_{KS} \, |\nu\mathbf{R}_e\rangle \, U^{\dagger}_{\nu n}(\mathbf{k}) \tag{1.76}$$

where the relation is exact on the $\mathbf{k}$ grid of points where H_{KS} has been resolved. Otherwise, we can interpret Eq. 1.76 as a way to interpolate $\epsilon_{n\mathbf{k}}$ on an arbitrary point in the BZ, if $\langle \nu' \mathbf{0}| H_{KS} |\nu \mathbf{R}_p\rangle$ is small enough for large $\mathbf{R}_p$; in order to use Eq. 1.76 we would need the matrices U at any arbitrary point. A practical calculation scheme is obtained considering the Wannier transform of the Hamiltonian operator:

$$\tilde{H}^{KS} = \sum_{p} e^{-i\mathbf{k}\cdot\mathbf{R}_p} \langle \nu' \mathbf{0}| H_{KS} |\nu \mathbf{R}_p\rangle \tag{1.77}$$

Diagonalizing $\tilde{H}^{KS}$ we find the interpolated electronic energies and the U matrices, which may be now used to interpolate one electron operators in the same spirit of Eq. 1.76. To sum up the procedure, one calculates the matrix elements of a certain spatially localized operator on the Bloch basis set, on a relatively coarse grid; then, one switches to the MLWFs representation; finally, one back interpolates into the $\mathbf{k}$-space on arbitrary points. The interpolation is good when the decay of the operators in the Wannier basis set is fast. This interpolation method has be applied successfully to electronic properties such as the velocities and Berry curvature [31, 98].

We have now a method to interpolate the electronic quantities entering in the electronic BTE. As regards the phonon properties, the Wannier interpolation reduces to the standard Fourier interpolation:

$$\omega^2_{\lambda\mathbf{q}} = \sum_{\substack{\alpha i \beta j \\ p'}} e^{-i\mathbf{q}\cdot\mathbf{R}_{p'}} e^{\lambda}_{\alpha i}(\mathbf{q})^{\dagger} \langle \alpha i \mathbf{0}| D |\beta j \mathbf{R}_{p'}\rangle e^{\lambda}_{\beta j}(\mathbf{q}) \tag{1.78}$$

where with the notation $\langle \alpha i \mathbf{0}|$ we indicate the displacement of the i-th atom along the α-th crystal coordinate in the primitive cell located at $\mathbf{R}_{p'} = \mathbf{0}$ (same for $|\beta j \mathbf{R}_{p'}\rangle$).

Now, the only quantity left to be interpolated is the EPC matrix element. In that case we can apply both the procedures for electronic and phonon interpolation to write:

$$\begin{aligned} g^{\lambda}_{n'\mathbf{k}+\mathbf{q},n\mathbf{k}} = & \sum_{\substack{\nu\nu' p \\ \alpha i p'}} e^{-i\left(\mathbf{k}\cdot\mathbf{R}_p + \mathbf{q}\cdot\mathbf{R}_{p'}\right)} \times \\ & \times U_{n'\nu'}(\mathbf{k}+\mathbf{q}) \langle \nu' \mathbf{0}| \frac{\partial V_{KS}}{\partial u_{\alpha i p}} |\nu \mathbf{R}_{p'}\rangle U^{\dagger}_{\nu m}(\mathbf{k}) e^{\lambda}_{\alpha i}(\mathbf{q}) \left(\frac{\hbar}{2M_i\omega_{\lambda\mathbf{q}}}\right)^{1/2} \end{aligned} \tag{1.79}$$

Eq. 1.79 is an efficient way to interpolate the EPC when $\langle \nu' \mathbf{0}| \partial_{\alpha i p} V_{KS} |\nu \mathbf{R}_{p'}\rangle$ is analytical and short ranged; in insulators and semiconductors, one has to single out possible non analytical terms due to dipolar and quadrupolar contributions that originates from singularities of the dielectric function [99, 100, 101, 22].

A successful software infrastructure that study the Wannier interpolation is implemented in WANNIER90 as described in Refs. [32, 33]. The Wannier interpolation method for the EPC has been implemented for the first time in EPW as described in Refs. [30, 34]. Such infrastructures, in conjunction with first-principle codes that give access to the electronic and vibrational properties of materials, are fundamental in order to calculate the physical quantities on very fine grids and converge the transport properties accurately.

1.7 Kubo-Greenwood formula

As discussed in the introduction to this thesis, the use of the Boltzmann formalism is not always justified. When the components of a system do not behave as quasi-classical particles with well defined dispersion relations and sufficiently long lifetimes, we have to resort to a more general formalism that correlates the response of a system to external perturbations to in equilibrium properties. Such properties need now to be expressed as averages over the whole system rather than on a defined subset of it.

One of the most important results regarding systems described by statistical mechanics is the relation between the thermal fluctuations and the response to external perturbations. This argument dates back to Einstein relations, even though the complete formal description of the connections is due to two seminal papers of Kubo [58, 59].

In general, we consider a time-independent Hamiltonian $\hat{H}$ subjected to a time-dependent perturbation $F(t)$ which couples to some observable $\hat{B}$ of the system [102]. We define:

$$\hat{H}_F(t) = \hat{H} + F(t)\hat{B} \tag{1.80}$$

as the total Hamiltonian of the system. We suppose that for $t \leq t_0$ the external perturbation is absent and that the system is in thermal equilibrium with a reservoir. In the Schrödinger picture, the time evolution operator between t_0 and a generic time t, at first order in the external perturbation, is:

$$\hat{U}(t, t_0) = e^{-\frac{i}{\hbar}\hat{H}(t-t_0)} \left[\hat{1} - \frac{i}{\hbar}\int_{t_0}^{t} \hat{B}(t' - t_0)F(t')dt'\right] \tag{1.81}$$

Now we would like to understand how the average values of a system observable change with time; in particular we consider an operator $\hat{A}$ with thermal equilibrium average $\langle\hat{A}\rangle_0$ at t_0 and we want to evaluate its average at a generic time $\langle\hat{A}\rangle_F(t)$. We

can write:

$$\langle \hat{A} \rangle_0 = \sum_N P_N \langle N | \hat{A} | N \rangle \tag{1.82}$$

where $|N\rangle$ is a set of eigenstates of the time-independent Hamiltonian $\hat{H}$ and P_N is the Boltzmann weight $P_n = \frac{e^{-\beta E_N}}{Z}$ where Z is the partition function, E_N are the eigenenergies of the eigenstates $|N\rangle$ and $\beta = \frac{1}{k_B T}$. We can now define the expectation value at later times as [102]:

$$\langle \hat{A} \rangle_F(t) = \sum_N P_N \langle N(t) | \hat{A} | N(t) \rangle \tag{1.83}$$

where the states are evolved in time with the time operator of Eq. 1.81. Using the previous results one can write:

$$\langle \hat{A} \rangle_F(t) - \langle \hat{A} \rangle_0 = -\frac{i}{\hbar} \int_{t_0}^{t} \langle [\hat{A}(t-t'), \hat{B}] \rangle_0 F(t') dt' \tag{1.84}$$

where $[,]$ is the commutator operator and we have used the time independence of the unperturbed Hamiltonian to write the time dependence with the variable $t - t' > 0$; we can let $t_0 \to -\infty$ without losing generality. The same result can be obtained studying the time evolution of the density matrix operator $\hat{\rho}$ that determines the probabilities P_N and defining the variation of the expectation value as $\mathrm{Tr}\,[(\hat{\rho}_F(t) - \hat{\rho}_0)A]$[58] where Tr is the trace operation. The importance of Eq. 1.84 is evident: the out of equilibrium response of the operator $\hat{A}$ is governed by an expectation value performed on the equilibrium distribution.

From Eq. 1.84 we can define the retarded adiabatic response function of the system as:

$$\chi_{AB}(t - t') = -\frac{i}{\hbar} \theta(t - t') \langle [\hat{A}(t - t'), B] \rangle_0 \tag{1.85}$$

where $\theta(t)$ is the Heaviside step functions—the difference between adiabatic and isothermal responses is presented in App. B. In usual calculations, one is interested in the response of a system to periodic perturbations of the form:

$$F(t) = F_\omega e^{-i(\omega + i\eta)t} + c.c. \tag{1.86}$$

where $c.c.$ means complex conjugate. In order for the system to have a thermal equilibrium at $t_0 = -\infty$, we have introduced a small η in Eq. 1.86 to switch on the perturbation adiabatically; we can take the limit $\eta \to 0$ at the end on the calculation.

Inserting Eq. 1.86 inside Eq. 1.84 we obtain:

$$\langle \hat{A} \rangle(\omega) \coloneqq \langle \hat{A} \rangle_F(\omega) - \langle \hat{A} \rangle_0 = \chi_{AB}(\omega) F_\omega \tag{1.87}$$

$$\chi_{AB}(\omega) = -\frac{i}{\hbar} \lim_{\eta \to 0} \int_0^\infty \langle [\hat{A}(\tau), \hat{B}] \rangle_0 e^{-i(\omega + i\eta)\tau} d\tau \tag{1.88}$$

where χ_{AB} and F are contracted on all the indexes that are not the frequency. To our aims, we are interested in the response of a system to an external electromagnetic field. In this case, we can consider the following Hamiltonian of N electrons in mutual interaction:

$$\hat{H}_{\mathbf{A}}(t) = \frac{1}{2m_e} \sum_i \left(\hat{\mathbf{p}}_i + \frac{e}{c} \mathbf{A}(\hat{\mathbf{r}}_i, t) \right)^2 + U(\hat{\mathbf{r}}_1, .., \hat{\mathbf{r}}_N) \tag{1.89}$$

where $\mathbf{A}$ is the vector potential in the Weyl gauge. Linearising the Hamiltonian with respect to the vector potential we obtain:

$$\hat{H}_{\mathbf{A}} = \hat{H} + \frac{e}{c} \int \hat{\mathbf{j}}_{\mathbf{p}}(\mathbf{r}) \cdot \mathbf{A}(\mathbf{r}, t) d\mathbf{r} \tag{1.90}$$

where:

$$\hat{\mathbf{J}}_{\mathbf{p}}(\mathbf{r}) = \frac{1}{2m_e} \sum_i [\hat{\mathbf{p}}_i \delta(\mathbf{r} - \hat{\mathbf{r}}_i) + \delta(\mathbf{r} - \hat{\mathbf{r}}_i) \hat{\mathbf{p}}_i] \tag{1.91}$$

is the total paramagnetic density current, which is not gauge invariant[1]. Its expectation values is:

$$\langle \mathbf{J}_{\mathbf{p}\alpha} \rangle(\mathbf{q}, \omega) = \frac{e}{c} \sum_{\mathbf{q}'\beta} \chi_{J_{\mathbf{p}\alpha} J_{\mathbf{p}\beta}}(\mathbf{q}, \mathbf{q}', \omega) \mathbf{A}_{\mathbf{p}\beta}(\mathbf{q}', \omega) \tag{1.92}$$

where here χ is the response function in the Fourier transform of:

$$\chi_{J_{\mathbf{p}\alpha} J_{\mathbf{p}\beta}}(\mathbf{r}, \mathbf{r}', t) = -\frac{i}{\hbar} \theta(t) \langle [\hat{\mathbf{J}}_{\mathbf{p}\alpha}(\mathbf{r}, t), \hat{\mathbf{J}}_{\mathbf{p}\beta}(\mathbf{r}')] \rangle_0 \tag{1.93}$$

One is then interested in the expectation value of the physical current, which is the sum of the total paramagnetic and diamagnetic currents (and whose operator is proportional to $\hat{\mathbf{v}}_i$ and not $\hat{\mathbf{p}}_i$):

$$\hat{\mathbf{J}}(\mathbf{r}) = \hat{\mathbf{J}}_{\mathbf{p}}(\mathbf{r}) + \frac{e}{m_e c} \hat{n}(\mathbf{r}) \mathbf{A}(\mathbf{r}) \tag{1.94}$$

The related response function is:

$$\chi^J_{\alpha\beta}(\mathbf{q}, \mathbf{q}', \omega) = \frac{n(\mathbf{q}, \omega)}{m_e} \delta(\mathbf{q} - \mathbf{q}') \delta_{\alpha\beta} + \chi_{J_{\mathbf{p}\alpha} J_{\mathbf{p}\beta}}(\mathbf{q}, \mathbf{q}', \omega) \tag{1.95}$$

[1] The current should be written $\hat{\mathbf{J}}_{\mathbf{p}} = \frac{1}{2} \sum_i [\hat{\mathbf{v}}_{\mathbf{i}} \delta(\mathbf{r} - \hat{\mathbf{r}}_{\mathbf{i}}) + \delta(\mathbf{r} - \hat{\mathbf{r}}_{\mathbf{i}}) \hat{\mathbf{v}}_{\mathbf{i}}]$. We can substitute $\hat{\mathbf{v}}_{\mathbf{i}} \to \frac{\hat{\mathbf{p}}_{\mathbf{i}}}{m_e}$ to obtain the paramagnetic component of the current only if we assume velocity-independent interactions amongst particles [103, 104]

We now consider the response to an uniform electric field $\mathbf{E}(t)$, that can be described by a vector potential of the form $\mathbf{A}(\omega) = -\frac{ic}{\omega}\mathbf{E}(\omega)$. In this case, Eq. 1.84 becomes:

$$-eJ_\alpha(\mathbf{0},\omega) = \frac{ie^2}{\omega}\sum_\beta \chi^J_{\alpha\beta}(\mathbf{0},\mathbf{0},\omega)E_\beta(\omega) \tag{1.96}$$

where we can identify immediately the complex conductivity tensor $\mathscr{S}$:

$$\mathscr{S}_{\alpha\beta}(\omega) = \frac{ie^2}{\omega}\chi^J_{\alpha\beta}(\mathbf{0},\mathbf{0},\omega) \tag{1.97}$$

From the previous equation, the complex conductivity tensor can be rewritten in the spectral representation in two equivalent ways [105]:

$$\mathscr{S}_{\alpha\beta}(\omega) = \frac{in(\mathbf{0},\omega)}{m\omega}\delta_{\alpha\beta} + \frac{i}{\omega\Omega}\sum_{MN}\frac{e^{-\beta E_N} - e^{-\beta E_M}}{Z}\frac{\langle N|\,\hat{J}_{\mathbf{p}\alpha}\,|M\rangle\,\langle M|\,\hat{J}_{\mathbf{p}\beta}\,|N\rangle}{\hbar(\omega+i\eta) - (E_M - E_N)} \tag{1.98}$$

$$\mathscr{S}_{\alpha\beta}(\omega) = \frac{i\hbar}{\Omega}\sum_{MN}\frac{e^{-\beta E_N} - e^{-\beta E_M}}{Z(E_M - E_N)}\frac{\langle N|\,\hat{J}_{\mathbf{p}\beta}\,|M\rangle\,\langle M|\,\hat{J}_{\mathbf{p}\alpha}\,|N\rangle}{\hbar(\omega+i\eta) - (E_M - E_N)} \tag{1.99}$$

Assuming now that our system is formed by a collection of electrons following a one particle Hamiltonian, as in the case of DFT, we can recast Eq. 1.99 as a function of one particle quantities and operators [60]:

$$\mathscr{S}_{\alpha\beta}(\omega) = i\frac{2e^2\hbar^3}{m_e^2\Omega}\sum_{mm'}\frac{f^0(\epsilon_{m'}) - f^0(\epsilon_m)}{\epsilon_m - \epsilon_{m'}}\frac{\langle m|\,\hat{j}_{\mathbf{p}\alpha}\,|m'\rangle\,\langle m'|\,\hat{j}_{\mathbf{p}\beta}\,|m\rangle}{\epsilon_m - \epsilon_{m'} - \hbar\omega + i\delta/2} \tag{1.100}$$

where $\hat{\mathbf{j}}$ is now the one particle paramagnetic current operator, proportional to the velocity operator $\hat{\mathbf{v}} = [\hat{H}, \hat{\mathbf{r}}]$ [2]. To obtain the response to a static perturbation, one should perform the limit $\omega \to 0$ in the above expressions. If the system is composed by atoms and electrons, as in crystals, Eq. 1.100 is justified in the adiabatic approximation picture; nonetheless, if calculated for one single atomic configuration, Eq. 1.100 only contains the response to an external perturbation in the form of an electromagnetic field. Indeed, for a DFT system another source of perturbation is the vibrational motion of nuclei; in the semi-classical approximation, this can be taken in account by averaging Eq. 1.100 over a set of nuclear configurations extracted from a MD simulation at temperature T. To our knowledge, only recently the limits of this procedure

[2] In the limit $m' \to m$ we have $\frac{f^0(\epsilon_{m'}) - f^0(\epsilon_m)}{\epsilon_m - \epsilon m'} \to -\frac{\partial f^0}{\partial \epsilon_m}$

have been formally discussed [106], but a complete investigation is still lacking.

Up to now we have considered the response of a system to a mechanical external perturbation, i.e. to an $F(t)$ which couple to some observable $\hat{B}$ of the system. When the external perturbation is a thermal gradient instead, the same picture does not hold. Nonetheless, in this case the coefficients that enter the Onsager relations may still be calculated as an expectation value of appropriate current operators [59]. In particular, referring to the notations of Sec. 1.2, we have:

$$L_{11\alpha\beta}(\omega) = \int_0^\infty dt e^{i\omega t} \int_0^\beta d\lambda \langle \hat{J}_\alpha \hat{J}_\beta(t + i\hbar\lambda)\rangle \tag{1.101}$$

$$L_{12\alpha\beta}(\omega) = \int_0^\infty dt e^{i\omega t} \int_0^\beta d\lambda \langle \hat{J}_\alpha \hat{Q}_\beta(t + i\hbar\lambda)\rangle \tag{1.102}$$

$$L_{21\alpha\beta}(\omega) = \int_0^\infty dt e^{i\omega t} \int_0^\beta d\lambda \langle \hat{Q}_\alpha \hat{J}_\beta(t + i\hbar\lambda)\rangle \tag{1.103}$$

$$L_{22\alpha\beta}(\omega) = \int_0^\infty dt e^{i\omega t} \int_0^\beta d\lambda \langle \hat{Q}_\alpha \hat{Q}_\beta(t + i\hbar\lambda)\rangle \tag{1.104}$$

$$\tag{1.105}$$

where $\hat{\mathbf{Q}}$ is the total quantum-mechanical operator associated to an heat flow current (analogously as $\hat{\mathbf{J}}$ is the total operator representing charge density current), and care to limits is implicit. As shown in Ref. [107], the real Onsager coefficient for independent electrons can be brought in the following form [103]:

$$L_{ij\alpha\beta} = \lim_{\omega\to 0}(-1)^{i+j}\frac{2\pi e^2\hbar^3}{m_e^2\Omega}\sum_{mm'}\frac{f^0(\epsilon_{m'}) - f^0(\epsilon_m)}{\epsilon_m - \epsilon_{m'}}(\epsilon_{m'} - \mu)^{i-1}(\epsilon_m - \mu)^{j-1}\times \\ \langle m|\nabla_\alpha|m'\rangle\langle m'|\nabla_\beta|m\rangle\,\delta(\epsilon_m - \epsilon_{m'} - \hbar\omega) \tag{1.106}$$

In the above formula the electronic states are all-electron wavefunctions; in the PAW formalism [108]—that we will use when performing calculations in Chapter 5— the matrix elements involving the gradients can be conveniently treated as in Ref. [103].

As mentioned above, to include the atomic degrees of freedom we average Eq. 1.106 over the nuclear thermal configurations, where we consider the electronic quantities as a function of the classical nuclear coordinates R, without time dependence in the adiabatic approximation.

As we have learnt in this and the previous sections, we can compute the conductivity of a system (and the other transport coefficients) within two seemingly different pictures. The first one relies on the existence of well-defined quasi-particles that weakly

interact and whose thermodynamics is governed by the Boltzmann master equation. The second one is based on the general theory for the response of a system to a small external perturbation expressed via the Kubo formula. To bridge the two approaches—at least for normal metals—we refer to Ref. [13]. Here, the current-current correlation function is calculated via a diagrammatic approach to equilibrium expectation values that includes the leading order approximation to the electron-phonon self-energy. This is *different* from the approximated approached used to write down Eq. 1.100. It is in general shown that the Kubo formula can be expressed in function of a quantity $\chi_{n\mathbf{k}}(\omega)$ that satisfies a generalized BTE equation, which reduces to Eq. 1.58 in the limit of vanishing ω (the result is even more general and provides separate BTEs for phonons and electrons; nonetheless, the phonons may be considered at equilibrium as explained previously in this chapter). Also, in the same limit the conductivity formula reduces to Eq. 1.70. We can therefore state that the calculation of the dc conductivity tensor by means of Eq. 1.70, where $\chi_{n\mathbf{k}}$ is the solution of the BTE with the collisional integral written using the Fermi golden rule, is *equivalent* to calculate the Kubo formula in the perturbative approach using the leading order approximation to the electron-phonon self-energy (and therefore including an infinite subset of diagrams in the calculation of the electron propagator). This generalized BTE derived in Ref. [13] can be used in order to correct the results coming from the first order perturbation theory calculation of the infrared absorption of normal metals, as done in Ref. [109]. This correction is expected to be relevant when the EPC coupling cannot be considered very small.

Chapter 2

Boltzmann equation from non equilibrium Green's functions

In this chapter, after having discussed the BTE and its solution from a phenomenological perspective in Chap. 1, we give a detailed and formal derivation of Eq. 1.58 from the Non Equilibrium Green's Functions (NEGF) theory. Despite Kadanoff and Baym [110] and Mahan [111] discussed the derivation for the homogeneous gas case, and Kita [11] extended the discussion to metallic one band models with the inclusion of impurity scattering only, a general approach that keeps in account a more realistic description of materials and scattering mechanisms is missing. For this reason in this chapter, on the footsteps of what already done in the literature, we give a derivation which avoid strong assumptions on the system under consideration as much as possible.

This chapter is intended to be technical, and one may jump directly to the last section where a generalized BTE is derived in the semiclassical limit and its reduction to the form of Eq. 1.58 is discussed. Nonetheless, we find interesting to highlight the fact that the BTE is profoundly well-founded and it naturally stems from physically sound approximations of the NEGFs. In particular, this sheds a different light over the results that will be presented in the following chapters on specific materials, as we will exactly know in which hypotesis they are valid and what degree of accuracy they have. A rather basic knowledge of the non equilibrium theory is needed to derive the BTE from first principles, so that a very brief introduction to the methodology is given in the first section of this chapter; for details we refer to the abundant literature [112, 113, 110].

Also, we want to mention that in this chapter we will adopt a notation where the variables on which a function depends are kept in paranthesis instead of subscripts as much as possible, in order to facilitate readibility of the (sometimes) very long expressions. The dependence of Green's function upon external field will always be

implicit, if not stated otherwise. Also, f and n without any apex will be used to indicate the statistical Fermi-Dirac and Bose-Einstein statistics, while the apexes ^{0} will be reserved to equilibrium quantities of non-interacting systems and $\dot{}^0$ to equilibrium quantities of interacting systems.

2.1 Keldysh-Contour formalism and Dyson's equations

It is very common to evaluate thermal averages of a physical observable $\hat{O}$. For an isolated system with Hamiltonian $\hat{H}$, this task can be performed by doing $\langle\hat{O}\rangle = \mathrm{Tr}\{\hat{\rho}\hat{O}\}$ where Tr is the trace operation and $\hat{\rho}$ is the density matrix operator, which in the canonical ensamble is identified by $\hat{\rho} = \frac{e^{-\beta\hat{H}}}{\mathrm{Tr}\{e^{-\beta\hat{H}}\}}$. In the case of an isolated system, at the thermodynamical equilibrium we have that $\langle\hat{O}\rangle$ is independent of time.

Things change when a system is isolated before $t < t_0$ but then a perturbation is turned on at $t = t_0$, so that its Hamiltonian becomes $\hat{H}(t)$ for $t \geq t_0$. In the Heisenberg picture for the time evolution of operators, we can write for the expectation value for $t > t_0$:

$$O(t) \coloneqq \langle\hat{O}_H(t)\rangle = \mathrm{Tr}\{\hat{\rho}\hat{O}_H(t)\} \tag{2.1}$$

where $\hat{O}_H(t) = \hat{U}(t_0,t)\hat{O}\hat{U}(t,t_0)$ and the time evolution operator satisfies:

$$\begin{aligned} i\frac{\partial}{\partial t}\hat{U}(t,t') &= \hat{H}(t)\hat{U}(t,t') \\ i\frac{\partial}{\partial t'}\hat{U}(t,t') &= -\hat{U}(t,t')\hat{H}(t') \end{aligned} \tag{2.2}$$

with boundary condition $\hat{U}(t,t) = 1$. The above equation is solved formally by:

$$\hat{U}(t,t') = \begin{cases} \hat{T}e^{-\int_{t'}^{t} d\bar{t}\hat{H}(\bar{t})} & t > t' \\ \hat{\bar{T}}e^{-\int_{t'}^{t} d\bar{t}\hat{H}(\bar{t})} & t < t' \end{cases} \tag{2.3}$$

where $\hat{T}$ is the time-ordering operator while $\hat{\bar{T}}$ is the anti-time-ordering operator. If one extends the definition of the time evolution operator to immaginary times then one can rewrite Eq. 2.1 as:

$$O(t) = \frac{\mathrm{Tr}\{\hat{U}(-i\beta,t_0)\hat{U}(t_0,t)\hat{O}\hat{U}(t,t_0)\}}{\mathrm{Tr}\{\hat{U}(-i\beta,t_0)\}} \tag{2.4}$$

A compact expression for Eq. 2.4 can be obtained if we define a time variable z living

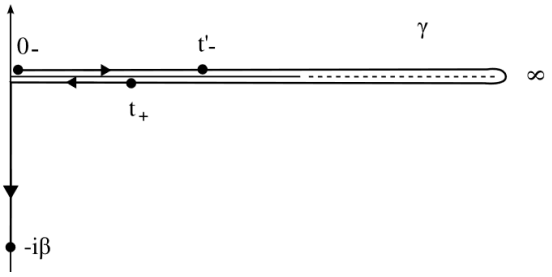

Figure 2.1: Keldysh contour γ (reprinted from Ref. [112]) with $t_0 = 0$ and extendend to real infinite times.

on the contour of Fig. 2.1:

$$O(z) = \frac{\mathrm{Tr}\{\hat{T}_c e^{-i\int_\gamma d\bar{z}\hat{H}(\bar{z})}\hat{O}(z)\}}{\mathrm{Tr}\{\hat{T}_c e^{-i\int_\gamma d\bar{z}\hat{H}(\bar{z})}\}} \tag{2.5}$$

where the contour ordering operator $\hat{T}_c$ moves operators with later contour variable to the left. In summary, we have introduced a formalism in order to calculate non equilibrium expectation values of physical observables on the contour represented in Fig. 2.1. The difference between this formalism and equilibrium theory is that the Keldysh contour explicitly avoids to deal with transition probabilities between different states [114]. In other words, non equilibrium theory cannot be expressed via expectation values of the fields between asymptotic states in the far past and in the far future as usually done in equilibrium theory. Here, at zero temperature in fact one can adopt the "adiabatic switching" technique and show, using the Gell-Mann-Low theorem, that asymptotic ground states are related via $|t = -\infty\rangle = e^{i\phi}\,|t = +\infty\rangle$ where ϕ is a generic phase [115]. Out of equilibrium, this supposition may not hold, expecially if dissipative processes take place. Therefore the expectation values are to be done between asymptotic states at equal times, i.e. at infinite past; the immediate consequence is that the theory cannot be expressed as a function of a single type of Green's function (or two, if we consider also the analyitic continuation to immaginary times in case of finite-temperature averages).

To be practical, we now consider the following Hamiltonian:

$$\hat{H} = \hat{H}^0 + \hat{H}^i + \hat{H}'(t) := \hat{H}^{\dot{0}} + \hat{H}'(t) \tag{2.6}$$

where $\hat{H}^0$ represents the Hamiltonian of a system composed by free particles, $\hat{H}^i$ is their mutual interaction and $\hat{H}'(t)$ is an external perturbing potential which has the property that is switched on at t_0; $\hat{H}^{\dot{0}}$ is the hamiltonian of the interacting system in

absence of external perturbations. We now define the following correlation functions [111]:

$$G^{<}(\mathbf{r}_1 t_1, \mathbf{r}_2 t_2) = i\langle \Psi^{\dagger}(\mathbf{r}_2 t_2)\Psi(\mathbf{r}_1 t_1)\rangle \tag{2.7}$$

$$G^{>}(\mathbf{r}_1 t_1, \mathbf{r}_2 t_2) = -i\langle \Psi(\mathbf{r}_1 t_1)\Psi^{\dagger}(\mathbf{r}_2 t_2)\rangle \tag{2.8}$$

$$G^{t}(\mathbf{r}_1 t_1, \mathbf{r}_2 t_2) = \theta(t_1 - t_2)G^{>}(\mathbf{r}_1 t_1, \mathbf{r}_2 t_2) + \theta(t_2 - t_1)G^{<}(\mathbf{r}_1 t_1, \mathbf{r}_2 t_2) \tag{2.9}$$

$$G^{\bar{t}}(\mathbf{r}_1 t_1, \mathbf{r}_2 t_2) = \theta(t_2 - t_1)G^{>}(\mathbf{r}_1 t_1, \mathbf{r}_2 t_2) + \theta(t_1 - t_2)G^{<}(\mathbf{r}_1 t_1, \mathbf{r}_2 t_2) \tag{2.10}$$

$$G^{r}(\mathbf{r}_1 t_1, \mathbf{r}_2 t_2) = G^{t}(\mathbf{r}_1 t_1, \mathbf{r}_2 t_2) - G^{<}(\mathbf{r}_1 t_1, \mathbf{r}_2 t_2) \tag{2.11}$$

$$G^{a}(\mathbf{r}_1 t_1, \mathbf{r}_2 t_2) = G^{t}(\mathbf{r}_1 t_1, \mathbf{r}_2 t_2) - G^{>}(\mathbf{r}_1 t_1, \mathbf{r}_2 t_2) \tag{2.12}$$

where $\Psi^{\dagger}(\mathbf{r}t)$ and $\Psi(\mathbf{r}t)$ are the electronic field operators in the Heisenberg representation and the six Green's functions are denoted respectively as "lesser", "greater","time-ordered","anti-time-ordered","retarded" and "advanced". The Heisenberg representation picture is switched to the interaction representation picture when perturbation theory is used. In the following we neglect initial correlations on the contour in the interaction representation [116], i.e. we neglect the perturbation expansion of the density matrix along the imaginary axis [117], and thus let $t_0 = -\infty$; this supposition can be justified only if we look at times which are very distant from external field appearance—even though this may be not a sufficient condition.

In equilibrium theory, for a non interacting DFT system with hamiltonian H^0, the expression for the lesser and greater Green's functions in momentum and frequency space are:

$$G^{<,0}(n\mathbf{k}, \omega) = 2\pi i f_{n\mathbf{k}}\delta(\omega - \epsilon^0_{n\mathbf{k}}) \tag{2.13}$$

$$G^{>,0}(n\mathbf{k}, \omega) = 2\pi i(1 - f_{n\mathbf{k}})\delta(\omega - \epsilon^0_{n\mathbf{k}}) \tag{2.14}$$

so that, when integrated over ω, the lesser and greater Green's functions contain the information on the particle statistics. $G^{<}$ and $G^{>}$ can therefore be seen as a generalization of the one particle Fermi-Dirac statistic, in the momentum and frequency phase space, when the system is perturbed (the same considerations apply to bosonic fields and Bose-Einstein statistic). With this in mind and wanting to derive the analogous of the BTE, one is eager to obtain an evolution equation for the lesser and greater Green's functions. The best way to do it is to start from the Dyson equation and derive it with respect to time. In non equilibrium theory the Dyson equation involve all the four independent different Green's functions listed in Eq. 2.12. Indeed, we consider the

matrix:

$$\tilde{G} = \begin{bmatrix} G^t & -G^< \\ G^> & -G^{\bar{t}} \end{bmatrix} \tag{2.15}$$

and the matrix:

$$\tilde{\Sigma} = \begin{bmatrix} \Sigma^t & -\Sigma^< \\ \Sigma^> & -\Sigma^{\bar{t}} \end{bmatrix}. \tag{2.16}$$

It can be shown that we can obtain a Dyson equation for $\tilde{G}$ in the form of (see Mahan [111]):

$$\begin{aligned} &\tilde{G}(\mathbf{r}_1 t_1, \mathbf{r}_2 t_2) = \tilde{G}^0(\mathbf{r}_1 t_1, \mathbf{r}_2 t_2) + \\ &\int_{-\infty}^{+\infty} d\mathbf{r}_3 dt_3 \int_{-\infty}^{+\infty} d\mathbf{r}_4 dt_4 \tilde{G}^0(\mathbf{r}_1 t_1, \mathbf{r}_3 t_3) \tilde{\Sigma}(\mathbf{r}_3 t_3, \mathbf{r}_4 t_4) \tilde{G}(\mathbf{r}_4 t_4, \mathbf{r}_2 t_2) \end{aligned} \tag{2.17}$$

or in the alternative but equivalent form:

$$\begin{aligned} &\tilde{G}(\mathbf{r}_1 t_1, \mathbf{r}_2 t_2) = \tilde{G}^0(\mathbf{r}_1 t_1, \mathbf{r}_2 t_2) + \\ &\int_{-\infty}^{+\infty} d\mathbf{r}_3 dt_3 \int_{-\infty}^{+\infty} d\mathbf{r}_4 dt_4 \tilde{G}(\mathbf{r}_1 t_1, \mathbf{r}_3 t_3) \tilde{\Sigma}(\mathbf{r}_3 t_3, \mathbf{r}_4 t_4) \tilde{G}^0(\mathbf{r}_4 t_4, \mathbf{r}_2 t_2) \end{aligned} \tag{2.18}$$

The above equations involve all the various Green's functions at the same time. Their coordinate dependence can be simplified in certain conditions; in fact, in crystals the Green's functions are usually not homogeneous in space, but they are homogeneous in time far from transients due to the switch on of the external perturbation. In this condition we can say that:

$$\tilde{G}^0(\mathbf{r}_1 t_1, \mathbf{r}_2 t_2) = \tilde{G}^0(\mathbf{r}_1, \mathbf{r}_2, t_1 - t_2). \tag{2.19}$$

Also, it is interesting to note that in crystals a certain degree of spatial homogeneity is reached. For example at thermal equilibrium, the value of the observables depending on the coordinates is the same when evaluated at $\mathbf{r}$ and $\mathbf{r} + \mathbf{t}$, where $\mathbf{t}$ is a generic combination of lattice vectors. This suggests to express the correlation functions on a basis set which keeps track of this invariance; this basis set is built with the Wannier functions generated by the Bloch functions of the crystal, that are introduced in Chap. 1. This will be of central importance for the approximations done in the following.

In this context we are interested mainly in two quantities: the one particle density for hole and electrons and the electronic current. The expectation values for the density,

starting from its form in second quantization, is:

$$n^e(\mathbf{r}_1, t_1) = \langle \hat{\Psi}^\dagger(\mathbf{r}_1, t_1)\hat{\Psi}(\mathbf{r}_1, t_1)\rangle = -iG^<(\mathbf{r}_1 t_1, \mathbf{r}_1 t_1) \tag{2.20}$$

For the electronic current we have the following expression for the paramagnetic current—or simply the component in absence of external fields:

$$\hat{\mathbf{J}}_\mathbf{p}(\mathbf{r},t) = \frac{e}{2}\sum_i (\hat{\mathbf{v}}_i\delta(\mathbf{r}-\mathbf{r}_i) + \delta(\mathbf{r}-\mathbf{r}_i)\hat{\mathbf{v}}_i) \tag{2.21}$$

where $\hat{\mathbf{v}}_i = [\hat{H}, \hat{\mathbf{r}}_i]$. The above expression can be simplified if we assume particle interactions that are independent of the velocity (such as for the case of one particle Hamiltonians with local pseudopotentials) by sending $\hat{\mathbf{v}}_\mathbf{i} \to \frac{\hat{\mathbf{p}}_\mathbf{i}}{m_e}$ [104, 113]. In this case we obtain [116]:

$$\mathbf{J}_\mathbf{p}(\mathbf{r},t) = -\frac{e}{2m_e}\left\{\left[\hat{\nabla}_{\mathbf{r}_1} - \hat{\nabla}_{\mathbf{r}_2}\right] G^<(\mathbf{r}_1, t_1, \mathbf{r}_2, t_2)\right\}_{\substack{\mathbf{r}_1=\mathbf{r}_2=\mathbf{r}\\ t_1=t_2=t}} \tag{2.22}$$

The total current operator in presence of a vector potential $\mathbf{A}(\mathbf{r},t)$ is instead:

$$\mathbf{J}_\mathbf{e}(\mathbf{r},t) = -\frac{e}{2m_e}\left\{\left[\hat{\nabla}_{\mathbf{r}_1} - \hat{\nabla}_{\mathbf{r}_2} - ie\left(\mathbf{A}(\mathbf{r}_1,t_1) + \mathbf{A}(\mathbf{r}_2,t_2)\right)\right] G^<(\mathbf{r}_1, t_1, \mathbf{r}_2, t_2)\right\}_{\substack{\mathbf{r}_1=\mathbf{r}_2=\mathbf{r}\\ t_1=t_2=t}} \tag{2.23}$$

If we express the electric field as gradient of a scalar potential, the paramagnetic is the only formal component of the total current; of course, the diamagnatic term will be contained in the Green's function by gauge invariance [see App. D and App. E for more details]. We finally remark that for both density and density-current operators, if spin degeneracy is broken, the above equations hold for each separate spin channel. It is evident from the above equations that the naive expectations raised by Eqs. 2.13 and 2.14 about the lesser Green's function centrality in transport theory find their justification in the second quantization expression for the current operator.

2.2 Retarded kinetic equation in the Wannier representation

To show the general procedure to find the kinetic equations for all the Green's functions in the Wannier representation, we focus on G^r and study the time evolution of its Dyson's equation. This is obtained applying the operator $i\partial/\partial t_1 - H^0(\mathbf{r}_1, -i\nabla_{\mathbf{r}_1})$ to

both members of equation 2.17, for the component involving G^r:

$$[i\frac{\partial}{\partial t_1} - H^0(\mathbf{r}_1, -i\nabla_{\mathbf{r}_1})]G^r(\mathbf{r}_1 t_1, \mathbf{r}_2 t_2) = \\ \delta(\mathbf{r}_1 - \mathbf{r}_2)\delta(t_1 - t_2) + \int_{-\infty}^{+\infty} d\mathbf{r}_3 dt_3 \Sigma^r(\mathbf{r}_1 t_1, \mathbf{r}_3 t_3) G^r(\mathbf{r}_3 t_3, \mathbf{r}_2 t_2) \tag{2.24}$$

where we used that at equilibrium:

$$\left[i\frac{\partial}{\partial t_1} - H^0(\mathbf{r}_1, -i\nabla_{\mathbf{r}_1})\right] \tilde{G}^0(\mathbf{r}_1 t_1, \mathbf{r}_2 t_2) = \delta(\mathbf{r}_1 - \mathbf{r}_2)\delta(t_1 - t_2)\tilde{I} \tag{2.25}$$

where $\tilde{I}$ is the 2×2 identity matrix.

The Feynmann rules for the diagrammatic expansion in the non equilibrium formalism are well explained by Rammer in Ref. [113]; the generalized features of Feynman diagrams with respect to equilibrium theory is that now they contain also product and summations over the matrix indexes that identify the Green's functions. We can extract from the self-energy the contribution given by $H'(\mathbf{r}_1 t_1) = U(\mathbf{r}_1 t_1)$. In fact, as showed in [113], its contribution to the Dyson equation may be written as:

$$\int_{-\infty}^{+\infty} d\mathbf{r}_3 dt_3 \tilde{G}^0(\mathbf{r}_1 t_1, \mathbf{r}_3 t_3) U(\mathbf{r}_3 t_3) \tilde{I} \tilde{G}(\mathbf{r}_3 t_3, \mathbf{r}_2 t_2) \tag{2.26}$$

so that for Eq. 2.24 we get:

$$[i\frac{\partial}{\partial t_1} - H^0(\mathbf{r}_1, -i\nabla_{\mathbf{r}_1}) - U(\mathbf{r}_1 t_1)]G^r(\mathbf{r}_1 t_1, \mathbf{r}_2 t_2) \\ = \delta(\mathbf{r}_1 - \mathbf{r}_2)\delta(t_1 - t_2) + \int_{-\infty}^{+\infty} d\mathbf{r}_3 dt_3 \Sigma^r(\mathbf{r}_1 t_1, \mathbf{r}_3 t_3) G^r(\mathbf{r}_3 t_3, \mathbf{r}_2 t_2) \tag{2.27}$$

where Σ now contains only terms which are formally equal to the equilibrium Feynman diagrams. At this point we express G^r in the Wannier function basis set as defined in Eq. 1.74, but by setting $U_{mn} = \delta_{mn}$. In this way we have a univoque identification between each Wannier function and the band energy to which it is referred—we will discuss later how different choices may be made. The result is:

$$G^r(\mathbf{R}n, \mathbf{R}'n', t_1, t_2) := \int_{-\infty}^{+\infty} d\mathbf{r'}_1 \int_{-\infty}^{+\infty} d\mathbf{r'}_2 \langle \mathbf{R}n|\mathbf{r'}_1\rangle G^r(\mathbf{r'}_1 t_1, \mathbf{r'}_2 t_2) \langle \mathbf{r'}_2|\mathbf{R}'n'\rangle \\ G^r(\mathbf{r}_1 t_1, \mathbf{r}_2 t_2) = \sum_{\substack{\mathbf{R}n \\ \mathbf{R}'n'}} \langle \mathbf{r}_1|\mathbf{R}n\rangle G^r(\mathbf{R}n, \mathbf{R}'n', t_1, t_2) \langle \mathbf{R}'n'|\mathbf{r}_2\rangle \tag{2.28}$$

We use the expansion on Wannier functions for every operator and function in Eq 2.27:

$$\delta(\mathbf{r}_1-\mathbf{r}_2)\delta(t_1-t_2)\rightarrow\delta_{\mathbf{R}n,\mathbf{R}'n'}\delta(t_1-t_2) \tag{2.29}$$
$$H^0(\mathbf{r}_1)\rightarrow H^0(\mathbf{R}n,\mathbf{R}'n') \tag{2.30}$$
$$U(\mathbf{r}_1,t_1)\rightarrow U(\mathbf{R}n,\mathbf{R}'n',t_1) \tag{2.31}$$
$$G^r(\mathbf{r}_1\mathbf{r}_2,t_1,t_2)\rightarrow G^r(\mathbf{R}n,\mathbf{R}'n',t_1,t_2) \tag{2.32}$$
$$\Sigma^r(\mathbf{r}_1\mathbf{r}_2,t_1,t_2)\rightarrow \Sigma^r(\mathbf{R}n,\mathbf{R}'n',t_1,t_2) \tag{2.33}$$

The explicit form for $U(\mathbf{r}_1,t_1)$ that we consider is:

$$U(\mathbf{r}_1,t_1)=-e\mathbf{E}\cdot\mathbf{r}_1, \tag{2.34}$$

and its matrix elements in Wannier functions are:

$$\begin{aligned}U(\mathbf{R}n,\mathbf{R}'n',t_1)=-e\mathbf{E}\cdot\langle\mathbf{R}n|\hat{\mathbf{r}}_1|\mathbf{R}'n'\rangle=\\ -e\mathbf{E}\cdot\langle(\mathbf{R}-\mathbf{R}')n|\hat{\mathbf{r}}_1|\mathbf{0}n'\rangle-e\mathbf{E}\cdot\mathbf{R}'\delta_{\mathbf{Rn},\mathbf{R}'n'}\end{aligned} \tag{2.35}$$

where the chain of equalities comes from the following translational property of the Wannier functions:

$$\begin{aligned}\langle\mathbf{r}+\mathbf{t}|\mathbf{R}n\rangle=\frac{V}{(2\pi)^3}\sum_{\mathbf{k}}e^{-i\mathbf{k}\cdot\mathbf{R}}\langle\mathbf{r}+\mathbf{t}|\mathbf{k}n\rangle=\frac{V}{(2\pi)^3}\sum_{\mathbf{k}}e^{-i\mathbf{k}\cdot\mathbf{R}}\langle\mathbf{r}|\mathbf{k}n\rangle e^{i\mathbf{k}\cdot\mathbf{t}}=\\ \frac{V}{(2\pi)^3}\sum_{\mathbf{k}}e^{-i\mathbf{k}\cdot(\mathbf{R}-\mathbf{t})}\langle\mathbf{r}|\mathbf{k}n\rangle=\langle\mathbf{r}|\mathbf{R}-\mathbf{t}n\rangle\end{aligned} \tag{2.36}$$

where $\mathbf{t}$ is a generic direct-space lattice vector; with the above formula and a change of variable in integration, Eq. 2.35 is obtained. It is to notice that Eq. 2.35 is valid even if the system is periodic in less than 3 dimensions. In such case, the above equalities are fully working only if the electric field is in a direction where periodicity is preserved, in order to use Bloch's functions properties in Eq. 2.36.

Eq. 2.27 in Wannier representation then becomes:

$$\begin{aligned}\sum_{\mathbf{R}^1n^1}[i\frac{\partial}{\partial t_1}\delta_{\mathbf{R}n,\mathbf{R}^1n^1}-H^0(\mathbf{R}n,\mathbf{R}^1n^1)\delta_{nn^1}+e\mathbf{E}\cdot\langle(\mathbf{R}-\mathbf{R}^1)n|\hat{\mathbf{r}}_1|\mathbf{0}n^1\rangle+\\ +e\mathbf{E}\cdot\mathbf{R}^1\delta_{\mathbf{R}n,\mathbf{R}^1n^1}]G^r(\mathbf{R}^1n^1,\mathbf{R}'n',t_1,t_2)=\delta_{\mathbf{R}n,\mathbf{R}'n'}\delta(t_1-t_2)+\\ \sum_{\mathbf{R}^1n^1}\int_{-\infty}^{+\infty}dt_3\Sigma^r(\mathbf{R}n,\mathbf{R}^1n^1,t_1,t_3)G^r(\mathbf{R}^1n^1,\mathbf{R}'n',t_3,t_2)\end{aligned} \tag{2.37}$$

The same equation but derived in the t_2 variable can be obtained applying the same procedure used to arrive to Eq. 2.37, but starting from Eq. 2.18. In this case one first uses that:

$$\left[-i\frac{\partial}{\partial t_2} - H^0(\mathbf{r}_2, i\nabla_{\mathbf{r}_2})\right] \tilde{G}^0(\mathbf{r}_1 t_1, \mathbf{r_2} t_2) = \delta(\mathbf{r}_1 - \mathbf{r}_2)\delta(t_1 - t_2)\tilde{I} \tag{2.38}$$

In this case one should be more careful with matrix indexes when passing to the Wannier basis set (see App. F). One obtains:

$$\begin{aligned}
&\sum_{\mathbf{R}^1 n^1} G^r(\mathbf{R}n, \mathbf{R^1}n^1, t_1, t_2)[-i\frac{\partial}{\partial t_2}\delta_{\mathbf{R}^1 n^1, \mathbf{R}'n'} - H^0(\mathbf{R}^1 n^1, \mathbf{R}'n')\delta_{n^1 n'} + \\
&e\mathbf{E}\cdot\langle(\mathbf{R^1} - \mathbf{R}')n^1|\hat{\mathbf{r}}_2|\mathbf{0}n\rangle + e\mathbf{E}\cdot\mathbf{R}^1\delta_{\mathbf{R^1}n^1,\mathbf{R}'n'}] = \delta_{\mathbf{R}n,\mathbf{R}'n'}\delta(t_1 - t_2) + \\
&\sum_{\mathbf{R}^1 n^1}\int_{-\infty}^{+\infty} dt_3 G^r(\mathbf{R}n, \mathbf{R^1}n^1, t_1, t_3)\Sigma^r(\mathbf{R}^1 n^1, \mathbf{R}'n', t_3, t_2)
\end{aligned} \tag{2.39}$$

where the time derivative operator is just simbolically on the right but it acts as $\frac{\partial}{\partial t_2}G^r$ (see App. F).

We now rewrite the correlation functions with the following change of variables:

$$G^r(\mathbf{R}n, \mathbf{R}'n', t_1, t_2) = G^r(\frac{\mathbf{R} + \mathbf{R}'}{2}, \mathbf{R} - \mathbf{R}', n, n', \frac{t_1 + t_2}{2}, t_1 - t_2) \tag{2.40}$$

Our assumption will be that the dependence of the Green's function over $\mathbf{R} + \mathbf{R}'$ is just due to the presence of the electric field, whereas other types of inhomogeneity are not present. In other words, we imagine a spatially homogeneous sample whose translational symmetry is broken only by the presence of an electric potential. We also define the following change of coordinate, analogous to what is know as Wigner transformation [111] (see App. C and E for a more detailed discussion over the Wigner transformation):

$$G^r(\mathbf{R}n, \mathbf{R}'n', t, t') = \sum_{\mathbf{k}}\int_{-\infty}^{\infty} d\omega e^{i\mathbf{k}\cdot(\mathbf{R}-\mathbf{R}')}e^{-i\omega(t_1 - t_2)}G^r(\mathbf{k}, \frac{\mathbf{R} + \mathbf{R}'}{2}, n, n', \frac{t_1 + t_2}{2}, \omega). \tag{2.41}$$

The same definition applies also to the self-energy. As long as Σ and G will appear as contracted over coordinates, we have to understand how to deal with the Wigner transform of products of the type:

$$\sum_{\mathbf{R}^1, n^1}\int_{-\infty}^{\infty} dt' A(\mathbf{R}n, \mathbf{R}^1 n^1, t_1, t')B(\mathbf{R}^1 n^1, \mathbf{R}'n', t', t_2) \tag{2.42}$$

This is done with a procedure known as gradient expansion, and is presented in App. C.

We now sum Eqs. 2.37 and 2.39 member by member, multiply by $\frac{1}{2}$ and apply the Wigner transform to both members of the obtained equation. We then make use of the results of App. C, where the change of variables $\Omega = \omega + e\mathbf{E}\cdot\frac{\mathbf{R}+\mathbf{R}'}{2}$ is implemented in order to obtain gauge invariant quantities—see App. E—to obtain:

$$\begin{aligned}
&\sum_{n^1}\left[\Omega\delta_{nn^1} - \epsilon^0_{n\mathbf{k}}\delta_{nn^1}\right] G^r(\mathbf{k},n^1,n',\Omega) + \frac{ie\mathbf{E}}{4}\cdot\nabla_{\mathbf{k}}\epsilon^0_{n\mathbf{k}}\delta_{nn^1}\frac{\partial}{\partial\Omega}G^{r,\dot{0}}(\mathbf{k},n^1,n',\Omega)+\\
&-\frac{ie\mathbf{E}}{4}\frac{\partial}{\partial\Omega}G^{r,\dot{0}}(\mathbf{k},n,n^1,\Omega)\cdot\nabla_{\mathbf{k}}\epsilon^0_{n'\mathbf{k}}\delta_{n^1n'}+\\
&+\frac{e}{2}\mathbf{E}\cdot\mathbf{A}(\mathbf{k},n,n^1)G^{r,\dot{0}}(\mathbf{k},n^1,n',\Omega)+\frac{e}{2}G^{r,\dot{0}}(\mathbf{k},n,n^1,\Omega)\mathbf{E}\cdot\mathbf{A}(\mathbf{k},n^1,n')+\\
&-\frac{1}{2}G^r(\mathbf{k},n,n^1)\Sigma^r(\mathbf{k},n^1,n')-\frac{1}{2}\Sigma^r(\mathbf{k},n,n^1)G^r(\mathbf{k},n,n^1)+\\
&-\frac{ie\mathbf{E}}{4}\Big[\nabla_{\mathbf{k}}G^{r,\dot{0}}(\mathbf{k},n,n^1,\Omega)\frac{\partial}{\partial\Omega}\Sigma^{r,\dot{0}}(\mathbf{k},n^1,n',\Omega)-\frac{\partial}{\partial\Omega}G^{r,\dot{0}}(\mathbf{k},n,n^1,\Omega)\nabla_{\mathbf{k}}\Sigma^{r,\dot{0}}(\mathbf{k},n^1,n',\Omega)+\\
&+\nabla_{\mathbf{k}}\Sigma^{r,\dot{0}}(\mathbf{k},n,n^1,\Omega)\frac{\partial}{\partial\Omega}G^{r,\dot{0}}(\mathbf{k},n^1,n',\Omega)-\frac{\partial}{\partial\Omega}\Sigma^{r,\dot{0}}(\mathbf{k},n,n^1,\Omega)\nabla_{\mathbf{k}}G^{r,\dot{0}}(\mathbf{k},n^1,n',\Omega)\Big]=1
\end{aligned} \tag{2.43}$$

where:

$$\mathbf{A}(\mathbf{k},n,n^1) = \sum_{\mathbf{R}} e^{-i\mathbf{k}\cdot\mathbf{R}} < \mathbf{R}n|\mathbf{r}|0n^1 > \tag{2.44}$$

and we have only retained first order terms in $\mathbf{E}$ in the gradient expansion of App. C.[1] Coherently, we keep/evaluate all the term at first order in the electric field. The above expression is clearly formidable, but it can be simplified. If indeed we assume that the Green's function is diagonal in the band index, so that different states are not mixed, and neglect the term in $\mathbf{A}$ we can simplify Eq. 2.43 into a much nicer expression:

$$\left[\Omega - \epsilon^0_{n\mathbf{k}} - \Sigma^r(\mathbf{k},n,\Omega)\right] G^r(\mathbf{k},n,\Omega) = 1 \tag{2.45}$$

where we have condensed the notation $(..,n,n,..)\to(..,n,..)$. The imposition of $n = n^1 = n'$ corresponds to neglect the terms in $\mathbf{A}$, since in their absence G^r and Σ^r are diagonal; coherently, we neglected the terms in $\mathbf{A}$ to reach Eq. 2.45. In principle, one

[1] Actually, we have kept only first orders in the expansion of the Green's function in the spatial and temporal center of mass. Since such expansion generates corrections in the electric field of the same order, we are in turn only keeping term which are first order in the electric field—see App. C and E for more details.

could find a basis set where the QBTE is diagonal (since all pieces are Hermitian—in particular, it holds that $\mathbf{A}(\mathbf{k},n,n') = \mathbf{A}^*(\mathbf{k},n',n)$ as a consequence of $\langle \mathbf{R}n|\,\mathbf{r}\,|\mathbf{0}n'\rangle = \langle \mathbf{0}n|\,\mathbf{r}\,|-\mathbf{R}n'\rangle$); one could try to understand if the U matrices that determine the gauge of the Wannier basis may be chosen so that they diagonalize Eq. 2.43. This will be attempted in future investigations. [2]

An analogous diagonal equation can be obtained by subtracting Eqs. 2.37 and 2.39:

$$i\frac{e}{2}\mathbf{E}\cdot\left[\left(1-\frac{\partial}{\partial\Omega}\Sigma^{r,\dot{0}}(\mathbf{k},n,\Omega)\right)\nabla_{\mathbf{k}}+\left(\nabla_{\mathbf{k}}\epsilon^0_{n\mathbf{k}}+\nabla_{\mathbf{k}}\Sigma^{r,\dot{0}}(\mathbf{k},n,\Omega)\right)\frac{\partial}{\partial\Omega}\right]G^{r,\dot{0}}(\mathbf{k},n,\Omega)=0 \tag{2.46}$$

The dependence on physical quantities of both expressions 2.45 and 2.46 is the same as obtained by Mahan in Ref. [111] for the case of the homogeneous electron gas, even though the quantities are calculated in a different way and we have had to neglect additional terms in $\mathbf{A}$. At first order in the electric field we simply obtain:

$$G^r(\mathbf{k},n,\Omega)=\frac{1}{\Omega-\epsilon^0_{n\mathbf{k}}-\Sigma^r(\mathbf{k},n,\Omega)} \tag{2.47}$$

Eq. 2.47 consistently solves also Eq. 2.46. In the next subsection we will take care of the expression of the self-energy.

2.3 Self Energy

The formalism for Feynmann diagrams in non-equilibrium theory is the same as the equilibrium one, with an additional summation over matrix indexes (see Rammer [116]). The matrix elements of specific Green's functions can be recovered with the Langreth rules. At equilibrium, the Fan-Migdal self energy can be expressed in the space-time coordinates as [78]:

$$\Sigma^{FM}(12)=\int d(34)G(13)\Gamma(324)W_{ph}(41^+) \tag{2.48}$$

where $3=(\mathbf{r_3},t_3)$ and so on; the expression for W_{ph} is, in the static approximation for the dielectric response function:

$$W_{ph}(12)=\sum_{\lambda,\lambda',\mathbf{q}} g^*(\mathbf{r}_2,\mathbf{q},\lambda)D(\mathbf{q},\lambda,\lambda',t_1,t_2)g(\mathbf{r}_2,\mathbf{q},\lambda) \tag{2.49}$$

[2] This task may be attempted in form of a power expansion in the U matrices, and this may lead to a BTE including quantum corrections in terms of Berry curvature (see Ref. [118]).

where $g(\mathbf{r},\mathbf{q},\nu)$ is defined as in [78] and D is the phonon propagator. We will also assume that the phonon propagator is the adiabatic one, to have:

$$W_{ph}(12) = \sum_{\lambda,\mathbf{q}} g^*(\mathbf{r}_2,\mathbf{q},\lambda) D(\mathbf{q},\lambda,t_1-t_2) g(\mathbf{r}_2,\mathbf{q},\lambda). \tag{2.50}$$

We will consider the case where no vertex approximations are present, so that $\Gamma(324) = \delta(32)\delta(24)$. In non equilibrium theory, we apply the Langreth rules [119] to obtain:

$$\begin{aligned}
&\Sigma^{FM,r}(12) = iG^r(12)W^<_{ph}(21) + iG^<(12)W^a_{ph}(21) = \\
&= iG^r(12)W^>_{ph}(12) + iG^<(12)W^r_{ph}(12) &(2.51)\\
&\Sigma^{FM,<}(12) = iG^<(12)W^>_{ph}(21) = iG^<(12)W^<_{ph}(21) &(2.52)\\
&\Sigma^{FM,>}(12) = iG^>(12)W^<_{ph}(21) = iG^>(12)W^>_{ph}(21) &(2.53)
\end{aligned}$$

The expression for the phonon adiabatic propagators are usually taken in the non interacting approximation (also the phonon population will always be considered the equilibrium one):

$$\begin{aligned}
D^<(\mathbf{q},\lambda,t) &= -i\left[(n_{\lambda\mathbf{q}}+1)e^{i\omega_{\lambda\mathbf{q}}t} + n_{\lambda\mathbf{q}}e^{-i\omega_{\lambda\mathbf{q}}t}\right] &(2.54)\\
D^>(\mathbf{q},\lambda,t) &= -i\left[(n_{\lambda\mathbf{q}}+1)e^{-i\omega_{\lambda\mathbf{q}}t} + n_{\lambda\mathbf{q}}e^{i\omega_{\lambda\mathbf{q}}t}\right] &(2.55)\\
D^r(\mathbf{q},\lambda,t) &= -i\left\{\theta(t)[e^{-i\omega_{\lambda\mathbf{q}}t} - e^{i\omega_{\lambda\mathbf{q}}t}]\right\} &(2.56)
\end{aligned}$$

Using the above expression and Eq. 2.53 and transforming into the frequency domain we obtain:

$$\begin{aligned}
&\Sigma^{FM,<}(\mathbf{r},\mathbf{r}',\omega) = \sum_{\lambda,\mathbf{q}} [G^<(\mathbf{r},\mathbf{r}',\omega+\omega_{\lambda\mathbf{q}})(n_{\lambda\mathbf{q}}+1) + G^<(\mathbf{r},\mathbf{r}',\omega-\omega_{\lambda\mathbf{q}})n_{\lambda\mathbf{q}}] \times \\
&\times g^*(\mathbf{r}_2,\mathbf{q},\lambda) g(\mathbf{r}_1,\mathbf{q},\lambda) &(2.57)
\end{aligned}$$

Taking matrix elements between Bloch functions we have:

$$\begin{aligned}
&\Sigma^{FM,<}(\mathbf{k},n,\omega) = \sum_{\substack{\lambda\mathbf{q}\\ n^1}} |g^\lambda_{n^1\mathbf{k}+\mathbf{q},n\mathbf{k}}|^2 \times \\
&\times \left[G^<(\mathbf{k}+\mathbf{q},n^1,\omega+\omega_{\lambda\mathbf{q}})(n_{\lambda\mathbf{q}}+1) + G^<(\mathbf{k}+\mathbf{q},n^1,\omega-\omega_{\lambda\mathbf{q}})n_{\lambda\mathbf{q}}\right]. &(2.58)
\end{aligned}$$

where we have used that:

$$g_{nn^1}(\mathbf{k},\mathbf{k^1},\mathbf{q},\lambda) = \int_{-\infty}^{+\infty} d\mathbf{r}_1 \Psi_{\mathbf{k},n}(\mathbf{r}_1)\Psi^*_{\mathbf{k^1},n^1}(\mathbf{r}_1) g(\mathbf{r_1},\mathbf{q},\lambda) =$$
$$\int_{-\infty}^{+\infty} d\mathbf{r}_1 \Psi_{\mathbf{k},n}(\mathbf{r}_1)\Psi^*_{\mathbf{k+q},n^1}(\mathbf{r}_1) g(\mathbf{r_1},\mathbf{q},\lambda) = g^{\lambda}_{n^1\mathbf{k+q},n\mathbf{k}} \tag{2.59}$$
$$g^*_{nn^1}(\mathbf{k},\mathbf{k^2},\mathbf{q},\lambda) = \int_{-\infty}^{+\infty} d\mathbf{r}_1 \Psi^*_{\mathbf{k},n}(\mathbf{r}_2)\Psi_{\mathbf{k^2},n^1}(\mathbf{r}_2) g^*(\mathbf{r_2},\mathbf{q},\lambda) =$$
$$\int_{-\infty}^{+\infty} d\mathbf{r}_1 \Psi^*_{\mathbf{k},n}(\mathbf{r}_2)\Psi_{\mathbf{k+q},n^1}(\mathbf{r}_2) g^*(\mathbf{r_2},\mathbf{q},\lambda) = g^{\lambda,*}_{n^1\mathbf{k+q},n\mathbf{k}} \tag{2.60}$$

We have therefore used momentum selection rules and the fact that the Green's function is assumed diagonal in the band index, so that $n^1 = n^2$. A similar expression is obtained for $\Sigma^>$:

$$\Sigma^{FM,>}(\mathbf{k},n,\omega) = \sum_{\substack{\lambda\mathbf{q}\\ n^1}} |g^{\lambda}_{n^1\mathbf{k+q},n\mathbf{k}}|^2 \times$$
$$\times \left[G^>(\mathbf{k}+\mathbf{q},n^1,\omega-\omega_{\lambda\mathbf{q}})(n_{\lambda\mathbf{q}}+1) + G^>(\mathbf{k}+\mathbf{q},n^1,\omega+\omega_{\lambda\mathbf{q}})n_{\lambda\mathbf{q}}\right]. \tag{2.61}$$

We can perform the same procedures for Σ^r; using the following formula:

$$\theta(t)f(t) \to \frac{f(\omega)}{2} + \frac{i}{2\pi}\int_{-\infty}^{\infty} \frac{f(\omega-\omega')}{\omega'} d\omega' \tag{2.62}$$

which is valid when the time transform has the sign as in Eq. 2.41, one can show that:

$$\Sigma^{FM,r}_{nn^1}(\mathbf{k},n,\omega) =$$
$$\sum_{\substack{\lambda\mathbf{q}\\ n^1}} |g^{\lambda}_{n^1\mathbf{k+q},n\mathbf{k}}|^2 \Big\{ \left[G^r(\mathbf{k}+\mathbf{q},n^1,\omega-\omega_{\lambda\mathbf{q}})(n_{\lambda\mathbf{q}}+1) + G^r(\mathbf{k}+\mathbf{q},n^1,\omega+\omega_{\lambda\mathbf{q}})n_{\lambda\mathbf{q}}\right] +$$
$$+ \frac{1}{2}\left[G^<(\mathbf{k}+\mathbf{q},n^1,\omega-\omega_{\lambda\mathbf{q}}) - G^<(\mathbf{k}+\mathbf{q},n^1,\omega+\omega_{\lambda\mathbf{q}})\right] +$$
$$+ \frac{i}{2\pi}\int_{-\infty}^{\infty} d\omega' \left[\frac{G^<(\mathbf{k}+\mathbf{q},n^1,\omega')}{\omega'-\omega+\omega_{\lambda\mathbf{q}}} - \frac{G^<(\mathbf{k}+\mathbf{q},n^1,\omega')}{\omega'-\omega-\omega_{\lambda\mathbf{q}}}\right] \Big\} \tag{2.63}$$

We can check how Eq. 2.63 is evaluated at equilibrium. Using:

$$\frac{1}{x-x_0+i\eta} = P\frac{1}{x-x_0} - i\pi\delta(x-x_0) \tag{2.64}$$

where P is the Cauchy principal value, and the expression for the Green's functions for non interacting particles we obtain:

$$\Sigma^{FM,r}_{nn^1}(\mathbf{k},n,\omega)=\sum_{\substack{\lambda\mathbf{q}\\ n^1}}|g^{\lambda}_{n^1\mathbf{k}+\mathbf{q},n\mathbf{k}}|^2\left[\frac{(n_{\lambda\mathbf{q}}+1-f_{n^1\mathbf{k}+\mathbf{q}})}{\omega-\epsilon^0_{n^1\mathbf{k}+\mathbf{q}}-\omega_{\lambda\mathbf{q}}+i\eta}+\frac{(n_{\lambda\mathbf{q}}+f_{n^1\mathbf{k}+\mathbf{q}})}{\omega-\epsilon^0_{n^1\mathbf{k}+\mathbf{q}}+\omega_{\lambda\mathbf{q}}+i\eta}\right] \tag{2.65}$$

which is formally equal to Eq. (55) of Ref. [111] and Eq. (157) of Ref. [78].

2.4 Lesser Green's function kinetic equation

We have the first two set of equations 2.45 and 2.63, which are equation to be solved coherently at first order in the electric field. These equations involve ^{r} and $^<$ quantities; our hope is that also the equation for $G^<$ involve only ^{r} and $^<$ quantities, so that this system of equation can be solved consistently.

As done for G^r we can try to start from equations Eq. 2.17 and Eq. 2.18 to obtain the evolution equation for the lesser Green's function. With the same kind of manipulations it can be shown that the equation for the $G^<$ in the momentum space can be written as:

$$\begin{aligned}&ie\mathbf{E}\cdot\left[(1-\frac{\partial\mathrm{Re}\Sigma^{r,\dot{0}}(\mathbf{k},n,\Omega)}{\partial\Omega})\nabla_{\mathbf{k}}+\nabla_{\mathbf{k}}(\epsilon^0_{n\mathbf{k}}+\mathrm{Re}\Sigma^{r,\dot{0}}(\mathbf{k},n,\Omega))\frac{\partial}{\partial\Omega}\right]G^{<,\dot{0}}(\mathbf{k},n,\Omega)+\\&-ie\mathbf{E}\cdot\left[\frac{\partial\Sigma^{<,\dot{0}}(\mathbf{k},n,\Omega)}{\partial\Omega}\nabla_{\mathbf{k}}\mathrm{Re}G^{r,\dot{0}}(\mathbf{k},n,\Omega)-\frac{\partial\mathrm{Re}G^{r,\dot{0}}(\mathbf{k},n,\Omega)}{\partial\Omega}\nabla_{\mathbf{k}}\Sigma^{<,\dot{0}}(\mathbf{k},n,\Omega)\right]=\\&\Sigma^{>}(\mathbf{k},n,\Omega)G^{<}(\mathbf{k},n,\Omega)-\Sigma^{<}(\mathbf{k},n,\Omega)G^{>}(\mathbf{k},n,\Omega)\end{aligned} \tag{2.66}$$

where we have used $G^t-G^{\bar{t}}=2\mathrm{Re}G^r$, $\Sigma^t-\Sigma^{\bar{t}}=2\mathrm{Re}\Sigma^r$, $G^t+G^{\bar{t}}=G^<+G^>$ and $\Sigma^t+\Sigma^{\bar{t}}=\Sigma^<+\Sigma^>$ to obtain the above formula. No terms have been neglected other then $\nabla_{\frac{\mathbf{R}+\mathbf{R}'}{2}}$, $\frac{\partial}{\partial\frac{t+t'}{2}}$ and second order terms in the electric field as done for the retarded equation; we further supposed that the Green's functions are always diagonal in the band index and coherently neglected terms in $\mathbf{A}$. We see that in order to solve for $G^<$ at first order in $\mathbf{E}$ we just need the equilibrium retarded Green's function given by the field independent term of Eq. 2.47. Substituting all the quantities with the correct field

order we obtain:

$$
\begin{aligned}
&- A^{\dot{0}}(\mathbf{k},n,\Omega)\frac{\partial f(\Omega)}{\partial\Omega}e\mathbf{E}\cdot\left\{\left[\nabla_{\mathbf{k}}\left(\epsilon^{0}_{n\mathbf{k}}+\mathrm{Re}\Sigma^{r,\dot{0}}(\mathbf{k},n,\Omega)\right)\right]\Gamma^{\dot{0}}(\mathbf{k},n,\Omega)+\right.\\
&\left.+\left(\Omega-\epsilon^{0}_{\mathbf{k}n}-\mathrm{Re}\Sigma^{r,\dot{0}}(\mathbf{k},n,\Omega)\right)\nabla_{\mathbf{k}}\Gamma^{\dot{0}}(\mathbf{k},n,\Omega)\right\}=\\
&\Sigma^{>}(\mathbf{k},n,\Omega)G^{<}(\mathbf{k},n,\Omega)-\Sigma^{<}(\mathbf{k},n,\Omega)G^{>}(\mathbf{k},n,\Omega)
\end{aligned}
\tag{2.67}
$$

where we have used that $G^{<,\dot{0}}(\mathbf{k},n,\Omega) = iA^{\dot{0}}(\mathbf{k},n,\Omega)f(\Omega)$ where $A^{\dot{0}}(\mathbf{k},n,\Omega) := i(G^{>,\dot{0}}-G^{<,\dot{0}}) = -2\mathrm{Im}G^{r,\dot{0}}(\mathbf{k},n,\Omega)$ is the spectral functions and $\Gamma^{\dot{0}}(\mathbf{k},n,\Omega) := \frac{i}{2}(\Sigma^{>,\dot{0}}-\Sigma^{<,\dot{0}}) = -\mathrm{Im}\Sigma^{r,\dot{0}}(\mathbf{k},n,\Omega)$ is the linewidth. The following relations hold between the spectral function and the relaxation time (it is worthwhile to stress that they are correct only at equilibrium and when vertex corrections are neglected):

$$
A^{\dot{0}}(\mathbf{k},n,\Omega)=\frac{2\Gamma^{\dot{0}}(\mathbf{k},n,\Omega)}{\Gamma^{\dot{0},2}(\mathbf{k},n,\Omega)+\left(\Omega-\epsilon^{0}_{n\mathbf{k}}-\mathrm{Re}\Sigma^{r,\dot{0}}(\mathbf{k},n,\Omega)\right)^{2}}
\tag{2.68}
$$

$$
\begin{aligned}
\Gamma^{\dot{0}}(\mathbf{k},n,\Omega)=\frac{1}{2}\sum_{\substack{\lambda\mathbf{q}\\ n^{1}}}|g^{\lambda}_{n^{1}\mathbf{k}+\mathbf{q},n\mathbf{k}}|^{2}\big[&\left(n_{\lambda\mathbf{q}}+1-f(\Omega-\omega_{\lambda\mathbf{q}})\right)A^{\dot{0}}(\mathbf{k}+\mathbf{q},n^{1},\Omega-\omega_{\lambda\mathbf{q}})+\\
&\left(n_{\lambda\mathbf{q}}+f(\Omega+\omega_{\lambda\mathbf{q}})\right)A^{\dot{0}}(\mathbf{k}+\mathbf{q},n^{1},\Omega+\omega_{\lambda\mathbf{q}})\big]
\end{aligned}
\tag{2.69}
$$

where Eq. 2.68 follows from the definitions of A and Γ whereas Eq. 2.69 follows from Eq. 2.63.

We now expand the lesser Green's functions around the equilibrium value as:

$$
G^{<}(\mathbf{k},n,\Omega)=iA^{\dot{0}}(\mathbf{k},n,\Omega)\left[f(\Omega)-\frac{\partial f(\Omega)}{\partial\Omega}\Lambda(\mathbf{k},n,\Omega)\right]
\tag{2.70}
$$

where Λ is linear in the external electric field. The expression for $G^{>}$ can be deduced from:

$$
G^{>}(\mathbf{k},n,\Omega)-G^{<}(\mathbf{k},n,\Omega)=2i\mathrm{Im}G^{r}(\mathbf{k},n,\Omega)=-iA(\mathbf{k},n,\Omega)
\tag{2.71}
$$

We finally obtain the Quantum Boltzmann Transport Equation (QBTE):

$$\mathbf{E}A^{\dot{0}}(\mathbf{k},n,\Omega)\cdot\mathbf{\Phi}\frac{\partial f(\Omega)}{\partial\Omega}=2\frac{\partial f(\Omega)}{\partial\Omega}\Gamma^{\dot{0}}(\mathbf{k},n,\Omega)\Lambda(\mathbf{k},n,\Omega)-\sum_{\substack{\lambda\mathbf{q}\\n^1}}|g^{\nu}_{n^1\mathbf{k}+\mathbf{q},n\mathbf{k}}|^2\frac{\partial f(\Omega)}{\partial\Omega}\times$$
$$\times\Big[\left(n_{\lambda\mathbf{q}}+1-f(\Omega-\omega_{\lambda\mathbf{q}})\right)A^{\dot{0}}(\mathbf{k}+\mathbf{q},n^1,\Omega-\omega_{\lambda\mathbf{q}})\Lambda(\mathbf{k}+\mathbf{q},n^1,\Omega-\omega_{\lambda\mathbf{q}})+$$
$$\left(n_{\lambda\mathbf{q}}+f(\Omega+\omega_{\lambda\mathbf{q}})\right)A^{\dot{0}}(\mathbf{k}+\mathbf{q},n^1,\Omega+\omega_{\lambda\mathbf{q}})\Lambda(\mathbf{k}+\mathbf{q},n^1,\Omega+\omega_{\lambda\mathbf{q}})\Big]$$
$$\Phi(\mathbf{k},n,\Omega)=\mathbf{v}^{\dot{0}}(\mathbf{k},n,\Omega)\Gamma^{\dot{0}}(\mathbf{k},n,\Omega)+\left(\Omega-\epsilon^0_{n\mathbf{k}}-\mathrm{Re}\Sigma^{r,\dot{0}}(\mathbf{k},n,\Omega)\right)\nabla_{\mathbf{k}}\Gamma^{\dot{0}}(\mathbf{k},n,\Omega)) \tag{2.72}$$

$$\mathbf{v}^{\dot{0}}(\mathbf{k},n,\Omega)=\nabla_{\mathbf{k}}\left(\epsilon^0_{n\mathbf{k}}+\mathrm{Re}\Sigma^{r,\dot{0}}(\mathbf{k},n,\Omega)\right) \tag{2.73}$$

where we have simplified a term $A^{\dot{0}}$ from both sides of the equation and used the following relations:

$$\begin{aligned}\frac{\partial f(\Omega+\omega_{\nu\mathbf{q}})}{\partial\Omega}[n_{\nu\mathbf{q}}+1-f(\Omega)]&=\frac{\partial f(\Omega)}{\partial\Omega}[n_{\nu\mathbf{q}}+f(\Omega+\omega_{\nu\mathbf{q}})]\\ \frac{\partial f(\Omega-\omega_{\nu\mathbf{q}})}{\partial\Omega}[n_{\nu\mathbf{q}}+f(\Omega)]&=\frac{\partial f(\Omega)}{\partial\Omega}[n_{\nu\mathbf{q}}+1-f(\Omega-\omega_{\nu\mathbf{q}})]\end{aligned} \tag{2.74}$$

To solve Eq. 2.72, one has to find the spectral function from the retarded Green's function at equilibrium; then one solves the equation with respect to Λ and reconstruct $G^<$, from which the current may be expressed as explained in App. D.

2.5 Semi-classical limit and BTE

In the previous sections we have derived the evolution equations for the Green's functions in presence of a small dc electric field, at leading order in the electron phonon coupling. These equations, under some simplifying hypotheses, give birth to the full QBTE of Eq. 2.72, which is an equation in the unknown $\Lambda(\mathbf{k},n,\Omega)$; its basic ingredients are the DFT and DFTP electronic energies and vibrational frequencies, the interacting spectral function, linewidth and self-energy, and the statistical weights of electrons and phonons. In principle, Eq. 2.72 can be solved for each $(\mathbf{k},n,\Omega)$. In practice, this is too hard to be done. In this section, we try to find the semi-classical limit to Eq. 2.72, i.e. the BTE presented in Chap. 1, which is less complicated to solve. The semi-classical limit consists in taking $\Gamma^{\dot{0}}\to 0$ (i.e. in the case of particle

with long enough lifetimes), for which we have:

$$A^{\dot{0}}(\mathbf{k},n,\Omega) \approx 2\pi\delta(\epsilon^0_{n\mathbf{k}} + Re\Sigma^{r,\dot{0}}(\mathbf{k},n,\Omega) - \Omega) \tag{2.75}$$

$$\Gamma^{\dot{0}}(\mathbf{k},n,\Omega) \approx \pi \sum_{\substack{\lambda\mathbf{q}\\ n^1}} |g^{\lambda}_{n^1\mathbf{k}+\mathbf{q},n\mathbf{k}}|^2 \big[\left(n_{\lambda\mathbf{q}} + 1 - f(\Omega - \omega_{\lambda\mathbf{q}})\right) \delta(\epsilon^0_{n^1\mathbf{k}+\mathbf{q}} - (\Omega - \omega_{\lambda\mathbf{q}})) +$$
$$\left(n_{\lambda\mathbf{q}} + f(\Omega + \omega_{\lambda\mathbf{q}})\right) \delta(\epsilon^0_{n^1\mathbf{k}+\mathbf{q}} - (\Omega + \omega_{\lambda\mathbf{q},}))\big] \tag{2.76}$$

Of course, the above equations are inconsistent, since the $\Gamma^{\dot{0}}$ coming from Eq. 2.76 is clearly finite. Nonetheless, they can be used whenever the dependence on Ω of the quantities entering the QBTE is smooth on a scale larger than $\Gamma^{\dot{0}}$.

The semi-classical limit of the QBTE of Eq. 2.72 is:

$$\mathbf{E}\cdot\mathbf{\Phi} = 2\Gamma^{\dot{0}}(\mathbf{k},n,\Omega)\Lambda(\mathbf{k},n,\Omega) - \sum_{\substack{\lambda\mathbf{q}\\ n^1}} |g^{\lambda}_{n^1\mathbf{k}+\mathbf{q},n\mathbf{k}}|^2 \times$$
$$\big[\left(n_{\lambda\mathbf{q}} + 1 - f(\Omega - \omega_{\lambda\mathbf{q}})\right) \delta^- \Lambda(\mathbf{k}+\mathbf{q}, n^1, \Omega - \omega_{\lambda\mathbf{q}}) +$$
$$\left(n_{\lambda\mathbf{q}} + f(\Omega + \omega_{\lambda\mathbf{q}})\right) \delta^+ \Lambda(\mathbf{k}+\mathbf{q}, n^1, \Omega + \omega_{\lambda\mathbf{q}})\big] \tag{2.77}$$

$$\delta^- = \delta(\epsilon^0_{n^1\mathbf{k}+\mathbf{q}} + \mathrm{Re}\Sigma^{r,\dot{0}}(\mathbf{k}+\mathbf{q}, n^1, \Omega - \omega_{\lambda\mathbf{q}})) - (\Omega - \omega_{\lambda\mathbf{q}})) \tag{2.78}$$

$$\delta^+ = \delta(\epsilon^0_{n^1\mathbf{k}+\mathbf{q}} + \mathrm{Re}\Sigma^{r,\dot{0}}(\mathbf{k}+\mathbf{q}, n^1, \Omega + \omega_{\lambda\mathbf{q}})) - (\Omega + \omega_{\lambda\mathbf{q}})) \tag{2.79}$$

$$\Phi(\mathbf{k},n,\Omega) = \mathbf{v}^{\dot{0}}(\mathbf{k},n,\Omega)\delta(\epsilon^0_{n\mathbf{k}} + \mathrm{Re}\Sigma^{r,\dot{0}}(\mathbf{k},n,\Omega) - \Omega). \tag{2.80}$$

Now we integrate both members with respect to Ω. The conditions to have non trivial solutions are:

$$\epsilon^0_{n\mathbf{k}} + \mathrm{Re}\Sigma^{r,\dot{0}}(\mathbf{k},n,\Omega) - \Omega = 0 \tag{2.81}$$

$$\epsilon^0_{n^1\mathbf{k}+\mathbf{q}} + \mathrm{Re}\Sigma^{r,\dot{0}}(\mathbf{k}+\mathbf{q}, n^1, \Omega - \omega_{\lambda\mathbf{q}}) - (\Omega - \omega_{\lambda\mathbf{q}}) = 0 \tag{2.82}$$

$$\epsilon^0_{n^1\mathbf{k}+\mathbf{q}} + \mathrm{Re}\Sigma^{r,\dot{0}}(\mathbf{k}+\mathbf{q}, n^1, \Omega + \omega_{\lambda\mathbf{q}}) - (\Omega + \omega_{\lambda\mathbf{q}}) = 0 \tag{2.83}$$

where the first condition can be used to isolate Ω and insert it in the other conditions. After this integration, an expression equivalent to Eq. 1.58 is reached, if one further discards the real part of the retarded self energy. In order to get the equivalence, one has to use that $\frac{1}{\tau^0} := \frac{1}{\tau^{SERTA}} = -2\mathrm{Im}\Sigma^{r,\dot{0}} = 2\Gamma^{\dot{0}}$, to identify $\Lambda(\mathbf{k},n,\epsilon^0_{n\mathbf{k}}) = \chi_{n\mathbf{k}}$, to

multiply both members by $-\frac{\partial f_{n\mathbf{k}}}{\partial \epsilon^0_{n\mathbf{k}}}$ and use:

$$(1+n_{\lambda\mathbf{q}}-f_{m\mathbf{k}+\mathbf{q}})f_{n\mathbf{k}}(1-f_{m\mathbf{k}})\delta(\epsilon^0_{n\mathbf{k}}-\epsilon^0_{m\mathbf{k}+\mathbf{q}}-\hbar\omega_{\lambda\mathbf{q}})= \tag{2.84}$$

$$=f_{n\mathbf{k}}(1-f_{m\mathbf{k}+\mathbf{q}})(n_{\lambda\mathbf{q}}+1)\delta(\epsilon^0_{n\mathbf{k}}-\epsilon^0_{m\mathbf{k}+\mathbf{q}}-\hbar\omega_{\lambda\mathbf{q}}) \tag{2.85}$$

$$(n_{\lambda\mathbf{q}}+f_{m\mathbf{k}+\mathbf{q}})f_{n\mathbf{k}}(1-f_{n\mathbf{k}})\delta(\epsilon^0_{n\mathbf{k}}-\epsilon^0_{m\mathbf{k}+\mathbf{q}}+\hbar\omega_{\lambda\mathbf{q}})= \tag{2.86}$$

$$=f_{n\mathbf{k}}(1-f_{n\mathbf{k}+\mathbf{q}})n_{\lambda\mathbf{q}}\delta(\epsilon^0_{n\mathbf{k}}-\epsilon^0_{m\mathbf{k}+\mathbf{q}}+\hbar\omega_{\lambda\mathbf{q}}) \tag{2.87}$$

and finally use the symmetry of the Π matrix of Eq. 1.58.

If one does not want to disregard $\mathrm{Re}\Sigma^{r,\dot{0}}$, one has to remember the following property:

$$\delta(\epsilon^0_{n\mathbf{k}}+\mathrm{Re}\Sigma^{r,\dot{0}}(\mathbf{k},n,\Omega)-\Omega)=\sum_i\frac{\delta(\Omega-\Omega_i)}{|1-\frac{\partial \mathrm{Re}\Sigma^{r,\dot{0}}(\mathbf{k},n,\Omega)}{\partial\Omega}|_{\Omega_i}}= \sum_i Z_i\delta(\Omega-\Omega_i) \tag{2.88}$$

where Ω_i are the solutions of Eq. 2.81, and Z_i are the so-called quasi-particle weights, which determine to which extent the quasi-particles are behaving as true particles. The same relation holds for Eqs. 2.82 and 2.83. This is a new feature coming from the semi-classical limit of the QBTE that enriches the kinetic picture of the BTE, and may be needed to describe conductivity in materials where the EPC interaction is particularly strong, so that Z_i is less than 1 by a significant amount.

Disregarding the real part of the self-energy we can write:

$$G^<(\mathbf{k},n,\Omega)=i\delta(\epsilon^0_{n\mathbf{k}}-\Omega)\big[f(\Omega)-\frac{\partial f(\Omega)}{\partial\Omega}\Lambda(\mathbf{k},n,\Omega)\big] \tag{2.89}$$

For homogeneous gas, the expression for the current following from transforming the electronic coordinates of Eq. 2.23 in Wigner coordinates would be [111]:

$$\mathbf{J}_e=\sum_n\int d^3k\frac{\mathbf{k}}{m_e}\int d\Omega G^<(\mathbf{k},n,\Omega) \tag{2.90}$$

Since for crystals the Wigner transformation has been done with respect to Wannier coordinates instead of electron ones, the generalization of the current expression from which we can then determine the conductivity tensor is:

$$\mathbf{J}_e=\sum_n\int d^3k\mathbf{v}_{n\mathbf{k}}\int d\Omega G^<(\mathbf{k},n,\Omega) \tag{2.91}$$

Eq. 2.91 is more formally justified in App. D.

Up to now we have just considered the case of a dc electric field. For a more generalized treatment of the case with an electromagnetic field, we refer to Ref. [11], where it is shown how gauge invariance can be treated via the introduction of modified Wannier functions that keep track of the Peierl's phase; the final BTE equation is still in the form of Eq. 1.58.

Finally, we compare the method presented in this chapter with the K-G approach presented in Chap. 1. The main difference between these two methods is that the K-G formula only deals with equilibrium quantities. Nonetheless, since we neglected initial correlations for NEGFs and we considered only times in the far future with respect to the external field appearance (and therefore we cannot access transients), the two approaches should be equivalent. Indeed, both of them bring to the same semi-classical Boltzmann equation.

Chapter 3

Magnetotransport phenomena in p-doped diamond

The first system that we investigate in this thesis is bulk p-doped diamond. As mentioned in the introduction, the theoretical interest on this system arises from the lack of a detailed understanding of its electrical transport properties. In particular, the value of its hole mobility is not known in details, neither experimentally nor theoretically; a broad range of values is present in literature and there is no consensus on the value of the intrinsically phonon-limited mobility. Moreover, the understanding of the precise contributions of different scattering mechanisms to transport properties in different temperature and doping regimes is missing. Another source of uncertainty is given by the relation between the drift and Hall mobilities; here, the knowledge of the Hall scattering factor is of crucial importance. The theoretical interest to study p-doped diamond also steams from the very large increase of the Seebeck coefficient value at low temperatures; this effect, which is way larger than in silicon, is due to the exceptional phonon-drag effect arising from the coupling of the electronic and vibrational systems. This is a consequence of the extraordinarily high thermal conductivity of diamond, which in turn follows from the very large out of equilibrium phonon populations. These populations couple to the electronic degrees of freedom and generate a drag effect which enhances the response of the compound to a thermal gradient.

In this chapter we will first start from the solution of the phonon BTE, which can be studied independently from the electronic BTE as the electron-phonon coupling term of Eq. 1.47 can be neglected (the low doping concentrations studied in this work allows us to do so). We will here compute the out of equilibrium phonon populations and the related thermal conductivity via the use of pre-existing codes (as explained below), and compare with experiments. Then, we will solve the complete electron BTE of Eq. 1.58, via the use of a massively parallelized in-house built code, in absence and presence of a magnetic field to deduce the conductivity tensor (and the related carrier

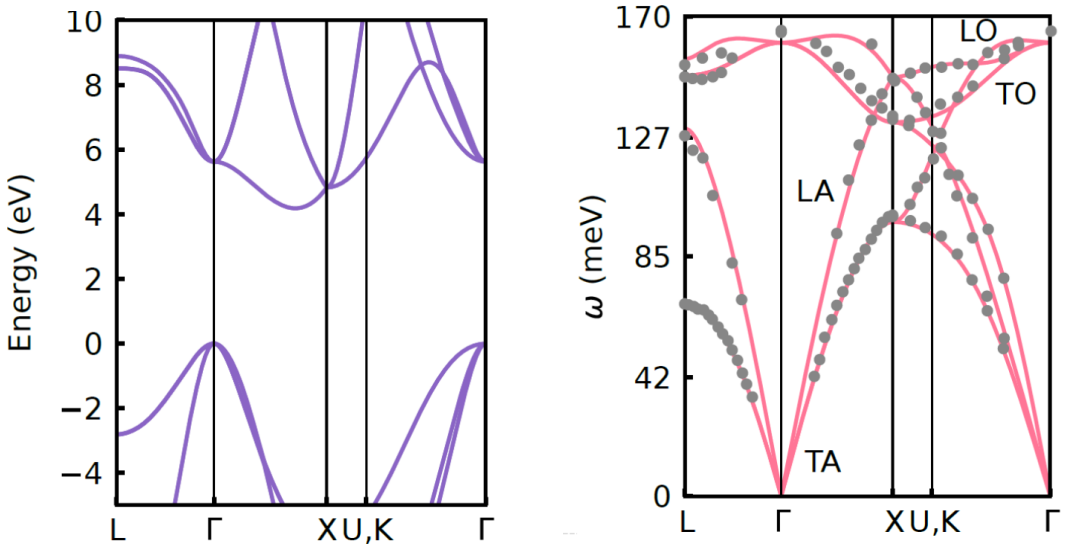

(a) **(b)**

Figure 3.1: (a) Electronic structure and (b) phonon dispersion of diamond crystal along high-symmetry lines; the grey dots are experimental neutron scattering data [120] .

mobility), the Seebeck coefficient, the Hall scattering factor, the magnetoresistance and the magneto-Seebeck coefficient. This will give us a complete description of the thermomagnetic phenomena in p-doped diamond.

3.1 Thermal conductivity

Diamond is a cubic crystal with a lattice parameter $a = 3.52$ Ang. To simulate its properties, we use DFT as implemented in QUANTUM ESPRESSO [66] within the local density approximation (LDA) [121]. We use a norm-conserving pseudopotential, a plane-wave expansion up to a 60 Ry cutoff and a BZ sampling with a $24 \times 24 \times 24$ Monkhorst-Pack mesh. The primitive cell of the crystal is described via the direct lattice vectors $\mathbf{v}_1 = (a/2)(-1, 0, 1)$, $\mathbf{v}_2 = (a/2)(0, 1, 1)$ and $\mathbf{v}_3 = (a/2)(-1, 1, 0)$. The electronic and phonon properties are summarized in Figs. 3.1a and 3.1b.
For cubic systems the thermal conductivity tensor k^{th}_{ij} is diagonal and can thus be represented by a single scalar quantity k^{th}. If we suppose that the thermal gradient in the medium is along the $\hat{x}$ direction, its expression reads as in Eq. 1.56. In order to calculate k^{th} we thus need to solve equation 1.53 to determine the out of equilibrium populations $\tilde{f}_{\lambda\mathbf{q}}$. To do this, we use the codes D3Q [27] (for the calculation of the P-scattering matrices) and THERMAL2 [25] (for the solution of the Boltzmann equation) that are part of QUANTUM ESPRESSO [66], together with in-house built post-processing tools; THERMAL2 implements a CG algorithm for the exact solution

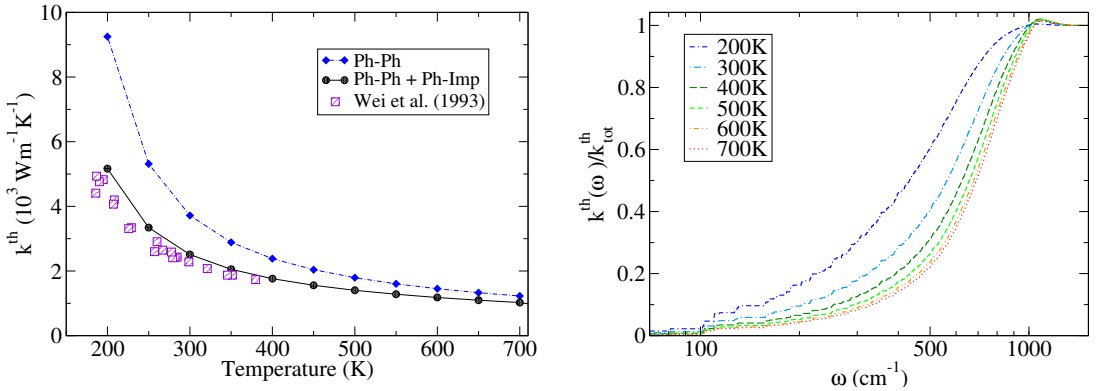

Figure 3.2: (a) Thermal conductivity for diamond crystal considering anharmonic phonon-phonon scattering only (blue diamonds) and phonon-phonon and isotopic scattering (black circles), compared with experimental data from [122] (violet squares); (b) Cumulative contribution of phonons at different frequencies to the diamond thermal conductivity, at different temperatures, when phonon-phonon scattering is the only source of scattering.

of equation 1.53; an exact solution is necessary for diamond because the SMA approximation leads to severely underestimated values of the thermal conductivity [25]. We obtain the out of equilibrium phonon populations $\tilde{f}_{\lambda\mathbf{q}}$ on a $30 \times 30 \times 30$ uniform $\mathbf{q}$-point mesh, for a range of temperatures going from 200K to 700K, and then calculate the thermal conductivity k^{th}. For all the calculation we use a Gaussian broadening of 10cm^{-1}. The calculation takes, per each temperature, around 48 hours on 600 processors on a Tier-1 supercomputing facility as ARCHER.

The calculated values of the thermal conductivity at different temperatures are presented in Fig. 3.2a. We first consider the phonon-phonon interaction as the only source of scattering, and see that the thermal conductivity is overestimated especially at low temperatures. Then, we take in account also isotopic scattering (with a natural concentration of impurities), modelled as in Ref. [25]. This inclusion reduces the thermal conductivity by a substantial factor at low temperatures, bringing it nearer to the experimental values.

It is interesting to analyse the cumulative contributions of different phonon frequencies to the thermal conductivity, at different temperatures, by means of Eq. 1.56. The result is given in Fig. 3.2b for the case where phonon-phonon scattering is the only source of scattering. Here we notice that, especially for higher temperatures, great part of the contribution comes from phonons with frequencies above 300cm^{-1}. This effect can be understood if we consider the exact numerical solution of Eq. 1.53, $\tilde{f}_{\lambda\mathbf{q}}$, for the first acoustic mode $\lambda = 1$ as a function of distance from the BZ center ($\lambda = 2, 3$ modes show the same behaviour); this is shown in Fig. 3.3a. Here we notice that the

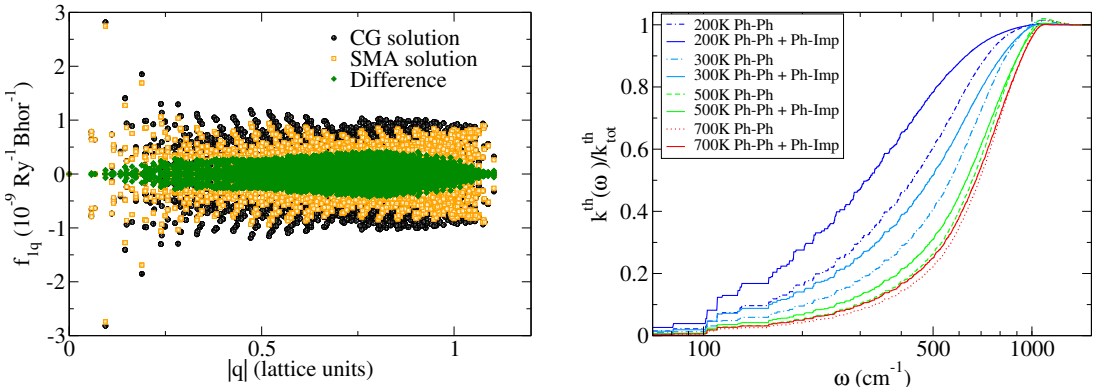

Figure 3.3: (a) $\tilde{f}_{1\mathbf{q}}$ at 300K, as a function of the distance of the $\mathbf{q}$-points from Γ (alat units), in case of exact solution (black circles) or SMA approximation (orange boxes) to Eq. 1.53; (b) Cumulative contribution of different phonons to the diamond thermal conductivity in absence (same values of Fig. 3.2b) and presence of phonon-impurity scattering.

absolute value of the solution decreases to a plateau. Since the $\mathbf{q}$-points number instead increases as $\propto q^3$, this causes the peripheral part of the BZ zone (corresponding to higher phonon frequencies) to dominate the contribution to the thermal conductivity. In Fig. 3.3b we show that when isotopic scattering is taken into account, the contribution to the thermal conductivity given by higher phonon-frequencies become less important, especially at low temperatures. This also means that the out of equilibrium populations relative to low frequency phonons are less sensitive to impurity presence and therefore their value is practically unchanged with respect to the phonon-phonon case.

As mentioned in the introduction of this thesis and in Chap. 1, the out of equilibrium populations of lattice vibrations have a crucial impact on the Seebeck coefficient of a semiconductor, especially at low temperatures. Indeed, they enter in the calculation of the phonon-drag scattering term of the electronic BTE. This term is a critical contribution to the electronic current in a crystal in presence of an external temperature gradient and thus needs to be computed very accurately. For this reason, we have to know the phonon populations on very fine $\mathbf{q}$-point meshes (up to $100 \times 100 \times 100$). Obtaining the exact solution of Eq. 1.53 on such a fine mesh is too demanding. Hence, the strategy here is to generate the exact values for the populations on a $30 \times 30 \times 30$ $\mathbf{q}$-points mesh and then linearly interpolate such values on the needed finer grid.

The major drawback of this strategy is that the diverging behaviour of the populations near Γ— evident from Fig. 3.3a—cannot be interpolated with a linear scheme; hence, we may lose some relevant information. Indeed, as we will see, the phonon-drag contribution to the Seebeck coefficient at sufficiently low temperatures (less than

350K) is highly dependent on the asymptotic behaviour of the phonon populations. To overcome this precision limit, we decide to use for the phonon population near Γ the values obtained with the SMA approximation. Our choice is motivated by the observation that, for sufficiently small $\mathbf{q}$-points, SMA or exact CG methods give very similar results near Γ— as seen from Fig. 3.3a. Our final interpolating scheme is shown in detail in Fig. 3.4a for the temperature of 200K.

To complete the discussion, we show in Fig. 3.4b the lifetimes used to calculate the SMA phonon population of Fig. 3.4a. We can clearly see the ω^2 dependence of the first acoustic branch lifetime at low frequencies. To obtain this result, it is crucial to apply the acoustic sum rules for the third order energy derivatives to the P-matrices of Eq. 1.53 in the following form [93]:

$$\sum_{ml} V^{(3)}_{\alpha\beta\gamma}(\mathbf{0}n, \mathbf{M}m, \mathbf{L}l) = 0 \tag{3.1}$$

where $V^{(3)}$ is the third derivative of the total energy with respect to displacement of atoms $n(l, m)$ in the cells $\mathbf{0}(\mathbf{M}, \mathbf{L})$ along the Cartesian coordinates $\alpha(\beta, \gamma)$. The ω^2 behaviour is coherent with the prediction of elastic theory [123] and thus indicates that our calculation contains the true asymptotic behaviour of $\tilde{f}_{\lambda\mathbf{q}}$.

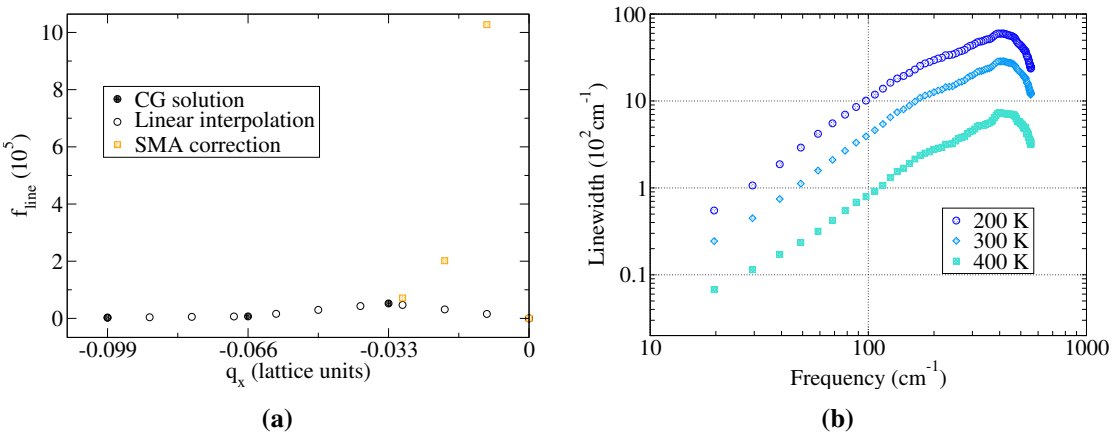

Figure 3.4: (a) Phonon out of equilibrium population at 200K on a chosen line for small $\mathbf{q}$-points, obtained by CG solution on a $30 \times 30 \times 30$ grid (black circles) linearly interpolated on a finer $100 \times 100 \times 100$ mesh (white circles) and by SMA calculation (orange squares). (b) Acoustic phonon linewidth (HWHM) as a function of phonon frequency, at different temperatures, for the first acoustic branch.

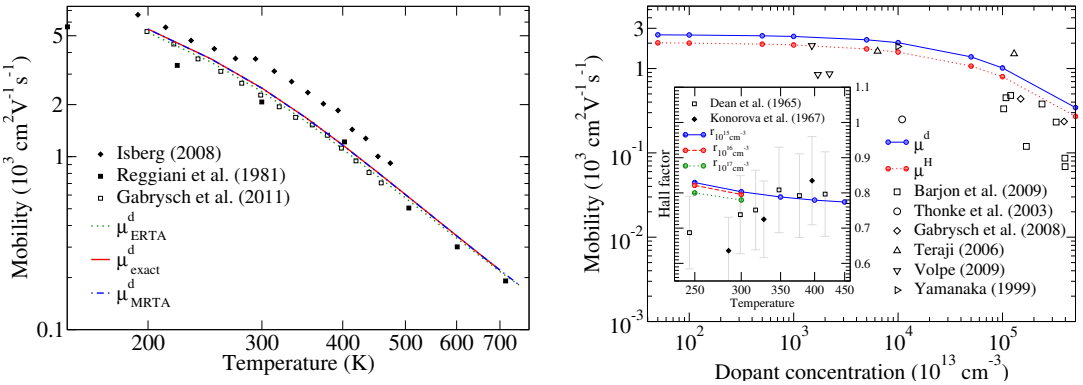

Figure 3.5: (a) Temperature dependence of hole drift mobility in p-doped diamond and comparison with approximations (ERTA and MRTA). Experimental values are from Ref. [41] (black diamonds), [45] (black squares) and [124] (white squares); (b) Doping dependence of μ^d and μ^H in p-doped diamond at 300K. Experimental data for Hall mobility taken from Ref. [125] (circles), [126] (left triangles), [127] (up triangles), [128] (diamonds), [129] (down triangles), [130] (squares). Inset: Hall scattering factor as function of temperature for Boron concentrations of 10^{15}cm^{-3} (blue circles), 10^{16}cm^{-3} (light blue circles) and 10^{17}cm^{-3} (green circles). Squares and diamonds refer to data obtained from μ^H in Refs. [131] and [132], respectively; in both cases μ^d is from Ref. [45]. An uncertainty of $\pm 15\%$ was estimated. [46]

3.2 Resistivity and mobility

Similarly to the case of thermal properties, the electric coefficients of a crystal are determined by the out of equilibrium thermodynamics of electrons or holes. For p-doped diamond, the presence of a certain density of acceptors N_A induces the presence of a well defined density of hole carriers n, which are effective carriers of positive charge that are responsible for the current flow. Amongst the electrical transport coefficients, the resistivity $\rho_{ij} = \sigma_{ij}^{-1}$ and the drift mobility $\mu^d_{ij} = \frac{\sigma_{ij}}{ne}$ are of crucial importance to engineer and design efficient electronic devices. In this section we will focus on these two material parameters for p-doped diamond crystal, in the framework of the exact numerical solution of the linearised BTE of Eq. 1.58; the evaluation of the Onsager coefficients follows from Eqs. 1.70, 1.71, 1.72 and 1.73. For diamond, the cubic symmetry implies that the transport tensors are diagonal in absence of magnetic fields and therefore we can fully describe the conductivity (and consequently the resistivity and the mobility) with just one scalar number σ (ρ and μ^d).

We start considering ρ and μ^d for the diamond crystal in absence of magnetic field, considering both electron-phonon and impurity scattering as described in Chap. 1. The values of the mobility are obtained solving Eq. 1.58 on a $\mathbf{k}$-points grid of dimensions $100 \times 100 \times 100$, including in the calculation states that lie down to 0.32eV below

the top valence band energy. The electron-phonon coupling elements are obtained from first principles on a $5 \times 5 \times 5$ coarse $\mathbf{k}$ and $\mathbf{q}$-grid and then interpolated on $100 \times 100 \times 100$ fine meshes with Wannier interpolation—as explained in Chap. 1; the value of the Gaussian smearing used to approximate the Dirac δ function with via finite-width Gaussian is 5meV. Spin orbit coupling has been neglected since the small split of the valence bands is not expected to dramatically change the value of the mobility.

We first solve Eq. 1.58 and compute the values of the drift mobility at a fixed acceptor density of $N_A = 10^{15}\text{cm}^{-3}$ in a range of temperatures going from 200K to 700K. This is the range of temperatures which is interesting for technological applications and generally investigated in experiments and theoretical works [132, 45]. The lower boundary of 200K on the temperature is due to the numerical precision involved in the calculation of the mobility. In fact, at low temperatures a very low percentage of electrons can reach the acceptor level and thus the number of holes in the valence band is, for the same reason, very small. This scenario poses a severe problem in the calculation of the mobility, because we both need very large $\mathbf{k}$-points grids to appropriately describe the bands energy near Γ and a very accurate numerical precision on the value of the chemical potential, to which the mobility is very sensitive especially at low temperatures. The result of the calculations is shown in Fig. 3.5a; here, we can see that the hole drift mobility for diamond at room temperature is around $2500\text{cm}^2\text{V}^{-1}\text{s}^{-1}$. Moreover, we can see that the mobility exhibits two different behaviours at low and high temperatures. At high temperature, the drift mobility is proportional to $\text{T}^{-2.96}$ whereas at low temperatures it is proportional to $\text{T}^{-1.70}$. Our results are in good agreement with the experimental result obtained by Gabrysch et al. [124] and Reggiani et al. [45]. At low temperatures the behaviour of our theoretical mobility is steeper than the traditional $\text{T}^{-\frac{3}{2}}$, deduced for crystals with spherical energy bands; this may be due to non-elasticity of scattering processes [133]. Microscopically, the T-dependence of the mobility at low and high temperatures can be lead back to the onset of high-frequency phonon scattering, which happens between 250K and 400K, as we will see later. As a final remark, we notice that from Fig. 3.5a that both the solutions of Eq. 1.58 within the ERTA or MRTA approximations gives results that are in good agreement with the full solution of the BTE, as it happens in the case of silicon [3]. The goodness of these approximations seems to be in general severely reduced in the case of polar materials [20].

Once we have studied the mobility as a function of temperature at a fixed dopant concentration, we can try to solve Eq. 1.58 keeping the temperature fixed and varying the dopant density. We shown in Fig. 3.5b the values of the hole drift mobility μ^d

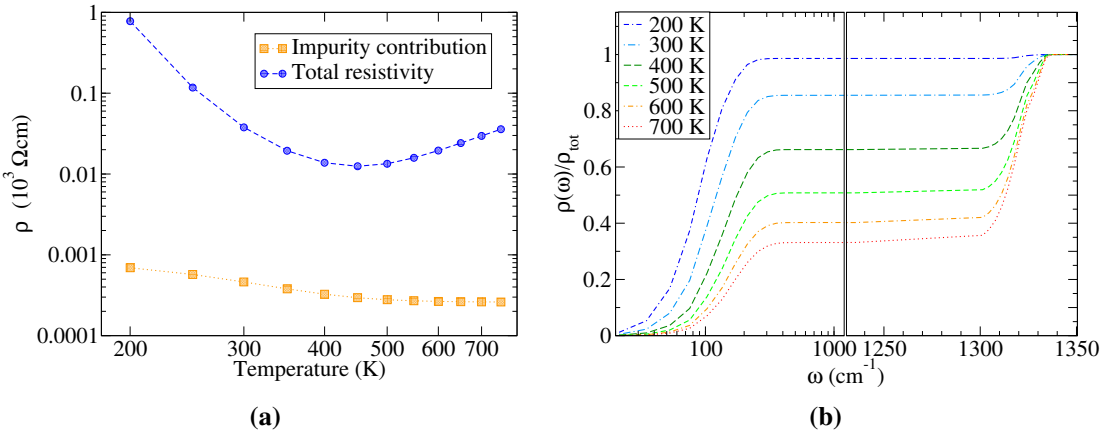

Figure 3.6: (a) Contribution of impurity scattering to total resistivity calculated via the variational formula of Eq. 3.4. (b) Phonon frequency cumulative contribution to total resistivity, for a doping of 10^{15}cm^{-3}. The frequency-axis is in logarithmic scale up to 1000cm^{-1} and in exponential scale for higher values.

for a fixed temperature of 300K and acceptor-impurities concentrations ranging from 10^{15}cm^{-3} to 10^{20}cm^{-3}. In particular, Fig. 3.5b shows that for low doping concentrations the mobility tends to an upper bound: this is the intrinsic value of the mobility obtained including only the electron-phonon interaction in the collisional term of the Boltzmann equation. In any case, our mobility results for concentration values above 10^{16}cm^{-3} should be taken with care because our electron-impurity interaction model may be unsuitable at high doping concentrations and because other scattering channels—such as electron-plasmons—may become important in the electric conduction mechanisms for p-diamond crystal.

From Fig. 3.5b we notice that the comparison with experiments is not straightforward. Indeed, the experimental mobilities can be spread out over one order of magnitude at a given boron content. This is a consequence of compensation effects due to deep level impurities. These effects can greatly affect electrical transport as they tend both to decrease the carrier concentration and increase the density of ionised impurities that can scatter charge carriers. Another difficulty comes from the fact that most experiments measure the Hall mobility μ^H, and not the drift mobility μ^d. Assuming an electric field along the $\hat{x}$ direction, these two quantities are related via the following relation:

$$\mu^H = \mu^d \frac{ne}{B_z} \frac{\sigma_{xy}(B_z)}{(\sigma)^2} = r\mu^d \tag{3.2}$$

where B_z is a vanishingly small magnetic field in the $\hat{z}$ direction, and r is known as the Hall scattering factor (or Hall coefficient factor). Therefore, to compare with experiment we need to solve Eq. 1.58 is presence of magnetic field; this will be matter

of the next section, but here we anticipate that in our calculations we find $r \approx 0.8$ with a weak dependence on doping and temperature, as can be seen in the inset of Fig. 3.5b. Therefore, we can rescale the drift mobility and obtain μ^H significantly lower than μ^d and closer to the higher experimental mobilities, as shown in Fig. 3.5b.

Once we have described the macroscopic dependence of electrical transport on temperature and doping, it is interesting to analyse its microscopical dependence on the scattering mechanisms; in order to do so, it is convenient to consider the resistivity ρ. This is because the resistivity can be expressed by means of a variational formula [15]:

$$\rho = \frac{4e^2 m_e^2}{V k_B T} \frac{\sum_{m\mathbf{k},m'\mathbf{k}'} \left(\chi_{m\mathbf{k}} - \chi_{m'\mathbf{k}'}\right)^2 \Pi_{m\mathbf{k},m'\mathbf{k}'}}{\left(\sum_{m\mathbf{k}} \mathbf{v}_{m\mathbf{k}} \cdot \mathbf{E} \chi_{m\mathbf{k}} \frac{\partial f^0}{\partial \epsilon_{m\mathbf{k}}}\right)^2}. \tag{3.3}$$

We can solve the BTE to find and then insert the exact solution $\chi_{m\mathbf{k}}$ in the variational formula 3.3; we can thus separate the scattering amplitudes:

$$\rho = \frac{4e^2 m_e^2}{V k_B T} \frac{\sum_{m\mathbf{k},m'\mathbf{k}'} \left(\chi_{m\mathbf{k}} - \chi_{m'\mathbf{k}'}\right)^2 \left[\Pi^{ph} + \Pi^{imp}\right]_{m\mathbf{k},m'\mathbf{k}'}}{\left(\sum_{m\mathbf{k}} \mathbf{v}_{m\mathbf{k}} \cdot \mathbf{E} \chi_{m\mathbf{k}} \frac{\partial f^0}{\partial \epsilon_{m\mathbf{k}}}\right)^2} \tag{3.4}$$

and obtain $\rho = \rho^{ph} + \rho^{imp}$. Unfortunately, ρ^{ph} and ρ^{imp} are not the resistivity due to electron-phonon or electron-impurity scattering separately, because in both cases they are calculated by means of the exact solution $\chi_{m\mathbf{k}}$ which contains information on all the scatterings; this separation is anyway a good index of the relative impact of the interactions on the electrical conduction. The result of this analysis is shown in figure 3.6a, where we can see that with a doping level of 10^{15}cm^{-3} phonon scattering is the main source of resistivity for p-doped diamond, at all temperatures.

We can go further in the analysis of the microscopic contribution to the resistivity by considering the following expression for the variational formula:

$$\rho(\omega) = \frac{4e^2 m_e^2}{V \beta} \frac{\sum_{m\mathbf{k},m'\mathbf{k}'} \left(\chi_{m\mathbf{k}} - \chi_{m'\mathbf{k}'}\right)^2 \Pi^{ph}_{m\mathbf{k},m'\mathbf{k}'}(\omega)}{\left(\sum_{m\mathbf{k}} \mathbf{v}_{m\mathbf{k}} \cdot \mathbf{E} \chi_{m\mathbf{k}} \frac{\partial f^0_{m\mathbf{k}}}{\partial \epsilon_{m\mathbf{k}}}\right)^2}. \tag{3.5}$$

where $\Pi^{ph}_{m\mathbf{k},m'\mathbf{k}'}(\omega)$ is the scattering term that includes only phonons of frequency lower than ω. The relative weight $\frac{\rho(\omega)}{\rho}$ against ω is plotted in figure 3.6b. It is here evident that with increasing temperature the frequency window relevant for the determination of resistivity widens. In particular, for temperatures below 300K the relative contribution of acoustic phonons (up to 300cm^{-1}) saturates the resistivity's value up to 90%, whereas

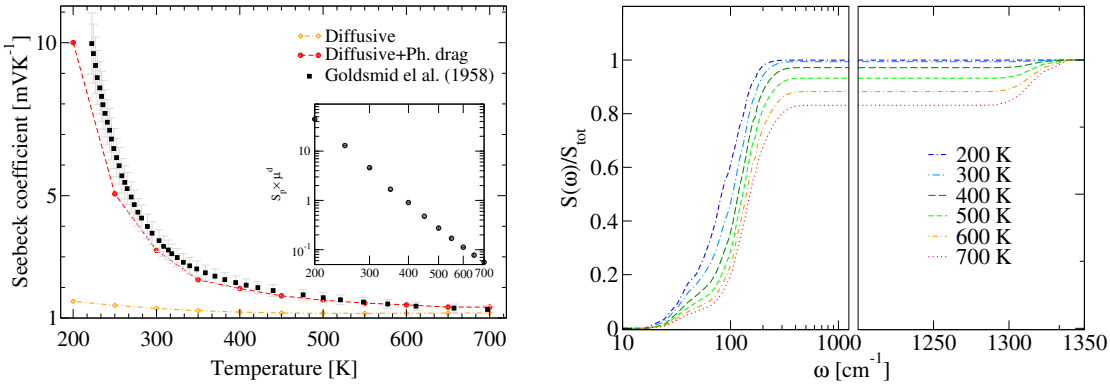

Figure 3.7: (a) Temperature dependence of the total (diffusive+phonon-drag) Seebeck coefficient (red circles) and of the diffusive contribution (orange diamond). Experimental values are taken from [47]. Inset: phonon drag component (S_p) times mobility as function of the temperature. (b) Phonon frequency cumulative analysis of the phonon drag contribution to the Seebeck coefficient.

for higher temperatures the onset of optical phonons (at around 1300cm^{-1}) gains importance for the total resistivity value. Phonons between 300cm^{-1} to 1300cm^{-1} seem to have no relevance for the resistivity values. Following this argument, we have a strong indication that the different mobility behaviour for high and low temperatures shown in figure 3.5a is discriminated by the onset of optical phonon scattering.

3.3 Seebeck coefficient

In this section we investigate the Seebeck coefficient S of p-doped diamond, defined via Eqs. 1.38, 1.70 and 1.71.

The relevant electronic states to be included for convergence are fewer than in the mobility case; indeed, all the needed information is contained in states lying down to 0.14eV under the highest valence electronic energy, which roughly correspond to the energy of the lowest optical phonon. The $\mathbf{k}$-points mesh used to converge the Seebeck is $100 \times 100 \times 100$. All the calculations have been performed with the same ab-initio matrix elements used for the mobility and the resistivity. We tested that no relevant temperature dependent corrections come from the computation of the ab-initio electron-phonon coupling on a denser coarse $\mathbf{k}$-grid.

The value of the Seebeck coefficient is presented in Fig. 3.7a, where we separately plot the diffusive component (i.e. without the phonon drag contribution) and the total value of the Seebeck coefficient in comparison with experimental data. The phonon out of equilibrium populations to insert in the phonon drag term have been calculated

exactly on a $30 \times 30 \times 30$ grid and then interpolated on a $100 \times 100 \times 100$ mesh with the procedure explained in Sec. 3.1 .

It is evident from Fig. 3.7a that the diffusive part of the Seebeck coefficient is relevant only for high temperatures (above 400K), whereas at low temperatures the phonon-drag component is dominating. This means that the diffusive model fails at low temperatures and that the electron-phonon interaction has to be taken in account to rightly compute the Seebeck coefficient. Overall, our calculation of the total Seebeck coefficient is in good agreement with the experimental findings; in particular, the $T^{-3/2}$ behaviour at low temperatures, which is the fingerprint of the scattering between electrons and phonon out of equilibrium populations, is well reproduced. The deviation at 200K from the experimental value could be related both to the experimental uncertainty and to the interpolation method of the phonon out of equilibrium populations.

As the thermal conductivity is significantly smaller in presence of isotopic scattering of lattice vibrations (Fig. 3.2a), as well as the phonon out of equilibrium populations, it is interesting to understand if the Seebeck change consistently in presence of lattice impurities. In our calculations we find that the Seebeck coefficient is practically unaffected by inclusion of isotopic scattering for lattice vibrations (the change of the value is of order 1%); the reason is that isotopic scattering affects almost only the behaviour of high-frequency phonons, as explained in Sec. 3.1, that have no significant impact on the Seebeck coefficient. In fact, the cumulative contribution of different phonon frequencies to the phonon drag fraction of the Seebeck coefficient is presented in Fig. 3.7b. The calculation is performed introducing a cutoff frequency $\tilde{\omega}$ such that for larger frequencies the out of equilibrium phonon population is put to 0. From Fig. 3.7b it is evident that the phonon drag portion of the Seebeck coefficient is mainly determined by phonons with frequencies below 300cm^{-1}, with a little contribution coming from higher frequencies and only at high temperature. Incidentally, this is also the proof that the phonon drag contribution of the Seebeck coefficient is particularly sensitive to the value of the acoustic phonon out of equilibrium populations near Γ. Therefore, the interpolation method of Sec. 3.1 of the phonon populations for sufficiently small $\mathbf{q}$-points is necessary to rightly reproduce the experimental value of the Seebeck coefficient.

3.4 Hall scattering factor, magnetoresistance and magneto-Seebeck

In the semi-classical picture, in presence of both and electric and a magnetic field, carriers are deflected from their straight trajectory. The current direction will depend on the direction of the magnetic field and on the symmetry of the crystal. For this reason, the relation between current and fields in the linear regime for the electric field and in presence of magnetic field is tensorial and we cannot use scalar quantities anymore to describe the transport properties of a material. From the point of view of the direct space symmetries of the crystal, this is due to the introduction of a privileged direction by the magnetic field. Microscopically, it follows from the loss of symmetry properties of the term $\tau_{m\mathbf{k}}(\mathbf{B})$ when a magnetic field is applied.

The Hall scattering factor, introduced in Eq. 3.2, is a quantity that connects the diagonal and out of diagonal components of the conductivity tensor. As mentioned in the introduction and in previous sections, the precise estimate of the Hall scattering factor is of fundamental importance to bridge experimental measurements and theoretical calculations of mobility and resistivity. In the inset of Fig. 3.5b we show the result of the calculation for the Hall scattering factor following from the solution of Eq. 1.58 in the linear regime for the magnetic field. We use a $\mathbf{k}$-points mesh of dimensions $85 \times 85 \times 85$ and consider electronic states lying down to 0.24eV below the top valence band energy. In our calculations we find that the Hall scattering factor falls below unity and is of around $r \approx 0.8$ for the range of temperature studied, in agreement with reported experimental estimates [46]. The experimental data indicate a possible decrease of the Hall scattering factor at low temperatures; our calculations show that this behaviour might be due to electron-impurity scattering, which is the mechanism that mostly affects the Hall scattering factor in this temperature range. Ref. [46] predicted two possible theoretical values of the Hall scattering factor, one lower and one greater than unity. These values were obtained in the relaxation time approximation using a parametrized parabolic electronic band structure around Γ. The lower values are smaller than ours but have a similar temperature dependence, with a minimum at around 350K.

The electronic BTE equation can also be solved in the non linear regime for the magnetic field[1]; this is important to calculate the variation of the diagonal resistivity components under the application of a generic magnetic field. A detailed comparison

[1]This is typically done in the study of the magnetoresistance—see, for instance, Ref. [90]. However, we are not aware of a theoretical justification for this procedure that follows from the arguments of Chap. 2. This will be matter of future investigations.

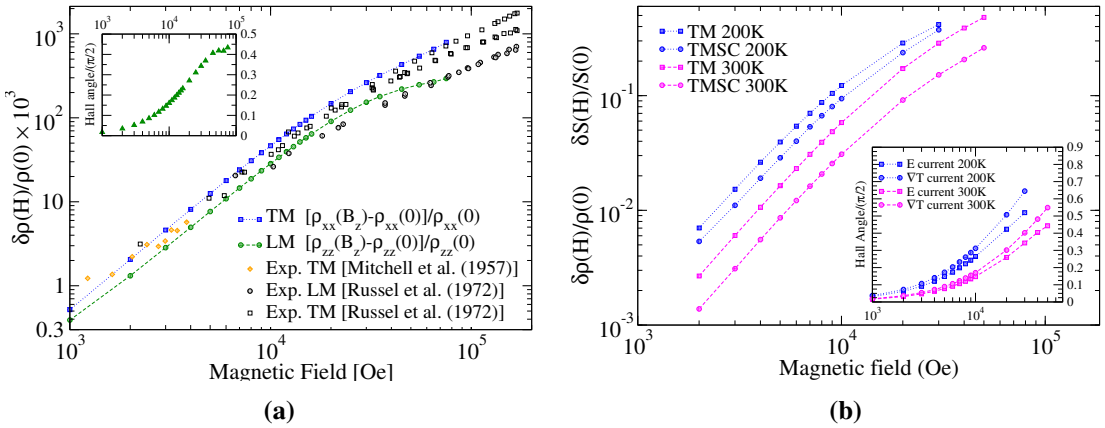

Figure 3.8: (a) Transversal magnetoresistance (TM) and longitudinal magnetoresistance (LM) for diamond crystal as a function of magnetic field strength, at 300K; experimental data are taken from Ref. [134] (orange squares) and Ref. [135] (black squares and circles); inset: Hall angle divided by $\frac{\pi}{2}$, as a function of the magnetic field. (b) Trasversal magnetoresistance (TM) and transversal magneto-Seebeck coefficient (TMSC) for diamond crystal as a function of magnetic field strength, at 200K and 300K. Inset: Hall angle divided by $\frac{\pi}{2}$ for the electric and thermal gradient contributions to the total electronic current, as a function of the magnetic field, at 200K and 300K.

between theory and experiments can be done by focussing on the magnetoresistance ($[\rho_{ij}(B_l) - \rho_{ij}(0)]/\rho_{ij}(0)$). Fig. 3.8a shows the values of the transversal and longitudinal magnetoresistance ($[\rho_{xx}(B_z) - \rho_{xx}(0)]/\rho_{xx}(0)$ and $[\rho_{zz}(B_z) - \rho_{zz}(0)]/\rho_{zz}(0)$) as a function of the magnetic field $\mathbf{B}$, which is taken along the $\hat{z}$ axis in our calculations. At low fields the values are proportional to the square of the magnetic field modulus $|\mathbf{B}|^2$, as expected from symmetry considerations [90]; at higher fields the behaviour strongly differs from the quadratic law. For all the magnetic fields considered in this work we find that the longitudinal magnetoresistance is smaller than the transversal one, in agreement with experimental data. It is to notice anyway that the available experimental data have been taken with respect to various different orientations of $\mathbf{B}$; this fact and the uncertain doping content of the samples may explain the difference between our calculation and the experimental data. As a measure of the strength of the magnetic fields considered here, in the inset of Fig. 3.8a (3.8b) we show the values for the Hall angle, i.e. the angle between $\mathbf{E}$ and $\mathbf{J}_e$ ($\nabla_{\mathbf{r}} T$ and $\mathbf{J}_Q$), as a function of the magnetic field strength. This quantity is expected to reach $\frac{\pi}{2}$ at very large magnetic fields when the magnetoresistance saturates [136].

When a temperature gradient is applied to the crystal in presence of a magnetic field, we will have a tensorial response also from the Seebeck coefficient $S(\mathbf{B})$. To understand the Seebeck response to the magnetic field, we start noticing that, when the phonon drag is the dominant driving force in Eq. 1.58, the Seebeck coefficient is

expected to be proportional to the mobility. This can be seen in the inset of Fig. 3.7a where we plot the product of the phonon drag component of the Seebeck coefficient and the mobility. The resultant curve is proportional to $\sim T^{-5.5}$ for low temperatures whereas the exponent increases a little for higher temperatures. This proportionality is consistent with previous simplified model previsions [137]. This interrelation between the two quantities can be exploited to further increase the Seebeck coefficient of diamond. This can be achieved when a temperature gradient is combined with a magnetic field that, as shown previously, tends to increase the resistivity—and therefore, reduce the mobility and increase the Seebeck.

In order to quantify the extent of this effect in diamond we computed the transversal magneto-Seebeck coefficient, shown in Fig.3.8b alongside the magnetoresistance, as a function of the intensity of the magnetic field. As expected, the behaviour of the two quantities is very similar, especially at low fields. While this has been observed in other semiconductors, such as germanium [138, 88], the interesting result here is the magnitude of the enhancement of the Seebeck coefficient at relatively high temperatures in presence of a magnetic field. For instance, we predict a relative change in the Seebeck coefficient at 200K and 10KOe that is about 4 times larger than in n-type germanium at the same temperature and magnetic field[138]. The enhancement goes up to about 30% in a magnetic field of 40KOe already at room temperature.

Chapter 4

Theory and computation of Hall scattering factor in graphene

The second system studied in this thesis is graphene. Since the discovery of its exceptional room-temperature mobility [48], graphene has attracted unprecedented interest and efforts to study its superior electrical properties and use them for advanced technological applications. Also, graphene represents a fundamental playground to study the impact of dimensionality on specific physical properties, and the possibility of exploiting them in electronic devices [139].

One of the defining properties of graphene is the linear energy-momentum dispersion with the conduction and valence bands intersecting at two special point $\mathbf{k} = \mathbf{K}$ and $\mathbf{k} = \mathbf{K}'$, called the Dirac points [140]. The Fermi velocity v_F, which characterizes the slopes of the conic energy bands, is around $10^6 \frac{\mathrm{m}}{\mathrm{s}}$. The consequences of this peculiar band dispersion on the electronic transport properties are remarkable [53]. In particular, the form of the allowed electron-phonon scattering times are different from the 3d counterparts both in scaling and amplitude; as a consequence, the value of the electric transport properties shows a temperature and carrier concentration dependence which is typical of graphene alone. Another distinguishing feature is the possibility to gate graphene by inducing a surplus of hole or electron carriers adjusting an external gate voltage. This allows to move the Fermi level E_F from the Charge Neutrality Point (CNP) at the intersection of the conic bands to the valence or conduction bands. This is one of the greatest achievements since it permits to directly control the carrier density and its charge, and therefore study in detail the electric transport properties. In particular, one can assess the hole and electron mobilities of the same sample.

Nonetheless, the experimental determination of mobility is not straightforward [141] and passes through the determination of the gate capacitance. In the general gate set-up for a 2d material, it is not uncommon to use the Hall effect in order to deduce the carrier density induced by the gate voltage and consequently calculate the

gate capacitance, or to directly study the Hall mobility [142, 143, 48, 144, 145]. When a gate set-up is not used, but graphene is grown on some support, it is common to evaluate the Hall mobility of the sample [146, 147, 148, 149, 150, 151, 152, 153, 154]. It is then of crucial importance to know the exact relations between the Hall factor and the carrier density and between the drift and Hall mobilities; both of these relations contain the value of the Hall scattering factor r, which is most often assumed to be unity (see, for instance, Refs. [48, 155]), but this assumption is based on studies performed on bulk semiconductors with quasi-parabolic band dispersion, where r commonly shows a weak dependence on temperature and scattering mechanisms. On the contrary in graphene, as we will show in this chapter, the intrinsic r follows non-trivial trends as a function of carrier concentration and temperature, with values that can be far greater or smaller than unity; this is due to the peculiar band structure and electron-phonon scattering mechanisms. For low carrier concentrations and temperatures below $\sim$ 300 K, we evaluate r using an analytical model that is derived from the Boltzmann Transport Equation (BTE) in the hypothesis of isotropic band energies and that depends on the density of states, v_F and the electron-phonon scattering rates, that can in turn be evaluated via simplified models. Above room temperature or at high carrier concentrations, the accuracy of the model has to be questioned. Indeed, here previous works have shown the necessity to exactly solve the BTE to accurately quantify the resistivity [16]. Therefore in these regimes we compute r via the full solution of the BTE, obtained by means of the most recent developments regarding the first-principles calculation of transport properties [3, 4, 21, 5], as explained in Chap. 1. The calculations are performed using a private version of EPW [34]—which is part of the QUANTUM ESPRESSO [66] package—where we implemented an highly scalable and strongly optimized numerical solution of the BTE, in presence or absence of external magnetic field.

In this chapter, before presenting our results for the Hall scattering factor, we present a numerical study of the electron-phonon coupling, the inverse scattering times and the drift mobility of graphene; all these ingredients are important in light of a comparison with existing model and known results. Once shown that the comparison is satisfactory, we will proceed to the prediction of the Hall scattering factor value in different regimes.

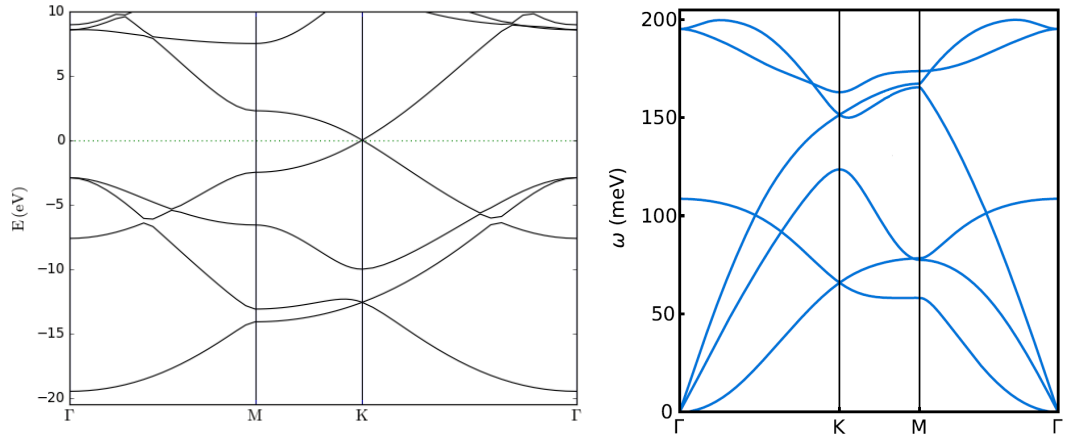

(a) **(b)**

Figure 4.1: (a) Electronic structure and (b) phonon branches of graphene along high-symmetry lines. The band structure displays the typical characteristic linear dispersion around the **K** high-symmetry point. As regards phonons, the linear behaviour of acoustic modes and the quadratic behaviour of flexural modes at small wave-vectors is clearly visible.

4.1 Computational details for an accurate electron-phonon coupling calculation

We follow here the procedure explained in App. A; the primitive cell is described via the lattice vectors $\mathbf{v}_1 = a(1,0,0)$, $\mathbf{v}_2 = a(-1/2,\sqrt{3}/2,0)$, $\mathbf{v}_3 = a(0,0,c)$ where $a = 2.46$ Ang and $c = 5.0$ (even though the stability of the transport coefficients has been tested against increases of the c parameter up to 10.0). Since we will compare with previous known results and analytical models, it is important to have very well converged values of the computational parameters. We work in the DFT framework using the QUANTUM ESPRESSO code [66] within the local density approximation (LDA) [121]. For the SCF calculation, we use a non-relativistic Norm-Conserving (NC) pseudopotential compatible with the PZ exchange-correlation functional [156, 121], a plane wave cutoff of 100Ry and a $\mathbf{k}$-point grid of dimensions $96 \times 96 \times 1$, to accurately compute the ground state of graphene. For the NSCF calculation, we use the same pseudopotential and cutoff, but we use a $\mathbf{k}$-point grid of dimensions $24 \times 24 \times 1$ (we will show in the next section that this is sufficient). The presence of a carrier density in graphene has been simulated within the rigid band approximation. In the case that the carrier density is generated by extrinsic impurities, this is the same technique used in similar transport calculations on bulk materials; otherwise, if graphene is studied in a gate configuration, such approximation is not appropriate for flexural phonons and for the "deformation potential" terms of the EPC, but luckily those terms

n (cm^{-2})	$\mathbf{k}/\mathbf{q}$-points grids	window (meV)	σ (meV)
$5 \times 10^{11} - 9 \times 10^{11}$	$1404 \times 1404 \times 1$	500	5
$1 \times 10^{12} - 4 \times 10^{12}$	$1080 \times 1080 \times 1$	500	5
$5 \times 10^{12} - 1 \times 10^{13}$	$1080 \times 1080 \times 1$	700	5

Table 4.1: Converged parameters for transport properties

do not contribute relevantly to transport properties [157]. For the DFPT calculations, we use a $\mathbf{q}$-point grid of dimensions $24 \times 24 \times 1$ and a strict threshold for convergence of the calculation (using a self-consistent threshold of 10^{-20} for the solution of the Sternheimer linear equation presented in Chap. 1). The electronic and vibrational properties obtained with the above methodologies are displayed in Figs.4.1a and 4.1b. The Wannier interpolation is performed with 5 basis functions, consisting in 3 sp^2-like orbitals centred on the bonds between a graphene atom and its first neighbours, and two pz-like orbitals centred on each of the graphene atoms in the primitive cell. The resulting MLWFs have spreads ranging from 0.6098Ang^2 to 2.7183Ang^2. Finally, we report in Tab. 4.1 the safe values for the fine grids, energy window from the Dirac cone energy and Gaussian smearing to obtain converged transport calculations with EPW. Convergence graphs are given in the next section.

In this section we study the convergence of the interpolated EPC matrix elements with respect to the *ab initio* values. Also, we compare the results with pre-existing models of the interaction. We put ourself at a momentum near $\mathbf{K}$, at a $\mathbf{k}$-point with Cartesian coordinates $\mathbf{k_1} = (0.3437500, 0.5953925, 0)$ (in units of $\frac{2\pi}{a}$, $\mathbf{k_1}$ belongs to the $48 \times 48 \times 1$ SCF grid and is on the line that connects the K and Γ points) and consider $\mathbf{q}$-points of the form $\mathbf{q} = \lambda \mathbf{k_1}$ with very small λ. $\mathbf{q}$ runs on the $\Gamma - K$ line. We compute the *ab initio* EPC $\langle n = 4, 5; \mathbf{k_1} + \mathbf{q} | \partial_{\lambda \mathbf{q}} V | m = 4, 5; \mathbf{k_1} \rangle$ (4 is the index for the π band, 5 is the index for the π^* band) and compare it with its Wannier interpolation obtained for different NSCF and DFPT grids in Panel 1. Since the $\Gamma - K$ line is a special line we have some symmetry constraints on the EPC matrix element values (as explained in Ref [158]); in particular, some elements need to be null on whole sectors of the line. Those elements are a clear indicator of the interpolation convergence: from Panel 1 we see that a NSCF $\mathbf{k}$-point grid of $24 \times 24 \times 1$ and a DPT $\mathbf{q}$-point grid of $24 \times 24 \times 1$ catch very well the behaviour of the *ab initio* EPC. We also mention that we tested the *ab initio* results under change of SCF grid (up to $144 \times 144 \times 1$) and of Gaussian smearing during the SCF cycle, finding no appreciable differences. In passing by, we notice that not all EPC matrix elements go to 0 when

$|\mathbf{q}| \to 0$, in opposition of what predicted in Ref. [158]; the reason is that the Hellmann-Feynman applied to Γ acoustic phonons (which are free of non-analyticity in graphene) reads:

$$\langle \mathbf{k}+\mathbf{q}n|\partial_{\lambda_{TA/LA}\mathbf{q}}V|\mathbf{k}n\rangle_{\mathbf{q}=0} \propto \frac{\partial \epsilon_{n\mathbf{k}}}{\partial \mathbf{q}}(\mathbf{q}=\mathbf{0}) = 0 \tag{4.1}$$

but this relation does not hold true in the case of different initial and final band indexes; in this case, we should instead use the Epstein formula [69] in order to deduce the values of the matrix elements, which result in general different from 0. Moreover, we also notice that the hole-electron symmetry for the modulus of the EPC matrix elements, which is usually assumed to hold in graphene (see for example Ref [52, 16]), results broken from our *ab initio* calculations; this is because the response function in a DFPT calculations depend on the ground state density, which in turn depends only on the occupied/valence states. A part from the above mentioned discrepancies, if we compare our results with models (such as the one in Ref [16]), we find an overall good agreement for the angular dependency of the EPC for the acoustic modes; for the optical phonons we find that the behaviour predicted from the models is oversimplified.

4.2 Convergence of transport quantities

In this section we present the convergence of transport quantities with respect to computational parameters. Referring to Panel 2 (a), we first notice the quadratic scaling of the relevant (active) $\mathbf{q}$-points $N_{\mathbf{q}}^{act.}$ contributing to the transport coefficient calculations inside the active energy window, consistent with the 2d dimensionality of the system; the time of the calculation increases with the $\mathbf{k}/\mathbf{q}$-point grids as $t \propto N_{\mathbf{k}}^{irr.} \times N_{\mathbf{q}}^{act.}$ where $N_{\mathbf{k}}^{irr.}$ is the number of irreducible points for a given grid. To explain this, we start noticing that the value of the EPC on a generic couple of $\mathbf{q}$ and $\mathbf{k}$ points can be obtained by using the relation [4]:

$$|g^{\lambda}_{n\mathbf{k},m\mathbf{k}+\mathbf{q}}|^2 = |g^{\lambda}_{nS\mathbf{k},mS(\mathbf{k}+\mathbf{q})}|^2 \tag{4.2}$$

where S is one of the symmetry operations associated with the star of $\mathbf{k}$. Therefore, we can reduce the calculation of the EPC elements choosing $\mathbf{k} \in IW$ (Irreducible Wedge of the BZ) and $\mathbf{q} \in BZ$. Eq. 4.2 holds for non-degenerate states, while for degenerate bands/phonons we just know that:

$$\sum_{mn\lambda} |g^{\lambda}_{n\mathbf{k},m\mathbf{k}+\mathbf{q}}|^2 = \sum_{mn\lambda} |g^{\lambda}_{nS\mathbf{k},mS(\mathbf{k}+\mathbf{q})}|^2 \tag{4.3}$$

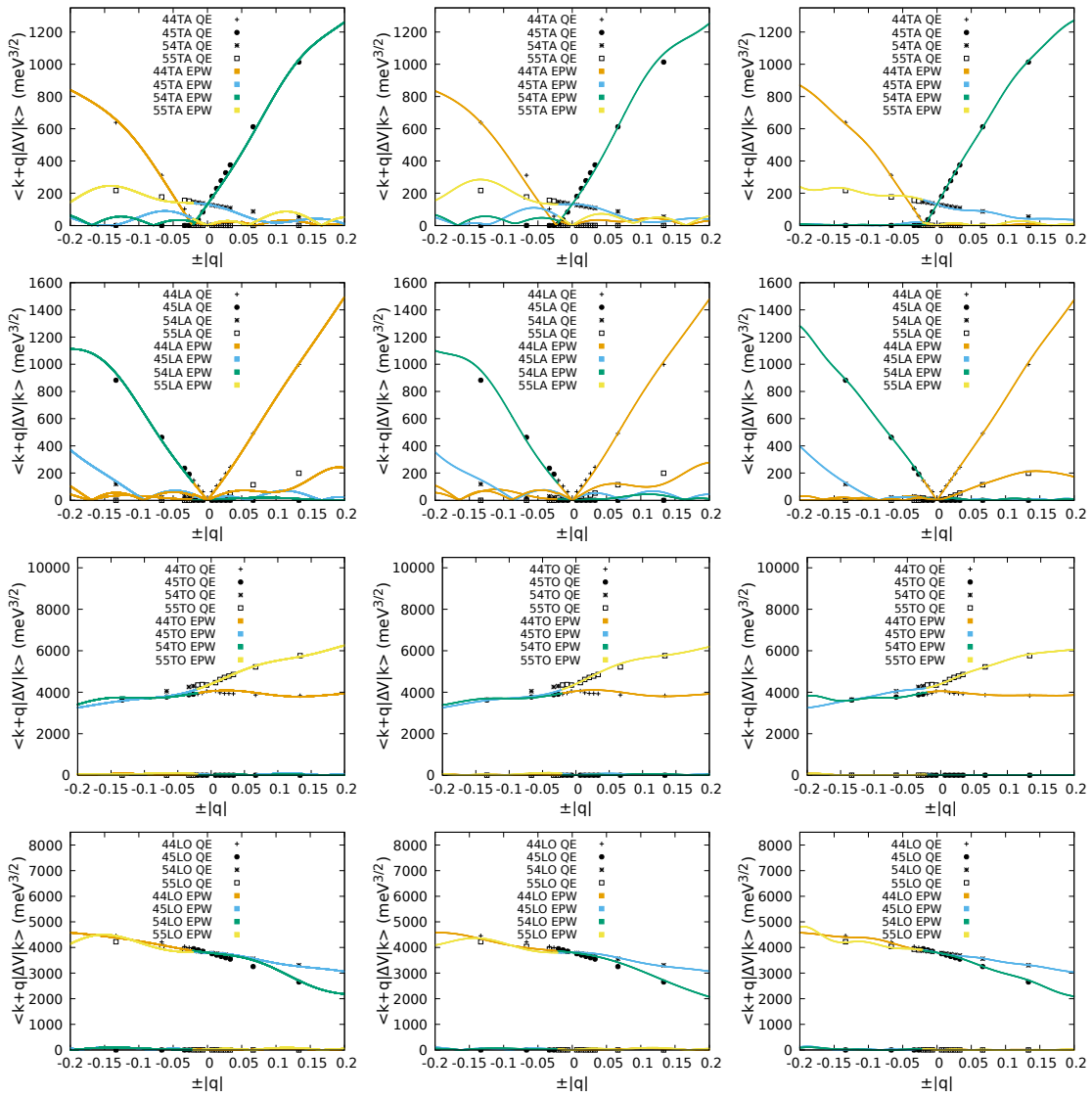

PANEL 1: Comparison between *ab initio* EPC and Wannier-interpolated EPC $[< n = 4, 5; \mathbf{k_1} + \mathbf{q}|\partial_{\lambda \mathbf{q}} V|m = 4, 5; \mathbf{k_1} >]$—4 and 5 represents the π and pi^* bands respectively. We compare different NSCF $\mathbf{k}$-point and DFPT $\mathbf{q}$-point grids for different λ modes, with $\mathbf{q}$ running on the $\Gamma - K$ line and $\mathbf{k_1} = (0.3437500, 0.5953925, 0)$. From top to bottom: TA mode, LA mode, TO mode, LO mode. First column: NSCF $24 \times 24 \times 1$ and DFPT $12 \times 12 \times 1$. Second column: NSCF $48 \times 48 \times 1$ and DFPT $12 \times 12 \times 1$. Third column: NSCF $24 \times 24 \times 1$ and DFPT $24 \times 24 \times 1$.

because of the gauge freedom within degenerate subspaces. A proper modification of the BTE where $\mathbf{v}_{n\mathbf{k}}$ is substituted by the matrix elements $\mathbf{v}_{n\mathbf{k},m\mathbf{k}'}$ (defined as in [31]) and $f_{n\mathbf{k}}$ by $f_{n\mathbf{k},m\mathbf{k}}$ should be implemented to make the Eq. 1.58 properly gauge invariant in degenerate subspaces (see for example [159] for an homogeneous system). Nonetheless, the set of degenerate points in a crystal is usually of null measure and

therefore for practical reasons this is never done. We also remind that the gauge freedom for degenerate vibrational modes does not affect the final results even using Eq. 1.58 because the phonon branches are always summed over. Therefore, practically, our procedure is to treat $|g|^2$ for degeneracy points in the same way as for non-degenerate ones, and then check that our grid dimensions are large enough to leave the results unaffected by the gauge choice. For $\mathbf{v}$, we adopt the gauge such that at each point the velocity matrix is diagonal and respects the lattice symmetry, so that transport quantities are recovered in the correct symmetrical form. In graphene, there is just one degeneracy point which is the Dirac cone center, so the observables are almost immediately gauge invariant. In passing by, we also mention that the property of Eq. 4.2 for symmetric operations belonging to the small group of $\mathbf{k}$ becomes:

$$|g^{\lambda}_{n\mathbf{k},m\mathbf{k+q}}|^2 = |g^{\lambda}_{nS\mathbf{k},mS\mathbf{k+q}}|^2 = |g^{\lambda}_{n\mathbf{k},mS\mathbf{k+q}}|^2 \tag{4.4}$$

and this property usually needs to be enforced numerically—and it is important to obtain transport tensors with the correct symmetries.

In Panel 2 we also show the convergence of (b) Fermi energy, (c) drift mobility and (d) Hall coefficient tensor components against the increase of the $\mathbf{k}/\mathbf{q}$-point grids, while keeping a fixed smearing of 5meV. The calculations are done for a carrier density of 10^{12}cm^{-2} and an active energy window extending 500meV below and above the Dirac cone center. The Fermi level at a given temperature converges to a precision of 10^{-3}eV at grids of dimensions $1080 \times 1080 \times 1$, whereas the difference between Fermi levels at 600K and 300K converges to a precision of 3×10^{-4}eV at the same grid. Regarding the mobility, we have two different behaviour for 300K and 600K that highlight the difficulty of converging the result at lower temperatures, where in general a smaller energy window around the Fermi level contributes to transport. At 300K we have a change of the mobility of 0.1% ($240\frac{\text{cm}^2}{\text{Vs}}$) at grids of dimensions $1080 \times 1080 \times 1$. As regards the Hall scattering factor, since graphene doesn't have rational ratios between Cartesian reciprocal lattice vectors, the Cartesian derivatives of the out of equilibrium populations in Eq. 1.58 cannot be done using a uniform $\mathbf{k}$-point grid; in this case, we take directional derivatives along the reciprocal lattice vectors and then rotate the resulting gradient to transform it into Cartesian coordinates. This operation is properly justified in the limit where the distance between grid points tends to 0; the symmetries of the physical quantities are recovered in such limit. We can

notice that at grids of dimensions $1080 \times 1080 \times 1$ the Hall scattering factor r^{xy} [1] is converged up to 3×10^{-2} and 5×10^{-3} for 300K and 600K respectively; the sum $r^{xy} + r^{yx}$, which should be 0 when the physical symmetries are recovered, is in this case 5×10^{-3} and 5×10^{-4} respectively. This is a good indicator that the grid points are close enough to evaluate the derivatives with the procedure described above. In Panel 2 we also show the convergence of e) the mobility and of f) Hall scattering factor with respect to smearing at fixed $\mathbf{k}/\mathbf{q}$-point grids of dimensions $1080 \times 1080 \times 1$. The carrier density considered here is 10^{12}cm^{-2}. In this case, we notice that for smearing values ranging from 2meV to 20meV the transport quantities are quite stable.

Other convergence tests, that we do not report, have been done for different carrier densities. The final converged parameters used in this work, as already mentioned in the previous section, are reported in Tab. 4.1.

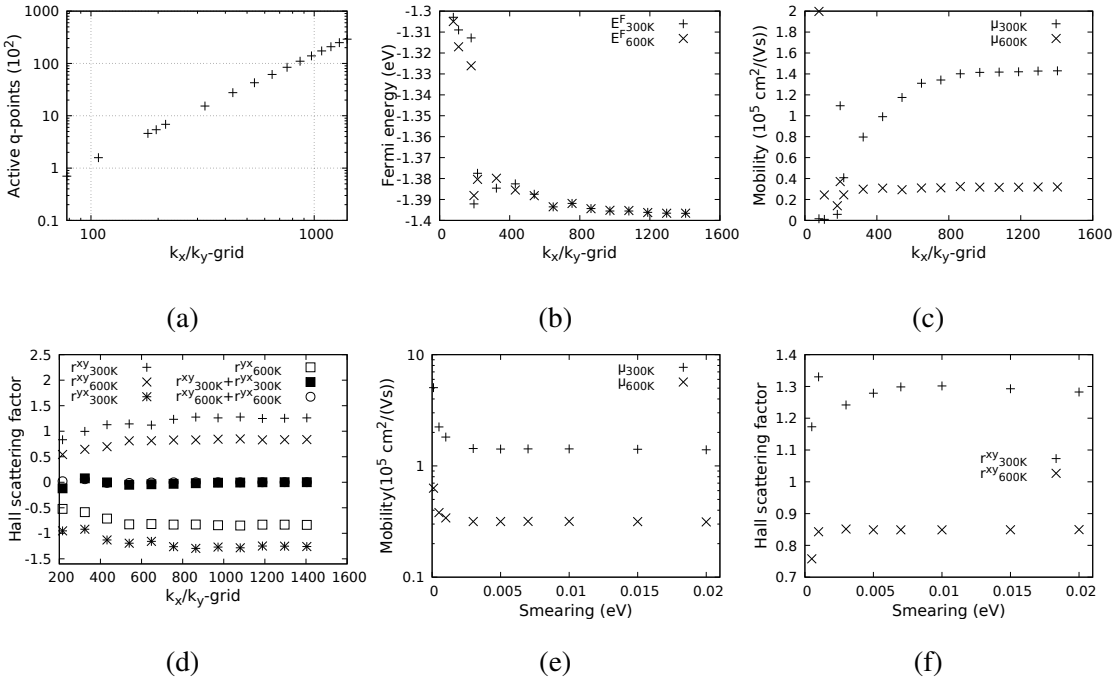

PANEL 2: (a) Number of active q-points within the active energy window against the size of the $\mathbf{k}/\mathbf{q}$-point grids. Convergence of (b) Fermi energy, (c) drift mobility and (d) Hall scattering tensor components against the size of the $\mathbf{k}/\mathbf{q}$-point grids with a fixed smearing of 5meV. Convergence of (e) drift mobility and (f) Hall scattering tensor components against the smearing value used at a fixed $1080 \times 1080 \times 1$ $\mathbf{k}/\mathbf{q}$-point grid.

[1] In Chap. 3 we introduced the Hall scattering factor for the particular case of an electric field along the $\hat{x}$ direction and a magnetic field along the $\hat{z}$ direction. Of course, the generalization of r to a tensorial form reads as $r^{ij} = \frac{ne}{|\mathbf{B}|}\left[\sigma(\mathbf{B})\left(\sigma^{-1}(\mathbf{0})\right)^2\right]_{ij}$

4.3 Drift mobility

Since the Hall scattering factor is a ratio of two components of the conductivity tensor, we start computing the intrinsic drift mobility of graphene and compare our results to the ones present in literature. The largest available experimental values estimates an intrinsic mobility of graphene of around $\sim$ 200 000 $\frac{\mathrm{cm}^2}{\mathrm{Vs}}$ [160, 155, 161]. These values are much higher than for the traditional semiconductors with quasi-parabolic band dispersion such as silicon, germanium or gallium-arsenide. Theoretical investigations of the mobility for graphene, done both via models or *ab initio* investigations [49, 51, 17, 162], also predict remarkably large values. In this work we study both the electron and the hole mobility. We have previously pointed out that the electron-hole symmetry is not fully respected by the electron-phonon coupling matrix elements. Moreover, the electron-hole symmetry is respected by the energy band structure only in the immediate proximity of the Dirac cone center. We show in Panel 3 that, nonetheless, the differences of the transport quantities between holes and electrons are quantitatively very small (for the Hall scattering factor, the sign change is expected because of the sign change of the carriers; the absolute value instead is very similar). Since the difference between the two is very small (with the hole mobility being higher of 7% at room temperature), we can concentrate just on the hole transport quantities.

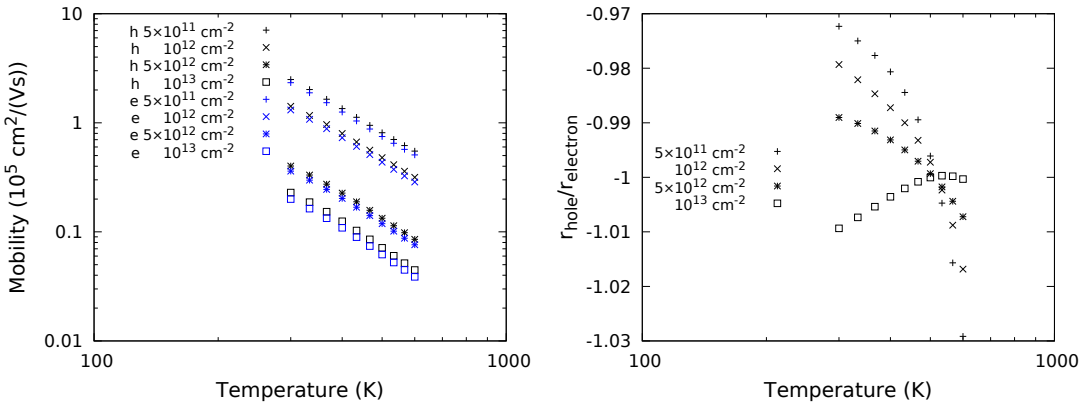

(a) (b)

PANEL 3: Temperature dependence, for different values of carrier concentration, of (a) hole and electron mobility; (b) ratio of hole and electron Hall scattering factors.

The behaviour of the hole mobility as a function of the carrier density is shown in Panel 4 (a). For low carrier concentrations, the mobility roughly behaves as $\mu \propto \mathrm{n}^{-0.85}$, in general agreement with previous predictions [49]. The temperature behaviour of the hole mobility for different doping concentrations is shown in Panel 4 (b). We witness

to a monotonic decrease of the mobility with increasing temperature, as it qualitatively happens also for traditional semiconductors; for low doping concentrations and around room temperature, we roughly have $\mu \propto \mathrm{T}^{-2.2}$. The value obtained for a carrier density of $10^{12}\mathrm{cm}^{-2}$ at room temperature is of $\sim 140\,000 \frac{\mathrm{cm}^2}{\mathrm{Vs}}$, in very good agreement with previous *ab initio* calculations and experimental results. In Panel 4 (c) we also show that the slope of the curve changes from $\mu \propto \mathrm{T}^{-2.2}$ to $\mu \propto \mathrm{T}^{-0.85}$ upon removal of the scattering between electrons and phonons with frequencies higher that $60\mathrm{meV}$, at a carrier density of $10^{12}\mathrm{cm}^{-2}$. This well reproduces the prediction of models that include only acoustic phonons [16]. We also check that the imposition of the quasielastic scattering condition (i.e. the neglect of the phonon frequencies inside the Dirac delta functions) still leads to the same temperature power $\mu \propto \mathrm{T}^{-0.85}$. We conclude therefore that optical phonons at room temperature are important in graphene to correctly describe the temperature behaviour of the mobility; on the contrary, optical phonons become less and less important as the temperature decreases, and already at 300K the acoustic scattering alone gives a mobility only 30% different from the value obtained considering full interactions. We will see in the following that, on the contrary, the determination of the Hall scattering factor includes the optical phonon scattering as a fundamental ingredient even at room temperature.

As regards technical details of the numerical solution of the BTE, Panel 5 shows a) the difference between the approximated SERTA approach and the full exact solution on the mobility and b) [c)] the convergence of the diagonal [off-diagonal] components of the conductivity tensor with respect to the iterations of the solving method. We can see that for the mobility the mismatch between the SERTA and the exact solution can reach up to 10% in the studied ranges; nonetheless, it is not as large as in other materials (such as GaAs [20] and GaN [163]). The plot of the iterations instead show a quick convergence of all the components of the conductivity tensor with the implemented method.

4.4 Hall scattering factor

4.4.1 Analytical model

As mentioned in the introduction, the Hall scattering factor is a fundamental quantity in order to bridge experimental results and theoretical calculations. In this section we present an analytical model that can be used at low carrier concentrations, where one could take advantage of several approximations to solve the BTE while maintaining an

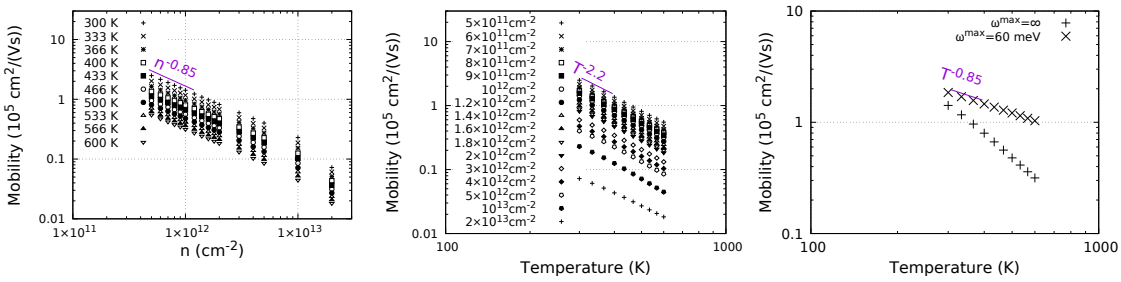

(a) (b) (c)

PANEL 4: Mobility as a function of (a) carrier concentration and (b) temperature. In (c), we plot the temperature dependence of mobility at a carrier density of 10^{12}cm^{-2} when all scattering mechanism are present and when just phonons below 60meV are considered.

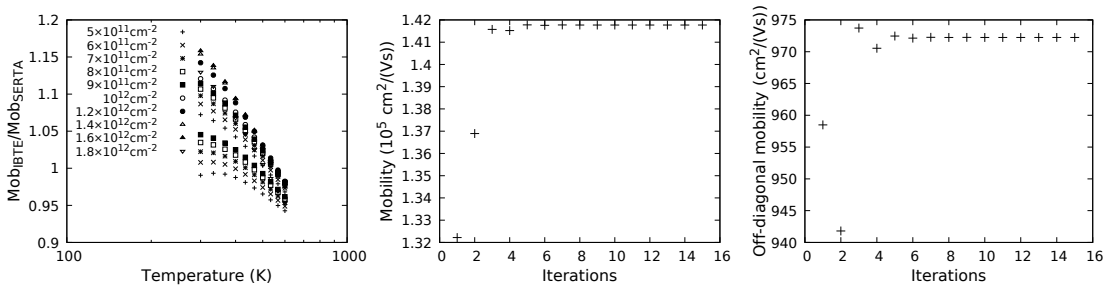

(a) (b) (c)

PANEL 5: (a) Temperature dependence of the ratio between the solution in the SERTA approximation and the exact solution, for different carrier concentrations; convergence with respect to the iterations of (b) mobility and (c) non-zero out of diagonal component of the mobility tensor when a magnetic field is present; the carrier concentration is 10^{12}cm^{-2} and computational parameter as in Tab. 4.1

high accuracy level. We then confirm and extends the results to different regimes using *ab initio* calculations.

To introduce the analytical model for r we start from the BTE of Eq. 1.58. If we were able to diagonalize the real symmetric scattering matrix $A_{n\mathbf{k},m\mathbf{k+q}}$ we could rewrite the Boltzmann equation in a basis $\{\overline{n\mathbf{k}}\}$ defined by (Einstein notation is used):

$$D_{\overline{n\mathbf{k}},\overline{m\mathbf{k}'}} = U_{\overline{n\mathbf{k}},l\mathbf{p}} A_{l\mathbf{p},j\mathbf{b}} U^{\dagger}_{j\mathbf{b},\overline{m\mathbf{k}'}} \tag{4.5}$$

where D is a diagonal matrix and U is the matrix of basis change between the basis $\{\overline{n\mathbf{k}}\}$ and $\{n\mathbf{k}\}$. The Boltzmann equation would then be exactly solved at linear order

in $\mathbf{B}$ by:

$$\chi_{n\mathbf{k}} = -\left(U^\dagger D^{-1} U\right)_{n\mathbf{k},m\mathbf{k}'} \frac{\partial f^0_{m\mathbf{k}'}}{\partial \epsilon_{m\mathbf{k}'}} \mathbf{v}_{m\mathbf{k}'} \cdot \mathbf{E} - \left(U^\dagger D^{-1} U\right)_{n\mathbf{k},m\mathbf{k}'} \frac{\partial f^0_{m\mathbf{k}'}}{\partial \epsilon_{m\mathbf{k}'}} \left(\mathbf{v}_{m\mathbf{k}'} \wedge \mathbf{B}\right) \cdot \left[\nabla_{\mathbf{k}'} \left\{ \left(U^\dagger D^{-1} U\right)_{m\mathbf{k}',l\mathbf{p}} \frac{\partial f^0_{l\mathbf{p}}}{\partial \epsilon_{l\mathbf{p}}} \mathbf{v}_{l\mathbf{p}} \cdot \mathbf{E} \right\}\right]. \tag{4.6}$$

The above result is equivalent to exactly solve the BTE; we can try to simplify it in order to describe some physical properties without having to go through all the numerics. In particular, we have already seen in Chap. 1 that some common approximations are based on the substitution:

$$\left(U^\dagger D^{-1} U\right)_{n\mathbf{k},m\mathbf{k}'} \to 1/\left(\frac{\partial f^0_{n\mathbf{k}}}{\partial \epsilon_{n\mathbf{k}}}\right) \delta_{n\mathbf{k},m\mathbf{k}'} \tau_{n\mathbf{k}} \tag{4.7}$$

Although in general the above replacement is an approximation, it can be shown that under the assumption of perfectly isotropic bands energies and a quasielastic scattering, Eq. 4.7 is *exact* provided that the scattering time is calculated as in Refs. [164, 16]. Instead, if one uses the SERTA approximation as presented in Eq. 1.59, the expression for the relaxation time is:

$$\frac{1}{\tau^{SERTA}_{n\mathbf{k}}} = 2\pi \sum_{m\lambda} \int \frac{d\mathbf{q}}{\Omega_{BZ}} |g^\lambda_{n\mathbf{k},m\mathbf{k}+\mathbf{q}}|^2 \times \left[(1 + n^0_{\lambda\mathbf{q}} - f^0_{m\mathbf{k}+\mathbf{q}}) \delta(\epsilon_{n\mathbf{k}} - \epsilon_{m\mathbf{k}+\mathbf{q}} - \omega_{\lambda\mathbf{q}}) + (n^0_{\lambda\mathbf{q}} + f^0_{m\mathbf{k}+\mathbf{q}}) \delta(\epsilon_{n\mathbf{k}} - \epsilon_{m\mathbf{k}+\mathbf{q}} + \omega_{\lambda\mathbf{q}})\right]. \tag{4.8}$$

Using Eq. 4.7 the BTE becomes ($e = \hbar = 1$):

$$-\mathbf{v}_{n\mathbf{k}} \cdot \mathbf{E} + \left(\mathbf{v}_{n\mathbf{k}} \wedge \mathbf{B}\right) \cdot \nabla_{\mathbf{k}} \chi_{n\mathbf{k}} = \tau^{-1}_{n\mathbf{k}} \chi_{n\mathbf{k}} \tag{4.9}$$

and to first order in the $\mathbf{B}$ field it is solved by:

$$\chi_{n\mathbf{k}} = -\mathbf{v}_{n\mathbf{k}} \cdot \mathbf{E} \tau_{n\mathbf{k}} - \left(\mathbf{v}_{n\mathbf{k}} \wedge \mathbf{B}\right) \cdot \left[\nabla_{\mathbf{k}} \left(\mathbf{v}_{n\mathbf{k}} \cdot \mathbf{E} \tau_{n\mathbf{k}}\right)\right] \tau_{n\mathbf{k}} \tag{4.10}$$

To eliminate the electric field, we notice that even with the magnetic field each term in the BTE is coherently linear in $\mathbf{E}$, so that the equation must be satisfied for every possible value and orientation of the electric field. Therefore we define $\chi_{n\mathbf{k}} = \mathbf{\Phi}_{n\mathbf{k}} \cdot \mathbf{E}$

and have, for each vectorial component:

$$\mathbf{\Phi}_{n\mathbf{k}} = -\mathbf{v}_{n\mathbf{k}}\tau_{n\mathbf{k}} - (\mathbf{v}_{n\mathbf{k}} \wedge \mathbf{B}) \cdot \nabla_{\mathbf{k}} (\mathbf{v}_{n\mathbf{k}}\tau_{n\mathbf{k}})\, \tau_{n\mathbf{k}} \tag{4.11}$$

For graphene, it is convenient to rewrite the above vectorial relation in cylindrical components around the special point $\mathbf{K}$ [we indicate the cylindrical components along $\hat{k}^\rho$ and $\hat{k}^\theta$ with ρ and θ]:

$$\Phi^\rho_{n\mathbf{k}}\hat{\rho} + \Phi^\theta_{n\mathbf{k}}\hat{\theta} = -\left(v^\rho_{n\mathbf{k}}\hat{\rho} + v^\theta_{n\mathbf{k}}\hat{\theta}\right)\tau_{n\mathbf{k}} - \sum_{LMN} \epsilon_{LMN} v^L_{n\mathbf{k}} B^M \nabla^N_{\mathbf{k}} \left[(v^\rho_{n\mathbf{k}}\hat{\rho} + v^\theta_{n\mathbf{k}}\hat{\theta})\tau_{n\mathbf{k}}\right] \tau_{n\mathbf{k}} \tag{4.12}$$

where the LMN components of the vectors are intended to be cylindrical, all the vectors are functions of (ρ, θ) and ϵ_{LMN} is the Levi-Civita tensor. Now we work in the hypothesis that we can write $\epsilon_{n\mathbf{k}} = \epsilon_n(\rho) = (-1)^n v_F \rho$ with $n = \{0, 1\}$, i.e. we reduce the problem to only the π and π^* electronic bands (this is valid in the immediate proximity of the Dirac cone). It follows that the electronic velocity is only radial. In this way also $\tau_{n\mathbf{k}}$ is a function of ρ alone because the scattering time has the same symmetries of the energy states [4]. Moreover, we are interested in the case of a magnetic field along the $\hat{z}$ direction. It follows that the only term which is retained from the vector product of Eq. 4.12 corresponds to $L = 1, M = 3, N = 2$:

$$\Phi^\rho_{n\mathbf{k}}\hat{\rho} + \Phi^\theta_{n\mathbf{k}}\hat{\theta} = -\left((-1)^n v_F \hat{\rho}\right)\tau_{n\mathbf{k}} + v_F B^z \nabla^\theta_{\mathbf{k}} \left(v_F \hat{\rho}\tau_{n\mathbf{k}}\right)\tau_{n\mathbf{k}} \tag{4.13}$$

which becomes:

$$\Phi^\rho_{n\mathbf{k}}\hat{\rho} + \Phi^\theta_{n\mathbf{k}}\hat{\theta} = -\left((-1)^n v_F \hat{\rho}\right)\tau_{n\mathbf{k}} + v_F B^z \frac{1}{\rho}\frac{\partial}{\partial\theta} \left(v_F \hat{\rho}\tau_{n\mathbf{k}}\right)\tau_{n\mathbf{k}} \tag{4.14}$$

Using the fact that $\frac{\partial}{\partial\theta}\hat{\rho} = \hat{\theta}$ we obtain to first order in the $\mathbf{B}$ field:

$$\Phi^\rho_{n\mathbf{k}} = -(-1)^n v_F \tau_{n\mathbf{k}} \tag{4.15}$$

$$\Phi^\theta_{n\mathbf{k}} = v_F^2 B^z \frac{1}{\rho}\tau^2_{n\mathbf{k}} \tag{4.16}$$

Now we define the quantity $S^{pol.}_{ij} = v_i \Phi_j$ (dropping for the moment $\{n\mathbf{k}\}$), which, when integrated, gives the conductivity. We transform this quantity in the Cartesian components via:

$$S^{cart.}_{ij} = \sum_{k,l} U^\dagger_{ik} S^{pol.}_{kl} U_{lj} \tag{4.17}$$

where the S on the left is expressed in Cartesian indexes, while on the right in polar. The matrix U is the matrix of basis change:

$$U = \begin{pmatrix} \cos(\theta) & \sin(\theta) \\ -\sin(\theta) & \cos(\theta) \end{pmatrix} \tag{4.18}$$

and therefore obtain:

$$S^{cart.} = v^{\rho} \begin{pmatrix} \Phi^{\rho}\cos^2(\theta) - \Phi^{\theta}\sin(\theta)\cos(\theta) & \Phi^{\rho}\cos(\theta)\sin(\theta) + \Phi^{\theta}\cos^2(\theta) \\ \Phi^{\rho}\sin(\theta)\cos(\theta) - \Phi^{\theta}\sin^2(\theta) & \Phi^{\rho}\sin^2(\theta) + \Phi^{\theta}\sin(\theta)\cos(\theta) \end{pmatrix} \tag{4.19}$$

We now express the conductivity tensor:

$$\sigma^{cart.} = -\frac{2}{\Omega\Omega_{BZ}} \sum_n \int_0^{\infty} \int_0^{2\pi} \rho d\rho d\theta v_n^{\rho} \frac{\partial f_n^0}{\partial \epsilon}(\epsilon_n(\rho)) \times \tag{4.20}$$

$$\times \begin{pmatrix} \Phi_n^{\rho}\cos^2(\theta) - \Phi_n^{\theta}\sin(\theta)\cos(\theta) & \Phi_n^{\rho}\cos(\theta)\sin(\theta) + \Phi_n^{\theta}\cos^2(\theta) \\ \Phi_n^{\rho}\sin(\theta)\cos(\theta) - \Phi_n^{\theta}\sin^2(\theta) & \Phi_n^{\rho}\sin^2(\theta) + \Phi_n^{\theta}\sin(\theta)\cos(\theta) \end{pmatrix} \tag{4.21}$$

Integrating the angular dependence (and remembering that $\Phi^{\rho,\theta}$ and $\frac{\partial f_n^0}{\partial \epsilon}$ do not have angular dependence, and putting $v_n^{\rho} \sim (-1)^n v_F$) we have:

$$\sigma^{cart.} = -(2\pi)^{-1} v_F \sum_n (-1)^n \int_0^{\infty} \rho d\rho \frac{\partial f_n^0}{\partial \epsilon}(\epsilon_n(\rho)) \begin{pmatrix} \Phi_n^{\rho} & \Phi_n^{\theta} \\ -\Phi_n^{\theta} & \Phi_n^{\rho} \end{pmatrix} \tag{4.22}$$

We notice that in absence of a magnetic field, the conductivity tensor is diagonal as expected for symmetry reasons, while in presence of a magnetic field the off diagonal components are opposite in sign. We now use Eq. 4.16 and find :

$$\sigma_{xx} = (2\pi)^{-1} v_F^2 \sum_n \int_0^{\infty} \rho d\rho \frac{\partial f_n^0}{\partial \epsilon}(\epsilon_n(\rho)) \tau_n(\epsilon_n(\rho)) \tag{4.23}$$

$$\sigma_{xy} = -(2\pi)^{-1} v_F^3 B_z \sum_n (-1)^n \int_0^{\infty} \rho d\rho \frac{\partial f_n^0}{\partial \epsilon}(\epsilon_n(\rho)) \frac{1}{\rho} \tau_n^2(\epsilon_n(\rho)) \tag{4.24}$$

where the scattering time depends only on the energy through the radial coordinate. It follows, using $\epsilon_n(\rho) = (-1)^n v_F \rho$ (restoring e and $\hbar$):

$$r = \frac{n_e|e|}{B_z}\frac{\sigma_{12}}{\sigma_{11}^2} = -2\pi v_F^2 \hbar^2 n_e \frac{\sum_n (-1)^n \int_{-\infty}^{\infty} d\epsilon \frac{\partial f_n^0}{\partial \epsilon} \tau_n^2(\epsilon)}{\left(\sum_n (-1)^n \int_{-\infty}^{\infty} d\epsilon \epsilon \frac{\partial f_n^0}{\partial \epsilon} \tau_n(\epsilon)\right)^2} \tag{4.25}$$

where all the quantities under integration sign are to be intended as functions of the

integration variable ϵ only. The $(-1)^n$ in the denominator compensates for the negative sign coming from the area element when $\epsilon < 0$, so that the contributions to the diagonal components are always positive. On the contrary, in the numerator it subtracts the contributions between hole and electron carriers; in condition of perfect hole-electron symmetry of the band structure (i.e., in the limit of low temperatures and low carrier concentrations) the two contributions tends to cancel out and r becomes very small. If the Fermi level is slightly different from the Dirac cone energy E_D, then one carrier type contribution will dominate and r will be non zero; since the hole and electron mobilities in graphene are practically the same, the value of r is expected to have a different sign when E_F is greater or lower than E_D.

As mentioned above, Eq. 4.25 is an exact expression for r for a system with perfectly isotropic band energies and in presence of quasi-elastic scattering. It can though be used as an approximated formula in conjunction with *ab initio* calculations if one identify $\tau_{n\mathbf{k}} = \tau_{n\mathbf{k}}^{SERTA}$; in this case, we have to find an expression for $\tau_{n\mathbf{k}}^{SERTA}$ as a function of energy alone. This is done by writing:

$$\tau(k^\rho(\epsilon)) = \frac{1}{2\pi}\int_0^{2\pi} dk'^\theta \tau_n(k^\rho(\epsilon), k'^\theta) = \tag{4.26}$$

$$\frac{1}{2\pi k^\rho(\epsilon)}\int_{-\infty}^{\infty}\int_{-\infty}^{\infty} dk'^x dk'^y \delta(\frac{\epsilon'(k'^x, k'^y)}{v_F} - k^\rho(\epsilon))\tau_n^{SERTA}(k'^x, k'^y) \tag{4.27}$$

where $\epsilon'(k^x, k^y)$ is the linear expression of the energy bands around the Dirac cone as a function of $\mathbf{k}$. Now, as long as we know τ for energies which are given by the *ab initio* calculations, we substitute the true energies in the expression above to obtain:

$$\tau(k^\rho(\epsilon)) = \frac{1}{2\pi k^\rho(\epsilon)}\int_{-\infty}^{\infty}\int_{-\infty}^{\infty} dk'^x dk'^y \delta(\frac{\epsilon^{FP}(k'^x, k'^y)}{v_F} - k^\rho(\epsilon))\tau_n^{SERTA}(k'^x, k'^y) \tag{4.28}$$

where FP stands for First Principles. Bringing everything in energy (and restoring $\hbar$):

$$\tau_n(\epsilon) = (-1)^n \frac{v_F^2 \Omega_{BZ} \hbar^2}{2\pi\epsilon N_{\mathbf{k}}} \sum_{\mathbf{k}} \delta(\epsilon_{n\mathbf{k}}^{FP} - \epsilon)\tau_{n\mathbf{k}}^{SERTA} \tag{4.29}$$

where we note that the minus sign compensates the negative contributions coming from $\epsilon < 0$ for $n = 1$.

We conclude by saying that the use of the SERTA relaxation times to evaluate r is very instructive because, as we will see, it qualitatively catches the relevant behaviours of the Hall scattering factor; therefore, one can relate the behaviour of r to the scaling of the physical quasi-particles lifetimes.

4.4.2 Scaling and results

Using Eq. 4.25 we can predict the behaviour of r in different temperature regimes by considering the energy and temperature scaling laws of $\tau_n(\epsilon)$. In the *Bloch-Gruneisen (BG) regime* ($T < T_{BG} = 2\hbar v_{TA/LA} k_F / k_B$ where $v_{TA/LA}$ is the transverse/longitudinal acoustic sound velocity and k_F is the Fermi quasi-momentum) a close expression of τ_n as a function of energy is non-trivial [16, 165]; nonetheless, we can evaluate it at E_F as $\tau_n(E_F) \propto \frac{(k_B T)^4}{E_F}$ [49]; all the other quantities in Eq. 4.25 can be conveniently evaluated at $\epsilon = E_F$ since $\frac{\partial f_n^0}{\partial \epsilon} \approx -\delta(\epsilon - E_F)$. Thanks to these considerations we expect that in this regime r behaves as a constant $r \propto n_e / D(E_F)^2$, where $D(E_F)$ is the density of states at the Fermi level and at low temperatures it holds that $n_e \propto \pm \int_{E_F}^{E_D=0} E dE = \pm E_F^2/2$. In the *equipartition (EP) regime* ($T_{BG} < T < 270$K, where the upper bound is determined by the temperature at which the population of the A_1' phonon mode becomes non-negligible [16]) we have that $\hbar\omega_{\lambda_{TA/LA}\mathbf{q}} << k_B T$, that the EPC scattering is quasielastic and that the change of the electronic populations is not appreciable over a length $\hbar\omega_{\lambda_{TA/LA}\mathbf{q}}$ around E_F; the expression for the inverse scattering time is then found to scale as $|\epsilon| k_B T$. However, note that, at $\epsilon = 0$, the true total scattering rate $1/\tau_n(\epsilon)$ cannot be exactly zero because of non-vanishing contributions due to scattering with optical phonons, higher order scatterings or possible scattering with defects or boundaries. We give estimates for such additional scattering channels, that can give an idea of the validity of the scaling of the scattering time, in App. G. The validity of the scaling of $1/\tau_n(\epsilon)$ is assumed to be dominated by the finite size effects and hold true up to 1meV below/above E_D. It is thus clear that in the BG regime the numerator of Eq. 4.25 can reach large numerical values while the denominator quickly converges thanks to the ϵ in the integrand. In the BG regime we thus expect unusually large values of r, especially for low carrier concentrations.

We can verify the previous scaling considerations by inputting the scattering models for acoustic phonons of Refs. [16, 49] inside Eq. 4.25. The scattering parameters are evaluated at a DFT level. In the EP regime, for completeness, we include also inelastic scattering with the A_1' and Γ phonon modes as modelled in Ref. [16] and using Matthiessen's rule. While the inclusion of inelastic terms makes Eq. 4.25 never exact, since Γ phonons scattering is here totally negligible and the scattering from A_1' phonons is very weak (although non-zero), we expect Eq. 4.25 to be accurate. We show in Fig. 4.2 that r increases in the EP regime with decreasing doping, with values reaching ~ 4 at ~ 30meV below the Dirac cone and ~ 150K (around 1.5×10^{11}cm^{-2}). At higher temperatures and at low carrier concentrations we witness instead to low values of r (~ 0.5) because E_F is very near E_D; the spread of the Fermi-Dirac distribution is large

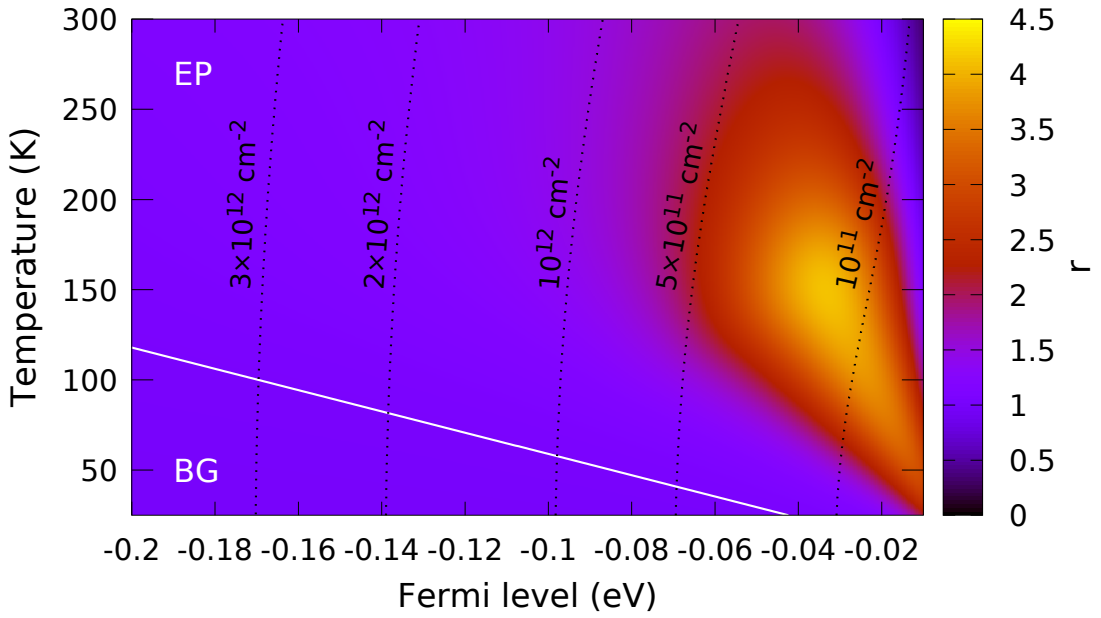

Figure 4.2: Hall scattering factor r as a function of temperature and Fermi level (corresponding carrier concentrations are indicated with dashed lines) obtained using Eq. 4.25 with $\tau^0_{n\mathbf{k}}$ from Ref. [49, 16]. We used a cutoff of 1 meV around the Dirac cone. The white line separates the Bloch-Gruneisen (BG) and the equipartition (EP) regimes.

and therefore both electrons and holes carriers contribute to the value of r substantially but with different signs, or in other words we have a cancellation of the scattering times at the numerator of Eq. 4.25 which is not challenged by a sharp variation of $\frac{\partial f^0_{n\mathbf{k}}}{\epsilon_{n\mathbf{k}}}$. The temperature and carrier density dependence of r is instead very mild in the BG regime; its value is around unity when using the DFT parameters. To test the robustness of these results, we can also evaluate Eq. 4.25 using the *ab initio* GW parameters given in Ref. [16] for both the EPC parameters and v_F; in this case we obtain very similar values for r holding the Fermi level fixed. The Hall scattering factor value is instead increased by $\sim 30\%$ over the whole range of considered temperatures if we compare the calculations at equal carrier concentrations. These changes are mostly due to v_F, not to the EPC parameters. Indeed, if we evaluate Eq. 4.25 at equal carrier densities using the GW EPC parameters but we keep v_F at its DFT value, the Hall scattering factor is very similar to r^{DFT}. This result is very interesting because it opens up the possibility to engineer r through Fermi velocity modification, which is experimentally possible as shown in Ref. [56]).

We can now proceed to study the high-temperature regime ($T > 270$ K) for a broad range of carrier concentrations. As mentioned above, in this regime the validity of Eq. 4.25 and of simplified models for $\tau_{n\mathbf{k}}$ is not given straight away. In particular, one would expect the importance of *ab initio* calculations in this regime as a consequence

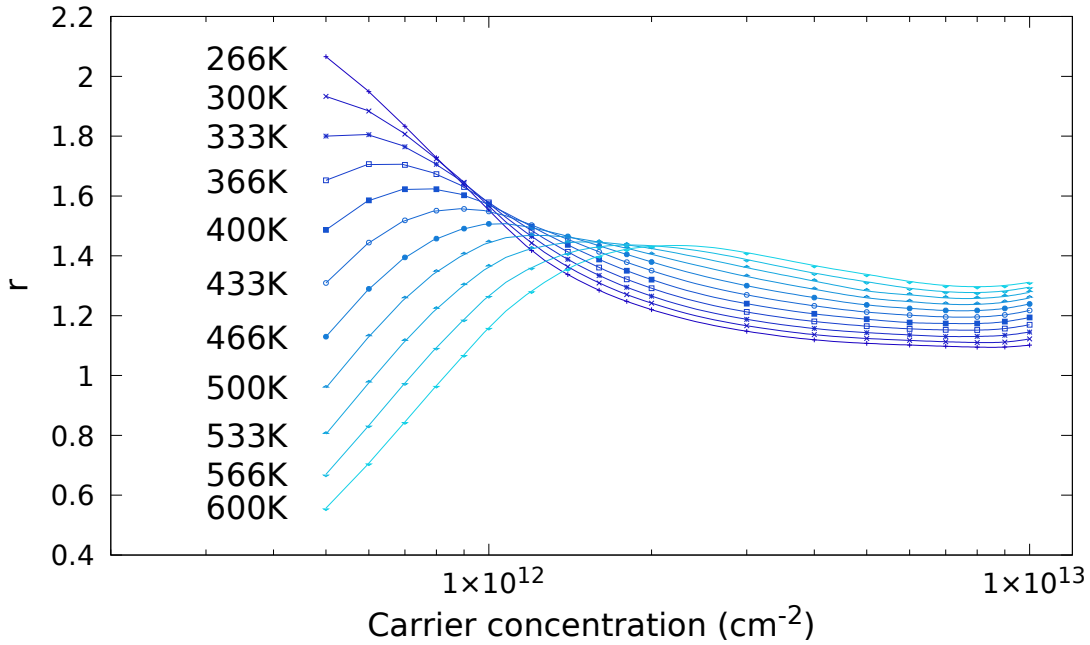

Figure 4.3: Hall scattering factor r obtained from the full *ab initio* solution of the BTE as a function of carrier concentrations, at different temperatures.

of *i*) the grown relevance of inelastic scattering, *ii*) the lack of an accurate and simple model for the optical EPC at Γ, *iii*) the inaccuracy of Matthiesen's rule and *iv*) the limited validity of the symmetry-based models for the EPC to the specific region of $\mathbf{k}$ points that are very close to the Dirac cone. We thus need to rely on the full *ab initio* solution of the BTE equation; the result for r is shown in Fig. 4.3. We notice that there is a cross-over in the temperature dependence of r at concentrations $10^{12}\text{cm}^{-2} < n < 2 \times 10^{12}\text{cm}^{-2}$. The low carrier concentrations regime shows that r decreases with temperature, a trend consistent with the one of Fig. 4.2. In the second regime ($n > 2 \times 10^{12}\text{cm}^{-2}$) r instead has gentle dependences on T and n.

Surprisingly, the *ab initio* values of r (Fig. 4.3) can be well reproduced in an extended range of temperatures and carrier concentrations by using the analytical model of Eq. 4.25, with the inclusion of both the acoustic and optical scattering rates of Ref. [16] using the Matthiesen's Rule. This agreement is shown in Fig. 4.4 where, as an example, we show the behaviour of r at $5 \times 10^{11}\text{cm}^{-2}$ and at $1.2 \times 10^{12}\text{cm}^{-2}$ (one of the carrier densities where r displays the cross-over in the temperature dependence observed in Fig. 4.3) It is crucial to point out than such an outstanding agreement happens despite the inaccuracy of the models in describing the resistivity at high temperatures and carrier densities [16]. The analytical model turning out to be a valid tool to compute r is due to compensation of scaling effects between the numerator and the

denominator of Eq. 4.25. A similar argument is also given for other transport quantities that are expressed as ratios, as the Seebeck coefficient (see, for instance, Refs. [3, 166, 65] where different computational approaches are analysed in various materials).

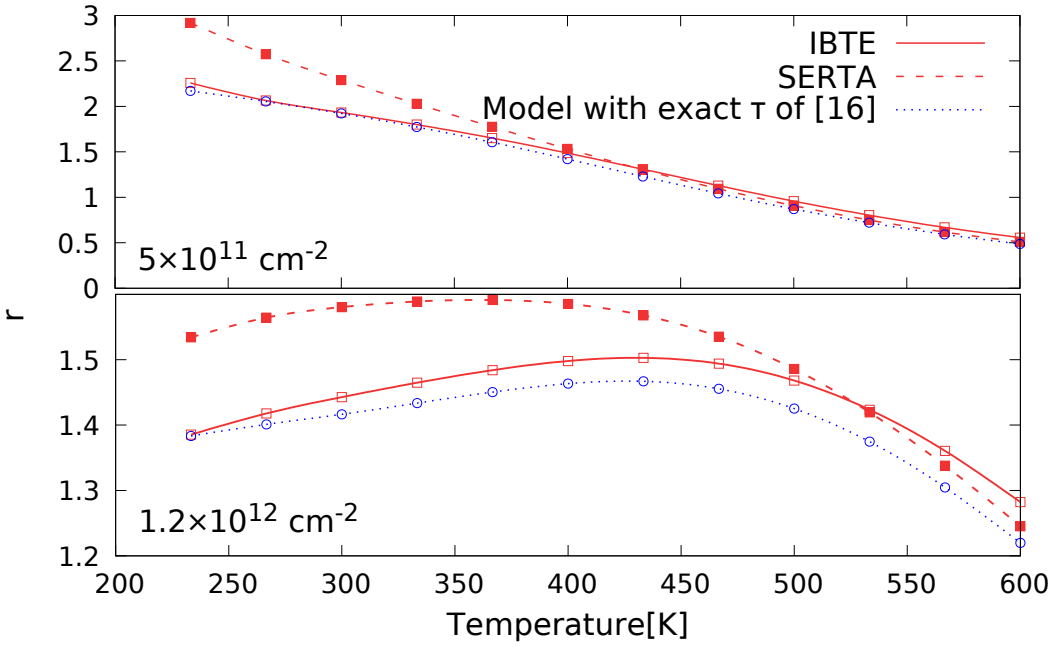

Figure 4.4: Comparison among the values of r as a function of temperature obtained from the full iterative solution of the BTE (IBTE) (continuous red line), using the SERTA approximation (dashed red line) and from the model discussed in the text (dotted blue line) at a carrier concentration of $5 \times 10^{11}\text{cm}^{-2}$ (top panel) and $1.2 \times 10^{12}\text{cm}^{-2}$ (bottom panel).

In Fig. 4.4 we also plot the temperature dependence of r in the SERTA approximation. It is interesting to notice that this approximation is slightly less precise than using the exact scattering times for isotropic band structures and quasi-elastic scattering, especially at low temperatures; nonetheless, it still captures the physical trends of the exact solution. Therefore the SERTA approximation can be conveniently used to analyse and understand the microscopic mechanisms that are at the basis of behaviour of r at high carrier concentrations. Indeed, in Fig. 4.5 we present the SERTA inverse scattering times for different carrier concentrations ($5 \times 10^{11}\text{cm}^{-2}$, $5 \times 10^{12}\text{cm}^{-2}$ and 10^{13}cm^{-2}) at 300K. We can see that the (almost) linear behaviour of $1/\tau_{\mathbf{k}}^{SERTA}$ around E_D, which is the distinguishing mark of acoustic phonon scattering, is evident for the lowest carrier concentrations; instead, it tends to disappear with increasing n. In addition, the fingerprint of optical phonon emission, i.e. the peak situated at around 200 meV above E_D, translates to lower energies while maintaining its energy at around

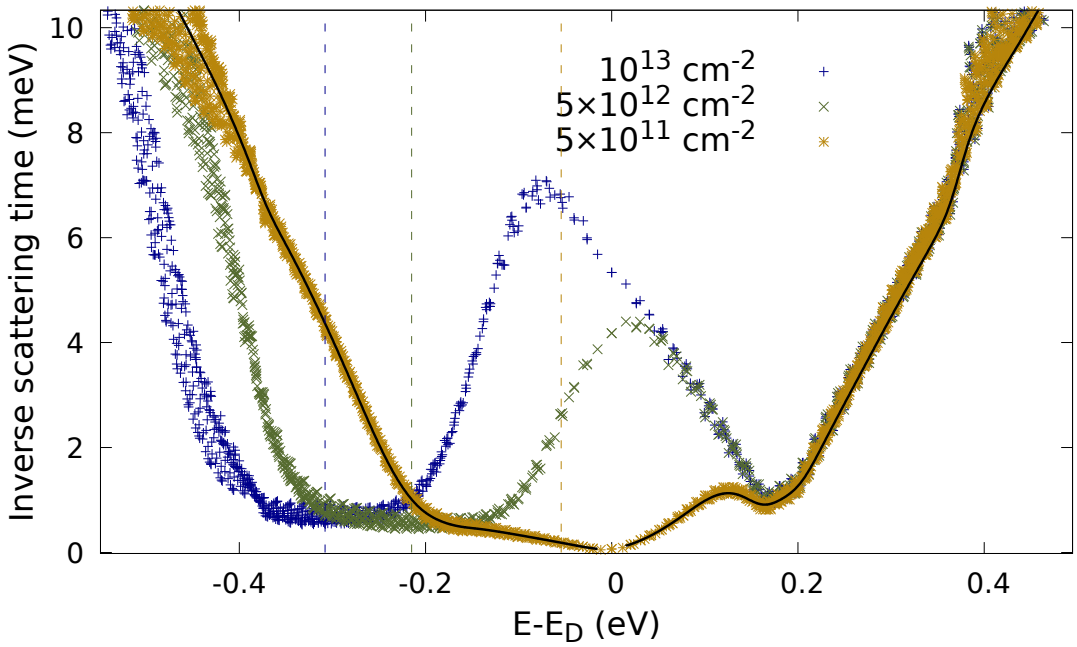

Figure 4.5: *Ab initio* scattering rate for three different doping concentrations (5×10^{11} cm^{-2}, 5×10^{12} cm^{-2} and 10^{13} cm^{-2}) at 300K, as a function of the distance from the Dirac cone energy. The black continuous line is the fit of the SERTA scattering time done via Eq. 4.29, which can be inserted in Eq. 4.25. The vertical dashed lines represent the Fermi levels for each doping concentration.

200 meV above E_F (indicated in the picture by vertical dashed lines for each concentration). This implies that at large carrier concentration the numerator of Eq. 4.25 does not present singular behaviours. We thus expect r to be much less sensitive to the form/nature of the scattering (in general, the denominator of Eq. 4.25, closely related to μ^d, is in this regime smoothly behaved). The final result is that the spread of the values of the Hall scattering factor as a function of temperature is strongly reduced.

In conclusion, we have determined from first principles the intrinsic behaviour of the Hall scattering factor in graphene for a wide range of carrier densities and temperatures. Our results show that at large carrier densities the strong coupling with optical phonons makes r weakly temperature dependent with values around unity. On the contrary, at low doping, the same quantity presents a strong temperature dependence with values much larger than unity below room temperature; this is a consequence of the nature of the acoustic scattering close to the Dirac cone and of the two-dimensional conic geometry of the bands. Therefore, the common practice of assuming $r = 1$ in Hall measurements should require careful examination in two-dimensional materials with non-parabolic band dispersion. As a final remark, we stress that our results also show that, even though for generic transport quantities a precise solution of the BTE is

needed in order to accurately determine their value and trends, for the Hall scattering factor the expression of Eq. 4.25 with analytic scattering models is an accurate and simple tool to compute the qualitative and quantitative values of r in a wide range of temperatures and carrier densities.

Chapter 5

First-principles study of electronic transport and structural properties of $Cu_{12}Sb_4S_{13}$ in its high-temperature phase

The Cu-Sb-S system has generated great interest amongst the family of copper-based semiconductors because of its appealing structural, electronic and thermal transport properties. In particular, Cu-Sb-S compounds display a large range of band gaps and extremely low thermal conductivities. Non-toxicity and abundance of the constituent elements are also key advantages that make the Cu-Sb-S system an ideal playground to design new materials for sustainable thermoelectric devices. In this perspective, the tetrahedrite $Cu_{12}Sb_4S_{13}$ is of particular interest since it shows a remarkably high zT value, approximately 0.6 at 700 K, which comes from a very low thermal conductivity (below 1 $Wm^{-1}K^{-1}$ from 300 to 700 K) and a high power factor [61].

In spite of a large effort in characterising the material (see, for instance, Refs. [61, 167, 168, 169, 170]), a detailed understanding of the transport coefficients is still missing. This can possibly prevent further optimisations of the compound and related thermoelectric devices. In particular, the relative electronic and lattice contributions to the very low thermal conductivity is not clear. In addition, the temperature dependence of the electrical resistivity appears to vary considerably in the available experimental data and a full *ab initio* theoretical approach that investigates the scattering mechanisms is still missing. In this, of particular interest is the effect on the carriers of a very peculiar lattice dynamics, that shows soft phonons at zero temperature, strong anharmonicity and unusually large anisotropic atomic displacement parameters as shown in diffraction studies [171].

In order to address all these issues we have initially carried out an extensive study

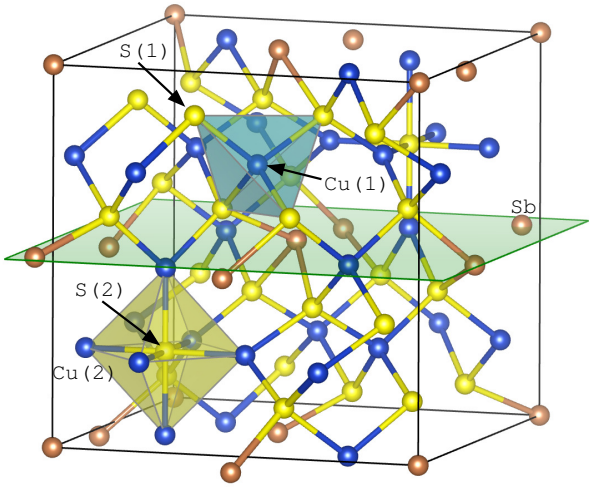

Figure 5.1: Tetrahedrite cubic conventional cell. S atoms are yellow, Cu atoms are blue and Sb atoms are orange.

of the structural stability of the high-temperature phase of tetrahedrite. In particular, this is done by analysing the structural relationship between the tetrahedrite and the simpler fematinite structure (Cu_3SbS_4), which under optimal doping shows comparably good thermoelectric properties [172, 173]. As it will be clear, tetrahedrite can be seen as a fematinite-based structure with an ordered arrangement of S-vacancies. Beside shedding new light on the caged nature of tetrahedrite and on its anharmonic structure [171], that are at the origin of the low lattice thermal conductivity, this also shows that S-vacancies are the natural doping mechanism for the Cu-Sb-S compound; indeed, the starting Cu_3SbS_4 structure is a semiconducting material with a gap of about 0.8 eV and it shows a zT of 0.6 at 600 K under Ge or Sn doping.

We have then investigated the temperature dependence of the electronic transport properties of the compound. In order to do this, we have averaged the Kubo-Greenwood (K-G) formula for independent particles on snapshots of *ab-initio* molecular-dynamics (AIMD) simulations at different temperatures, as successfully done in other systems (see for instance Ref. [63]). The calculations have been performed using VASP [67, 68] together with a in-house built post-processing tool [1]. The need for this approach, instead of a Boltzmann transport formalism, is justified principally by the inherent incorporation of the interaction between electrons and classical lattice vibrations as well as classical anharmonicity effects. These are supposed to stabilise the high-temperature phase of the tetrahedrite structure, that instead displays unstable soft phonons at zero-temperature [61]. This kind of calculation evaluates the intrinsic transport properties of the material and their temperature dependence: we find that the

[1] Publicly available at https://github.com/conodipaola/kg4vasp

Seebeck coefficient is in very good agreement with experiments and that the phonon-limited resistivity shows a fairly temperature independent behaviour, with remarkably low values that are not too far from the lowest experimental values [168]. Finally, the Lorenz number is significantly lower than the free electron value; this is an important result in the perspective of grasping the relative importance of the lattice and electronic contributions to the thermal conductivity.

5.1 Computational details

The DFT calculations were performed using the projector augmented wave method (PAW) [108] as implemented in the Vienna *ab initio* simulation package (VASP) [67, 68]. We used the Perdew, Burke and Ernzerhof (PBE) exchange-correlation functional [174] for all the calculations with a plane wave energy cutoff of 550 eV and a $3 \times 3 \times 3$ grid of k-points to sample the Brillouin zone of the conventional unit cell. Lattice parameters and internal positions were fully relaxed (but constraining the cell to be tetragonal). Formation energies are calculated as $E_{form.} = \frac{E_0 - \sum_{i=1}^{N_t} n_i E_i}{N_a}$ where E_0 is the ground state total energy of the system with N_a atoms in the unit cell, N_t is the number of different types of atoms in the unit cell, and n_i and E_i are the number of atoms of type i and their ground state total energy in a bulk configuration. We compute the Onsager coefficients $L_{ij}(\omega)$ in the static dc limit for the electronic field for each ionic configuration in the supercell according to the K-G formula of Eq. 1.106. The temperature dependence of the transport coefficients (defined as in Eq. 1.35) is obtained by a simple average over snapshots extracted from a molecular dynamics simulation [63]. We used simulation cells of 232 atoms ($2 \times 2 \times 1$ supercells). Initially we performed NPT runs with the Parrinello-Rahman scheme in the Nosé -Poincaré approach for isothermal sampling [175]; we set the time-step to 1 fs and the thermostat period to 1.11 ps; the barostat is used with fictitious masses of 10^{-3} amu. These AIMD simulations were run for a time span of 5 ps, which was enough to calculate the averaged cell parameters at different temperatures. As a second step, we performed NVT runs using a Langevin thermostat. We used a drift parameter of 1.0 ps^{-1} and performed simulations of about 8.5 ps with a time-step of 1 fs; the first 4.5 ps have been used to safely reach thermal equilibration. After equilibration we extracted snapshots of nuclear positions every 500 AIMD steps. For every snapshot we have performed static electronic DFT calculations and used the output to evaluate the Kubo formula. While in the AIMD simulations we used a k-points grid of $1 \times 1 \times 3$, for every snapshot we used a denser grid of $3 \times 3 \times 6$; for the smearing we used the Fermi-Dirac function with

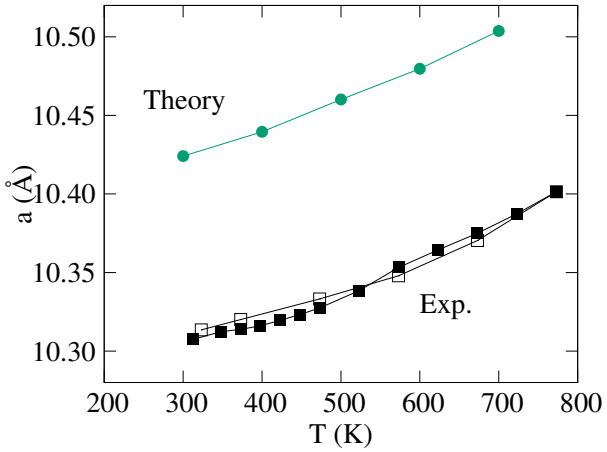

Figure 5.2: Lattice parameter as a function of temperature. Experimental data are from the supplementary material of Ref. [177] and obtained from cooling (empty squares) and heating (full squares).

the electronic temperature corresponding to the temperature of the system. The chemical potential obtained from the *ab initio* calculation was then consequently used in the Kubo formula. The Dirac delta functions have been approximated with Gaussians of spread 40 meV. One method to choose the broadening is to impose the removal of all the small oscillations in the optical conductivity that are due to the discretization of band structure [176]. The stability with respect to changes of the Gaussian broadening is checked by increasing its value and estimating the changes in the transport coefficients. For instance, at 300K the resistivity changes by less than 5% when we change the smearing from 20 meV to 70 meV. It is also worth to stress that we used a cell of 232 atoms that is a tetragonal supercell; nonetheless, the conductivity tensor is diagonal with the proper symmetry for a cubic system. We intend this to be a quite clear indication of convergence of the transport coefficients with respect to the cell size.

The electronic transport parameters were also computed via the BTE within the Constant Relaxation Time (CRT) approximation, using the BoltzWann code [33] on the DFT band structure of the symmetric high-temperature phase of tetrahedrite.

5.2 Crystal structure

Above room temperature tetrahedrite possess a cubic structure ($I\bar{4}3m$). The conventional cell is made of 58 atoms and is shown in Fig. 5.1, with an experimental lattice parameter of $a_{exp} = 10.32$Ang [178, 179]. Our DFT calculations predict

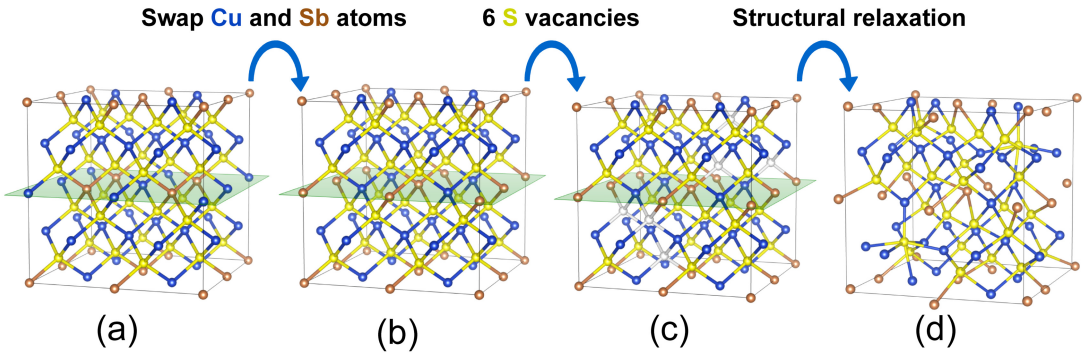

Figure 5.3: (a) $2 \times 2 \times 1$ supercell of fematinite, Cu_3SbS_4; (b) structure obtained by swapping Cu and Sb atoms within the green (001) plane; (c) structure in which 6 S atoms are removed (white atoms); (d) Relaxed structure obtained starting from (c). Color scheme for the atoms are as in Fig. 5.1.

$a_{DFT} = 10.40$Ang, in agreement with results reported in literature [61]. The temperature dependence of the lattice parameter, deduced from AIMD NPT simulations, is shown in Fig. 5.2 together with a comparison to experimental data. In this high temperature phase there are five distinct crystallographic sites, namely, Cu(1): 12d, Cu(2): 12e, Sb: 8c, S(1): 24g, and S(2): 2a. The Cu(1) atoms are four-fold coordinated at the centre of tetrahedrons of S(1) atoms, whereas the Cu(2) atoms are three-fold coordinated at the vertices of octahedrons at the centre of which there are S(2) atoms. The Sb atoms are on [001] planes at the apex of trigonal pyramids with S(1) atoms. In order to better understand the structure of this complex compound, it is useful to establish a connection between the structures of the tetrahedrite and of the simpler fematinite. In order to do so we consider a $2 \times 2 \times 1$ supercell of the fematinite structure, containing 64 atoms (Fig. 5.3a). This supercell is almost cubic since the primitive cell of the fematinite phase is tetragonal ($I\bar{4}2m$) with experimental cell parameters of 5.39Ang and $c = 10.75$Ang[173]; moreover, the average of the supercell lattice parameters is close to the tetrahedrite one. At this point, the link between the tetrahedrite and the fematinite structures is established in the following two-step procedure: i) swap Cu and Sb atoms in the highlighted (001) plane as shown in Fig. 5.3 (b) (or, equivalently, slip the highlighted plane in the $< 110 >$ direction), and then ii) remove 6 S atoms from the supercell [see Fig. 5.3 (c)], thus recovering the tetrahedrite stoichiometry. If the system is now relaxed, the resulting structure (Fig. 5.3 (d)) is cubic (with a lattice parameter of 10.39Ang) and quite similar to the tetrahedrite. The only main difference is a small distortion of the octahedral pattern that is not observed in the high-T phase of tetrahedrite (see Fig. 5.1). This result is not very surprising because at low temperatures in tetrahedrite there are hints of a first order structural transition happening around

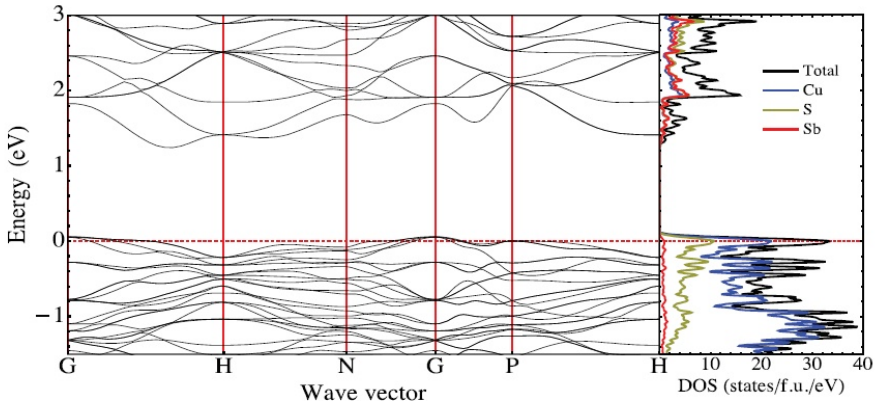

Figure 5.4: Band structure and DOS of $Cu_{12}Sb_4S_{13}$, reprinted from Ref. [61].

70 K; this transition modifies the size of the cell and introduces distortions in the local symmetry for $T < 70$ K (this transition is still object of an active experimental investigation [167, 180, 181, 182, 62]). In addition, the instability at low temperatures is evident also from zero temperature calculations of the phonon spectrum of the high-T symmetric phase [61], as we will see in the next section.

To conclude the discussion about the connection between tetrahedrite and fematinite, it is interesting to compare the stability of the structures suggested in Fig. 5.3. Our calculations show that the formation energies of the initial and final structures in Fig. 5.3 are the same to a good precision, their values being -0.241 eV. The formation energy of the high-T symmetric phase (Fig. 5.1) is instead 2 meV higher. It is also interesting to observe that the formation energy of the intermediate step (b) of Fig. 5.3, where Cu and Sb are exchanged, is only 6 meV higher than the fematinite one. These structure calculations show that the clustering of sulphur vacancies in neighbouring positions turns out to be very convenient. These results, beside highlighting the link between tetrahedrite and fematinite, also directly show that the Cu-Sb-S crystalline compounds can be quite flexible and open to a variety of energetically competitive structures, with sulphur vacancies playing a very active role in this process.

5.3 Electronic and vibrational properties

Our calculation of the electronic structure of the high-temperature phase of $Cu_{12}Sb_4S_{13}$ is in good agreement with results already reported in literature (shown in Fig. 5.4). The density of states (DOS) in Figs. 5.4 and 5.5 clearly shows that the compound is metallic but it can be interpreted as an heavily doped p-type semiconductor. This is because the Fermi level lies near the top valence bands formed by sulphur 3p and copper 3d hybridised states; the bottom of the conduction band lies at about 1.25 eV from the

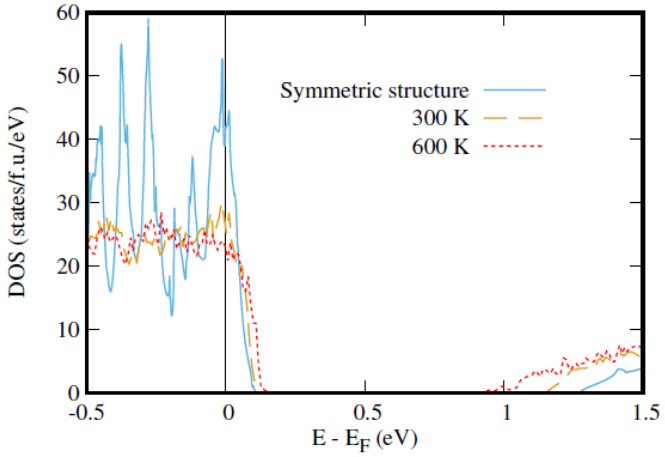

Figure 5.5: Comparison between the DOS of the symmetric structure in Fig. 5.1 (solid blue line) and the snapshot averaged DOS at 300 K (orange dashed line) and at 600 K (red dotted line). E_F is the Fermi level.

Fermi level. This large band gap is in agreement with other theoretical results [61], but it is lower than the experimental gaps reported in literature that vary between 1.7 eV and 1.9 eV. [183, 184] The electronic structure of tetrahedrite is very different from the one of fematinite. Indeed, as discussed in Refs. [172, 173], fematinite is a semiconductor with a smaller band gap of around 0.6 eV; here, the DOS at the top of the valence band can be easily fitted with a proper DOS effective mass that can be used in a parabolic band model to predict the thermoelectric properties of the compound under hole doping. The tetrahedrite displays instead a rather complex and spiky DOS around the Fermi level, far from being compatible with a parabolic model able to predict the transport properties behaviours. In Fig. 5.5 we show the effect of thermal motion of atoms on the electronic DOS of the compound, at 300 K and 600 K, obtained by averaging snapshots of the AIMD simulations. Our results clearly show that thermal motion leads to a visible flattening of the DOS peaks obtained at zero-T for the symmetric structure; also, we witness to a sensible decrease of the energy gap between the Fermi level and the bottom of the conduction band.

Finally, we show in Fig. 5.6 the phonon dispersion of the high-T phase of $Cu_{12}Sb_4S_{13}$ at zero-T. As already anticipated, several soft modes (negative phonons) are present over all the wave-vector spectrum. This means that the structure is highly unstable at low temperature and undergoes a reconstruction process, and anharmonic effects are of fundamental importance to stabilize the structure above 70K.

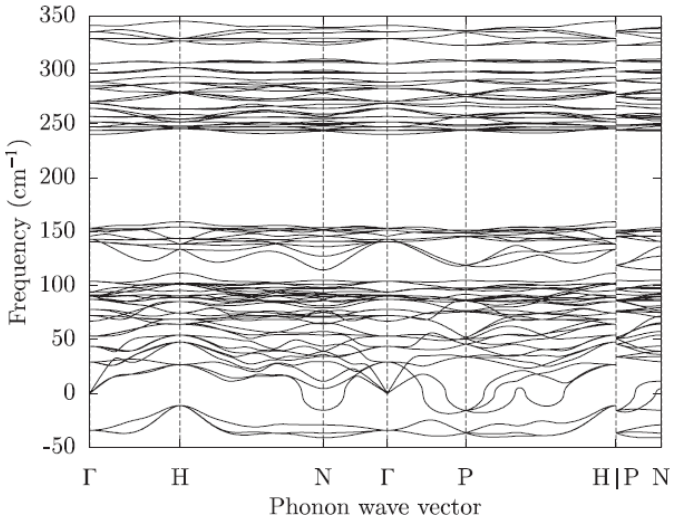

Figure 5.6: Phonon dispersion of $Cu_{12}Sb_4S_{13}$,reprinted from Ref. [61].

5.4 Thermoelectric transport coefficients

In this section we discuss the thermoelectric transport properties of the tetrahedrite compound and their temperature dependence. In Fig. 5.7 we compare the intrinsic phonon-limited resistivity $\rho = 1/\sigma$ computed with the K-G approach and the experimental results. Most of the experimental data show a metallic-kind increase of the resistivity as a function of temperature and this trend is in good agreement with our theoretical results. Nonetheless, the experimental points have a quite sensitive spread as a result of extrinsic effects (e.g. defects, impurities and polycrystallinity) that in different samples can be of different importance. Our values for the phonon-limited resistivity (about 0.5×10^{-5} Ω m at 600 K) are intended as an inferior limit for the ideal pure sample and are not too far from the lowest experimental values reported in literature [168, 170], which are about 1×10^{-5} Ω m. These values are quite low for an undoped mineral in the Cu-Sb-S family. Indeed, for instance, nano structured Sn doped fematinite at optimal doping for thermoelectric efficiency (a carrier concentration of about 5×10^{20} cm^{-3}) has a resistivity between 1×10^{-5} Ω m and 1.8×10^{-5} Ω m, respectively at 300K and 600K [173].

It is now very interesting to notice that the temperature dependence of our theoretical results and of the experimental results with the lowest resistivity [168, 170] can be reproduced also by tuning the carrier lifetime τ in the CRT approach for the Boltzmann formalism, that uses only the DFT band structure of the symmetric high-temperature phase of tetrahedrite. For instance, as shown in Fig. 5.7, the experimental data in Ref. [168] can be fitted in a broad temperature range using an empirical carrier lifetime of 5.6 fs. The same fitting can be done on our theoretical result and in this

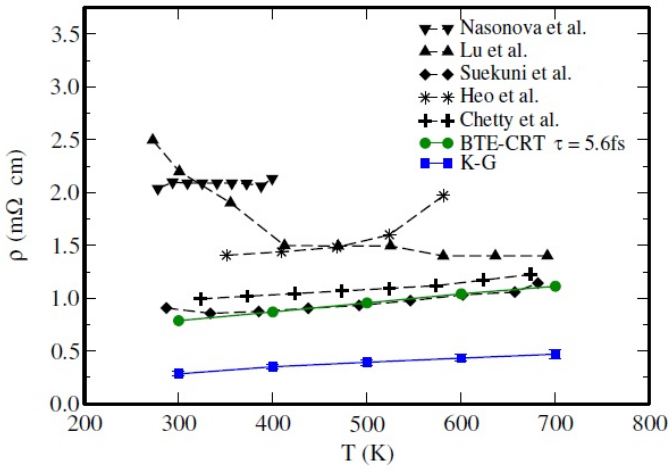

Figure 5.7: Resistivity as a function of temperature. The blue squares (green circles) are the K-G (BTE-CRT) results. The black symbols are the experimental data: the down triangles are from Ref. [167], the up triangles from Ref. [61], the diamonds from Ref. [168], the stars from Ref. [169], and the plus symbols from Ref. [170]. The error bars in the K-G results are smaller than the symbols used.

case the phonon-limited carrier lifetime is 16 fs, which has to be considered the upper bound of the carrier lifetime in pristine tetrahedrite.

The fact that the temperature dependence of the resistivity is so well captured by the Boltzmann approach in a very simple approximation as the CRT suggests that the temperature dependence of the carrier scattering time due to the electron-phonon coupling is not of fundamental importance in this material.

In Fig. 5.8 we show our results for the Seebeck coefficient as a function of temperature. The theoretical data are in very good agreement with experiments, both in the K-G and the BTE-CRT formalisms. This agreement between different approximate theoretical approaches is not novel for the Seebeck coefficient (for instance, see the analysis done for simple semiconductors [3, 4]) even when the scattering time has a well defined temperature dependence; a fortiori, as we discussed above, for this material where the resistivity can be reproduced in a wide range of temperatures using the equilibrium band structure of the symmetric phase and a carrier relaxation time independent of temperature, it is reasonable to expect a good agreement between the different approaches. The values of the Seebeck coefficient are appreciably high in this pristine system. For instance, the predicted value at 600 K, about 100 μV/K, is almost as high as the values found in fematinite at optimal Sn doping, about 130 μV/K [173]. These values of S and ρ lead to an undoped compound with a quite high power factor, S^2/ρ. The highest reported experimental values of the power factor at 600 K are

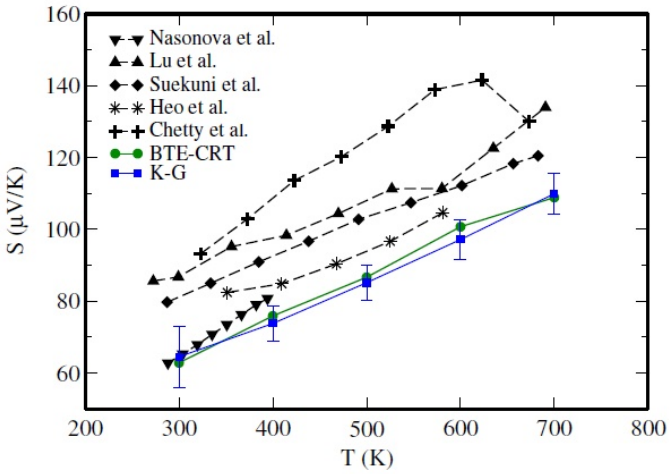

Figure 5.8: Seebeck coefficient as a function of temperature. The symbols are as in Fig. 5.7.

between 1.2 and 1.4 mW/(K^{2}m) [168, 170, 185], but our calculations suggest the possibility of further improvement to about 2 mW/(K^{2}m).

In Fig. 5.9 we show the results for the Lorenz number, $L = \kappa_e/(\sigma T)$. This quantity is important to isolate the electronic contribution κ_e to the thermal conductivity using the experimental values of the electrical conductivity. In this way, it is possible to extract the lattice thermal conductivity κ_L from experiments using $\kappa_L = \kappa_{exp} - \kappa_e$. Our calculations show that even if tetrahedrite displays a transport metallic behaviour above room temperature, the values of L obtained with the K-G formalism are almost temperature-independent but substantially lower than the free-electron value in the Wiedemann-Franz law ($L_0 = 2.44 \times 10^{-8}W\Omega$ K^{-2}). In addition, contrary to what observed for the Seebeck coefficient, the BTE-CRT approach gives values for L slightly higher than the K-G ones, with a slightly different temperature trend. Here, the difference between the approaches is not surprising because, as shown in other models [186] and *ab initio* [3] calculations, the Lorenz number is tendentially more sensitive to the details of the carrier scattering mechanisms.

These predictions for L are interesting as they show that the electronic contribution to the thermal conductivity extracted using the free-electron value for L (as done, for instance, in Refs. [168, 61]) can be significantly overestimated, up to about 50%; this can lead to a severe underestimation of the intrinsic lattice thermal conductivity of tetrahedrite. For instance, in Ref. [61] the reported value of the experimental thermal conductivity is of about 1.45 W/(m K) at 600 K and the lattice contribution is estimated using an L_0 of about 0.4 W/(m K); if the estimation is instead done using L from our calculations within the K-G approach, the value for κ_L is of about 0.8 W/(m K) ($\kappa_L \approx 0.6$ W/(m K) using L from the BTE-CRT approach), suggesting that the lattice

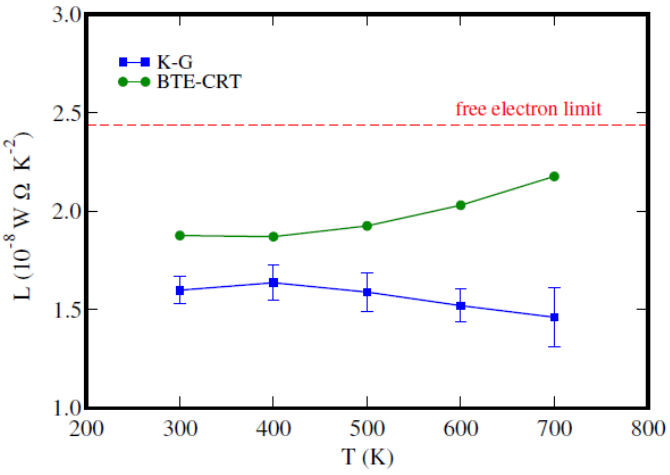

Figure 5.9: Lorenz number as a function of temperature. The blue squares (green circles) are the K-G (BTE-CRT) results; the red dashed line is free-electron value in the Wiedemann-Franz law ($L_0 = 2.44 \times 10^{-8}$WΩ K^{-2}).

thermal conductivity of the compound is certainly low, but it can be very similar to the electronic contribution.

Conclusion

In this work we addressed the theory and computation of transport properties of crystals in presence of external fields (thermal gradients and electromagnetic fields) via the solution of the linearised BTE or using the Kubo response formalism. In the theoretical section, we have given a detailed description of both methods, with a particular attention on the derivation of the BTE from NEGFs. Indeed, we showed that the BTE for the electronic statistical distribution is obtained as the semi-classical limit of the evolution equation for the lesser Green's function, integrated over the frequency domain. We also showed how the various transport observables in this limit coincide with their intuitive microscopic definitions; we discussed their gauge invariance and how in solids this is tightly connected to the use of Wannier functions basis sets. The whole of these arguments serves as a proof of the general validity and precision of the methods and of the results of this work. Successively, we have validated the theory reproducing experimental data and used it to predict behaviours of transport quantities on materials of interest. Firstly, we have explored from first-principles the intrinsic limits of the thermoelectric properties of p-doped diamond and their dependence upon dopant concentration, temperature and magnetic field. We found that the phonon-limited drift mobility is around 2500 $\mathrm{cm}^2/\mathrm{V}^{-1}\mathrm{s}^{-1}$ at room temperature, which is in agreement with the most recent experiments but not compatible with some extraordinary high values (around 3800 $\mathrm{cm}^2/\mathrm{V}^{-1}\mathrm{s}^{-1}$) reported in the literature. The temperature dependence of this quantity is remarkable since we can identify two regimes where the power law is very different as a consequence of different scattering mechanisms (acoustic phonons at low temperatures, high phonons at high temperatures). As regards the Seebeck coefficient, the diffusive component is not remarkable in value or trends, but the phonon-drag component—whose description requires the numerical solution of the phonon BTE—presents unique features at low temperatures. We also predicted that the Seebeck coefficient can be enhanced at room temperature in presence of an external magnetic field by as much as 30% at 40kOe, in line with the magnetoresistivity behaviour. On a more general footing, our results give a detailed microscopic characterisation of the carrier dynamics in diamond and are intended to provide a useful reference for the analysis and simulation of diamond-based electronic devices. Also,

the use and validation of our theoretical modelization here turns out to be a promising tool to calculate magneto-transport coefficients in doped semiconductors as well as in metallic systems.

We have then focused on two dimensional materials and, in particular, graphene. Here, we have determined from both first principles and models the intrinsic behaviour of the Hall scattering factor in a wide range of doping and temperatures. This quantity is very important in extracting the carrier density and the drift mobility from experiments. We find that at large dopings r is weakly temperature dependent, with values around unity, due to the coupling with optical phonons. At low doping, r presents a sharp temperature dependence with values much larger/lower than unity below 300K; this is due to the acoustic electron-phonon scattering rate close to the Dirac cone and to the two-dimensional conic geometry of the bands. This suggests that in two-dimensional materials with non-parabolic band dispersion the common practice of assuming $r = 1$ in experiments or theoretical calculations should require careful examination. Finally, it is worth pointing out that, even though the careful *ab-initio* description of r is very demanding, simple models which contain the basic physical ingredient can predict the value of the Hall scattering factor within a great accuracy. Practically, a better understanding of the Hall scattering factor in graphene—and a simple tool to calculate it—can be of great importance to explore and optimise graphene-based devices. For instance, a direction of particular interest is the current research on graphene Hall sensors, that have the potential to outperform traditional magnetic sensors based on semiconductors [187, 188, 189, 190].

When our BTE approach cannot be applied, such as in materials with soft phonons modes, we switch to the Kubo formalism. The case study that we considered here is the tetrahedrite $Cu_{12}Sb_4S_{13}$, a compound of potential technological applications. We have shown that the structural variety of the Cu-Sb-S network allows a description of tetrahedrite in terms of a semiconductor modified by an ordered arrangement of S-vacancies. The Kubo-Greenwood approach has allowed us to predict two important thermoelectric quantities, the phonon-limited electrical resistivity and the Lorenz number. The predicted resistivity turns out to be quite low for an undoped compound in the Cu-Sb-S system. The lowest experimental data reported in literature are not too far from the predicted intrinsic values: this clearly shows that the quality of the samples studied in experiments is high, but it also suggests the possibility of further improvements of the electronic transport properties. The Lorenz number has turned out to be substantially lower than what expected for the free-electron value, often used to estimate the electronic and lattice contributions to the thermal conductivity in experiments. Thus our result provides a more accurate reference to analyse thermal transport in this

compound. Finally, it is important to stress that the K-G approach has been key to predict transport properties in this system. Nonetheless, our analysis has also allowed us to show that the use of a less computationally demanding BTE-CRT approach is quite effective to reproduce the temperature trends of transport quantities such as the resistivity and the Seebeck coefficient in this complex compound.

In conclusion, in this work I developed theoretical tools and computational infrastructures in order to study the trends of transport quantities in 3d and 2d materials. In particular, I focused on the development and on the implementation of a new and reliable solver for the BTE in presence of a magnetic field; I also extensively worked on the systematic optimization of the existing solvers for the BTE in presence of electric field alone. In the cases that have been studied, my predictions are in line with theoretical expectations and, more importantly, they are in general good agreement with experimental data. The developments of this work will be available in the official repository of the EPW code at `https://gitlab.com/QEF/q-e/-/tree/develop/EPW`. With more than 30,000 lines of FORTRAN90 code written, the scalable and optimized tools developed here allow to obtain the exact numerical solution of the BTE equation on extremely dense grids for increasingly complex systems; together with the current exciting perspective of exascale computing, I believe that these advances will be of fundamental importance in the investigation of the *ab-initio* transport properties of crystals in the next years.

Appendix A

Work-flow/Flowchart of transport calculation from first principles

In this Appendix we present the work-flow of the practical calculations that are based on the theory presented in Chap. 1. Our practical procedure for the calculation of the transport quantities in crystals consists in various steps. For the BTE approach, as explained in Refs. [4, 3, 5, 64], we proceed in line with the following steps:

1. Self-Consistent-Field (SCF) calculation of the ground state density of the system by the means of standard ab-initio DFT techniques;
2. Non-Self-Consistent-Field (NSCF) calculation of the wave-functions $\Psi_{n\mathbf{k}}$ and band structure $\epsilon_{n\mathbf{k}}$ of the system using the SCF ground state density;
3. Density Functional Perturbation Theory (DFPT) calculation of the phonon spectrum of the system and variation of the electronic self consistent Khon-Sham potential $\partial_{\lambda\mathbf{q}} V^{SCF}$ with respect to a phonon mode $\{\lambda\mathbf{q}\}$ of frequency $\omega_{\lambda\mathbf{q}}$;
4. Calculation of the Electron Phonon Coupling (EPC) matrix $g^{\lambda}_{n\mathbf{k},m\mathbf{k}+\mathbf{q}}$ using DFPT $\partial_{\lambda\mathbf{q}} V^{SCF}$ and NSCF $\Psi_{n\mathbf{k}}$;
5. Wannier-scheme interpolation of the band structure energies, band velocities, phonon energies and EPC elements on very fine grids;
6. Solution of the BTE equation to obtain the out of equilibrium population $f_{n\mathbf{k}}$;
7. Calculation of the transport properties tensors by means of Eqs. 1.73.

The previous steps are graphically represented in the flowchart of Fig. A.1. For the first 4 steps we have used the Quantum Espresso (QE) code [66] and for the last 2 we have used a pre-release version of the EPW code [34, 35].

For the calculations involving the Kubo-Greenwood formalism, we work with the following steps, as explained in Ref. [65]:

1. *Ab initio* NPT Molecular Dynamics (MD) to equilibrate the volume of the system;
2. *Ab initio* NVT MD to simulate the thermal motion of the atoms;
3. SCF calculation on snapshots of the MD simulation;
4. NSCF and calculation of optical matrix elements (expectation values of the nabla operator);
5. Calculation of the conductivity by means of the Kubo-Formula of Eq. 1.106.

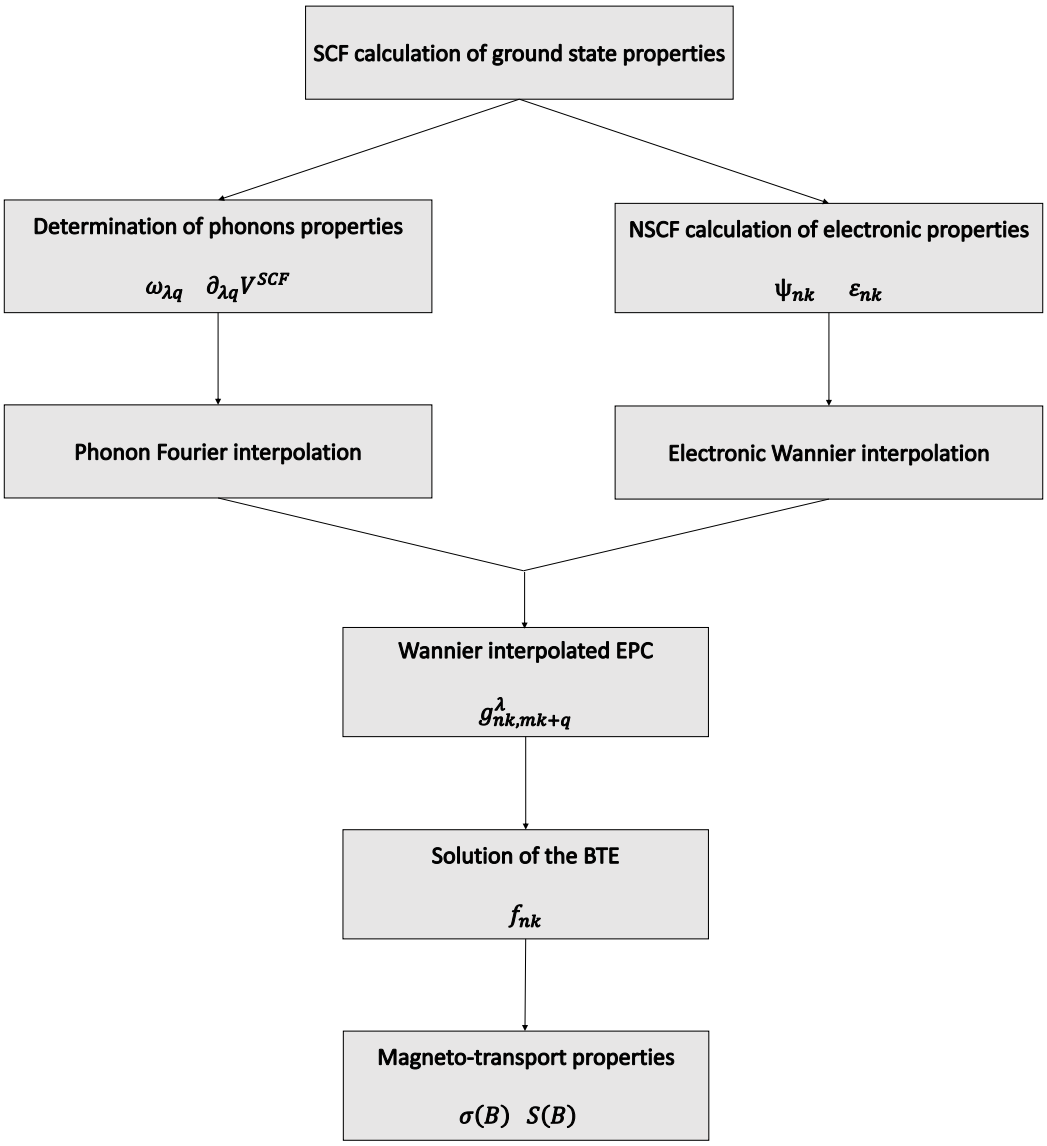

Figure A.1: Logical procedure followed in the implementation of the theory presented in Chap. 1

Appendix B

Difference between adiabatic and isothermal responses

Eq. 1.83 is valid when the states of a system follow a unitary dynamics. This is true if the system is totally isolated from the sorrounding environment or, more realistically, if it can be evolved so slowly that transistions between orthogonal states are not allowed. In this case, the P_N are constant in time and therefore can be put equal to the in-equilibrium ones. By the way, when one approaches the limit $\omega \to 0$, the adiabatic approximation is doomed to fail because the system will inevitably interact with the sorrounding environment on long time scales. It follows that such probabilities cannot be constant in such limit.

Before looking at how the linear response changes if we take in account the coupling to the external bath, let us introduce the Lehmann representation for the adiabatic susceptibility. Starting from Eq. 1.85, we can write the commutator in a basis set of eigenstates and obtain in the frequency domain:

$$\chi_{AB}(\omega) = \sum_{mn} \frac{P_m - P_n}{\omega - (E_n - E_m) + i\eta} A_{mn} B_{nm} \tag{B.1}$$

where $\eta \to 0^+$. The isothermal response is defined for zero frequency as [102] (compare with Eq. 1.87):

$$\chi_{AB}^{isoth.} = \lim_{F \to 0} \frac{\mathrm{Tr}[\hat{A}\hat{\rho}_F] - \mathrm{Tr}[\hat{A}\hat{\rho}_{F=0}]}{F} \tag{B.2}$$

$$\hat{\rho}_F = \frac{e^{-\beta \hat{H}_F}}{Z_F} \tag{B.3}$$

With few manipulations one can show that the Lehmann representation of the isothermal response function becomes:

$$\chi_{AB}^{isoth.} = \sum_{n \neq m} \frac{P_m - P_n}{E_m - E_n} A_{mn} B_{nm} - \beta \left(\sum_n P_n A_{nn} B_{nn} - \langle \hat{A} \rangle_0 \langle \hat{B} \rangle_0 \right) \tag{B.4}$$

where we recognize that the first piece is Eq. B.1 evaulated at null frequency. If we now define the operators $\left[\hat{A}_0\right]_{nm} = \hat{A}_{nn}\delta_{nm}$ and $\left[\hat{B}_0\right]_{nm} = \hat{B}_{nn}\delta_{nm}$ as done in Ref. [102], the previous expression becomes:

$$\chi_{AB}^{isoth.} = \lim_{\omega \to 0} \sum_{n \neq m} \frac{P_m - P_n}{E_m - E_n} A_{mn} B_{nm} - \beta \left(\langle \hat{A}_0 \hat{B}_0 \rangle_0 - \langle \hat{A}_0 \rangle_0 \langle \hat{B}_0 \rangle_0 \right) \tag{B.5}$$

so that the two responses are equal whenever we can neglect the correlations between the diagonal elements of $\hat{A}$ and $\hat{B}$ at initial times. The difference between the two responses is not limited to the Kubo formalisms, but it is in general intrinsic in the study of non equilibrium systems[1].

[1] For example, the study of the expectation value of Eq. 2.1 with a unitary dynamics is the analogue of the adiabatic response of the Kubo formalism

Appendix C

Gradient expansion

The transform of Eq. 2.42 is:

$$\sum_{\substack{\mathbf{R}-\mathbf{R}'\\ \mathbf{R^1}n^1}} \int_{-\infty}^{\infty} d(t-t')dt^1 e^{-i\mathbf{k}\cdot(\mathbf{R}-\mathbf{R}')} e^{i\omega(t-t')} A(\mathbf{R}n, \mathbf{R^1}n^1, t, t^1) B(\mathbf{R^1}n^1, \mathbf{R}'n', t^1, t') =$$
$$\sum_{\substack{\mathbf{R}-\mathbf{R}'\\ \mathbf{R^1}n^1}} \int_{-\infty}^{\infty} d(t-t')dt^1 e^{-i\mathbf{k}\cdot(\mathbf{R}-\mathbf{R}')} e^{i\omega(t-t')} A(\mathbf{R}-\mathbf{R^1}, \frac{\mathbf{R}+\mathbf{R^1}}{2}, n, n^1, t-t^1, \frac{t+t^1}{2})\times$$
$$\times B(\mathbf{R^1}-\mathbf{R}', \frac{\mathbf{R^1}+\mathbf{R}'}{2}, n^1, n', t^1-t', \frac{t^1+t'}{2}). \tag{C.1}$$

Now we change the sum index $\mathbf{R}^1 \to \mathbf{R}-\mathbf{R^1} = \tilde{\mathbf{R}}^{\mathbf{1}}$, and the transform is:

$$\sum_{\substack{\mathbf{R}-\mathbf{R}'\\ \tilde{\mathbf{R}}^{\mathbf{1}}, n^1}} \int_{-\infty}^{\infty} d(t-t')dt^1 e^{-i\mathbf{k}\cdot(\mathbf{R}-\mathbf{R}')} e^{i\omega(t-t')} A(\tilde{\mathbf{R}}^{\mathbf{1}}, \mathbf{R}-\frac{\tilde{\mathbf{R}}^{\mathbf{1}}}{2}, n, n^1, t-t^1, \frac{t+t^1}{2})\times$$
$$\times B(\mathbf{R}-\tilde{\mathbf{R}}^{\mathbf{1}}-\mathbf{R}', \frac{\mathbf{R}-\tilde{\mathbf{R}}^{\mathbf{1}}+\mathbf{R}'}{2}, n^1, n', t^1-t', \frac{t^1+t'}{2}) \tag{C.2}$$

I express the variables as functions of $\frac{\mathbf{R}+\mathbf{R}'}{2} = \mathbf{R}'_\dagger$ and $\mathbf{R}-\mathbf{R}' = \tilde{\mathbf{R}}'$:

$$\sum_{\substack{\tilde{\mathbf{R}}'\tilde{\mathbf{R}}^{\mathbf{1}}\\ n^1}} \int_{-\infty}^{\infty} d(t-t')dt^1 e^{-i\mathbf{k}\cdot\tilde{\mathbf{R}}'} e^{i\omega(t-t')} A(\tilde{\mathbf{R}}^{\mathbf{1}}, \mathbf{R}'_\dagger + \frac{\tilde{\mathbf{R}}'-\tilde{\mathbf{R}}^{\mathbf{1}}}{2}, n, n^1, t-t^1, \frac{t+t^1}{2})\times$$
$$\times B(\tilde{\mathbf{R}}'-\tilde{\mathbf{R}}^{\mathbf{1}}, \mathbf{R}'_\dagger - \frac{\tilde{\mathbf{R}}^{\mathbf{1}}}{2}, n^1, n', t^1-t', \frac{t^1+t'}{2}) \tag{C.3}$$

I repeat the same operation for the time variables, with $t - t^1 = \tilde{t}^1$, $\frac{t+t'}{2} = t'_\dagger$ and $t - t' = \tilde{t}'$:

$$-\sum_{\substack{\tilde{\mathbf{R}}',\tilde{\mathbf{R}}^{\mathbf{1}} \\ n^1}} \int_{-\infty}^{\infty} d\tilde{t}' d\tilde{t}^1 e^{-i\mathbf{k}\cdot\tilde{\mathbf{R}}'} e^{i\omega\tilde{t}'} A(\tilde{\mathbf{R}}^{\mathbf{1}}, \mathbf{R}'_\dagger + \frac{\tilde{\mathbf{R}}' - \tilde{\mathbf{R}}^{\mathbf{1}}}{2}, n, n^1, \tilde{t}^1, t'_\dagger + \frac{\tilde{t}' - \tilde{t}^1}{2}) \times$$
$$\times B(\tilde{\mathbf{R}}' - \tilde{\mathbf{R}}^{\mathbf{1}}, \mathbf{R}'_\dagger - \frac{\tilde{\mathbf{R}}^{\mathbf{1}}}{2}, n^1, n', \tilde{t}' - \tilde{t}^1, t'_\dagger - \frac{\tilde{t}^1}{2}) \tag{C.4}$$

Now we perform the last change of variables, calling $\tilde{\mathbf{R}}_{\mathbf{z}} = \tilde{\mathbf{R}}' - \tilde{\mathbf{R}}^{\mathbf{1}}$ and $\tilde{t}_z = \tilde{t}' - \tilde{t}^1$:

$$\sum_{\tilde{\mathbf{R}}_{\mathbf{z}},\tilde{\mathbf{R}}^{\mathbf{1}},n^1} \int_{-\infty}^{\infty} d\tilde{t}1 d\tilde{t}_z e^{-i\mathbf{k}\cdot(\tilde{\mathbf{R}}_{\mathbf{z}}+\tilde{\mathbf{R}}^{\mathbf{1}})} e^{i\omega(\tilde{t}_z+\tilde{t}^1)} A(\tilde{\mathbf{R}}^{\mathbf{1}}, \mathbf{R}'_\dagger + \frac{\tilde{\mathbf{R}}_{\mathbf{z}}}{2}, n, n^1, \tilde{t}^1, t'_\dagger + \frac{\tilde{t}_z}{2}) \times$$
$$B(\tilde{\mathbf{R}}_{\mathbf{z}}, \mathbf{R}'_\dagger - \frac{\tilde{\mathbf{R}}^{\mathbf{1}}}{2}, n^1, n', \tilde{t}_z, t'_\dagger - \frac{\tilde{t}^1}{2}) \tag{C.5}$$

The gradient expansion is performed at this point. The sum over all the cells of the crystal is intended to be extended over the whole dimension of the crystal; the time integral is from $-\infty$ to $+\infty$; nonetheless we suppose that our functions have a big but finite support where their variation with respect to the coordinate is smooth.[1] With this in mind, we expand A and B in the following way:

$$A(\tilde{\mathbf{R}}^{\mathbf{1}}, \mathbf{R}'_\dagger + \frac{\tilde{\mathbf{R}}_{\mathbf{z}}}{2}, n, n^1, \tilde{t}^1, t'_\dagger + \frac{\tilde{t}_z}{2}) = A(\tilde{\mathbf{R}}^{\mathbf{1}}, \mathbf{R}'_\dagger, n, n^1, \tilde{t}^1, t'_\dagger) +$$
$$+ \frac{\Delta}{\Delta \mathbf{R}'_\dagger} A(\tilde{\mathbf{R}}^{\mathbf{1}}, \mathbf{R}'_\dagger, n, n^1, \tilde{t}^1, t'_\dagger) \cdot \frac{\tilde{\mathbf{R}}_{\mathbf{z}}}{2} + \frac{\partial}{\partial t'_\dagger} A(\tilde{\mathbf{R}}^{\mathbf{1}}, \mathbf{R}'_\dagger, n, n^1, \tilde{t}^1, t'_\dagger) \frac{\tilde{t}_z}{2} \tag{C.6}$$
$$B(\tilde{\mathbf{R}}_{\mathbf{z}}, \mathbf{R}'_\dagger - \frac{\tilde{\mathbf{R}}^{\mathbf{1}}}{2}, n^1, n', \tilde{t}_z, t'_\dagger - \frac{\tilde{t}^1}{2}) = B(\tilde{\mathbf{R}}_{\mathbf{z}}, \mathbf{R}'_\dagger, n^1, n', \tilde{t}_z, t'_\dagger) +$$
$$- \frac{\Delta}{\Delta \tilde{\mathbf{R}}^{\mathbf{1}}} B(\tilde{\mathbf{R}}_{\mathbf{z}}, \mathbf{R}'_\dagger, n^1, n', \tilde{t}_z, t'_\dagger) \cdot \frac{\tilde{\mathbf{R}}^{\mathbf{1}}}{2} - \frac{\partial}{\partial \tilde{t}^1} B(\tilde{\mathbf{R}}_{\mathbf{z}}, \mathbf{R}'_\dagger, n^1, n', \tilde{t}_z, t'_\dagger) \frac{\tilde{t}^1}{2} \tag{C.7}$$

where Δ is referred to the fact that it is a finite difference derivative because the distance between Wannier functions is not infinitesimal; if the functions are varying enough smoothly we treat the finite differences as proper derivatives and the sums as

[1] Experimentally, there is a bound on the time of observation of a system and the dimension of a crystal.

proper integrals. With this expansion equation C.5 becomes:

$$A(\star)B(\star') + \frac{i}{2}\nabla_{\mathbf{R}'_\dagger}A(\star)\cdot\nabla_{\mathbf{k}}B(\star') - \frac{i}{2}\nabla_{\mathbf{k}}A(\star)\cdot\nabla_{\mathbf{R}'_\dagger}B(\star') + \\ - \frac{i}{2}\frac{\partial}{\partial t'_\dagger}A(\star)\cdot\frac{\partial}{\partial\omega}B(\star') + \frac{i}{2}\frac{\partial}{\partial\omega}A(\star)\cdot\frac{\partial}{\partial t'_\dagger}B(\star') \tag{C.8}$$

$$\star = \mathbf{k}, \mathbf{R}'_\dagger, n, n^1, \omega, t'_\dagger \tag{C.9}$$

$$\star' = \mathbf{k}, \mathbf{R}'_\dagger, n^1, n', \omega, t'_\dagger \tag{C.10}$$

where the sum over n^1 is implicit. In this passage we do not need to suppose that the system is periodical in all the 3 spatial directions; in fact, the vectors $\mathbf{k}$ and $\mathbf{R}$ are d-dimensional where d is the number of periodical dimensions. It follows that the gradients are to be thought as d-dimensional gradients. More specifically, the functions A and B will not bring additional dependence on the non periodical coordinates because these coordinates have been integrated out in equation 2.28.

Now we want to single out the dependence of A and B with respect to the electric field. To this aim, we change the functional forms to $A = A(\mathbf{k}, \mathbf{R}'_\dagger, n, n^1, \Omega, t'_\dagger)$ and $B = B(\mathbf{k}, \mathbf{R}'_\dagger, n^1, n', \Omega, t'_\dagger)$ where $\Omega = \omega + e\mathbf{E}\cdot\mathbf{R}'_\dagger$; this same kind of change of variables is adopted in Ref. [191] for the electron gas. The most important reason behind this is the insurance of the gauge invariance of the physical observables that are expressed via the Green's functions. In particular, the Green's function expressed as a function of Ω instead of ω is gauge invariant, and so are its evolution equations. For the interested reader, this is shown in details in App. E. With this change of variable we have that:

$$\frac{\partial}{\partial\omega}A(\mathbf{k}, \mathbf{R}'_\dagger, n, n^1, \omega, t'_\dagger) = \frac{\partial}{\partial\Omega}A(\mathbf{k}, \mathbf{R}'_\dagger, n, n^1, \Omega, t'_\dagger)$$
$$\nabla_{\mathbf{R}'_\dagger}A(\mathbf{k}, \mathbf{R}'_\dagger, n, n^1, \omega, t'_\dagger) = \nabla_{\mathbf{R}'_\dagger}A(\mathbf{k}, \mathbf{R}'_\dagger, n, n^1, \Omega, t'_\dagger) + e\mathbf{E}\frac{\partial}{\partial\Omega}A(\mathbf{k}, \mathbf{R}'_\dagger, n, n^1, \Omega, t'_\dagger) \tag{C.11}$$

and the same for B. We obtain at the end:

$$A(\star)B(\star') + \frac{i}{2}\nabla_{\mathbf{R}'_\dagger}A(\star)\cdot\nabla_{\mathbf{k}}B(\star') + \frac{ie\mathbf{E}}{2}\frac{\partial}{\partial\Omega}A(\star)\cdot\nabla_{\mathbf{k}}B(\star') - \frac{i}{2}\nabla_{\mathbf{k}}A(\star)\cdot\nabla_{\mathbf{R}'_\dagger}B(\star') + \\ - \frac{ie\mathbf{E}}{2}\nabla_{\mathbf{k}}A(\star)\cdot\frac{\partial}{\partial\Omega}B(\star') - \frac{i}{2}\frac{\partial}{\partial t'_\dagger}A(\star)\cdot\frac{\partial}{\partial\Omega}B(\star') + \frac{i}{2}\frac{\partial}{\partial\Omega}A(\star)\cdot\frac{\partial}{\partial t'_\dagger}B(\star') \tag{C.12}$$

$$\star = \mathbf{k}, \mathbf{R}'_\dagger, n, n^1, \Omega, t'_\dagger \tag{C.13}$$

$$\star' = \mathbf{k}, \mathbf{R}'_\dagger, n^1, n', \Omega, t'_\dagger \tag{C.14}$$

where the sum over n^1 is implicit. It is worth noticing again that for these passages we do not need to assume that the system is periodical in all the 3 directions, given that the electric field can be expressed as a d-dimensional vector (i.e. it has to be zero in the non periodical directions).

We suppose now that all the spatial dependence has been included in the Ω variable. We therefore neglect all the spatial gradient. Moreover, we suppose to be studying the steady state situation. This is coherent with our choice of neglecting initial correlation (we could nonetheless study some time-dependent phenomena, but not the initial transient when the external fields are turned on). In this case expression C.12 simplifies to:

$$A(\mathbf{k}, n, n^1, \Omega)B(\mathbf{k}, n^1, n', \Omega) + \frac{ie\mathbf{E}}{2}\frac{\partial}{\partial\Omega}A(\mathbf{k}, n, n^1, \Omega)\cdot\nabla_{\mathbf{k}}B(\mathbf{k}, n^1, n', \Omega)+$$
$$-\frac{ie\mathbf{E}}{2}\nabla_{\mathbf{k}}A(\mathbf{k}, n, n^1, \Omega)\cdot\frac{\partial}{\partial\Omega}B(\mathbf{k}, n^1, n', \Omega) \tag{C.15}$$

where the sum over n^1 is implicit.

Appendix D

Current expression

We start from the operatorial definition of the paramagnetic current in absence of external fields:

$$\hat{\mathbf{J}}_{\mathbf{p}}(\mathbf{r}t) = \frac{e}{2}\sum_i \left[\hat{\mathbf{v}}_i\delta(\mathbf{r}-\hat{\mathbf{r}}_i) + \delta(\mathbf{r}-\hat{\mathbf{r}}_i)\hat{\mathbf{v}}_i\right] \tag{D.1}$$

Using the second quantization rules for the expression of the one-particle operator matrix elements we have:

$$\hat{\mathbf{J}}_{\mathbf{p}}(\mathbf{r}t) = \frac{e}{2}\sum_{\mathbf{k}n,\mathbf{k}'n'} \langle \mathbf{k}n|\, \hat{\mathbf{J}}_{\mathbf{p}}(\mathbf{r})\, |\mathbf{k}'n'\rangle\, \hat{c}^{\dagger}_{\mathbf{k}n}(t)\hat{c}_{\mathbf{k}'n'}(t) \tag{D.2}$$

where $\hat{c}^{\dagger}_{\mathbf{k}n}$ and $\hat{c}_{\mathbf{k}'n'}$ are creation and destruction operators in the Bloch basis set in the Heisenberg picture. $\hat{c}^{\dagger}_{\mathbf{k}n}(-\infty)$ and $\hat{c}_{\mathbf{k}'n'}(-\infty)$ are referred to the Bloch basis that diagonalize the free Hamiltonian. This is always possible because we can always adiabatically switch on the interaction long time before the external perturbation is applied; when evaluating their average we are still in the assumption that we can disregard the perturbative expansion of the immaginary portion of the interaction contour. The matrix elements are expressed as (remembering that the velocity operator is diagonal in $\mathbf{k}$ [192]):

$$\begin{aligned}\langle \mathbf{k}n|\, \hat{\mathbf{J}}_{\mathbf{p}}(\mathbf{r})\, |\mathbf{k}'n'\rangle = \sum_m \big[&\langle \mathbf{k}n|\, \hat{\mathbf{v}}\, |\mathbf{k}m\rangle\, \langle \mathbf{k}m|\, \delta(\mathbf{r}-\hat{\mathbf{r}}_1)\, |\mathbf{k}'n'\rangle + \\ &\langle \mathbf{k}n|\, \delta(\mathbf{r}-\hat{\mathbf{r}}_1)\, |\mathbf{k}'m\rangle\, \langle \mathbf{k}'m|\, \hat{\mathbf{v}}\, |\mathbf{k}'n'\rangle\big]\end{aligned} \tag{D.3}$$

and inserting the completeness relation $\int d\mathbf{r}'\, \langle \mathbf{r}'|\mathbf{r}'\rangle = 1$ and using $\delta(\mathbf{r}-\hat{\mathbf{r}}_1)\, |\mathbf{r}'\rangle = \delta(\mathbf{r}-\mathbf{r}')\, |\mathbf{r}'\rangle$ we have:

$$\begin{aligned}\langle \mathbf{k}n|\, \hat{\mathbf{J}}_{\mathbf{p}}(\mathbf{r})\, |\mathbf{k}'n'\rangle = \sum_{\mathbf{k}m} \big[&\langle \mathbf{k}n|\, \hat{\mathbf{v}}\, |\mathbf{k}m\rangle\, \phi_{\mathbf{k}m}(\mathbf{r})\phi^{*}_{\mathbf{k}'n'}(\mathbf{r}) + \\ &\phi_{\mathbf{k}n}(\mathbf{r})\phi^{*}_{\mathbf{k}'m}(\mathbf{r})\, \langle \mathbf{k}'m|\, \hat{\mathbf{v}}\, |\mathbf{k}'n'\rangle\big]\end{aligned} \tag{D.4}$$

Therefore we have:

$$\langle \hat{\mathbf{J}}_{\mathbf{p}}(\mathbf{r}t)\rangle = \frac{e}{2}\sum_{\mathbf{k}n\mathbf{k}'n'm}\big[\langle \mathbf{k}n|\,\hat{\mathbf{v}}\,|\mathbf{k}m\rangle\,\phi_{\mathbf{k}m}(\mathbf{r})\phi^{*}_{\mathbf{k}'n'}(\mathbf{r}) + \phi_{\mathbf{k}n}(\mathbf{r})\phi^{*}_{\mathbf{k}'m}(\mathbf{r})\,\langle \mathbf{k}'m|\,\hat{\mathbf{v}}\,|\mathbf{k}'n'\rangle\big]\langle \hat{c}^{\dagger}_{\mathbf{k}n}(t)\hat{c}_{\mathbf{k}'n'}(t)\rangle \tag{D.5}$$

Now we can express:

$$\langle \hat{c}^{\dagger}_{\mathbf{k}n}(t)\hat{c}_{\mathbf{k}'n'}(t)\rangle = \sum_{\mathbf{R}\mathbf{R}'}\langle \hat{w}^{\dagger}_{\mathbf{R}n}(t)\hat{w}_{\mathbf{R}'n'}(t)\rangle e^{-i\mathbf{k}\cdot\mathbf{R}+i\mathbf{k}'\cdot\mathbf{R}'} = \sum_{\mathbf{R}\mathbf{R}'}G^{<}(\mathbf{R},\mathbf{R}',n,n',t,t)e^{-i\mathbf{k}\cdot\mathbf{R}+i\mathbf{k}'\cdot\mathbf{R}'} \tag{D.6}$$

where $\hat{w}^{\dagger}_{\mathbf{R}n}(t)$ and $\hat{w}_{\mathbf{R}'\mathbf{n}'}(t)$ are creation and destruction operator in the Wannier basis set. If we were able to identify $\mathbf{k}=\mathbf{k}'$ then the r.h.s. of the above expression is exactly the quantity that obeys the BTE, with all the procedure explained in the main text. Now the expression for the current is:

$$\langle \hat{\mathbf{J}}_{\mathbf{p}}(\mathbf{r}t)\rangle = \frac{e}{2}\sum_{\mathbf{k}n\mathbf{k}'n'm\mathbf{R}\mathbf{R}'}\big[\langle \mathbf{k}n|\,\hat{\mathbf{v}}\,|\mathbf{k}m\rangle\,\phi_{\mathbf{k}m}(\mathbf{r})\phi^{*}_{\mathbf{k}'n'}(\mathbf{r}) + \phi_{\mathbf{k}n}(\mathbf{r})\phi^{*}_{\mathbf{k}'m}(\mathbf{r})\,\langle \mathbf{k}'m|\,\hat{\mathbf{v}}\,|\mathbf{k}'n'\rangle\big]G^{<}(\mathbf{R},\mathbf{R}',n,n',t,t)e^{-i\mathbf{k}\cdot\mathbf{R}+i\mathbf{k}'\cdot\mathbf{R}'} \tag{D.7}$$

Our coarse graining operation now will be to average the current over the whole crystal, and use the orthogonality relations for Bloch functions:

$$\langle \hat{\mathbf{J}}^{\mathbf{TOT}}_{\mathbf{p}}(t)\rangle = e\sum_{\mathbf{k}nn'\mathbf{R}\mathbf{R}'}\langle \mathbf{k}n|\,\hat{\mathbf{v}}\,|\mathbf{k}n\rangle\,G^{<}(\mathbf{R},\mathbf{R}',n,n',t,t)e^{-i\mathbf{k}\cdot(\mathbf{R}-\mathbf{R}')} = \tag{D.8}$$

$$e\int d\omega\sum_{\mathbf{k}n\mathbf{R}^{+}}\langle \mathbf{k}n|\,\hat{\mathbf{v}}\,|\mathbf{k}n\rangle\,G^{<}(\mathbf{k},\mathbf{R}^{+},n,\omega) \tag{D.9}$$

where we have introduced the variables $\mathbf{R}^{+}=\frac{\mathbf{R}+\mathbf{R}'}{2}$ and $\mathbf{R}^{-}=\mathbf{R}-\mathbf{R}'$, we have used the assumption that the Green's function is diagonal in band indexes[1] and passed to integration over frequency using that $G^{<}$ depends only on the difference of the times. Therefore the total current is the average of currents that can be considered as the coarse graining of the current in the unit cell at $\mathbf{R}^{+}$. Therefore, the cell-dependent current is:

$$\langle \mathbf{J}_{\mathbf{p}}(\mathbf{R}^{+})\rangle = e\sum_{\mathbf{k}n}\int d\omega\,\langle \mathbf{k}n|\,\hat{\mathbf{v}}\,|\mathbf{k}n\rangle\,G^{<}(\mathbf{k},\mathbf{R}^{+},n,\omega) \tag{D.10}$$

[1] As in Chap. 2, we are supposing that we are neglecting terms in $\mathbf{A}$; this is a coherent approximation also for the velocity, whose out of diagonal components in the band indexes are proportional to $\mathbf{A}$.

which is in the same form of 2.91, with the difference that the expression is valid in absence of external fields.

In order to derive the expression of the total current $\mathbf{J_e}$ in presence of external fields, we use the procedure of App. E to express the current as a function of a gauge independent Green's function. This procedure consists in introducing the Peierl's phase in Eq. D.6 (see App. E) to remove the gauge dependence of the Green's function in the Wannier basis set. Repeating the same passages, in the case of a dc electric field Eq. D.9 becomes:

$$\langle \hat{\mathbf{J}}_{\mathbf{e}}^{\mathbf{TOT}}(\mathbf{R}^+) \rangle = e \int d\Omega \sum_{\mathbf{k}n\mathbf{R}^+} \langle \mathbf{k}n | \, \hat{\mathbf{v}} \, | \mathbf{k}n \rangle \, G^<(\mathbf{k}, \mathbf{R}^+, n, \Omega) \tag{D.11}$$

where the important difference is the substitution $\omega \to \Omega = \omega + e\mathbf{E} \cdot \mathbf{R}^+$ (see App. E). Thus, it is important that Eq. 2.91 is applied to the solution of the QBTE where the change of variables of App. C has been performed.

Appendix E

Gauge invariance of the lesser Green's function

In this appendix we show more details of what anticipated in Chap. 2 and App. C as regards the gauge invariance of the Green's functions. In particular, we will provide a general receipt to express the Green's functions in coordinates that ensure gauge invariance in presence of electromagnetic fields. In the particular case of a dc electric field, we will show the equivalence with the change of variables introduced in C. In the following, we will drop band indexes since they are not necessary for the derivation.

We start considering the Green's function $G^<(\mathbf{r_1}t_1, \mathbf{r_2}t_2)$ for the homogeneous electron gas. As done by Mahan in Ref. [191], one goes in the Wigner representation introducing the variables:

$$\begin{aligned} \mathbf{r}^+ &= \frac{\mathbf{r}_1 + \mathbf{r}_2}{2} \\ \mathbf{r}^- &= \mathbf{r}_1 - \mathbf{r}_2 \\ t^+ &= \frac{t_1 + t_2}{2} \\ t^- &= t_1 - t_2 \end{aligned} \tag{E.1}$$

We first consider the Dyson equation for the non equilibrium Green's functions in the form of Eq. 2.17. It can be easily be shown that upon a gauge transformation in the form:

$$\begin{aligned} \mathbf{A}(\mathbf{rt}) &\rightarrow \mathbf{A}(\mathbf{r}, \mathbf{t}) + \nabla_{\mathbf{r}}\chi(\mathbf{r}, \mathbf{t}) \\ \phi(\mathbf{r}, t) &\rightarrow \phi(\mathbf{r}, t) - \frac{\partial\chi(\mathbf{r}, t)}{\partial t} \end{aligned} \tag{E.2}$$

the Green's functions transform in the following way[11]:

$$\tilde{G}(\mathbf{r_1}t_1, \mathbf{r_2}t_2) \rightarrow e^{i[\chi(\mathbf{r_1},t_1)-\chi(\mathbf{r_2},t_2)]}\tilde{G}(\mathbf{r_1}t_1, \mathbf{r_2}t_2) \tag{E.3}$$

Now we can define, for each Green's function, the appropriate gauge invariant expression in the Wigner representation as :

$$\tilde{G}(\mathbf{r_1}t_1, \mathbf{r_2}t_2) = e^{i\int_{\bar{r}_2}^{\bar{r}_1}\bar{A}(\bar{r})\cdot d\bar{r}}\int d\mathbf{k}e^{i\mathbf{k}\cdot\mathbf{r}^-}e^{-i\Omega t^-}\tilde{G}(\mathbf{k}, \Omega, \mathbf{r}^+, t^+) \tag{E.4}$$

where $\bar{r}_1 = \mathbf{r_1}t_1$, $\bar{r}_2 = \mathbf{r_2}t_2$, $\bar{A}(\bar{r}) = (\mathbf{A}(\mathbf{r}t), -\phi(\mathbf{r}t))$, $I(\bar{r}_1, \bar{r}_2) = e^{i\int_{\bar{r}_2}^{\bar{r}_1}\bar{A}(\bar{r})\cdot d\bar{r}}$ and the integration is done on the straight line that connect $\bar{r}_1$ to $\bar{r}_2$. Now, if one performs a gauge transformation following Eq. E.2, we have:

$$I(\bar{r}_1, \bar{r}_2) \rightarrow I(\bar{r}_1, \bar{r}_2)e^{i[\chi(\mathbf{r_1},t_1)-\chi(\mathbf{r_2},t_2)]} \tag{E.5}$$

because we are integrating a 4-dimensional gradient over a line, and therefore all the gauge information is manifestly included in $I(\bar{r}_1, \bar{r}_2)$. The conclusion is that with this definition $\tilde{G}(\mathbf{k}, \Omega, \mathbf{r}^+, t^+)$ is manifestly gauge invariant, with gauge invariant evolution equations. An example of application of E.4 is for a dc electric field expressed only via the potential $\phi(\mathbf{r}, t) = -e\mathbf{E}\cdot\mathbf{r}$. The line integral has to be evaluated on the path :

$$\bar{r}(s) = (1-s)(\mathbf{r_2}, t_2) + s(\mathbf{r_1}, t_1) \tag{E.6}$$

so that it becomes:

$$\int_{\bar{r}_2}^{\bar{r}_1}\bar{A}(\bar{r})\cdot d\bar{r} = \int_0^1 \bar{A}(s)\cdot\frac{\partial\bar{r}(s)}{\partial s}ds = \int_0^1 e\mathbf{E}\cdot\left[(1-s)\mathbf{r_2} + s\mathbf{r_1}\right](t_1-t_2)ds = \mathbf{E}\cdot\mathbf{r}^+t^- \tag{E.7}$$

For example, for the lesser Green's function:

$$G^<(\mathbf{r_1}t_1, \mathbf{r_2}t_2) = e^{i\mathbf{E}\cdot\mathbf{r}^+\mathbf{t}^-}\int d\mathbf{k}d\Omega e^{i\mathbf{k}\cdot\mathbf{r}^-}e^{-i\Omega t^-}G^<(\mathbf{k}, \Omega, \mathbf{r}^+, t^+) \tag{E.8}$$

The above equation *defines* the Wigner transformation for which we are sure that $G^<(\mathbf{k}, \Omega, \mathbf{r}^+, t^+)$ is a gauge invariant quantity. If in our definition of Wigner transformation we do not put the prefactor dependent on the electric field, then we must rescale the Wigner coordinates accordingly, in order to rightly identify the gauge invariant

Green's function. Indeed, this is what has been done by Mahan in Ref. [111]—even if there the change of variable is introduced from another point of view. The above procedure is nonetheless more general and can be applied to any kind of electromagnetic field.

In crystals the situation is a bit different, because we do not deal directly with $\mathbf{r}^+$ and $\mathbf{r}^-$, but with:

$$\begin{aligned} \mathbf{R}^+ &= \frac{\mathbf{R}_1 + \mathbf{R}_2}{2} \\ \mathbf{R}^- &= \mathbf{R}_1 - \mathbf{R}_2 \end{aligned} \tag{E.9}$$

where $\mathbf{R_1}$ and $\mathbf{R_2}$ are direct lattice vectors (or Wannier functions indexes). In this case the most convenient basis set where to expand the Green's functions is a generalization of the Wannier functions obtained via the Peierl's substitution:

$$|\tilde{\mathbf{R}}\rangle = e^{i\frac{e}{\hbar}\int_{\mathbf{R}}^{\mathbf{r}} \mathbf{A}(\mathbf{r}'t')d\mathbf{r}'} |\mathbf{R}\rangle \tag{E.10}$$

where $\mathbf{r}'$ runs along the direct line that connects $\mathbf{r}$ and $\mathbf{R}$ [193]. In this case the right gauge invariant Wigner transformation of the Green's function is [194]:

$$\tilde{G}(\mathbf{R_1}, t_1, \mathbf{R_2}, t_2) = e^{i\int_{\bar{R}_2}^{\bar{R}_1} \bar{A}(\bar{R})\cdot d\bar{R}} \int d\mathbf{k} d\omega e^{i\mathbf{k}\cdot\mathbf{R}^-} e^{-i\Omega t^-} \tilde{G}(\mathbf{k}, \Omega, \mathbf{R}^+, t^+) \tag{E.11}$$

where $\bar{R}_1 = \mathbf{R_1} t_1$, $\bar{R}_2 = \mathbf{R_2} t_2$, $\bar{A}(\bar{R}) = (\mathbf{A}(\mathbf{R}t), -\phi(\mathbf{R}t))$, $I(\bar{R}_1, \bar{R}_2) = e^{i\int_{\bar{R}_2}^{\bar{R}_1} \bar{A}(\bar{R})\cdot d\bar{R}}$ and the integration is done on the straight line that connect $\bar{R}_1$ to $\bar{R}_2$. Notice that the gauge invariance has been shifted from the $\mathbf{r}$ space coordinate to the $\mathbf{R}$ lattice coordinates.

With the same exact procedure as for the homogeneous gas case, we have that for the dc electric field expressed via a scalar potential the gauge invariant lesser Green's functions expressed in the generalized Wannier basis is:

$$G^<(\mathbf{R_1}t_1, \mathbf{R_2}t_2) = e^{i\mathbf{E}\cdot\mathbf{R}^+ t^-} \int d\mathbf{k} d\omega e^{i\mathbf{k}\cdot\mathbf{R}^-} e^{-i\Omega t^-} G^<(\mathbf{k}, \Omega, \mathbf{R}^+, t^+) \tag{E.12}$$

Again, if the prefactor is not taken in account correctly in the Wigner transformation—as in Eq. 2.41—then one has to adopt an appropriate change of variable—as in App. C—to make the Green's function gauge invariant. The inverse transform of Eq. E.12

is:

$$G^{<}(\mathbf{k},\Omega,\mathbf{R}^{+},t^{+}) = \int d\mathbf{R}^{-}dt^{-}e^{-i\mathbf{k}\cdot\mathbf{R}^{-}}e^{i\left(\Omega-\mathbf{E}\cdot\mathbf{R}^{+}\right)t^{-}}G^{<}(\mathbf{R_1}t_1,\mathbf{R_2}t_2) \tag{E.13}$$

To sum up, if one transforms the appropriate Green's functions evolution equations in presence of a dc electric field from the direct space to the reciprocal space using Eq. E.13, then one obtains gauge invariant equations—that are the same that we obtained in Chap 2 with the trick of the variable change. Also, with this transform one obtains Eq. C.12 directly from the transform of Eq. C.5,C.6 and C.7. Again, we stress that the procedure described in this chapter is general and can be extended to any electromagnetic field.

Appendix F

Field operators and equations of motion

Let's consider a one particle Hamiltonian that may be written in second quantization on a general basis as:

$$\hat{H}^0 = \sum_{ij} h_{ij} \hat{c}_i^\dagger \hat{c}_j \tag{F.1}$$

then the evolution equations for the annihilation e creation operator are:

$$\begin{aligned} i\frac{\partial}{\partial t}\hat{c}_I(t) &= -[\hat{H}^0, \hat{c}_I(t)] = -\sum_{ij} h_{ij}[\hat{c}_i^\dagger(t)\hat{c}_j(t), \hat{c}_I(t)] = \sum_j h_{Ij}\hat{c}_j(t) \\ i\frac{\partial}{\partial t}\hat{c}_I^\dagger(t) &= -[\hat{H}^0, \hat{c}_I^\dagger(t)] = -\sum_{ij} h_{ij}[\hat{c}_i^\dagger(t)\hat{c}_j(t), \hat{c}_I^\dagger(t)] = -\sum_i h_{iI}\hat{c}_i^\dagger(t) \end{aligned} \tag{F.2}$$

where we used that for fermions:

$$\begin{aligned} [\hat{A}\hat{B}, \hat{C}] &= \hat{A}\{\hat{B}, \hat{C}\} - \{\hat{A}, \hat{C}\}\hat{B} \\ \{\hat{A}(x,t), \hat{A}(x',t)\} &= \{\hat{A}(x',t), \hat{A}(x,t)\} = \delta(x - x') \end{aligned} \tag{F.3}$$

where $\{,\}$ is the anticommumator operator for fermionic fields. Let's see the implication of the above rules on the time evolution of the Green's functions. Let's define for example the lesser Green's function on the Bloch basis set:

$$G^{<,0}(n\mathbf{k}, t_1, t_2) = i\langle \hat{c}_{\mathbf{k}n}^\dagger(t_2)\hat{c}_{\mathbf{k}n}(t_1)\rangle \tag{F.4}$$

We now see that:

$$i\frac{\partial}{\partial t_1}G^{<,0}(n\mathbf{k}, t_1, t_2) = i\epsilon_{n\mathbf{k}}^0\langle \hat{c}_{\mathbf{k}n}^\dagger(t_2)\hat{c}_{\mathbf{k}n}(t_1)\rangle \tag{F.5}$$

$$i\frac{\partial}{\partial t_2}G^{<,0}(n\mathbf{k}, t_1, t_2) = -i\epsilon_{n\mathbf{k}}^0\langle \hat{c}_{\mathbf{k}n}^\dagger(t_2)\hat{c}_{\mathbf{k}n}(t_1)\rangle \tag{F.6}$$

that can be rewritten as:

$$\left[i\frac{\partial}{\partial t_1} - \epsilon^0_{n\mathbf{k}}\right] G^{<,0}(n\mathbf{k}, t_1, t_2) = 0 \tag{F.7}$$

$$\left[-i\frac{\partial}{\partial t_2} - \epsilon^0_{n\mathbf{k}}\right] G^{<,0}(n\mathbf{k}, t_1, t_2) = 0 \tag{F.8}$$

that are the same expression that can obtained taking the matrix elements of Eqs. 2.25 and 2.38 between Bloch functions. In the Wannier basis set instead, we have:

$$G^{<,0}(\mathbf{R}n, \mathbf{R}'n', t_1, t_2) = i\langle \hat{w}^\dagger_{\mathbf{R}'n'}(t_2)\hat{w}_{\mathbf{R}n}(t_1)\rangle \tag{F.9}$$

where $\hat{w}$ and $\hat{w}^\dagger$ are defined as in App. D and:

$$i\frac{\partial}{\partial t_1}G^{<,0}(\mathbf{R}n, \mathbf{R}'n', t_1, t_2) = \sum_{\mathbf{R}^1 n^1} iH^0_{\mathbf{R}n,\mathbf{R}^1n^1}\langle \hat{w}^\dagger_{\mathbf{R}'n'}(t_2)\hat{w}_{\mathbf{R}^1n^1}(t_1)\rangle \tag{F.10}$$

$$i\frac{\partial}{\partial t_2}G^{<,0}(\mathbf{R}n, \mathbf{R}'n', t_1, t_2) = -\sum_{\mathbf{R}^1 n^1} iH^0_{\mathbf{R}^1n^1,\mathbf{R}n}\langle \hat{w}^\dagger_{\mathbf{R}^1n^1}(t_2)\hat{w}_{\mathbf{R}n}(t_1)\rangle \tag{F.11}$$

which become:

$$\sum_{\mathbf{R}^1 n^1}[i\frac{\partial}{\partial t_1}\delta_{\mathbf{R}n,\mathbf{R^1}n^1} - H^0_{\mathbf{R}n,\mathbf{R}^1n^1}]G^{<,0}(\mathbf{R^1}n^1, \mathbf{R}'n', t_1, t_2) = 0 \tag{F.12}$$

$$\sum_{\mathbf{R}^1 n^1}(-i\frac{\partial}{\partial t_2}\delta_{\mathbf{R^1}n^1,\mathbf{R}'n'})G^{<,0}(\mathbf{R}n, \mathbf{R^1}n^1, t_1, t_2) - G^{<,0}(\mathbf{R}n, \mathbf{R}^1n^1, t_1, t_2)H^0_{\mathbf{R^1}n^1,\mathbf{R}'n'} = 0 \tag{F.13}$$

Eq. F.13 may be rewritten *formally* as:

$$\sum_{\mathbf{R}^1 n^1} G^{<,0}(\mathbf{R}n, \mathbf{R}^1n^1, t_1, t_2)[-i\frac{\partial}{\partial t_2}\delta_{\mathbf{R^1}n^1,\mathbf{R}'n'} - H^0_{\mathbf{R^1}n^1,\mathbf{R}'n'}] = 0 \tag{F.14}$$

where the time derivative operator is intended to act on the Green's function. We can generalize also Eq. 2.25 and 2.38 to:

$$\sum_k \left[i\frac{\partial}{\partial t_1}\delta_{ik} - H^0_{ik}\right]\tilde{G}^0_{kj}(t_1, t_2) = \delta_{ij}\delta(t_1 - t_2)\tilde{I}$$

$$\sum_k \tilde{G}^0_{ik}(t_1, t_2)\left[-i\frac{\partial}{\partial t_2}\delta_{kj} - H^0_{kj}\right] = \delta_{ij}\delta(t_1 - t_2)\tilde{I} \tag{F.15}$$

It is worth mentioning also that the transformation between second quantized operators also determines the sign of the $\mathbf{k}$ exponent of the Wigner transform of Eq. 2.41.

Indeed, using Eq. 1.74 we have:

$$\hat{w}^{\dagger}_{\mathbf{R}'n'} = \sum_{\mathbf{k}} e^{-i\mathbf{k}\cdot\mathbf{R}'} \hat{c}^{\dagger}_{\mathbf{k}n} \tag{F.16}$$

$$\hat{w}_{\mathbf{R}'n'} = \sum_{\mathbf{k}} e^{i\mathbf{k}\cdot\mathbf{R}'} \hat{c}^{\dagger}_{\mathbf{k}n} \tag{F.17}$$

which implies:

$$G^{<}(\mathbf{R}n, \mathbf{R}'n) = i\langle \hat{w}^{\dagger}_{\mathbf{R}'n'} \hat{w}_{\mathbf{R}n} \rangle = i \sum_{\mathbf{k}} e^{i\mathbf{k}\cdot(\mathbf{R}-\mathbf{R}')} \langle \hat{c}^{\dagger}_{\mathbf{k}'n'} \hat{c}_{\mathbf{k}n} \rangle = \sum_{\mathbf{k}} e^{i\mathbf{k}\cdot(\mathbf{R}-\mathbf{R}')} G^{<}(\mathbf{k}, n) \tag{F.18}$$

Appendix G

Dirac cone integration cutoff

In this appendix we give some estimates for effects that limit the validity of the scaling of the scattering time.

1. Finite size effects: graphene flakes have finite size and therefore the size of the samples puts a cutoff for the minimum $\mathbf{k}$ vector (and consequently energy states) available in the system. In particular, if we consider a graphene flake of dimensions $1\mu\text{m}^2$, then we expect that we cannot get nearer than approximatively 1 meV to the Dirac cone. Of course, for graphene flakes of larger dimensions we can implement smaller cutoffs and expect slightly larger peak values for r.

2. Optical phonon scattering: the scattering time of the optical phonons in the EP regime is not completely 0, but at $\epsilon = 0$ for the lowest optical mode A_1' at $\mathbf{q} = \mathbf{K}$ it is expected to evaluate to [16]:

$$\frac{1}{\tau_{A_1'}(\epsilon=0)} = \frac{\beta_{\mathbf{K}}^2}{\mu_S}\frac{1}{(\hbar v_F)^2}\frac{\hbar/2}{1-f^0(0)}\times\left[3n^0_{A_1'}(1-f^0(\hbar\omega_{A_1'})) + (n^0_{A_1'}+1)(1-f^0(-\hbar\omega_{A_1'}))\right] \tag{G.1}$$

where $\beta_{\mathbf{K}}$ is the optical gauge field, $\omega_{A_1'}$ is the frequency and $n^0_{A_1'}$ the occupation of the A_1' mode and μ_S is the graphene sheet mass density. In this case, the inverse scattering time depends both on T and on E_F; since below room temperature $n_{A_1'} < 0.004 \ll 1$ we can simplify the previous expression in:

$$\frac{1}{\tau_{A_1'}(\epsilon=0)} = \frac{\beta_{\mathbf{K}}^2}{\mu_S}\frac{1}{(\hbar v_F)^2}\frac{\hbar/2}{1-f^0(0)}\left[3n^0_{A_1'}(1-f^0(\hbar\omega_{A_1'})) + (1-f^0(-\hbar\omega_{A_1'}))\right]. \tag{G.2}$$

If we now take $|E_F| << \omega_{A_1'}$ (with E_F referred to E_D), which is true in the low doping regime ($n << 10^{13} cm^{-2}$), we have that the expression can be simplified as:

$$\frac{1}{\tau_{A_1'}(\epsilon=0)} = \frac{\beta_{\mathbf{K}}^2}{\mu_S}\frac{1}{(\hbar v_F)^2}\hbar\left[3n^0_{A_1'}\frac{e^{\hbar\omega_{A_1'}/k_BT}}{e^{\hbar\omega_{A_1'}/k_BT}+1} + \frac{e^{-\hbar\omega_{A_1'}/k_BT}}{e^{-\hbar\omega_{A_1'}/k_BT}+1}\right] \tag{G.3}$$

which evaluates to $\frac{1}{\tau} \approx 7 \times 10^{10} s^{-1}$ at room temperature.

3. Many-body effects: there exist an all-order relation between the many-body linewidths and the spectral function if we disregard vertex corrections to the self-energy. This relation is given by Eqs. 2.68 and 2.69. These two relations may not be satisfied at the same time when Γ and A are evaluated at the leading order. In general, one assumes that the linewidths are small enough to treat the spectral function as a delta function, and then one evaluates $\Gamma_{n\mathbf{k}}(\Omega)$ for $\Omega = \epsilon_{n\mathbf{k}}$ to find the scattering time in the SERTA approximation, i.e. Eq. 4.8. If one instead substitutes again the linewidths in the expression to evaluate finite-width correction to the spectral function, also the expression for the linewidth will be modified consequently, in a self-consistent loop. Usually one assumes that the first step is indeed sufficient to give a good evaluation of the linewidth. This is true for example if one wants to evaluate the diagonal component of the conductivity tensor: the integral at the denominator of Eq. 4.25 is well behaved even when $\tau_n^{-1}(\epsilon) \propto |\epsilon| k_B T$. For the Hall factor instead, one have to re-evaluate the linewidth at least with two iterations of the described procedure in order to obtain a non-diverging Hall factor. This procedure of course considers only a subset of all the diagrams which may contribute to corrections, but we assume that the self-consistent solution of Eqs. 2.68 and 2.69 gives a reasonable estimate of the many-body effect on the linewidths; in other words, we assume that this iteration can give us a reasonable order of magnitude of the linewidth value at the Dirac cone, which cannot be zero since a diverging Hall factor is unphysical. The second iteration of the evaluation of the linewidths reads (we always neglect the real part of the self-energy):

$$
\begin{aligned}
&A_{n^1\mathbf{k}+\mathbf{q}}(\epsilon_{n\mathbf{k}} - \omega_{\lambda\mathbf{q}}) = \frac{2\alpha\epsilon_{n^1\mathbf{k}+\mathbf{q}}}{(\alpha\epsilon_{n^1\mathbf{k}+\mathbf{q}})^2 + (\epsilon_{n\mathbf{k}} - \omega_{\lambda\mathbf{q}} - \epsilon_{n^1\mathbf{k}+\mathbf{q}})^2} \\
&A_{n^1\mathbf{k}+\mathbf{q}}(\epsilon_{n\mathbf{k}} + \omega_{\lambda\mathbf{q}}) = \frac{\alpha\epsilon_{n^1\mathbf{k}+\mathbf{q}}}{(\alpha\epsilon_{n^1\mathbf{k}+\mathbf{q}})^2 + (\epsilon_{n\mathbf{k}} + \omega_{\lambda\mathbf{q}} - \epsilon_{n^1\mathbf{k}+\mathbf{q}})^2} \\
&\Gamma_{n\mathbf{k}}(\epsilon_{n\mathbf{k}}) = \frac{1}{2}\sum_{\mathbf{q}\lambda n^1} |g_{nn^1\lambda}(\mathbf{k},\mathbf{q})|^2 \big[\left(n^0_{\lambda\mathbf{q}} + 1 - f^0(\epsilon_{n\mathbf{k}} - \omega_{\lambda\mathbf{q}})\right) A_{n^1\mathbf{k}+\mathbf{q}}(\epsilon_{n\mathbf{k}} - \omega_{\lambda\mathbf{q}}) + \\
&\left(n^0_{\lambda\mathbf{q}} + f^0(\epsilon_{n\mathbf{k}} + \omega_{\lambda\mathbf{q}})\right) A_{n^1\mathbf{k}+\mathbf{q}}(\epsilon_{n\mathbf{k}} + \omega_{\lambda\mathbf{q}}) \big] \approx \\
&\frac{1}{2}\sum_{\mathbf{q}\lambda n^1} |g_{nn^1\lambda}(\mathbf{k},\mathbf{q})|^2 \big[\left(2n^0_{\lambda\mathbf{q}} + 1\right) A_{n^1\mathbf{k}+\mathbf{q}}(\epsilon_{n\mathbf{k}}) \big] \propto \\
&\alpha(\hbar v_F)^2 \sum_{\mathbf{q}n^1} \frac{\alpha\epsilon_{n^1\mathbf{k}+\mathbf{q}}}{(\alpha\epsilon_{n^1\mathbf{k}+\mathbf{q}})^2 + (\epsilon_{n\mathbf{k}} - \epsilon_{n^1\mathbf{k}+\mathbf{q}})^2} \propto \alpha \int_0^\Lambda d\epsilon' \frac{\alpha\epsilon'^2}{(\alpha\epsilon')^2 + (\epsilon - \epsilon')^2}
\end{aligned}
\tag{G.4}
$$

where we have used the approximation of quasi-elastic scattering and we have indicated with Λ the cutoff due to acoustic phonon scattering ($\Lambda <= 60$meV, which is

the portion of phonons which give linear dispersion of the inverse scattering time; in principle, the cutoff has a temperature dependence due to the fact that the approximation $f^0(\epsilon_{n\mathbf{k}} + \hbar\omega_{\lambda\mathbf{q}}) = f^0(\epsilon_{n\mathbf{k}} - \hbar\omega_{\lambda\mathbf{q}})$ is valid for a subset of phonons in dependence of T) and $\alpha \ll 1$ so that the quasi-particle picture is qualitatively still valid (we indeed know that the 0-th iteration of the linewidth calculations gives $\alpha \approx \frac{2\beta^2_{TA/LA} k_B T}{\mu_S v^2_{TA/LA}(\hbar v_F^2)}$ where $\beta_{TA/LA}$ is the acoustic gauge field and $v_{TA/LA}$ is the phonon velocity [16], so that $\alpha \approx 10^{-3}$ at room temperature). It follows that:

$$\frac{1}{\tau(\epsilon)} \propto \alpha \frac{\alpha}{(1+\alpha^2)^2}\Big[\epsilon' + \alpha^2\epsilon' + (\frac{\epsilon}{\alpha} - \alpha\epsilon)\arctan(\frac{-\epsilon + \epsilon' + \alpha^2\epsilon'}{\alpha\epsilon}) + \tag{G.5}$$

$$\epsilon \log(\epsilon^2 - 2\epsilon\epsilon' + (1+\alpha^2)\epsilon'^2)\Big]_{\epsilon'=0}^{\epsilon'=\Lambda} \qquad \epsilon < \Lambda \tag{G.6}$$

which is always positive and has the finite limit $\frac{1}{\tau(\epsilon=0)} \propto \frac{1}{\hbar}\frac{\alpha^2\Lambda}{1+\alpha^2}$ which is, at room temperature, $\frac{1}{\tau(\epsilon=0)} \approx 4 \times 10^8 s^{-1}$ and has a quadratic dependence on the temperature ($\frac{1}{\tau(\epsilon=0)} \approx 10^8 s^{-1}$ at 200K and $\frac{1}{\tau(\epsilon=0)} \approx 5 \times 10^7 s^{-1}$ at 100K). Even though this is not reproduced by the usual Fermi golden rule, if α is small enough the change to the τ in shape for $\epsilon > \alpha\Lambda \approx 0.06$meV is negligible, but for $\epsilon < \alpha\Lambda$ it is fundamental in order to get convergence of the numerator of Eq. 4.25 at any finite temperature. Since the previous choice of Λ suppose that the contributes of higher phonons do not count, we nonetheless notice that an increase of the cutoff impact linearly on the inverse of the scattering time, so that the previous estimates for the order of magnitude hold true for every $\Lambda < \omega^{ph.}_{MAX}$; moreover, we do not expect that the expansion of $\frac{1}{\tau}$ in powers of Λ is strongly dependent on the non-linear terms.

Bibliography

[1] Lars Onsager. "Reciprocal Relations in Irreversible Processes. I." In: *Phys. Rev.* 37 (4 1931), pp. 405–426. DOI: 10.1103/PhysRev.37.405. URL: https://link.aps.org/doi/10.1103/PhysRev.37.405.

[2] Lars Onsager. "Reciprocal Relations in Irreversible Processes. II." In: *Phys. Rev.* 38 (12 1931), pp. 2265–2279. DOI: 10.1103/PhysRev.38.2265. URL: https://link.aps.org/doi/10.1103/PhysRev.38.2265.

[3] Mattia Fiorentini and Nicola Bonini. "Thermoelectric coefficients of n-doped silicon from first principles via the solution of the Boltzmann transport equation". In: *Phys. Rev. B* 94 (8 2016), p. 085204. DOI: 10.1103/PhysRevB.94.085204. URL: https://link.aps.org/doi/10.1103/PhysRevB.94.085204.

[4] Francesco Macheda and Nicola Bonini. "Magnetotransport phenomena in p-doped diamond from first principles". In: *Phys. Rev. B* 98 (20 2018), p. 201201. DOI: 10.1103/PhysRevB.98.201201. URL: https://link.aps.org/doi/10.1103/PhysRevB.98.201201.

[5] Samuel Poncé et al. "First-principles calculations of charge carrier mobility and conductivity in bulk semiconductors and two-dimensional materials". In: *Reports on Progress in Physics* 83.3 (2020), p. 036501. DOI: 10.1088/1361-6633/ab6a43. URL: https://doi.org/10.1088%2F1361-6633%2Fab6a43.

[6] Lucas Lindsay et al. "Perspective on ab initio phonon thermal transport". In: *Journal of Applied Physics* 126.5 (2019), p. 050902. DOI: 10.1063/1.5108651. eprint: https://doi.org/10.1063/1.5108651. URL: https://doi.org/10.1063/1.5108651.

[7] Kim Sharp and Franz Matschinsky. "Translation of Ludwig Boltzmann's Paper "On the Relationship between the Second Fundamental Theorem of the Mechanical Theory of Heat and Probability Calculations Regarding the Conditions for Thermal Equilibrium" Sitzungberichte der Kaiserlichen Akademie

der Wissenschaften. Mathematisch-Naturwissen Classe. Abt. II, LXXVI 1877, pp 373-435 (Wien. Ber. 1877, 76:373-435). Reprinted in Wiss. Abhandlungen, Vol. II, reprint 42, p. 164-223, Barth, Leipzig, 1909". In: *Entropy* 17.4 (2015), 1971–2009. ISSN: 1099-4300. DOI: 10.3390/e17041971. URL: http://dx.doi.org/10.3390/e17041971.

[8] R. Peierls. "Zur kinetischen Theorie der Wärmeleitung in Kristallen". In: *Annalen der Physik* 395.8 (1929), pp. 1055–1101. ISSN: 1521-3889. DOI: 10.1002/andp.19293950803. URL: http://dx.doi.org/10.1002/andp.19293950803.

[9] Gordon Baym and Leo P. Kadanoff. "Conservation Laws and Correlation Functions". In: *Phys. Rev.* 124 (2 1961), pp. 287–299. DOI: 10.1103/PhysRev.124.287. URL: https://link.aps.org/doi/10.1103/PhysRev.124.287.

[10] Gordon Baym. "Self-Consistent Approximations in Many-Body Systems". In: *Phys. Rev.* 127 (4 1962), pp. 1391–1401. DOI: 10.1103/PhysRev.127.1391. URL: https://link.aps.org/doi/10.1103/PhysRev.127.1391.

[11] Takafumi Kita and Hiromasa Yamashita. "Quantum Transport Equation for Bloch Electrons in Electromagnetic Fields". In: *Journal of the Physical Society of Japan* 77.2 (2008), pp. 024711–024711. DOI: 10.1143/jpsj.77.024711.

[12] Richard E. Prange and Leo P. Kadanoff. "Transport Theory for Electron-Phonon Interactions in Metals". In: *Phys. Rev.* 134 (3A 1964), A566–A580. DOI: 10.1103/PhysRev.134.A566. URL: https://link.aps.org/doi/10.1103/PhysRev.134.A566.

[13] T. Holstein. "Theory of transport phenomena in an electron-phonon gas". In: *Annals of Physics* 29.3 (1964), pp. 410 –535. ISSN: 0003-4916. DOI: https://doi.org/10.1016/0003-4916(64)90008-9. URL: http://www.sciencedirect.com/science/article/pii/0003491664900089.

[14] Yu.G. Gurevich and O.L. Mashkevich. "The electron-phonon drag and transport phenomena in semiconductors". In: *Physics Reports* 181.6 (1989), pp. 327 –394. ISSN: 0370-1573. DOI: https://doi.org/10.1016/0370-1573(89)90011-2. URL: http://www.sciencedirect.com/science/article/pii/0370157389900112.

[15] J M. Ziman. *Electrons and Phonons: The Theory of Transport Phenomena in Solids*. Jan. 2001.

[16] Thibault Sohier et al. "Phonon-limited resistivity of graphene by first-principles calculations: Electron-phonon interactions, strain-induced gauge field, and Boltzmann equation". In: *Phys. Rev. B* 90 (12 2014), p. 125414. DOI: 10.1103/PhysRevB.90.125414. URL: https://link.aps.org/doi/10.1103/PhysRevB.90.125414.

[17] Tue Gunst et al. "First-principles method for electron-phonon coupling and electron mobility: Applications to two-dimensional materials". In: *Phys. Rev. B* 93 (3 2016), p. 035414. DOI: 10.1103/PhysRevB.93.035414. URL: https://link.aps.org/doi/10.1103/PhysRevB.93.035414.

[18] Jin-Jian Zhou and Marco Bernardi. "Ab initio electron mobility and polar phonon scattering in GaAs". In: *Phys. Rev. B* 94 (20 2016), p. 201201. DOI: 10.1103/PhysRevB.94.201201. URL: https://link.aps.org/doi/10.1103/PhysRevB.94.201201.

[19] Fanchen Meng et al. "Phonon-limited carrier mobility and temperature-dependent scattering mechanism of 3C-SiC from first principles". In: *Phys. Rev. B* 99 (4 2019), p. 045201. DOI: 10.1103/PhysRevB.99.045201. URL: https://link.aps.org/doi/10.1103/PhysRevB.99.045201.

[20] Jinlong Ma, Arun S. Nissimagoudar, and Wu Li. "First-principles study of electron and hole mobilities of Si and GaAs". In: *Phys. Rev. B* 97 (4 2018), p. 045201. DOI: 10.1103/PhysRevB.97.045201. URL: https://link.aps.org/doi/10.1103/PhysRevB.97.045201.

[21] Samuel Poncé, Elena R. Margine, and Feliciano Giustino. "Towards predictive many-body calculations of phonon-limited carrier mobilities in semiconductors". In: *Phys. Rev. B* 97 (12 2018), p. 121201. DOI: 10.1103/PhysRevB.97.121201. URL: https://link.aps.org/doi/10.1103/PhysRevB.97.121201.

[22] Guillaume Brunin et al. "Electron-Phonon beyond Fröhlich: Dynamical Quadrupoles in Polar and Covalent Solids". In: *Phys. Rev. Lett.* 125 (13 2020), p. 136601. DOI: 10.1103/PhysRevLett.125.136601. URL: https://link.aps.org/doi/10.1103/PhysRevLett.125.136601.

[23] Vatsal A. Jhalani et al. "Piezoelectric Electron-Phonon Interaction from Ab Initio Dynamical Quadrupoles: Impact on Charge Transport in Wurtzite GaN". In: *Phys. Rev. Lett.* 125 (13 2020), p. 136602. DOI: 10.1103/PhysRevLett.125.136602. URL: https://link.aps.org/doi/10.1103/PhysRevLett.125.136602.

[24] Giorgia Fugallo et al. "Thermal Conductivity of Graphene and Graphite: Collective Excitations and Mean Free Paths". In: *Nano Letters* 14.11 (2014), pp. 6109–6114. ISSN: 1530-6984. DOI: 10.1021/nl502059f. URL: https://doi.org/10.1021/nl502059f.

[25] Giorgia Fugallo et al. "Ab initio variational approach for evaluating lattice thermal conductivity". In: *Phys. Rev. B* 88 (4 2013), p. 045430. DOI: 10.1103/PhysRevB.88.045430. URL: https://link.aps.org/doi/10.1103/PhysRevB.88.045430.

[26] A. Ward et al. "Ab initio theory of the lattice thermal conductivity in diamond". In: *Phys. Rev. B* 80 (12 2009), p. 125203. DOI: 10.1103/PhysRevB.80.125203. URL: https://link.aps.org/doi/10.1103/PhysRevB.80.125203.

[27] Lorenzo Paulatto, Francesco Mauri, and Michele Lazzeri. "Anharmonic properties from a generalized third-order ab initio approach: Theory and applications to graphite and graphene". In: *Phys. Rev. B* 87 (21 2013), p. 214303. DOI: 10.1103/PhysRevB.87.214303. URL: https://link.aps.org/doi/10.1103/PhysRevB.87.214303.

[28] Davide Campi et al. "First-principles calculation of lattice thermal conductivity in crystalline phase change materials: GeTe, $\mathbf{Sb_2Te_3}$, and $\mathbf{Ge_2Sb_2Te_5}$". In: *Phys. Rev. B* 95 (2 2017), p. 024311. DOI: 10.1103/PhysRevB.95.024311. URL: https://link.aps.org/doi/10.1103/PhysRevB.95.024311.

[29] Nicola Marzari et al. "Maximally localized Wannier functions: Theory and applications". In: *Rev. Mod. Phys.* 84 (4 2012), pp. 1419–1475. DOI: 10.1103/RevModPhys.84.1419. URL: https://link.aps.org/doi/10.1103/RevModPhys.84.1419.

[30] Feliciano Giustino, Marvin L. Cohen, and Steven G. Louie. "Electron-phonon interaction using Wannier functions". In: *Phys. Rev. B* 76 (16 2007), p. 165108. DOI: 10.1103/PhysRevB.76.165108. URL: https://link.aps.org/doi/10.1103/PhysRevB.76.165108.

[31] Jonathan R. Yates et al. "Spectral and Fermi surface properties from Wannier interpolation". In: *Phys. Rev. B* 75 (19 2007), p. 195121. DOI: 10.1103/PhysRevB.75.195121. URL: https://link.aps.org/doi/10.1103/PhysRevB.75.195121.

[32] Arash A. Mostofi et al. "wannier90: A tool for obtaining maximally-localised Wannier functions". In: *Computer Physics Communications* 178.9 (2008), pp. 685 –699. ISSN: 0010-4655. DOI: https://doi.org/10.1016/j.cpc.2007.11.016. URL: http://www.sciencedirect.com/science/article/pii/S0010465507004936.

[33] Giovanni Pizzi et al. "BoltzWann: A code for the evaluation of thermoelectric and electronic transport properties with a maximally-localized Wannier functions basis". In: *Computer Physics Communications* 185.1 (2014), pp. 422 – 429. ISSN: 0010-4655. DOI: https://doi.org/10.1016/j.cpc.2013.09.015. URL: http://www.sciencedirect.com/science/article/pii/S0010465513003160.

[34] Jesse Noffsinger et al. "EPW: A program for calculating the electron–phonon coupling using maximally localized Wannier functions". In: *Computer Physics Communications* 181.12 (2010), pp. 2140 –2148. ISSN: 0010-4655. DOI: https://doi.org/10.1016/j.cpc.2010.08.027. URL: http://www.sciencedirect.com/science/article/pii/S0010465510003218.

[35] S. Poncé et al. "EPW: Electron–phonon coupling, transport and superconducting properties using maximally localized Wannier functions". In: *Computer Physics Communications* 209 (2016), pp. 116 –133. ISSN: 0010-4655. DOI: https://doi.org/10.1016/j.cpc.2016.07.028. URL: http://www.sciencedirect.com/science/article/pii/S0010465516302260.

[36] Ricardo S Sussmann. *CVD diamond for electronic devices and sensors*. Vol. 26. John Wiley & Sons, 2009.

[37] N. Tranchant et al. "High mobility single crystal diamond detectors for dosimetry: Application to radiotherapy". In: *Diamond and Related Materials* 17.7 (2008). Proceedings of Diamond 2007, the 18th European Conference on Diamond, Diamond-Like Materials, Carbon Nanotubes, Nitrides and Silicon Carbide, pp. 1297 –1301. ISSN: 0925-9635. DOI: https://doi.org/10.1016/j.diamond.2008.03.025. URL: http://www.sciencedirect.com/science/article/pii/S0925963508002562.

[38] Chris J.H. Wort and Richard S. Balmer. "Diamond as an electronic material". In: *Materials Today* 11.1 (2008), pp. 22 –28. ISSN: 1369-7021. DOI: http://dx.doi.org/10.1016/S1369-7021(07)70349-8. URL: http://www.sciencedirect.com/science/article/pii/S1369702107703498.

[39] A. A. Altukhov et al. "Application of Diamond in High Technology". In: *Inorganic Materials* 40.1 (2004), S50–S70. ISSN: 1608-3172. DOI: 10.1023/B:INMA.0000036328.94568.7c. URL: https://doi.org/10.1023/B:INMA.0000036328.94568.7c.

[40] Jan Isberg et al. "High Carrier Mobility in Single-Crystal Plasma-Deposited Diamond". In: *Science* 297.5587 (2002), pp. 1670–1672. ISSN: 0036-8075. DOI: 10.1126/science.1074374. eprint: http://science.sciencemag.org/content/297/5587/1670.full.pdf. URL: http://science.sciencemag.org/content/297/5587/1670.

[41] Jan Isberg et al. "Temperature dependence of hole drift mobility in high-purity single-crystal CVD diamond". In: *physica status solidi (a)* 202.11 (2005), pp. 2194–2198. ISSN: 1862-6319. DOI: 10.1002/pssa.200561915. URL: http://dx.doi.org/10.1002/pssa.200561915.

[42] H. Pernegger et al. "Charge-carrier properties in synthetic single-crystal diamond measured with the transient-current technique". In: *Journal of Applied Physics* 97.7 (2005), p. 073704. DOI: 10.1063/1.1863417. eprint: http://dx.doi.org/10.1063/1.1863417. URL: http://dx.doi.org/10.1063/1.1863417.

[43] Miloš Nesladek et al. "Charge transport in high mobility single crystal diamond". In: *Diamond and Related Materials* 17.7 (2008). Proceedings of Diamond 2007, the 18th European Conference on Diamond, Diamond-Like Materials, Carbon Nanotubes, Nitrides and Silicon Carbide, pp. 1235 –1240. ISSN: 0925-9635. DOI: http://dx.doi.org/10.1016/j.diamond.2008.03.015. URL: http://www.sciencedirect.com/science/article/pii/S0925963508002367.

[44] Hendrik Jansen et al. "Temperature dependence of charge carrier mobility in single-crystal chemical vapour deposition diamond". In: *Journal of Applied Physics* 113.17 (2013), p. 173706. DOI: 10.1063/1.4802679. eprint: http://dx.doi.org/10.1063/1.4802679. URL: http://dx.doi.org/10.1063/1.4802679.

[45] L. Reggiani et al. “Hole-drift velocity in natural diamond”. In: *Phys. Rev. B* 23 (6 1981), pp. 3050–3057. DOI: 10.1103/PhysRevB.23.3050. URL: https://link.aps.org/doi/10.1103/PhysRevB.23.3050.

[46] Lino Reggiani, David Waechter, and Stefan Zukotynski. “Hall-coefficient factor and inverse valence-band parameters of holes in natural diamond”. In: *Phys. Rev. B* 28 (6 1983), pp. 3550–3555. DOI: 10.1103/PhysRevB.28.3550. URL: https://link.aps.org/doi/10.1103/PhysRevB.28.3550.

[47] H J Goldsmid, C C Jenns, and D A Wright. “The Thermoelectric Power of a Semiconducting Diamond”. In: *Proceedings of the Physical Society* 73.3 (1959), p. 393. URL: http://stacks.iop.org/0370-1328/73/i=3/a=306.

[48] K. S. Novoselov et al. “Electric Field Effect in Atomically Thin Carbon Films”. In: *Science* 306.5696 (2004), pp. 666–669. ISSN: 0036-8075. DOI: 10.1126/science.1102896. eprint: https://science.sciencemag.org/content/306/5696/666.full.pdf. URL: https://science.sciencemag.org/content/306/5696/666.

[49] E. H. Hwang and S. Das Sarma. “Acoustic phonon scattering limited carrier mobility in two-dimensional extrinsic graphene”. In: *Phys. Rev. B* 77 (11 2008), p. 115449. DOI: 10.1103/PhysRevB.77.115449. URL: https://link.aps.org/doi/10.1103/PhysRevB.77.115449.

[50] R S Shishir and D K Ferry. “Intrinsic mobility in graphene”. In: *Journal of Physics: Condensed Matter* 21.23 (2009), p. 232204. DOI: 10.1088/0953-8984/21/23/232204. URL: https://doi.org/10.1088%2F0953-8984%2F21%2F23%2F232204.

[51] K. M. Borysenko et al. “First-principles analysis of electron-phonon interactions in graphene”. In: *Phys. Rev. B* 81 (12 2010), p. 121412. DOI: 10.1103/PhysRevB.81.121412. URL: https://link.aps.org/doi/10.1103/PhysRevB.81.121412.

[52] Cheol-Hwan Park et al. “Electron–Phonon Interactions and the Intrinsic Electrical Resistivity of Graphene”. In: *Nano Letters* 14.3 (2014). PMID: 24524418, pp. 1113–1119. DOI: 10.1021/nl402696q. URL: http://dx.doi.org/10.1021/nl402696q.

[53] S. Das Sarma et al. "Electronic transport in two-dimensional graphene". In: *Rev. Mod. Phys.* 83 (2 2011), pp. 407–470. DOI: 10.1103/RevModPhys.83.407. URL: https://link.aps.org/doi/10.1103/RevModPhys.83.407.

[54] Dmitri K. Efetov and Philip Kim. "Controlling Electron-Phonon Interactions in Graphene at Ultrahigh Carrier Densities". In: *Phys. Rev. Lett.* 105 (25 2010), p. 256805. DOI: 10.1103/PhysRevLett.105.256805. URL: https://link.aps.org/doi/10.1103/PhysRevLett.105.256805.

[55] R.S. Popovic. *Hall Effect Devices: Magnetic Sensors and Characterization of Semiconductors*. Taylor & Francis, 1991. ISBN: 9780750300964.

[56] Choongyu Hwang et al. "Fermi velocity engineering in graphene by substrate modification". In: *Scientific Reports* 2.1 (2012), p. 590. ISSN: 2045-2322. DOI: 10.1038/srep00590. URL: https://doi.org/10.1038/srep00590.

[57] Raffaello Bianco et al. "Second-order structural phase transitions, free energy curvature, and temperature-dependent anharmonic phonons in the self-consistent harmonic approximation: Theory and stochastic implementation". In: *Phys. Rev. B* 96 (1 2017), p. 014111. DOI: 10.1103/PhysRevB.96.014111. URL: https://link.aps.org/doi/10.1103/PhysRevB.96.014111.

[58] Ryogo Kubo. "Statistical-Mechanical Theory of Irreversible Processes. I. General Theory and Simple Applications to Magnetic and Conduction Problems". In: *Journal of the Physical Society of Japan* 12.6 (1957), pp. 570–586. DOI: 10.1143/JPSJ.12.570. eprint: https://doi.org/10.1143/JPSJ.12.570. URL: https://doi.org/10.1143/JPSJ.12.570.

[59] Ryogo Kubo, Mario Yokota, and Sadao Nakajima. "Statistical-Mechanical Theory of Irreversible Processes. II. Response to Thermal Disturbance". In: *Journal of the Physical Society of Japan* 12.11 (1957), pp. 1203–1211. DOI: 10.1143/JPSJ.12.1203. eprint: https://doi.org/10.1143/JPSJ.12.1203. URL: https://doi.org/10.1143/JPSJ.12.1203.

[60] L. Calderín, V.V. Karasiev, and S.B. Trickey. "Kubo–Greenwood electrical conductivity formulation and implementation for projector augmented wave datasets". In: *Computer Physics Communications* 221 (2017), pp. 118 –142. ISSN: 0010-4655. DOI: https://doi.org/10.1016/j.cpc.2017.08.008. URL: http://www.sciencedirect.com/science/article/pii/S0010465517302539.

[61] Xu Lu et al. “High Performance Thermoelectricity in Earth-Abundant Compounds Based on Natural Mineral Tetrahedrites”. In: *Advanced Energy Materials* 3.3 (2013), pp. 342–348. DOI: 10.1002/aenm.201200650. eprint: https://onlinelibrary.wiley.com/doi/pdf/10.1002/aenm.201200650. URL: https://onlinelibrary.wiley.com/doi/abs/10.1002/aenm.201200650.

[62] Sebastian O. Long et al. “Jahn–Teller Driven Electronic Instability in Thermoelectric Tetrahedrite”. In: *Advanced Functional Materials* 30.12 (2020), p. 1909409. DOI: 10.1002/adfm.201909409. eprint: https://onlinelibrary.wiley.com/doi/pdf/10.1002/adfm.201909409. URL: https://onlinelibrary.wiley.com/doi/abs/10.1002/adfm.201909409.

[63] Dario Alfè, Monica Pozzo, and Michael P. Desjarlais. “Lattice electrical resistivity of magnetic bcc iron from first-principles calculations”. In: *Phys. Rev. B* 85 (2 2012), p. 024102. DOI: 10.1103/PhysRevB.85.024102. URL: https://link.aps.org/doi/10.1103/PhysRevB.85.024102.

[64] Francesco Macheda et al. “Theory and Computation of Hall Scattering Factor in Graphene”. In: *Nano Letters* 20.12 (2020), pp. 8861–8865. ISSN: 1530-6984. DOI: 10.1021/acs.nanolett.0c03874. URL: https://doi.org/10.1021/acs.nanolett.0c03874.

[65] Cono Di Paola et al. “First-principles study of electronic transport and structural properties of $Cu_{12}Sb_4S_{13}$ in its high-temperature phase”. In: *Phys. Rev. Research* 2 (3 2020), p. 033055. DOI: 10.1103/PhysRevResearch.2.033055. URL: https://link.aps.org/doi/10.1103/PhysRevResearch.2.033055.

[66] Paolo Giannozzi et al. “QUANTUM ESPRESSO: a modular and open-source software project for quantum simulations of materials”. In: *Journal of Physics: Condensed Matter* 21.39 (2009), p. 395502. URL: http://stacks.iop.org/0953-8984/21/i=39/a=395502.

[67] G. Kresse and J. Hafner. “Ab initio molecular dynamics for liquid metals”. In: *Phys. Rev. B* 47 (1 1993), pp. 558–561. DOI: 10.1103/PhysRevB.47.558. URL: https://link.aps.org/doi/10.1103/PhysRevB.47.558.

[68] G. Kresse and J. Hafner. "Ab initio molecular-dynamics simulation of the liquid-metal–amorphous-semiconductor transition in germanium". In: *Phys. Rev. B* 49 (20 1994), pp. 14251–14269. DOI: 10.1103/PhysRevB.49.14251. URL: https://link.aps.org/doi/10.1103/PhysRevB.49.14251.

[69] G. Grosso and G.P. Parravicini. *Solid State Physics*. Elsevier Science, 2000. ISBN: 9780080481029. URL: https://books.google.co.uk/books?id=L5RrQbbvWn8C.

[70] A. Marco Saitta et al. "Giant Nonadiabatic Effects in Layer Metals: Raman Spectra of Intercalated Graphite Explained". In: *Phys. Rev. Lett.* 100 (22 2008), p. 226401. DOI: 10.1103/PhysRevLett.100.226401. URL: https://link.aps.org/doi/10.1103/PhysRevLett.100.226401.

[71] M. Born and R. Oppenheimer. "Zur Quantentheorie der Molekeln". In: *Annalen der Physik* 389.20 (1927), pp. 457–484. DOI: https://doi.org/10.1002/andp.19273892002. eprint: https://onlinelibrary.wiley.com/doi/pdf/10.1002/andp.19273892002. URL: https://onlinelibrary.wiley.com/doi/abs/10.1002/andp.19273892002.

[72] P. Hohenberg and W. Kohn. "Inhomogeneous Electron Gas". In: *Phys. Rev.* 136 (1964), B864.

[73] W. Kohn and L. J. Sham. "Self-Consistent Equations Including Exchange and Correlation Effects". In: *Phys. Rev.* A1133 (1965), p. 140.

[74] E.K.U. Gross, E. Runge, and O. Heinonen. *Many-Particle Theory,* Taylor & Francis, 1991. ISBN: 9780750301558. URL: https://books.google.it/books?id=_6y_72b9HbkC.

[75] Paolo Giannozzi et al. "Ab initio calculation of phonon dispersions in semiconductors". In: *Phys. Rev. B* 43 (9 1991), pp. 7231–7242. DOI: 10.1103/PhysRevB.43.7231. URL: https://link.aps.org/doi/10.1103/PhysRevB.43.7231.

[76] Matteo Calandra, Gianni Profeta, and Francesco Mauri. "Adiabatic and nonadiabatic phonon dispersion in a Wannier function approach". In: *Phys. Rev. B* 82 (16 2010), p. 165111. DOI: 10.1103/PhysRevB.82.165111. URL: https://link.aps.org/doi/10.1103/PhysRevB.82.165111.

[77] Stefano Baroni et al. “Phonons and related crystal properties from density-functional perturbation theory”. In: *Rev. Mod. Phys.* 73 (2 2001), pp. 515–562. DOI: 10.1103/RevModPhys.73.515. URL: https://link.aps.org/doi/10.1103/RevModPhys.73.515.

[78] Feliciano Giustino. “Electron-phonon interactions from first principles”. In: *Rev. Mod. Phys.* 89 (1 2017), p. 015003. DOI: 10.1103/RevModPhys.89.015003. URL: https://link.aps.org/doi/10.1103/RevModPhys.89.015003.

[79] P B Allen and V Heine. “Theory of the temperature dependence of electronic band structures”. In: *Journal of Physics C: Solid State Physics* 9.12 (1976), pp. 2305–2312. DOI: 10.1088/0022-3719/9/12/013. URL: https://doi.org/10.1088%2F0022-3719%2F9%2F12%2F013.

[80] L.D. Landau and E.M. Lifshitz. *Statistical Physics: Volume 5*. v. 5. Elsevier Science, 2013. ISBN: 9780080570464. URL: https://books.google.it/books?id=VzgJN-XPTRsC.

[81] A. Piróth and J. Sólyom. *Fundamentals of the Physics of Solids: Volume II: Electronic Properties*. Fundamentals of the Physics of Solids. Springer Berlin Heidelberg, 2008. ISBN: 9783540853152. URL: https://books.google.it/books?id=XSo-a2n43xEC.

[82] S.R. de Groot and P. Mazur. *Non-equilibrium Thermodynamics*. Dover Books on Physics. Dover Publications, 1984. ISBN: 9780486647418. URL: https://books.google.it/books?id=HFAIv43rlGkC.

[83] S. R. de Groot and P. Mazur. “Extension of Onsager’s Theory of Reciprocal Relations. I”. In: *Phys. Rev.* 94 (2 1954), pp. 218–224. DOI: 10.1103/PhysRev.94.218. URL: https://link.aps.org/doi/10.1103/PhysRev.94.218.

[84] P. Mazur and S. R. de Groot. “Extension of Onsager’s Theory of Reciprocal Relations. II”. In: *Phys. Rev.* 94 (2 1954), pp. 224–226. DOI: 10.1103/PhysRev.94.224. URL: https://link.aps.org/doi/10.1103/PhysRev.94.224.

[85] P. Mazur and S.R. de Groot. “On Onsager’s relations in a magnetic field”. In: *Physica* 19.1 (1953), pp. 961 –970. ISSN: 0031-8914. DOI: https://doi.org/10.1016/S0031-8914(53)80108-4. URL: http://www.sciencedirect.com/science/article/pii/S0031891453801084.

[86] Nicholas A. Mecholsky et al. "Theory of band warping and its effects on thermoelectronic transport properties". In: *Phys. Rev. B* 89 (15 2014), p. 155131. DOI: 10.1103/PhysRevB.89.155131. URL: https://link.aps.org/doi/10.1103/PhysRevB.89.155131.

[87] Nicholas A. Mecholsky et al. "Anisotropy Effects on the Thermoelectric Electronic Transport Coefficients". In: *Energy Harvesting and Systems* 2.1 (1Apr. 2015), pp. 15 –24. DOI: https://doi.org/10.1515/ehs-2014-0041. URL: https://www.degruyter.com/view/journals/ehs/2/1/article-p15.xml.

[88] C. Herring, T. H. Geballe, and J. E. Kunzler. "Phonon-Drag Thermomagnetic Effects in n-Type Germanium. I. General Survey". In: *Phys. Rev.* 111 (1 1958), pp. 36–57. DOI: 10.1103/PhysRev.111.36. URL: https://link.aps.org/doi/10.1103/PhysRev.111.36.

[89] N.W. Ashcroft and N.D. Mermin. *Solid State Physics*. Cengage Learning, 2011. ISBN: 9788131500521. URL: https://books.google.co.uk/books?id=x_s_YAAACAAJ.

[90] William Jones and Norman H March. *Theoretical solid state physics*. London: Wiley, 1973. URL: http://cds.cern.ch/record/104669.

[91] Bolin Liao et al. "Significant Reduction of Lattice Thermal Conductivity by the Electron-Phonon Interaction in Silicon with High Carrier Concentrations: A First-Principles Study". In: *Phys. Rev. Lett.* 114 (11 2015), p. 115901. DOI: 10.1103/PhysRevLett.114.115901. URL: https://link.aps.org/doi/10.1103/PhysRevLett.114.115901.

[92] Nakib H. Protik and David A. Broido. "Coupled transport of phonons and carriers in semiconductors: A case study of n-doped GaAs". In: *Phys. Rev. B* 101 (7 2020), p. 075202. DOI: 10.1103/PhysRevB.101.075202. URL: https://link.aps.org/doi/10.1103/PhysRevB.101.075202.

[93] Nicola Bonini, Jivtesh Garg, and Nicola Marzari. "Acoustic Phonon Lifetimes and Thermal Transport in Free-Standing and Strained Graphene". In: *Nano Letters* 12.6 (2012), pp. 2673–2678. ISSN: 1530-6984. DOI: 10.1021/nl202694m. URL: https://doi.org/10.1021/nl202694m.

[94] Nicola Bonini et al. "Phonon Anharmonicities in Graphite and Graphene". In: *Phys. Rev. Lett.* 99 (17 2007), p. 176802. DOI: 10.1103/PhysRevLett.99.176802. URL: https://link.aps.org/doi/10.1103/PhysRevLett.99.176802.

[95] Andrea Cepellotti and Nicola Marzari. "Thermal Transport in Crystals as a Kinetic Theory of Relaxons". In: *Phys. Rev. X* 6 (4 2016), p. 041013. DOI: 10.1103/PhysRevX.6.041013. URL: https://link.aps.org/doi/10.1103/PhysRevX.6.041013.

[96] Carlo Jacoboni and Lino Reggiani. "The Monte Carlo method for the solution of charge transport in semiconductors with applications to covalent materials". In: *Rev. Mod. Phys.* 55 (3 1983), pp. 645–705. DOI: 10.1103/RevModPhys.55.645. URL: https://link.aps.org/doi/10.1103/RevModPhys.55.645.

[97] J. R. Meyer and F. J. Bartoli. "Phase-shift calculation of electron mobility in n-type silicon at low temperatures". In: *Phys. Rev. B* 24 (4 1981), pp. 2089–2100. DOI: 10.1103/PhysRevB.24.2089. URL: https://link.aps.org/doi/10.1103/PhysRevB.24.2089.

[98] Xinjie Wang et al. "Ab initio calculation of the anomalous Hall conductivity by Wannier interpolation". In: *Phys. Rev. B* 74 (19 2006), p. 195118. DOI: 10.1103/PhysRevB.74.195118. URL: https://link.aps.org/doi/10.1103/PhysRevB.74.195118.

[99] P. Vogl. "Microscopic theory of electron-phonon interaction in insulators or semiconductors". In: *Phys. Rev. B* 13 (2 1976), pp. 694–704. DOI: 10.1103/PhysRevB.13.694. URL: https://link.aps.org/doi/10.1103/PhysRevB.13.694.

[100] R. Resta. "Deformation-potential theorem in metals and in dielectrics". In: *Phys. Rev. B* 44 (20 1991), pp. 11035–11041. DOI: 10.1103/PhysRevB.44.11035. URL: https://link.aps.org/doi/10.1103/PhysRevB.44.11035.

[101] Carla Verdi and Feliciano Giustino. "Fröhlich Electron-Phonon Vertex from First Principles". In: *Phys. Rev. Lett.* 115 (17 2015), p. 176401. DOI: 10.1103/PhysRevLett.115.176401. URL: https://link.aps.org/doi/10.1103/PhysRevLett.115.176401.

[102] Gabriele Giuliani and Giovanni Vignale. *Quantum Theory of the Electron Liquid*. Cambridge University Press, 2005. DOI: 10.1017/CBO9780511619915.

[103] S. Mazevet et al. "Calculations of the transport properties within the PAW formalism". In: *High Energy Density Physics* 6.1 (2010), pp. 84 –88. ISSN: 1574-1818. DOI: https://doi.org/10.1016/j.hedp.2009.06.004. URL: http://www.sciencedirect.com/science/article/pii/S1574181809000664.

[104] J. M. Luttinger. "Theory of Thermal Transport Coefficients". In: *Phys. Rev.* 135 (6A 1964), A1505–A1514. DOI: 10.1103/PhysRev.135.A1505. URL: https://link.aps.org/doi/10.1103/PhysRev.135.A1505.

[105] P.B. Allen. "Chapter 6 Electron Transport". In: *Conceptual Foundations of Materials*. Ed. by Steven G. Louie and Marvin L. Cohen. Vol. 2. Contemporary Concepts of Condensed Matter Science. Elsevier, 2006, pp. 165 –218. DOI: https://doi.org/10.1016/S1572-0934(06)02006-3. URL: http://www.sciencedirect.com/science/article/pii/S1572093406020063.

[106] James Dufty et al. "On the Kubo-Greenwood model for electron conductivity". In: *Contributions to Plasma Physics* 58.2-3 (2018), pp. 150–154. DOI: https://doi.org/10.1002/ctpp.201700102. eprint: https://onlinelibrary.wiley.com/doi/pdf/10.1002/ctpp.201700102. URL: https://onlinelibrary.wiley.com/doi/abs/10.1002/ctpp.201700102.

[107] G V Chester and A Thellung. "The Law of Wiedemann and Franz". In: *Proceedings of the Physical Society* 77.5 (1961), pp. 1005–1013. DOI: 10.1088/0370-1328/77/5/309. URL: https://doi.org/10.1088%2F0370-1328%2F77%2F5%2F309.

[108] G. Kresse and D. Joubert. "From ultrasoft pseudopotentials to the projector augmented-wave method". In: *Phys. Rev. B* 59 (3 1999), pp. 1758–1775. DOI: 10.1103/PhysRevB.59.1758. URL: https://link.aps.org/doi/10.1103/PhysRevB.59.1758.

[109] P. B. Allen. "Electron-Phonon Effects in the Infrared Properties of Metals". In: *Phys. Rev. B* 3 (2 1971), pp. 305–320. DOI: 10.1103/PhysRevB.3.305. URL: https://link.aps.org/doi/10.1103/PhysRevB.3.305.

[110] L.P. Kadanoff and G. Baym. *Quantum Statistical Mechanics: Green's Function Methods in Equilibrium and Nonequilibrium Problems*. Frontiers in Physics. A Lecture Note and Reprint Series. Benjamin, 1962. URL: https://books.google.it/books?id=L0VAAAAAIAAJ.

[111] G.D. Mahan. "Quantum transport equation for electric and magnetic fields". In: *Physics Reports* 145.5 (1987), pp. 251 –318. ISSN: 0370-1573. DOI: https://doi.org/10.1016/0370-1573(87)90004-4. URL: http://www.sciencedirect.com/science/article/pii/0370157387900044.

[112] R. van Leeuwen et al. "Introduction to the Keldysh Formalism". In: *Time-Dependent Density Functional Theory*. Ed. by Miguel A.L. Marques et al. Berlin, Heidelberg: Springer Berlin Heidelberg, 2006, pp. 33–59. ISBN: 978-3-540-35426-0. DOI: 10.1007/3-540-35426-3_3. URL: https://doi.org/10.1007/3-540-35426-3_3.

[113] Jørgen Rammer. *Quantum Field Theory of Non-equilibrium States*. Cambridge University Press, 2007. DOI: 10.1017/CBO9780511618956.

[114] Julian Schwinger. "Brownian Motion of a Quantum Oscillator". In: *Journal of Mathematical Physics* 2.3 (1961), pp. 407–432. DOI: 10.1063/1.1703727. eprint: https://doi.org/10.1063/1.1703727. URL: https://doi.org/10.1063/1.1703727.

[115] A.L. Fetter and J.D. Walecka. *Quantum Theory of Many-particle Systems*. Dover Books on Physics. Dover Publications, 2003. ISBN: 9780486428277. URL: https://books.google.it/books?id=0wekf1s83b0C.

[116] J. Rammer and H. Smith. "Quantum field-theoretical methods in transport theory of metals". In: *Rev. Mod. Phys.* 58 (2 1986), pp. 323–359. DOI: 10.1103/RevModPhys.58.323. URL: https://link.aps.org/doi/10.1103/RevModPhys.58.323.

[117] J Maciejko. *An Introduction to Nonequilibrium Many-Body Theory*. Lecture notes, 2007.

[118] Christian Wickles and Wolfgang Belzig. "Effective quantum theories for Bloch dynamics in inhomogeneous systems with nontrivial band structure". In: *Phys. Rev. B* 88 (4 2013), p. 045308. DOI: 10.1103/PhysRevB.88.045308. URL: https://link.aps.org/doi/10.1103/PhysRevB.88.045308.

[119] H. Ness et al. "GW approximations and vertex corrections on the Keldysh time-loop contour: Application for model systems at equilibrium". In: *Phys. Rev. B* 84 (19 2011), p. 195114. DOI: 10.1103/PhysRevB.84.195114. URL: https://link.aps.org/doi/10.1103/PhysRevB.84.195114.

[120] J. L. Warren et al. “Lattice Dynamics of Diamond”. In: *Phys. Rev.* 158 (3 1967), pp. 805–808. DOI: 10.1103/PhysRev.158.805. URL: https://link.aps.org/doi/10.1103/PhysRev.158.805.

[121] J. P. Perdew and Alex Zunger. “Self-interaction correction to density-functional approximations for many-electron systems”. In: *Phys. Rev. B* 23 (10 1981), pp. 5048–5079. DOI: 10.1103/PhysRevB.23.5048. URL: https://link.aps.org/doi/10.1103/PhysRevB.23.5048.

[122] Lanhua Wei et al. “Thermal conductivity of isotopically modified single crystal diamond”. In: *Phys. Rev. Lett.* 70 (24 1993), pp. 3764–3767. DOI: 10.1103/PhysRevLett.70.3764. URL: https://link.aps.org/doi/10.1103/PhysRevLett.70.3764.

[123] Conyers Herring. “Role of Low-Energy Phonons in Thermal Conduction”. In: *Phys. Rev.* 95 (4 1954), pp. 954–965. DOI: 10.1103/PhysRev.95.954. URL: https://link.aps.org/doi/10.1103/PhysRev.95.954.

[124] Markus Gabrysch et al. “Electron and hole drift velocity in chemical vapor deposition diamond”. In: *Journal of Applied Physics* 109.6 (2011), p. 063719. DOI: 10.1063/1.3554721. eprint: https://doi.org/10.1063/1.3554721. URL: https://doi.org/10.1063/1.3554721.

[125] Klaus Thonke. “The boron acceptor in diamond”. In: *Semiconductor Science and Technology* 18.3 (2003), S20. URL: http://stacks.iop.org/0268-1242/18/i=3/a=303.

[126] S. Yamanaka et al. “Low-Compensated Boron-Doped Homoepitaxial Diamond Films Using Trimethylboron”. In: *physica status solidi (a)* 174.1 (1999), pp. 59–64. ISSN: 1521-396X. DOI: 10.1002/(SICI)1521-396X(199907)174:1<59::AID-PSSA59>3.0.CO;2-A. URL: http://dx.doi.org/10.1002/(SICI)1521-396X(199907)174:1<59::AID-PSSA59>3.0.CO;2-A.

[127] T. Teraji et al. “Highly efficient doping of boron into high-quality homoepitaxial diamond films”. In: *Diamond and Related Materials* 15.4 (2006). Diamond 2005, pp. 602 –606. ISSN: 0925-9635. DOI: https://doi.org/10.1016/j.diamond.2006.01.011. URL: http://www.sciencedirect.com/science/article/pii/S0925963506000185.

[128] Markus Gabrysch et al. “Compensation in boron-doped CVD diamond”. In: *physica status solidi (a)* 205.9 (2008), pp. 2190–2194. ISSN: 1862-6319. DOI: 10.1002/pssa.200879711. URL: http://dx.doi.org/10.1002/pssa.200879711.

[129] Pierre-Nicolas Volpe et al. “High hole mobility in boron doped diamond for power device applications”. In: *Applied Physics Letters* 94.9 (2009), p. 092102. DOI: 10.1063/1.3086397. eprint: https://doi.org/10.1063/1.3086397. URL: https://doi.org/10.1063/1.3086397.

[130] J. Barjon et al. “Resistivity of boron doped diamond”. In: *physica status solidi (RRL) – Rapid Research Letters* 3.6 (2009), pp. 202–204. ISSN: 1862-6270. DOI: 10.1002/pssr.200903097. URL: http://dx.doi.org/10.1002/pssr.200903097.

[131] E.A. Konorova and S. Shevchenko. In: *Fiz. Tekh. Poluprovodn.(Sov. Phys.-Semicond.)* 1 (364 1967).

[132] P. J. Dean, E. C. Lightowlers, and D. R. Wight. “Intrinsic and Extrinsic Recombination Radiation from Natural and Synthetic Aluminum-Doped Diamond”. In: *Phys. Rev.* 140 (1A 1965), A352–A368. DOI: 10.1103/PhysRev.140.A352. URL: https://link.aps.org/doi/10.1103/PhysRev.140.A352.

[133] L. Gherardi, A. Pellacani, and C. Jacoboni. “Velocity autocorrelation function and low-temperature mobility of electrons in silicon”. In: *Lettere al Nuovo Cimento (1971-1985)* 14.7 (1975), pp. 225–232. ISSN: 1827-613X. DOI: 10.1007/BF02745630. URL: https://doi.org/10.1007/BF02745630.

[134] E W J Mitchell and P T Wedepohl. “Magnetoresistance of a p-type Semiconducting Diamond”. In: *Proceedings of the Physical Society. Section B* 70.5 (1957), p. 527. URL: http://stacks.iop.org/0370-1301/70/i=5/a=410.

[135] Kenneth J. Russell and William J. Leivo. “High-Field Magnetoresistance of Semiconducting Diamond”. In: *Phys. Rev. B* 6 (12 1972), pp. 4588–4592. DOI: 10.1103/PhysRevB.6.4588. URL: https://link.aps.org/doi/10.1103/PhysRevB.6.4588.

[136] John A. Swanson. “Saturation Hall Constant of Semiconductors”. In: *Phys. Rev.* 99 (6 1955), pp. 1799–1807. DOI: 10.1103/PhysRev.99.1799. URL: https://link.aps.org/doi/10.1103/PhysRev.99.1799.

[137] Conyers Herring. "Theory of the Thermoelectric Power of Semiconductors". In: *Phys. Rev.* 96 (5 1954), pp. 1163–1187. DOI: 10.1103/PhysRev.96.1163. URL: https://link.aps.org/doi/10.1103/PhysRev.96.1163.

[138] M. C. Steele. "Magnetic Field Dependence of the Seebeck Effect in Germanium". In: *Phys. Rev.* 107 (1 1957), pp. 81–83. DOI: 10.1103/PhysRev.107.81. URL: https://link.aps.org/doi/10.1103/PhysRev.107.81.

[139] Rong Wang et al. "Graphene based functional devices: A short review". In: *Frontiers of Physics* 14.1 (2018), p. 13603. ISSN: 2095-0470. DOI: 10.1007/s11467-018-0859-y. URL: https://doi.org/10.1007/s11467-018-0859-y.

[140] A. H. Castro Neto et al. "The electronic properties of graphene". In: *Rev. Mod. Phys.* 81 (1 2009), pp. 109–162. DOI: 10.1103/RevModPhys.81.109. URL: https://link.aps.org/doi/10.1103/RevModPhys.81.109.

[141] Nan Ma and Debdeep Jena. "Carrier statistics and quantum capacitance effects on mobility extraction in two-dimensional crystal semiconductor field-effect transistors". In: *2D Materials* 2.1 (2015), p. 015003. DOI: 10.1088/2053-1583/2/1/015003. URL: https://doi.org/10.1088%2F2053-1583%2F2%2F1%2F015003.

[142] R. S. Gonnelli et al. "Temperature Dependence of Electric Transport in Few-layer Graphene under Large Charge Doping Induced by Electrochemical Gating". In: *Scientific Reports* 5.1 (2015), p. 9554. ISSN: 2045-2322. DOI: 10.1038/srep09554. URL: https://doi.org/10.1038/srep09554.

[143] N. R. Pradhan et al. "Hall and field-effect mobilities in few layered p-WSe_2 field-effect transistors". In: *Scientific Reports* 5.1 (2015), p. 8979. ISSN: 2045-2322. DOI: 10.1038/srep08979. URL: https://doi.org/10.1038/srep08979.

[144] Morgan A. Brown et al. "Hall Effect Measurements of the Double-Layer Capacitance of the Graphene–Electrolyte Interface". In: *The Journal of Physical Chemistry C* 123.37 (2019), pp. 22706–22710. ISSN: 1932-7447. DOI: 10.1021/acs.jpcc.9b03935. URL: https://doi.org/10.1021/acs.jpcc.9b03935.

[145] S. Dröscher et al. "Quantum capacitance and density of states of graphene". In: *Applied Physics Letters* 96.15 (2010), p. 152104. DOI: 10.1063/1.3391670. eprint: https://doi.org/10.1063/1.3391670. URL: https://doi.org/10.1063/1.3391670.

[146] J. L. Tedesco et al. "Hall effect mobility of epitaxial graphene grown on silicon carbide". In: *Applied Physics Letters* 95.12 (2009), p. 122102. DOI: 10.1063/1.3224887. eprint: https://doi.org/10.1063/1.3224887. URL: https://doi.org/10.1063/1.3224887.

[147] Gabriele Calabrese et al. "Inkjet-printed graphene Hall mobility measurements and low-frequency noise characterization". In: *Nanoscale* 12 (12 2020), pp. 6708–6716. DOI: 10.1039/C9NR09289G. URL: http://dx.doi.org/10.1039/C9NR09289G.

[148] Christos Dimitrakopoulos et al. "Effect of SiC wafer miscut angle on the morphology and Hall mobility of epitaxially grown graphene". In: *Applied Physics Letters* 98.22 (2011), p. 222105. DOI: 10.1063/1.3595945. eprint: https://doi.org/10.1063/1.3595945. URL: https://doi.org/10.1063/1.3595945.

[149] L. A. Falkovsky. "Unusual field and temperature dependence of the Hall effect in graphene". In: *Phys. Rev. B* 75 (3 2007), p. 033409. DOI: 10.1103/PhysRevB.75.033409. URL: https://link.aps.org/doi/10.1103/PhysRevB.75.033409.

[150] Damon B. Farmer et al. "Charge trapping and scattering in epitaxial graphene". In: *Phys. Rev. B* 84 (20 2011), p. 205417. DOI: 10.1103/PhysRevB.84.205417. URL: https://link.aps.org/doi/10.1103/PhysRevB.84.205417.

[151] Wenjuan Zhu et al. "Carrier scattering, mobilities, and electrostatic potential in monolayer, bilayer, and trilayer graphene". In: *Phys. Rev. B* 80 (23 2009), p. 235402. DOI: 10.1103/PhysRevB.80.235402. URL: https://link.aps.org/doi/10.1103/PhysRevB.80.235402.

[152] Matthew J. Hollander et al. "Enhanced Transport and Transistor Performance with Oxide Seeded High-κ Gate Dielectrics on Wafer-Scale Epitaxial Graphene". In: *Nano Letters* 11.9 (2011), pp. 3601–3607. ISSN: 1530-6984. DOI: 10.1021/nl201358y. URL: https://pubs.acs.org/doi/abs/10.1021/nl201358y.

[153] Yike Hu et al. "Structured epitaxial graphene: growth and properties". In: *Journal of Physics D: Applied Physics* 45.15 (2012), p. 154010. DOI: 10.1088/0022-3727/45/15/154010. URL: https://doi.org/10.1088%2F0022-3727%2F45%2F15%2F154010.

[154] E. Tiras et al. "Effective mass of electron in monolayer graphene: Electron-phonon interaction". In: *Journal of Applied Physics* 113.4 (2013), p. 043708. DOI: 10.1063/1.4789385. eprint: https://doi.org/10.1063/1.4789385. URL: https://doi.org/10.1063/1.4789385.

[155] K.I. Bolotin et al. "Ultrahigh electron mobility in suspended graphene". In: *Solid State Communications* 146.9 (2008), pp. 351 –355. ISSN: 0038-1098. DOI: https://doi.org/10.1016/j.ssc.2008.02.024. URL: http://www.sciencedirect.com/science/article/pii/S0038109808001178.

[156] John P. Perdew and Yue Wang. "Accurate and simple analytic representation of the electron-gas correlation energy". In: *Phys. Rev. B* 45 (23 1992), pp. 13244–13249. DOI: 10.1103/PhysRevB.45.13244. URL: https://link.aps.org/doi/10.1103/PhysRevB.45.13244.

[157] Thibault Sohier, Matteo Calandra, and Francesco Mauri. "Density functional perturbation theory for gated two-dimensional heterostructures: Theoretical developments and application to flexural phonons in graphene". In: *Phys. Rev. B* 96 (7 2017), p. 075448. DOI: 10.1103/PhysRevB.96.075448. URL: https://link.aps.org/doi/10.1103/PhysRevB.96.075448.

[158] J. L. Mañes. "Symmetry-based approach to electron-phonon interactions in graphene". In: *Phys. Rev. B* 76 (4 2007), p. 045430. DOI: 10.1103/PhysRevB.76.045430. URL: https://link.aps.org/doi/10.1103/PhysRevB.76.045430.

[159] Robert F. Snider. "Quantum-Mechanical Modified Boltzmann Equation for Degenerate Internal States". In: *The Journal of Chemical Physics* 32.4 (1960), pp. 1051–1060. DOI: 10.1063/1.1730847. eprint: https://doi.org/10.1063/1.1730847. URL: https://doi.org/10.1063/1.1730847.

[160] S. V. Morozov et al. "Giant Intrinsic Carrier Mobilities in Graphene and Its Bilayer". In: *Phys. Rev. Lett.* 100 (1 2008), p. 016602. DOI: 10.1103/PhysRevLett.100.016602. URL: https://link.aps.org/doi/10.1103/PhysRevLett.100.016602.

[161] K. S. Novoselov et al. “A roadmap for graphene”. In: *Nature* 490.7419 (2012), pp. 192–200. ISSN: 1476-4687. DOI: 10.1038/nature11458. URL: https://doi.org/10.1038/nature11458.

[162] Oscar D Restrepo et al. “A first principles method to simulate electron mobilities in 2D materials”. In: *New Journal of Physics* 16.10 (2014), p. 105009. DOI: 10.1088/1367-2630/16/10/105009. URL: https://doi.org/10.1088%2F1367-2630%2F16%2F10%2F105009.

[163] Samuel Poncé, Debdeep Jena, and Feliciano Giustino. “Hole mobility of strained GaN from first principles”. In: *Phys. Rev. B* 100 (8 2019), p. 085204. DOI: 10.1103/PhysRevB.100.085204. URL: https://link.aps.org/doi/10.1103/PhysRevB.100.085204.

[164] T. Kawamura and S. Das Sarma. “Phonon-scattering-limited electron mobilities in $Al_xGa_{1-x}As$/GaAs heterojunctions”. In: *Phys. Rev. B* 45 (7 1992), pp. 3612–3627. DOI: 10.1103/PhysRevB.45.3612. URL: https://link.aps.org/doi/10.1103/PhysRevB.45.3612.

[165] Khoe Van Nguyen and Yia-Chung Chang. “Full consideration of acoustic phonon scatterings in two-dimensional Dirac materials”. In: *Phys. Chem. Chem. Phys.* 22 (7 2020), pp. 3999–4009. DOI: 10.1039/C9CP05740D. URL: http://dx.doi.org/10.1039/C9CP05740D.

[166] F Rittweger, N F Hinsche, and I Mertig. “Phonon limited electronic transport in Pb”. In: *Journal of Physics: Condensed Matter* 29.35 (2017), p. 355501. DOI: 10.1088/1361-648x/aa7b56. URL: https://doi.org/10.1088%2F1361-648x%2Faa7b56.

[167] Daria I. Nasonova et al. “Low-Temperature Structure and Thermoelectric Properties of Pristine Synthetic Tetrahedrite $Cu_{12}Sb_4S_{13}$”. In: *Chemistry of Materials* 28.18 (2016), pp. 6621–6627. ISSN: 0897-4756. DOI: 10.1021/acs.chemmater.6b02720. URL: https://doi.org/10.1021/acs.chemmater.6b02720.

[168] Koichiro Suekuni et al. “High-performance thermoelectric mineral $Cu_{12-x}Ni_xSb_4S_{13}$ tetrahedrite”. In: *Journal of Applied Physics* 113.4 (2013), p. 043712. DOI: 10.1063/1.4789389. eprint: https://doi.org/10.1063/1.4789389. URL: https://doi.org/10.1063/1.4789389.

[169] Jaeseok Heo et al. "Enhanced Thermoelectric Performance of Synthetic Tetrahedrites". In: *Chemistry of Materials* 26.6 (2014), pp. 2047–2051. ISSN: 0897-4756. DOI: 10.1021/cm404026k. URL: https://doi.org/10.1021/cm404026k.

[170] R. Chetty et al. "Thermoelectric properties of Co substituted synthetic tetrahedrite". In: *Acta Materialia* 100 (2015), pp. 266 –274. ISSN: 1359-6454. DOI: https://doi.org/10.1016/j.actamat.2015.08.040. URL: http://www.sciencedirect.com/science/article/pii/S1359645415006175.

[171] Wei Lai et al. "From Bonding Asymmetry to Anharmonic Rattling in $Cu_{12}Sb_4S_{13}$ Tetrahedrites: When Lone-Pair Electrons Are Not So Lonely". In: *Advanced Functional Materials* 25.24 (2015), pp. 3648–3657. DOI: 10.1002/adfm.201500766. eprint: https://onlinelibrary.wiley.com/doi/pdf/10.1002/adfm.201500766. URL: https://onlinelibrary.wiley.com/doi/abs/10.1002/adfm.201500766.

[172] Kan Chen et al. "Theory-Guided Synthesis of an Eco-Friendly and Low-Cost Copper Based Sulfide Thermoelectric Material". In: *The Journal of Physical Chemistry C* 120.48 (2016), pp. 27135–27140. ISSN: 1932-7447. DOI: 10.1021/acs.jpcc.6b09379. URL: https://doi.org/10.1021/acs.jpcc.6b09379.

[173] Kan Chen et al. "Enhanced thermoelectric performance of Sn-doped Cu_3SbS_4". In: *J. Mater. Chem. C* 6 (31 2018), pp. 8546–8552. DOI: 10.1039/C8TC02481B. URL: http://dx.doi.org/10.1039/C8TC02481B.

[174] John P. Perdew, Kieron Burke, and Matthias Ernzerhof. "Generalized Gradient Approximation Made Simple". In: *Phys. Rev. Lett.* 77 (18 1996), pp. 3865–3868. DOI: 10.1103/PhysRevLett.77.3865. URL: https://link.aps.org/doi/10.1103/PhysRevLett.77.3865.

[175] E. Hernández. "Metric-tensor flexible-cell algorithm for isothermal–isobaric molecular dynamics simulations". In: *The Journal of Chemical Physics* 115.22 (2001), pp. 10282–10290. DOI: 10.1063/1.1416867. eprint: https://aip.scitation.org/doi/pdf/10.1063/1.1416867. URL: https://aip.scitation.org/doi/abs/10.1063/1.1416867.

[176] M. P. Desjarlais, J. D. Kress, and L. A. Collins. "Electrical conductivity for warm, dense aluminum plasmas and liquids". In: *Phys. Rev. E* 66 (2 2002),

p. 025401. DOI: 10.1103/PhysRevE.66.025401. URL: https://link.aps.org/doi/10.1103/PhysRevE.66.025401.

[177] Gabin P. L. Guélou et al. "The impact of manganese substitution on the structure and properties of tetrahedrite". In: *Journal of Applied Physics* 126.4 (2019), p. 045107. DOI: 10.1063/1.5110696. eprint: https://doi.org/10.1063/1.5110696. URL: https://doi.org/10.1063/1.5110696.

[178] Petr Levinsky et al. "Thermoelectric properties of the tetrahedrite–tennantite solid solutions $Cu_{12}Sb_{4-x}As_xS_{13}$ and $Cu_{10}Co_2Sb_{4-y}As_yS_{13}$ (0 <= x,y <= 4)". In: *Phys. Chem. Chem. Phys.* 21 (8 2019), pp. 4547–4555. DOI: 10.1039/C9CP00213H. URL: http://dx.doi.org/10.1039/C9CP00213H.

[179] L.L. Huang et al. "Preparation and enhanced thermoelectric performance of Pb-doped tetrahedrite $Cu_{12-x}Pb_xSb_4S_{13}$". In: *Journal of Alloys and Compounds* 769 (2018), pp. 478 –483. ISSN: 0925-8388. DOI: https://doi.org/10.1016/j.jallcom.2018.07.335. URL: http://www.sciencedirect.com/science/article/pii/S0925838818328366.

[180] Hiromi I. Tanaka et al. "Metal–Semiconductor Transition Concomitant with a Structural Transformation in Tetrahedrite $Cu_{12}Sb_4S_{13}$". In: *Journal of the Physical Society of Japan* 85.1 (2016), p. 014703. DOI: 10.7566/JPSJ.85.014703. eprint: https://doi.org/10.7566/JPSJ.85.014703. URL: https://doi.org/10.7566/JPSJ.85.014703.

[181] A. F. May et al. "Structural phase transition and phonon instability in $Cu_{12}Sb_4S_{13}$". In: *Phys. Rev. B* 93 (6 2016), p. 064104. DOI: 10.1103/PhysRevB.93.064104. URL: https://link.aps.org/doi/10.1103/PhysRevB.93.064104.

[182] Venkatesha R. Hathwar et al. "Low-Temperature Structural Phase Transitions in Thermoelectric Tetrahedrite, $Cu_{12}Sb_4S_{13}$, and Tennantite, $Cu_{12}As_4S_{13}$". In: *Crystal Growth & Design* (2019). ISSN: 1528-7483. DOI: 10.1021/acs.cgd.9b00385. URL: https://doi.org/10.1021/acs.cgd.9b00385.

[183] Joel van Embden et al. "Near-Infrared Absorbing $Cu_{12}Sb_4S_{13}$ and Cu_3SbS_4 Nanocrystals: Synthesis, Characterization, and Photoelectrochemistry". In: *Journal of the American Chemical Society* 135.31 (2013), pp. 11562–11571. ISSN: 0002-7863. DOI: 10.1021/ja402702x. URL: https://doi.org/10.1021/ja402702x.

[184] Raymond Jeanloz and Mary L. Johnson. "A note on the bonding, optical spectrum and composition of tetrahedrite". In: *Physics and Chemistry of Minerals* 11.1 (1984), pp. 52–54. ISSN: 1432-2021. DOI: 10.1007/BF00309375. URL: https://doi.org/10.1007/BF00309375.

[185] Sahil Tippireddy et al. "Electronic and thermoelectric properties of Zn and Se double substituted tetrahedrite". In: *Phys. Chem. Chem. Phys.* 20 (45 2018), pp. 28667–28677. DOI: 10.1039/C8CP05479G. URL: http://dx.doi.org/10.1039/C8CP05479G.

[186] E. Flage-Larsen and O. Prytz. "The Lorenz function: Its properties at optimum thermoelectric figure-of-merit". In: *Applied Physics Letters* 99.20 (2011), p. 202108. DOI: 10.1063/1.3656017. eprint: https://doi.org/10.1063/1.3656017. URL: https://doi.org/10.1063/1.3656017.

[187] Bingyan Chen et al. "Exploration of sensitivity limit for graphene magnetic sensors". In: *Carbon* 94 (2015), pp. 585 –589. ISSN: 0008-6223. DOI: https://doi.org/10.1016/j.carbon.2015.07.040. URL: http://www.sciencedirect.com/science/article/pii/S0008622315300634.

[188] Guibin Song, Mojtaba Ranjbar, and Richard A. Kiehl. "Operation of graphene magnetic field sensors near the charge neutrality point". In: *Communications Physics* 2.1 (2019), p. 65. ISSN: 2399-3650. DOI: 10.1038/s42005-019-0161-5. URL: https://doi.org/10.1038/s42005-019-0161-5.

[189] David Collomb, Penglei Li, and Simon J. Bending. "Nanoscale graphene Hall sensors for high-resolution ambient magnetic imaging". In: *Scientific Reports* 9.1 (2019), p. 14424. ISSN: 2045-2322. DOI: 10.1038/s41598-019-50823-8. URL: https://doi.org/10.1038/s41598-019-50823-8.

[190] Brian T. Schaefer et al. "Magnetic field detection limits for ultraclean graphene Hall sensors". In: *Nat. Commun.* 11 (2020), p. 4163. DOI: 10.1038/s41467-020-18007-5. URL: https://doi.org/10.1038/s41467-020-18007-5.

[191] G.D. Mahan. *Many-Particle Physics*. Physics of Solids and Liquids. Springer US, 2000. ISBN: 9780306463389. URL: https://books.google.it/books?id=xzSgZ4-yyMEC.

[192] E.I. Blount. "Formalisms of Band Theory". In: ed. by Frederick Seitz and David Turnbull. Vol. 13. Solid State Physics. Academic Press, 1962, pp. 305 –373. DOI: https://doi.org/10.1016/S0081-1947(08)60459-2. URL: http://www.sciencedirect.com/science/article/pii/S0081194708604592.

[193] J. M. Luttinger. "The Effect of a Magnetic Field on Electrons in a Periodic Potential". In: *Phys. Rev.* 84 (4 1951), pp. 814–817. DOI: 10.1103/PhysRev.84.814. URL: https://link.aps.org/doi/10.1103/PhysRev.84.814.

[194] Takafumi Kita. "Entropy in Nonequilibrium Statistical Mechanics". In: *Journal of the Physical Society of Japan* 75.11 (2006), p. 114005. DOI: 10.1143/JPSJ.75.114005. eprint: https://doi.org/10.1143/JPSJ.75.114005. URL: https://doi.org/10.1143/JPSJ.75.114005.